

Engineering Optimization: Methods and Applications

Anand J. Kulkarni *Editor*

# Optimization Methods for Product and System Design



Springer

# **Engineering Optimization: Methods and Applications**

## **Series Editors**

Anand J. Kulkarni, Institute of Artificial Intelligence, Dr. Vishwanath Karad MIT World Peace University, Pune, Maharashtra, India

Amir H. Gandomi, Engineering & Information Technology, University of Technology Sydney, Sydney, NSW, Australia

Seyedali Mirjalili, Brisbane, QLD, Australia

Nikos D. Lagaros, National Technical University of Athens, Athens, Greece

Warren Liao, Department of Construction Management and Industrial Engineering, Louisiana State University, Baton Rouge, LA, USA

Optimization carries great significance in both human affairs and the laws of nature. It refers to a positive and intrinsically human concept of minimization or maximization to achieve the best or most favorable outcome from a given situation. Besides, as the resources are becoming scarce there is a need to develop methods and techniques which will make the systems extract maximum from minimum use of these resources, i.e. maximum utilization of available resources with minimum investment or cost of any kind. The resources could be any, such as land, materials, machines, personnel, skills, time, etc. The disciplines such as mechanical, civil, electrical, chemical, computer engineering as well as the interdisciplinary streams such as automobile, structural, biomedical, industrial, environmental engineering, etc. involve in applying scientific approaches and techniques in designing and developing efficient systems to get the optimum and desired output. The multifaceted processes involved are designing, manufacturing, operations, inspection and testing, forecasting, scheduling, costing, networking, reliability enhancement, etc. There are several deterministic and approximation-based optimization methods that have been developed by the researchers, such as branch-and-bound techniques, simplex methods, approximation and Artificial Intelligence-based methods such as evolutionary methods, Swarm-based methods, physics-based methods, socio-inspired methods, etc. The associated examples are Genetic Algorithms, Differential Evolution, Ant Colony Optimization, Particle Swarm Optimization, Artificial Bee Colony, Grey Wolf Optimizer, Political Optimizer, Cohort Intelligence, League Championship Algorithm, etc. These techniques have certain advantages and limitations and their performance significantly varies when dealing with a certain class of problems including continuous, discrete, and combinatorial domains, hard and soft constrained problems, problems with static and dynamic in nature, optimal control, and different types of linear and nonlinear problems, etc. There are several problem-specific heuristic methods are also existing in the literature.

This series aims to provide a platform for a broad discussion on the development of novel optimization methods, modifications over the existing methods including hybridization of the existing methods as well as applying existing optimization methods for solving a variety of problems from engineering streams. This series publishes authored and edited books, monographs, and textbooks. The series will serve as an authoritative source for a broad audience of individuals involved in research and product development and will be of value to researchers and advanced undergraduate and graduate students in engineering optimization methods and associated applications.

Anand J. Kulkarni  
Editor

# Optimization Methods for Product and System Design

 Springer

*Editor*

Anand J. Kulkarni  
Institute of Artificial Intelligence  
Dr. Vishwanath Karad MIT World Peace  
University  
Pune, India

ISSN 2731-4049

ISSN 2731-4057 (electronic)

Engineering Optimization: Methods and Applications

ISBN 978-981-99-1520-0

ISBN 978-981-99-1521-7 (eBook)

<https://doi.org/10.1007/978-981-99-1521-7>

© The Editor(s) (if applicable) and The Author(s), under exclusive license to Springer Nature Singapore Pte Ltd. 2023

This work is subject to copyright. All rights are solely and exclusively licensed by the Publisher, whether the whole or part of the material is concerned, specifically the rights of translation, reprinting, reuse of illustrations, recitation, broadcasting, reproduction on microfilms or in any other physical way, and transmission or information storage and retrieval, electronic adaptation, computer software, or by similar or dissimilar methodology now known or hereafter developed.

The use of general descriptive names, registered names, trademarks, service marks, etc. in this publication does not imply, even in the absence of a specific statement, that such names are exempt from the relevant protective laws and regulations and therefore free for general use.

The publisher, the authors, and the editors are safe to assume that the advice and information in this book are believed to be true and accurate at the date of publication. Neither the publisher nor the authors or the editors give a warranty, expressed or implied, with respect to the material contained herein or for any errors or omissions that may have been made. The publisher remains neutral with regard to jurisdictional claims in published maps and institutional affiliations.

This Springer imprint is published by the registered company Springer Nature Singapore Pte Ltd.

The registered company address is: 152 Beach Road, #21-01/04 Gateway East, Singapore 189721, Singapore

# Preface

Product designers develop the features and functionality of the products based on the market demands, needs, trends, cost, predicted performance, novelty as well as ease of manufacturing. The emerging areas of product and system design involve apparel jewellery, automotive, furniture, households, packaging, manufacturing, etc. It is important for the designers to optimize each and every facet of the possible final product to make it functional as desired and acceptable in the market. The term product design is not only limited to the design of merely a product; but also, a system or a process. The optimization of associated machine-tools, outlet stores, supply chain management system, web interface and many more require minute level optimization which finally contribute to the sale, success and reputation. This edited book provides a platform to discuss the state-of-the-art developments associated with traditional as well as advanced single objective as well as multi-objective/criteria optimization methods for addressing problems associated with performance enhancement of the products and systems design. The book in detail discusses the core ideas, underlying principles, mathematical formulations, critical reviews and experimentations and solutions to the complex problems from within the domains such as mechanical engineering design and manufacturing, fault detection and diagnosis, control systems, financial systems, machine learning in medical image processing as well as problems from operations research domain. It may serve as a valuable reference to the academic as well as industry practitioners involving in improving the efficiency, cost, performance and durability of the products and systems. The contributions of the book may further give impetus to explore new avenues leading towards multi-disciplinary research discussions associated with resilience and sustainability of the existing systems.

Every chapter submitted to the book has been critically evaluated by at least two expert reviewers. The critical suggestions by the reviewers helped the authors of the individual chapter to enrich the quality in terms of experimentation, performance evaluation, representation, etc. The book may serve as a valuable reference for the researchers working in the domain of development and application of the optimization methods for solving complex problems from a variety of product and systems design.

The book is divided into four parts. The review and state-of-the-art single-objective as well as multi-objective/criteria optimization methods for solving engineering design problems as well as systems optimization are discussed in Part I. They include problems from manufacturing as well as control systems, fault diagnosis domain. Part II is dedicated to the application of Cohort Intelligence algorithm solving a variety of problems from financial domain, such as efficient management of the bank asset liability, problems modelled as Goal Programming problems. Part III provides rich and detailed work on the application of the machine learning algorithms for the classification of the tomography images as well as brain tumour and Alzheimer disease prognosis using deep learning approach. Part IV discusses two distinguished contributions including a Genetic Algorithm based assessment approach to maximize Tourist's Satisfaction.

## **Part I: Optimization in Engineering Design and Systems**

Chapter 1 “Multi-objective Optimization of Ventilated Brake Disc Based on Finite Element Simulation and League Championship Algorithm” considers an example of mechanical component with its design being simulated and optimized for the complex goals of maximizing heat transfer, minimizing weight and lifespan maximization. The well-proven NSGA-II and Multi-Objective League Championship Algorithm (MOLCA), three associated functions that fit these criteria are successfully solved.

Chapter 2 “Multi-response Optimization on Process Parameters of WEDM for Ti-6Al-4 V Alloy Using Grey Relational Approach” presents a complete investigation of the material removal rate and various significant surface roughness response parameters of the wire-cut electric discharge machining process. The work discusses optimization of various machining control parameters using the grey relational analysis. For carrying out the experimentation, traditional Taguchi DOE approach has been selected with four factors and three levels for designing the variation control table. The investigation suggests the most optimal process parameters for MRR and surface roughness performance characteristics of the significant machining parameters.

Chapter 3 “Tuning of Complex Coefficient Fractional Complex Order Controllers for a Generalized System Structure—An Optimisation Approach” proposes complex coefficient fractional complex order controllers for integer/fractional order systems containing complex coefficients and fractional complex order containing real/complex coefficients systems. An optimization approach is used to tune the controller parameters by considering both positive and negative frequency information of system with complex coefficients and complex order derivatives involving dead time. Numerical simulations are performed for a case study with the proposed and real-valued fractional order controllers.

Chapter 4 “A Review on Intelligent Optimization Techniques Based Fault Detection and Diagnosis in Power System Applications” presents a comprehensive review of computational intelligent optimization methods used for the Fault Detection and Diagnosis purpose in power transmission lines. The review focusses on the energy

efficiency by reducing transmission losses using efficient energy storage methods and improvement in the power quality and protection enhancing the reliability and operational performance through power management. It also addresses various Fault Detection and Diagnosis-related algorithms in power transmission line using computational intelligence techniques under varying load demands. The review may provide a valuable guidance and potential new research directions for selecting a suitable Fault Detection and Diagnosis method in power transmission line.

Chapter 5 “Prediction of Surface Roughness Using Desirability Concept and Support Vector Machine for Fused Deposition Modeling Part” provides an investigation on the effect of printing speed, layer thickness, extrusion temperature and infill percentage on the surface roughness of parts produced using Fused Deposition Modelling. An approach based on Response Surface Methodology and Design of Experiments yielded in significant reduction in the number of experimental runs. Optimum values of process parameters are determined using desirability concept which yielded the minimum surface roughness of the printed part.

Chapter 6 “An Extremum Model for the Performance Analysis of a Loop Heat Pipe Using Nano-fluids” presents the steady-state experimental analysis carried out to predict the loop heat pipe thermal performance using the Copper-Water Nano-fluid. The studies are performed for varied heat loads. It involves a parametric study for the thermal resistance, evaporator temperature and interface temperature of the heat pipe that affects its performance. The results highlighted the notable enhancement in the thermal characteristics of the heat pipe in comparison to the baseline case. The research reports significant reduction in the evaporator temperature and the thermal resistance of the heat pipe as well.

Chapter 7 “Selected Multi-criteria Decision-Making Methods and Their Applications to Product and System Design” five variations of Multi-criteria Decision-Making procedure with four normalization methods, weighting methods are described in very details. The MS Excel program, developed is also proposed and validated solving the chosen methods is also presented. Several Multi-criteria Decision-Making applications involving product and system design are successfully demonstrated showcasing the applicability and effectiveness.

## **Part II: Optimization for Financial Systems**

Chapter 8 “Cohort Intelligence Solution to Bank Asset Liability Management” addresses the important financial management objectives such as profit maximization, loss minimization and asset maximizing. These issues are categorized as multi-objective problems because they involve numerous conflicting objectives. Cohort Intelligence algorithm and the Goal Programming technique have been used to solve the problem. The effectiveness of this strategy is validated and demonstrated by the optimal results.

Chapter 9 “Cohort Intelligence Solution to Goal Programming Problems from Financial Management Domain” emphasizes that a good financial management



plays a critical role for the growth of any organization and the prevalent approach of achieving this is by setting priority-based goals which need to be optimized. In addition, the chapter proposes maximization of profit, loss reduction and asset maximization as goals to be achieved. The socio-inspired optimization algorithm referred to as Cohort Intelligence algorithm is applied to solve associated four financial real-world Goal Programming problems. A Static Penalty Function approach is adopted to achieve goals as constraints. The problems are referred to as Bank Financial Statement Optimization, Financial Structure Optimization, Financial Analysis of Non-Life Insurance Sector and Technical Analysis of Non-Life Insurance Sector.

Chapter 10 “Solving Asset and Liability Management Problem Using Cohort Intelligence and Goal Programming” highlights the dependency of an organization’s growth on sound financial management. The chapter addresses the problems of maximizing net profit, reducing non-performing assets and reducing loss. The Cohort Intelligence algorithm is used to solve asset and liability management problems. The solutions are validated by comparing with the existing methods.

### **Part III: Optimization for Image Processing**

Chapter 11 “Proposing a New Feature Clustering Method in Order to the Binary Classification of COVID-19 in Computed Tomography Images” proposes a new classification algorithm referred to as Curling Optimization Algorithm in which a valid database of CT scans is used in the training phase. The algorithm involves three main steps such as feature extraction using two pre-trained convolutional neural networks, dimension reduction process in combination with the DBSCAN and binary classification using Support Vector Machine. The accuracy of the classification yields a very high accuracy.

Chapter 12 “Deep Learning Framework for Brain Tumor and Alzheimer Disease Prognosis Using MRI Images” enables clear distinction in Brain Tumour and Alzheimer Disease using MRI. The proposed systems underlying Deep Learning Framework works on the pre-trained models that are VGG16, VGG 19, DenseNet201. The model is ordered into five classes Glioma Tumour, Meningioma Tumour, Pituitary Tumour, Alzheimer’s disease and No Tumour.

### **Part IV: Miscellaneous**

Chapter 13 “Genetic Algorithm to Maximize the Tourist’s Satisfaction: An Assessment of Technology Adoption for a Tourist App” proposes a tourism app to produce personalized trip itineraries. The app has embedded a genetic algorithm that searches for the best choices of places to maximize the tourist’s satisfaction. In order to evaluate tourists’ attitudes toward using the tourism app based on a genetic algorithm,

authors apply the practically important technology acceptance model. Results exhibited that most test participants found the tourism easier and acceptable and a strong positive correlation between attitude towards use and intention to use is also evident.

Pune, India

Anand J. Kulkarni

# Contents

## Part I Optimization in Engineering Design and Systems

<b>1 Multi-objective Optimization of Ventilated Brake Disc Based on Finite Element Simulation and League Championship Algorithm</b> .....	3
Ali Husseinzadeh Kashan, Somayyeh Karimiyan, Sadra Khodaei Anaraki, and Maryam Farahani	
<b>2 Multi-response Optimization on Process Parameters of WEDM for Ti-6Al-4 V Alloy Using Grey Relational Approach</b> .....	29
Ranjan Kumar and Kaushik Kumar	
<b>3 Tuning of Complex Coefficient Fractional Complex Order Controllers for a Generalized System Structure—An Optimisation Approach</b> .....	53
P. Sathishkumar and N. Selvagesan	
<b>4 A Review on Intelligent Optimization Techniques Based Fault Detection and Diagnosis in Power System Applications</b> .....	71
K. Vanchinathan and N. Selvagesan	
<b>5 Prediction of Surface Roughness Using Desirability Concept and Support Vector Machine for Fused Deposition Modeling Part</b> .....	89
Vijaykumar Jatti, Vinaykumar Jatti, Pawandeep Dhall, and Akshaykumar Patel	
<b>6 An Extremum Model for the Performance Analysis of a Loop Heat Pipe Using Nano-fluids</b> .....	97
Jobin Jose and Tapano Kumar Hotta	

**7 Selected Multi-criteria Decision-Making Methods and Their Applications to Product and System Design** ..... 107  
 Zhiyuan Wang, Seyed Reza Nabavi, and Gade Pandu Rangaiah

**Part II Optimization for Financial Systems**

**8 Cohort Intelligence Solution to Bank Asset Liability Management** ..... 141  
 Pranav Kulkarni, Aniket Nargundkar, Anand J. Kulkarni, and Apoorva Shastri

**9 Cohort Intelligence Solution to Goal Programming Problems from Financial Management Domain** ..... 157  
 Aayush P. Khandekar, Aniket Nargundkar, Anand J. Kulkarni, and Apoorva Shastri

**10 Solving Asset and Liability Management Problem Using Cohort Intelligence and Goal Programming** ..... 177  
 Ishan G. Gala, Aniket Nargundkar, Anand J. Kulkarni, and Apoorva Shastri

**Part III Optimization for Image Processing**

**11 Proposing a New Feature Clustering Method in Order to the Binary Classification of COVID-19 in Computed Tomography Images** ..... 193  
 Alireza Balavand and Soheyla Pahlevani

**12 Deep Learning Framework for Brain Tumor and Alzheimer Disease Prognosis Using MRI Images** ..... 217  
 Aditee Patil, Bhavana Tiple, and Madhura Phatak

**Part IV Miscellaneous**

**13 Genetic Algorithm to Maximize the Tourist’s Satisfaction: An Assessment of Technology Adoption for a Tourist App** ..... 235  
 M. A. Cosío-Léon, Anabel Martínez-Vargas, Misael Lopez-Sanchez, and Viridiana Silva-Rodríguez

# Editor and Contributors

## About the Editor

**Anand J. Kulkarni** holds a Ph.D. in Distributed Optimization from Nanyang Technological University, Singapore, an MS in Artificial Intelligence from the University of Regina, Canada, a Bachelor of Engineering from Shivaji University, India and a Diploma from the Board of Technical Education, Mumbai. He worked as a Research Fellow at Odette School of Business, University of Windsor, Canada. Anand worked with Symbiosis International University, Pune, India for over six years. He is currently working as a Professor and Associate Director of the Institute of Artificial Intelligence at MITWPU, Pune, India. His research interests include optimization algorithms, multi-objective optimization, continuous, discrete, and combinatorial optimization, swarm optimization, and self-organizing systems. Anand pioneered optimization methodologies such as Cohort Intelligence, Ideology Algorithm, Expectation Algorithm, and Socio Evolution & Learning Optimization Algorithm. Anand is the founder of Optimization and Agent Technology Research Lab and has published over 70 research papers in peer-reviewed reputed journals, chapters, and conferences along with 5 authored and 10 edited books. Anand is the lead series editor for Springer and Taylor & Francis as well as the editor of several Elsevier journals. He also writes on AI in several newspapers and magazines. Anand has delivered expert research talks in countries such as the USA, Canada, Singapore, Malaysia, India, and France.

## Contributors

**Alireza Balavand** Department of Industrial Engineering, Science and Research Branch, Islamic Azad University, Tehran, Iran

**M. A. Cosío-Léon** Universidad Politécnica de Pachuca, Zempoala, Hidalgo, Mexico

**Pawandeep Dhall** D.Y. Patil College of Engineering, Akurdi, Pune, Maharashtra, India

**Maryam Farahani** Faculty of Industrial and Systems Engineering, Tarbiat Modares University, Tehran, Iran

**Ishan G. Gala** Marathwada Mitramandal's College of Engineering, Pune, India

**Tapano Kumar Hotta** School of Mechanical Engineering, Vellore Institute of Technology, Vellore, Tamil Nadu, India

**Ali Husseinzadeh Kashan** Faculty of Industrial and Systems Engineering, Tarbiat Modares University, Tehran, Iran

**Vijaykumar Jatti** Symbiosis Institute of Technology, Pune, Maharashtra, India

**Vinaykumar Jatti** Symbiosis Institute of Technology, Pune, Maharashtra, India

**Jobin Jose** School of Mechanical Engineering, Vellore Institute of Technology, Vellore, Tamil Nadu, India

**Somayyeh Karimiyan** Department of Civil Engineering, Islamshahr Branch, Islamic Azad University, Islamshahr, Iran

**Aayush P. Khandekar** Vishwakarma Institute of Technology, Pune, India

**Sadra Khodaei Anaraki** Faculty of Industrial and Systems Engineering, Tarbiat Modares University, Tehran, Iran

**Anand J. Kulkarni** Dr. Vishwanath Karad, MIT World Peace University, Pune, India

**Pranav Kulkarni** Marathwada Mitramandal's College of Engineering, Pune, India

**Kaushik Kumar** Birla Institute of Technology, Mesra, Ranchi, India

**Ranjan Kumar** Birla Institute of Technology, Mesra, Ranchi, India

**Misael Lopez-Sanchez** Universidad Politécnica de Pachuca, Zempoala, Hidalgo, Mexico

**Anabel Martínez-Vargas** Universidad Politécnica de Pachuca, Zempoala, Hidalgo, Mexico

**Seyed Reza Nabavi** Department of Applied Chemistry, Faculty of Chemistry, University of Mazandaran, Babolsar, Iran

**Aniket Nargundkar** Symbiosis International (Deemed University), Symbiosis Institute of Technology, Lavale, Pune, India

**Soheyla Pahlevani** Department of Industrial Engineering, Electronic Branch, Islamic Azad University, Tehran, Iran

**Akshaykumar Patel** D.Y. Patil College of Engineering, Akurdi, Pune, Maharashtra, India

**Aditee Patil** MIT World Peace University, Pune, India

**Madhura Phatak** MIT World Peace University, Pune, India

**Gade Pandu Rangaiah** Department of Chemical and Biomolecular Engineering, National University of Singapore, Singapore, Singapore;  
School of Chemical Engineering, Vellore Institute of Technology, Vellore, India

**P. Sathishkumar** Department of Avionics, Indian Institute of Space Science and Technology, Department of Space, Government of India, Trivandrum, India

**N. Selvagesan** Department of Avionics, Indian Institute of Space Science and Technology, Thiruvananthapuram, Kerala, India

**Apoorva Shastri** Dr. Vishwanath Karad, MIT World Peace University, Pune, India

**Viridiana Silva-Rodríguez** Universidad Autónoma de San Luis Potosí, San Luis Potosí, San Luis Potosí, Mexico

**Bhavana Tiple** MIT World Peace University, Pune, India

**K. Vanchinathan** Department of Electrical and Electronics Engineering, Velalar College of Engineering and Technology, Thindal, Erode, Tamil Nadu, India

**Zhiyuan Wang** Department of Chemical and Biomolecular Engineering, National University of Singapore, Singapore, Singapore;  
Department of Continuing Education, DigiPen Institute of Technology Singapore, Singapore, Singapore

**Part I**  
**Optimization in Engineering Design**  
**and Systems**



# Chapter 1

## Multi-objective Optimization of Ventilated Brake Disc Based on Finite Element Simulation and League Championship Algorithm



Ali Husseinzadeh Kashan, Somayyeh Karimiyan, Sadra Khodaei Anaraki, and Maryam Farahani

**Abstract** Optimizing the design of mechanical components to achieve the desired goals and conditions is one of the most widely discussed topics in the field of optimization. In this research, the brake disc is considered as an example of mechanical component with its design being simulated and optimized to maximize heat transfer, minimize weight and maximize lifespan. Using the central composite design (CCD) technique, different tests are designed and simulated by Ansys 17 finite element software. Using NSGA-II and multi-objective league championship algorithm (MOLCA), three functions that fit these criteria are optimized. Results are merged and ranked by the ELECTRE method. The optimized brake disc experiences 32% better heat transfer, 12% less weight, and 37% longer lifetime relative to the original rigid disc.

**Keywords** Multi-objective optimization · Simulation · Multi-criteria decision making · Brake discs with ventilation

### 1.1 Introduction

The brake disc is one of the most important parts of a car being responsible for converting the kinetic energy of the vehicle into heat energy to slow it down. Approximately 99% of the kinetic energy content is absorbed by the brake disc and transferred to the environment during the friction of the disc with the brake pad. Due to the forces on brake discs and frequent thermal stresses, the brake disc experiences fatigue, ultimately causing its failure. Therefore, to be named a high-quality brake disc, one must transfer heat to the environment and have an acceptable lifetime. Methods like finite

---

A. Husseinzadeh Kashan (✉) · S. Khodaei Anaraki · M. Farahani  
Faculty of Industrial and Systems Engineering, Tarbiat Modares University, Tehran, Iran  
e-mail: [a.kashan@modares.ac.ir](mailto:a.kashan@modares.ac.ir)

S. Karimiyan  
Department of Civil Engineering, Islamshahr Branch, Islamic Azad University, Islamshahr, Iran

element analysis, solving equations related to problem conditions, and laboratory analysis have been used by researchers to study this topic.

In the work by (Kubota et al. 2000), the brake disc is optimized using the experimental method for weight, heat transfer, and vibration criteria. In Mackin et al. (2002), thermal cracking of a brake disc was studied by braking from the experimental and theoretical point of view and extracting the relating equations. In Galindo-Lopez and Tirovic (2008), the effect of cooling fins on heat transfer of the brake disc using the finite element method was studied. Investigation (Bagnoli et al. 2009) examines thermal fatigue in a cast-iron brake disc of a firefighter truck using finite element analysis and an experimental review of gray cast iron barriers.

In Hwang and Wu (2010), the temperature and thermal stress of braking in a braking disc with ventilation using finite element analysis was investigated. In Adamowicz and Grzes (2011), the brake disc temperature under repeated braking is studied by analyzing the equations of related convection heat transfer for the brake disc. In Belhocine and Bouchetara (2012), a brake disc with ventilation blades is examined by analyzing heat transfer equations and the finite element method, and the shape of brake discs is optimized with different materials for increasing heat transfer. In Munisamy et al. (2012) it is focused on the effect of ventilation fins curvature on temperature and heat transfer of a brake disc by using CFD. The effect of brake disc ventilation fin's angle on the heat transfer of brake disc was discussed in Munisamy et al. (2013). In Saiz et al. (2015), the thermal stresses of 3 discs with different ventilation fins were investigated. Using the Ansys software, temperature, tension, and strain caused by braking on a brake disc were extracted. In the study of Yan et al. (2015), the effect of ventilation holes of a brake disc on heat transfer was studied and the results of the finite element analysis were compared with the experimental results. In Tauviqirrahman et al. (2017), thermo-mechanical analysis of a brake disc with ventilation by the finite element method was studied and the ratio of heat transfer and stresses applied to the brake disc was calculated and concluded that: (a) by increasing the fin's number, heat transferring increases (b) the gradient of the von mises stress decreases (c) increasing fin's number doesn't change in the total deformation much. In Kakandar et al. (2017) by simulating CEA/FEA and the Taguchi design of experiment method, the fatigue factors in the design of the brake disc have been introduced. In Chopade and Valavade (2016), the effect of four different cross-sections on the shape of the brake disc's fins have been analyzed by a finite elemental and experimental analysis on the heat transfer of the brake disc. Finally, the fins with a TRV (taper radial vanes) shape had the best heat transfer at all speeds.

## 1.2 Research Method

In this chapter, the Brake Disc of a "Pride" vehicle has been used, with mechanical properties and geometric dimensions obtained from the main manufacturer. Mechanical and physical properties such as density, elastic modulus, Poisson ratio, ultimate

tensile and compressive strengths, specific heat capacity, coefficient of heat transfer and data on mechanical fatigue of the gray cast iron used in the brake disc are presented in Tables 1.13 and 1.14 of Appendix 1.

### 1.2.1 Design of Experiments

Using the Central Composite Inscribed (CCI) design technique for two different geometries of brake discs, 135 experiments were designed for disc A and 90 for disc B.

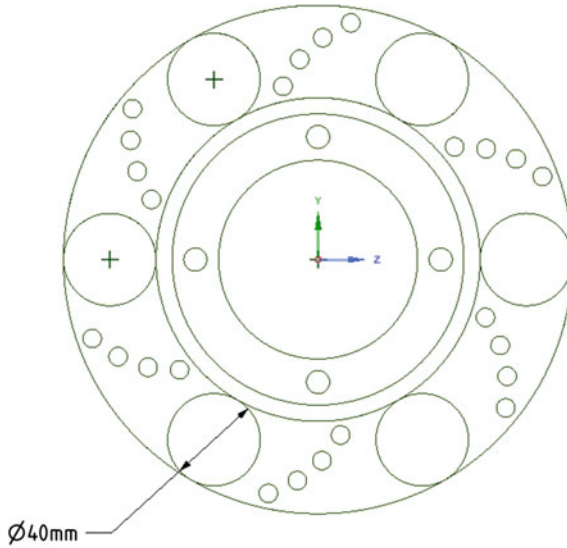
#### 1.2.1.1 Response Criteria

In this study, three criteria of average disc surface temperature, lifetime, and weight were considered as response criteria, where minimizing the average surface and weight of the disc, as well as maximizing its life was to be obtained.

- *Average temperature:* By braking, the kinetic force of the vehicle is converted into thermal energy by the friction between the brake disc and the pad, which is transferred to the surrounding environment. As the brake disc temperature increases, the brake linings and friction reduce. Modification of the brake disc design to maximize heat transfer is of great importance.
- *Disc lifespan:* The brake disc is under load due to the compressive force of the pad and the braking system, which causes its fatigue, making maximization of its life as a means to ensure its safety and reliability.
- *Weight of the disc:* Designed geometry and shape of the brake disc have significant effects on its weight. The weight could be significantly reduced through negligible variations in its design. Therefore, minimizing its weight (and the cast iron used in it) is of great importance which plays a major role in the production costs.

#### 1.2.1.2 Decision Variable for Brake Disc A

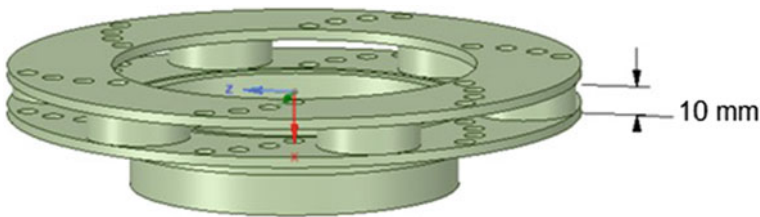
- *The radius of fins:* In the design of the ventilated disc A, there are cylindrical fins between the two-discs that connect the two disc plates. These fins act as a pillar in transmitting the force between the two-disc plates, which also play significant roles in both resistance and life of the disc, in addition to their effect on heat transfer of the disc with the environment through airflow. The radius of these cylinders is a continuous variable with upper and lower limits of 4 and 20 mm, respectively. Figure 1.1 shows the top view of the disc and the location of these cylinders.
- *Fin's height:* The height of the fins is another continuous variable considered in this study, which represents the distance between the two-disc plates; or in other words, the fin's height. The upper boundary of this height is 10 mm due to braking system design limitations, which means other parts of the brake system must be



**Fig. 1.1** The top view of the disc and the location of cylinders' fins

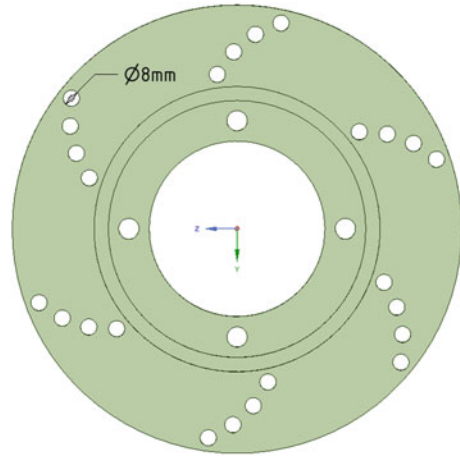
re-designed if the fin's height is needed to be more than 10 mm. As a result, the upper value is assumed to be 10 mm in this case, while the lower value is 1 mm. Figure 1.2 shows the 3D representation of the fin's height and the distance between the two-disc plates.

- *The radius of ventilation holes:* These holes are designed on both sides of the brake disc, which allow the air to flow and increase the heat transfer of the brake disc and accelerate the disc temperature drop. The lower boundary of these cavities radius is 1 mm, while the upper is 4 mm. It should be noted that the larger the holes are, the less is the area that can be contacted with the linings, which will hinder the braking system to work efficiently. In this research, the upper boundary of the diameter is selected such that it does not adversely affect the braking system. This parameter is shown in Fig. 1.3.
- *The number of fins:* In this research, the number of cylindrical fins is considered as a discrete variable with a lower and upper bound of 6 and 8, respectively.



**Fig. 1.2** The height of the fins and the distance between the two disc plates

**Fig. 1.3** Location of ventilation holes



**Table 1.1** The range of each decision variable in brake disc A

Decision variable	Fin's radius	Fin's height	The radius of ventilation holes	Ventilation holes number	Fin's number
Range	$4 \leq x_5 \leq 20$	$1 \leq x_4 \leq 10$	$1 \leq x_3 \leq 4$	$2 \leq x_2 \leq 6$ And integer	$6 \leq x_1 \leq 8$ And integer

- *The number of ventilation holes:* the number of brake ventilation holes in this study is a discrete variable that represents the number of holes between two successive cylindrical fins on both sides of the disc. In the design of the disc, there are rows of ventilation cavities on both sides of the disc equivalent to the number of cylindrical fins, which are designed in curve shapes with a radius of 90 mm. The number of these cavities is considered to be an integer with a lower bound of 2 and an upper of 6. Table 1.1 briefly summarizes the range of each decision variable in the brake disc A.

**1.2.1.3 Decision Variables for Brake Disc B**

Decision variables for brake disc B are the same as for A, with the only difference in the shape of the fins, which is rectangular in this disc. Therefore, the fin's width is used instead of the fin's radius. In Table 1.2, the scope of each decision criterion is briefly displayed on the brake disc B.

**Table 1.2** Range of each decision variables in brake disc B

Decision variables	Fin's width	Fin's height	The radius of ventilation holes	Ventilation holes number	Fin's number
Range	$2 \leq x_5 \leq 10$	$1 \leq x_4 \leq 10$	$1 \leq x_3 \leq 4$	$2 \leq x_2 \leq 4$ And integer	$10 \leq x_1 \leq 20$ And integer

## 1.2.2 Simulation and Design Results

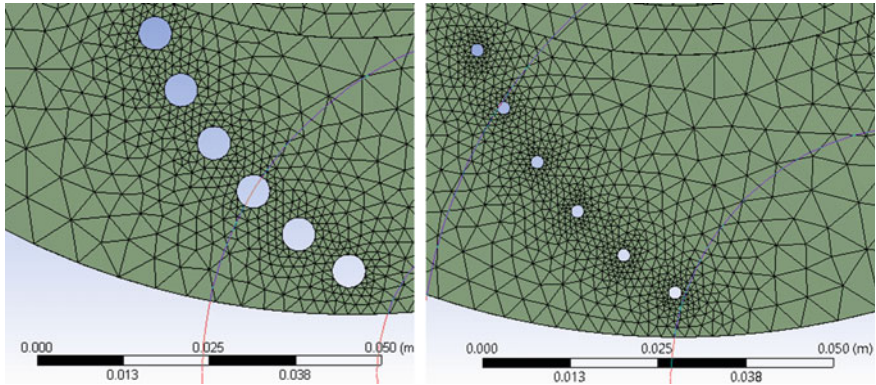
The Ansys SpaceClaim 17 software was used to design the brake disc and Ansys collection was utilized for simulation of the fluid and structural environment, as well as numerical solutions.

### 1.2.2.1 Simulation of the Fluid Environment in the CFX Module

In this module, all the rules governing fluids including fluid motion, turbulence, heat transfer, and forces applied to the structure are considered through numerical simulation. After importing the designed model into the module, the fluid environment around the disc is meshed, then in the next step, the boundary conditions are considered. Finally, when the model is solved, the required outputs are extracted, which are described below.

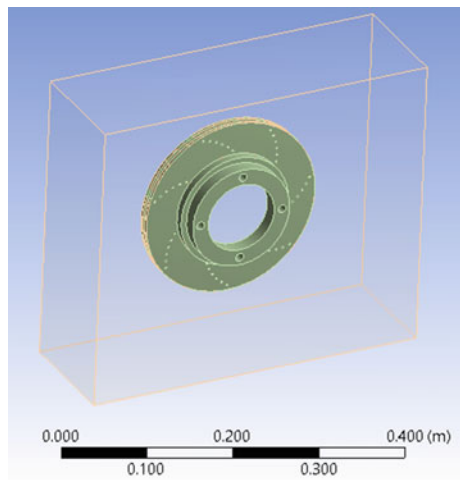
- *Network of nodes in a fluid environment:* Triangular mesh type was used with the maximum and minimum distance between two nodes of 5 cm and 0.5 mm, respectively. Based on the value of the decision variable in each design for the network, the shape of the mesh and node's distances are different. However, the average number of nodes for the fluid environment around the brake disc A is 150,000 and is 310,000 for disk B. For the brake disc A, 90,000 nodes, and for B, 170,000 nodes were meshed. Figure 1.4 shows the extent of mesh variations relative to the changes in the radius of the ventilation holes.
- *Applying boundary conditions in the fluid environment:* The Transient Rotor–Stator (TRS) boundary conditions are used in this project. The brake disc is immersed in the surrounding air. Figure 1.5 shows the brake disc and the surrounding air that are considered as a cube. The angular velocity of the brake discs is 1066 rpm and the ambient air hits fin grooves with a 100 km/h speed parallel to them. The initial temperature of the disc and ambient temperature are considered 20 °C. The braking time and the cooling time of the disc are both considered to be 100 s. The model was simulated in 20 stages at intervals of 10 s. The convergence accuracy of the simulation is considered to be 0.0001 and temperature is considered as its criterion.

In the design of the fluid environment around the brake disc, one air inlet and three open boundaries are considered. As shown in Fig. 1.6, the entering air is shown with black arrows while open boundaries are displayed with blue arrows. Open boundaries act as air outlet or inlet and vary depending on the movement of the fluid.



**Fig. 1.4** Variations of meshes relative to changes of ventilation holes radius

**Fig. 1.5** Brake disc and the surrounding air



- *Extracting results from the fluid analysis:* After calculating the simulated model in the CFX software, the required results such as speed, the average temperature of the disc surface, and forces applied to the disc are extracted. The amount of heat transfer is one of the response criteria in this study, which is measured by the average temperature of the contact surfaces of the lining and the brake disc. In Fig. 1.7, the average temperature of one brake disc is shown as an example.

**1.2.2.2 Simulation of the Structural Environment in the Ansys Structural Module**

In the structural environment, all dynamic and static forces and reciprocating forces of the brake disc are simulated and after the numerical analysis, the amount of

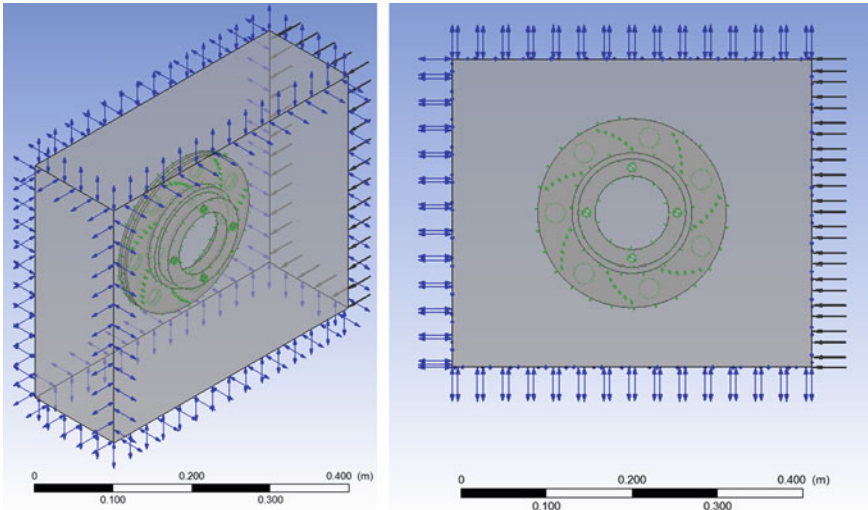


Fig. 1.6 Air inlet and three open boundaries in fluid simulation

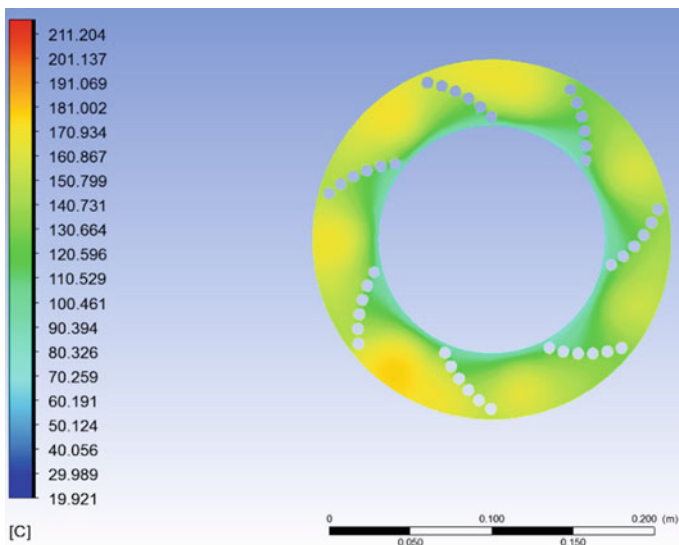
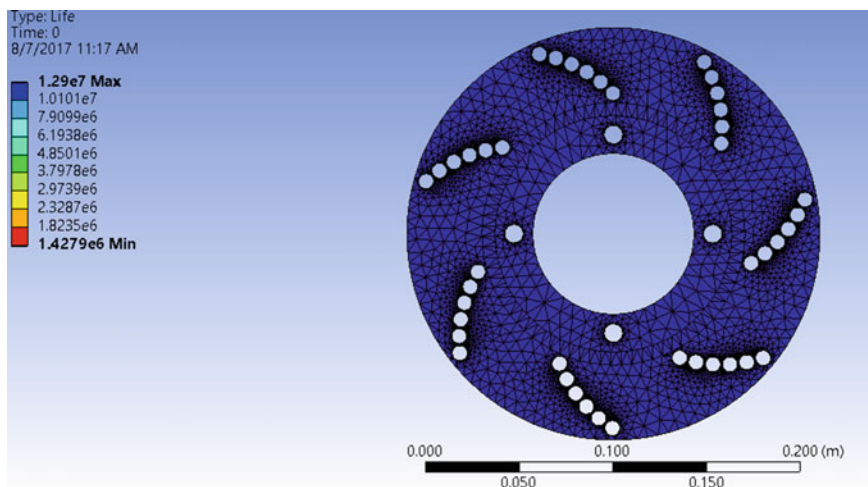


Fig. 1.7 The average temperature of the brake disc surface

deformation and lifespan, calculated based on the fatigue theories, are obtained as the output for one of response criteria.

- *Mesh grid in the structural environment:* The grid system used is triangular, and the maximum and minimum distance between two nodes is 2.5 mm 0.25 mm,





**Fig. 1.8** Illustration of the fatigue life of the brake disc

respectively. Based on the value of the decision variables in each design, the shape of the node network and the distances of the nodes are different. The average number of nodes for the brake disc A is 300,000 and for the brake disc B is 520,000. In the structural environment, the air around the disc is not analyzed and therefore not meshed.

- *Apply boundary conditions in the structural environment:* In this step, the supporting plans are selected in the software and the force of the lining to two surfaces of the disc is 9800N, perpendicular to the surface.
- *Extracting results from the structural analysis:* Lifespan and weight, two criteria considered in this research, are achievable at this stage. The average stress curve theory was used to analyze the fatigue phenomenon. In Fig. 1.8, the minimum lifespan of the brake disc is shown.

### ***1.2.3 Extracting the Fitted Functions on the Simulation Results***

By using the results of simulation of all the models defined in the design of the experiments, the functions fitted on the three response criteria are extracted by design expert software. In this study, for each disc, three functions with 5 variables were extracted.

## 1.2.4 Optimization

Two multi-objective optimization algorithms, namely the NSGA-II<sup>1</sup> and MOLCA<sup>2</sup> are used to optimize functions. The mentioned algorithms are employed to find optimal setting for the designing parameters.

### 1.2.4.1 NSGA-II Algorithm

This algorithm is based on a genetic algorithm, and by adding two essential operators to a single-objective genetic algorithm, it is converted into a multi-objective algorithm which provides a group of best solutions, known as the Pareto Front, rather than finding the best single-dimensional response. These two operators are:

- An operator that assigns a superiority (rank) based on non-dominated sorting and unlocking and fronting the members of the population.
- An operator that maintains the diversity of the solutions and their disparity among responses with equal ranks.

In Fig. 1.9, the pseudocode of NSGA-II is displayed.

### 1.2.4.2 MOLCA Algorithm

The MOLCA algorithm is designed based on the league championship algorithm (LCA), which has been proposed in Husseinzadeh Kashan (2014) and employed in Husseinzadeh Kashan et al. (2012, 2017, 2018, 2019a, 2020), Alizadeh and Husseinzadeh Kashan (2019), Alimoradi and Husseinzadeh Kashan (2018), Jalili et al. (2017), Husseinzadeh Kashan (2011), Husseinzadeh Kashan and Karimi (2010). LCA is the most prominent algorithm inspired from the field of sport. LCA is a population-based algorithm for global optimization in a continuous search space.

The main idea of LCA is based on an artificial match analysis process where a metaphorical SWOT analysis is used for generating new solutions. In order to investigate the LCA in detail, its pseudo-code is presented in Fig. 1.10.

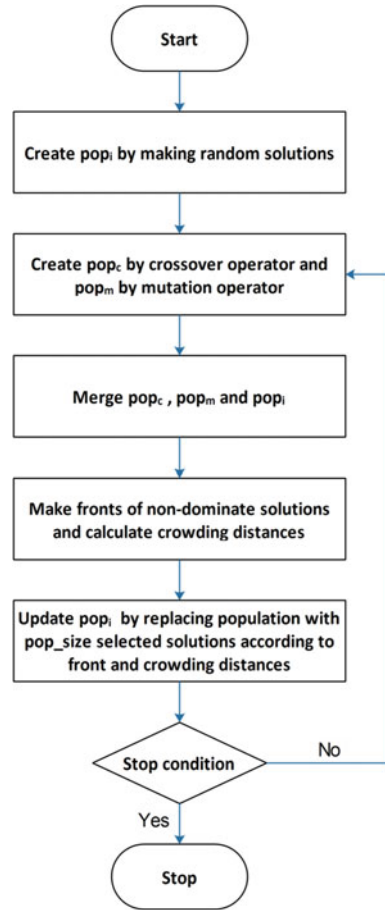
In the initial step, some parameters must be determined. These parameters include the number of iterations, the number of the season, control parameters, and the number of teams/individuals (Husseinzadeh Kashan 2014). The stopping criteria are satisfied when a certain number of seasons are passed in which a season includes several weeks or iterations. A solution in LCA is a vector whose length is equal to the number of variables. The value of the objective function (s) of each solution is called team strength. In the initial phase of LCA, a population of solutions is generated and evaluated. After initialization, the league schedule is generated based on a single round-robin schedule (Husseinzadeh Kashan 2014).

---

<sup>1</sup> Non-dominated sorting genetic algorithm-II.

<sup>2</sup> Multi-objective league of champions.

**Fig. 1.9** Pseudocode of NSGA-II



Let  $f(X = (x_1, x_2, \dots, x_n))$  be an  $n$  variable function that should be minimized over the decision space. A team formation (a solution) for team (individual)  $i$  at week (iteration)  $t$  can be represented by  $X_i^t = (x_{i1}^t, x_{i2}^t, \dots, x_{in}^t)$ , with  $f(X_i^t)$  indicating the fitness/function value (team strength) resulted from  $X_i^t$ . By  $B_i^t = (b_{i1}^t, b_{i2}^t, \dots, b_{in}^t)$ , we denote the best previously experienced formation of team  $i$  until week  $t$ , yielding the best function value for team  $i$ . To determine  $B_i^t$ , we employ a greedy selection between  $X_i^t$  and  $B_i^{t-1}$  based on the value of  $f(X_i^t)$  and  $f(B_i^{t-1})$ .

There is a procedure to identify the loser or winner team in LCA that its equation is as follows.

$$p_i^t = \frac{f(X_j^t) - \hat{f}}{f(X_j^t) + f(X_i^t) - 2\hat{f}} \tag{1.1}$$

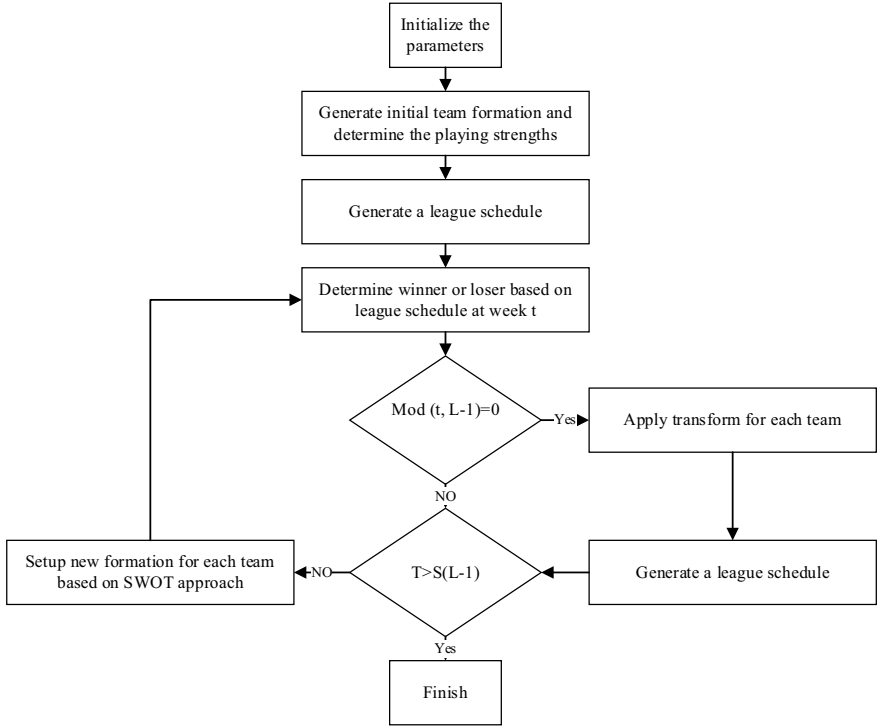





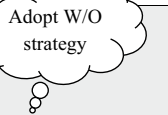
Fig. 1.10 Flowchart of LCA

According to Eq. 1.1 Let us consider teams  $i$  and  $j$  playing at week  $t$  with their formations  $X_i^t$  and  $X_j^t$  and playing strengths  $f(X_i^t)$  and  $f(X_j^t)$ , respectively. Let  $p_i^t$  denotes the chance of team  $i$  to beat team  $j$  at week  $t$  ( $p_j^t$  can be defined accordingly). Let also  $\hat{f}$  be an ideal value (e.g., a lower bound on the optimal function value). A random number between zero and one is generated. If this number is less than or equal to  $p_i^t$ , team  $i$  wins otherwise team  $j$  wins.

The main part of LCA is related to match analysis. LCA uses a SWOT strategy to generate a new solution. According to Fig. 1.11, SWOT shows that each team benefits from its internal evaluation and external evaluation of other teams. In this way, the match analysis for each team will be done before playing in two ways. Firstly, the performance of the team is considered based on its previous game; secondly, the performance of the opponent team is investigated based on its previous game.

By using the hypothetical SWOT matrix, we derive the possible actions for team  $i$  from the artificial match analysis based on the previous week's events in Fig. 1.11.

The given S/T, S/O, W/T, and W/O strategies in Fig. 1.11 show the reasonable strategies in different situations for an artificial team. Let us introduce the following indices:

	 <i>i had won</i> <i>l had won</i> Focusing on ...	 <i>i had won</i> <i>l had lost</i> Focusing on ...	 <i>i had lost</i> <i>l had won</i> Focusing on ...	 <i>i had lost</i> <i>l had lost</i> Focusing on ...
<b>S</b>	own strengths (or weaknesses of <i>j</i> )	own strengths (or weaknesses of <i>j</i> )	–	–
<b>W</b>	–	–	own weaknesses (or strengths of <i>j</i> )	own weaknesses (or strengths of <i>j</i> )
<b>O</b>	–	weaknesses of <i>l</i> (or strengths of <i>k</i> )	–	weaknesses of <i>l</i> (or strengths of <i>k</i> )
<b>T</b>	strengths of <i>l</i> (or weaknesses of <i>k</i> )	–	strengths of <i>l</i> (or weaknesses of <i>k</i> )	–

**Fig. 1.11** Hypothetical SWOT matrix derived from the artificial match analysis (Husseinzadeh Kashan 2014)

*l* : Based on the league schedule, the team with index *l* will play with team *i* at week *t* + 1.

*j* : Based on the league schedule, the team with index *j* has played with team *i* at week *t*.

*k* : Based on the league schedule, the team with index *k* has played with team *l* at week *t*.

Four situations occur according to Eqs. (1.2)–(1.5):

**If both *i* and *l* had won**, then a new solution is created based on the adaptation of the *S/T* strategy:

$$(S/T \text{ equation}) : x_{id}^{t+1} = b_{id}^t + y_{id}^t \left( \psi_1 r_1 (b_{id}^t - b_{kd}^t) + \psi_1 r_2 (b_{id}^t - b_{jd}^t) \right) \forall d = 1, \dots, n \tag{1.2}$$

**Else if *i* won but *l* had lost**, then a new solution is created based on the adaptation of *S/O* strategy:

$$(S/O \text{ equation}) : x_{id}^{t+1} = b_{id}^t + y_{id}^t \left( \psi_2 r_1 (b_{kd}^t - b_{id}^t) + \psi_1 r_2 (b_{id}^t - b_{jd}^t) \right) \forall d = 1, \dots, n \tag{1.3}$$

**Else if *i* had lost but *l* had won**, then a new solution is created based on the adaptation of *W/T* strategy:

$$(W/T \text{ equation}) : x_{id}^{t+1} = b_{id}^t + y_{id}^t \left( \psi_1 r_1 (b_{id}^t - b_{kd}^t) + \psi_2 r_2 (b_{jd}^t - b_{id}^t) \right) \quad \forall d = 1, \dots, n \quad (1.4)$$

**Else if** both  $i$  and  $l$  had lost, then a new solution is created based on the adaptation of W/O strategy:

$$(W/O \text{ equation}) : x_{id}^{t+1} = b_{id}^t + y_{id}^t \left( \psi_2 r_1 (b_{kd}^t - b_{id}^t) + \psi_2 r_2 (b_{jd}^t - b_{id}^t) \right) \quad \forall d = 1, \dots, n \quad (1.5)$$

**End if.**

According to Eqs. (1.2)–(1.5), in order to generate a new solution, the strengths and weakness of team  $i$  are investigated by considering the performance of team  $j$  and the opportunities and treats are investigated by considering the performance of team  $k$ . In the above equations,  $d$  is the variable or dimension index.  $r_1$  and  $r_2$  are uniform random numbers in  $[0, 1]$ .

$\psi_1$  and  $\psi_2$  are coefficients employed to scale the contribution of “retreat” or “approach” components, respectively. Also, the sign of the difference in the parentheses causes acceleration towards the winner or retreat from the loser.  $y_{id}^t$  is a binary change variable that indicates whether the  $d$ th element in the current best solution will change or not. Only  $y_{id}^t = 1$  allows making a change in the value of  $b_{id}^t$ . Let us define  $Y_i^t = (y_{i1}^t, y_{i2}^t, \dots, y_{in}^t)$  as the binary change array in which the number of ones is equal to  $q_i^t$ . It is reasonable that the number of changes made in  $B_i^t$  (i.e., the value of  $q_i^t$ ) be small. The following formula simulates the random number of changes made in  $B_i^t$  to get the new solution  $X_i^{t+1}$ .

$$q_i^t = \left\lceil \frac{\ln(1 - (1 - (1 - p_c)^{n-q_0+1})r)}{\ln(1 - p_c)} \right\rceil + q_0 - 1 : q_i^t \in \{q_0, q_0 + 1, \dots, n\} \quad (1.6)$$

where  $r$  is a random number in  $[0, 1]$  and  $p_c \in (0, 1)$  is a control parameter.  $q_0$  is the least number of changes realized during the artificial match analysis. The greater the value of  $p_c$ , the smaller number of changes are advised. After simulating the number of changes by (1.6),  $q_i^t$  number of elements are selected randomly from  $B_i^t$  and their value changes based on one of Eqs. (1.2)–(1.5). For greater details on the idea behind various equations developed in LCA, the reader may refer to Husseinzadeh Kashan (2014).

We exactly employ the same rationale used in NSGAI to develop the multi-objective version of LCA, noted as MOLCA.

### 1.3 Analysis of the Results

#### 1.3.1 Fitting a Function on Simulated Results

20 samples out of 135 and 90 experiments, and their simulation results for the two brake discs, are presented in Tables 1.15 and 1.16 (Appendix 2). Using these results, 3D functions are fitted to two brake discs. In Table 1.3, the parameters used in the fitted functions are shown.

Equations (1.7)–(1.9) are functions fitted for the weight, lifespan and average temperature values of the brake disc A, respectively.

$$\text{Mass} = 3.378 - 0.078A - 0.051B - 5.185 \times 10^{-3}C - 0.098D + 4.119 \times 10^{-3}E + 3.626 \times 10^{-3}AB + 4.604 \times 10^{-3}AD + 4.666 \times 10^{-3}BD - 5.522 \times 10^{-3}CE + 7.33 \times 10^{-4}A^2 \tag{1.7}$$

$$\text{Log}(\text{life} + 12900) = +1.563 + 0.155A + 0.383D \tag{1.8}$$

$$\begin{aligned} (\text{Average temperature})^{-1.57} = & +7.703 \times 10^{-4} - 4.626 \times 10^{-5}A + 9.395 \times 10^{-5}B - 1.37 \\ & \times 10^{-5}C - 4.341 \times 10^{-5}D - 1.849 \times 10^{-5}E + 1.152 \times 10^{-6}AB - 2.329 \times 10^{-6}AD + 4.714 \\ & \times 10^{-6}BD + 1.275 \times 10^{-6}BE + 3.972 \times 10^{-6}CE + 1.114 \times 10^{-6}A^2 - 5.096 \times 10^{-6}B^2 \end{aligned} \tag{1.9}$$

Equations (1.10)–(1.12) are functions fitted for weight, lifespan and average temperature values of the disc brake B, respectively.

$$\text{Mass} = +2.79 - 0.029A - 0.043B + 0.033C - 0.061D - 7.074 \times 10^{-3}E + 4.827 \times 10^{-3}AB + 7.274 \times 10^{-3}AD + 2.293 \times 10^{-3}BE \tag{1.10}$$

$$\text{Log}(\text{life}) = +0.0156 + 0.234A + 0.333D + 0.35E - 0.0108AE - 0.017DE \tag{1.11}$$

$$\begin{aligned} \text{Average temperature} = & +271.976 - 5.86A - 9.033B - 21.78C - 18.12E + 0.184BE \\ & +0.575A^2 + 0.418B^2 + 4.114C^2 + 0.601E^2 \end{aligned} \tag{1.12}$$

**Table 1.3** Definition of the parameters of the fitted functions

Parameters	Brake disc B	Brake disc A
A	Fin width	Fin diameter
B	Fin height	Fin height
C	Hole radius	Hole radius
D	Hole number	Fin number
E	Fin number	Hole number

**Table 1.4** R-squared indicator for fitted functions

Response objectives	R-squared for brake disc A (%)	R-squared for brake disc B (%)
Mass	96.60	77.23
Life	83.76	96.62
Average temperature	95.94	79.56

The accuracy of the fitted functions on the results of experiments for two brake discs are shown in Table 1.4.

### 1.3.2 Multi-Optimization by Meta-Heuristic Algorithms

By applying NSGA-II and MOLCA multi-objective algorithms, the three objective functions corresponding to brake discs A and B are optimized and the Pareto front solutions corresponding to each algorithm are obtained. In Table 1.5, the number of Pareto solutions of each algorithm is shown.

The three-variable function surfaces for brake disc A and B are shown in Figs. 1.12 and 1.13.

#### 1.3.2.1 Comparing the Results of the NSGA-II and MOLCA

Generally, two features are used to evaluate the quality of the Pareto front set. The first feature refers to the number of Pareto optimal solutions in the set. The second feature examines the accuracy of the solutions.

- *Quantitative index*: This index measures the number of optimal Pareto solutions. Obviously, by finding more solutions, the algorithm will be more effective. The number of solutions obtained from the two algorithms is shown in Table 1.5.
- *Quality index*: If the three functions be independently optimized, by comparing their value with the mean of the Pareto front of each algorithm, this index can be calculated. In Table 1.6, the optimal value of the single-objective functions is shown. In Table 1.7, the quality index of the algorithms is shown.

**Table 1.5** The number of resulting solutions in the Pareto front of each algorithm

Algorithm	Pareto front	
	Brake disc B	Brake disc A
NSGA-II	31	32
MOLCA	1269	594



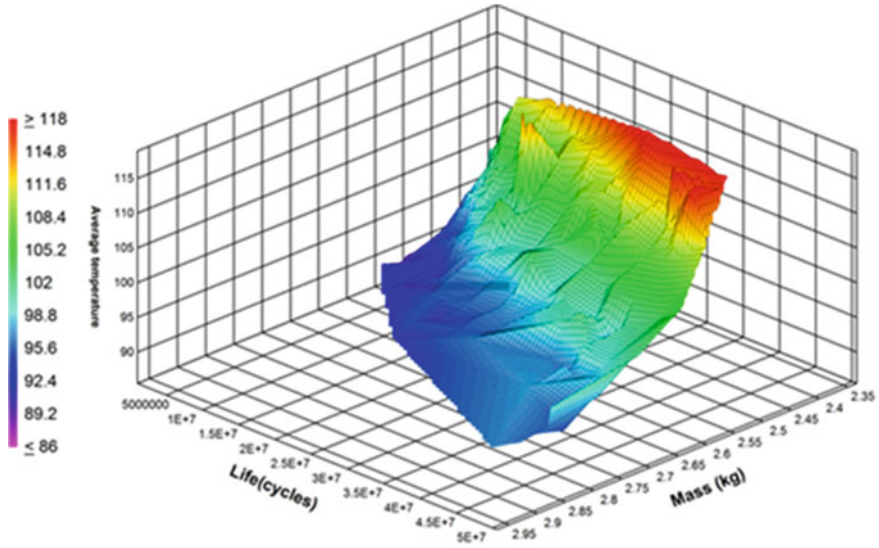


Fig. 1.12 Approximation of three-variable functions surface for brake disc A

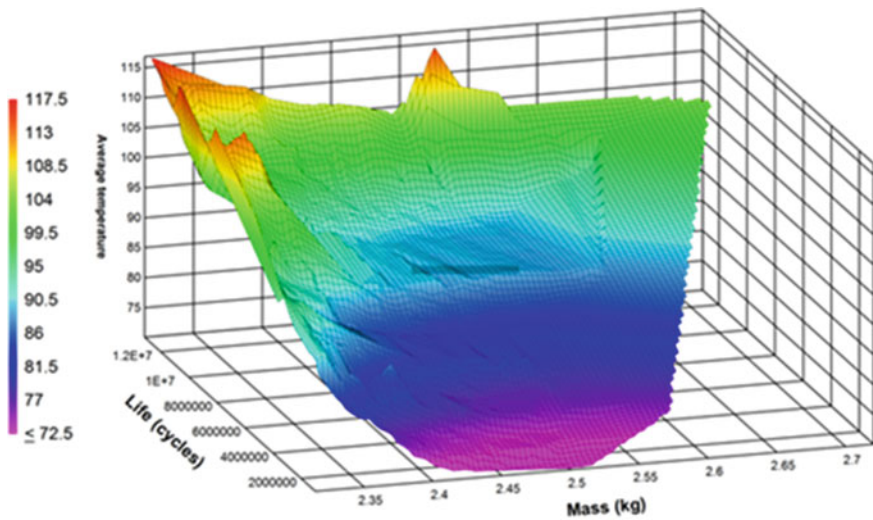


Fig. 1.13 Approximation of three-variable functions surface for brake disc B

According to the results, MOLCA reports better results in quantitative and qualitative indexes.

**Table 1.6** Optimal value of single objective functions

Criteria	Single objective optimal value
Weight of brake disc A	2.3 (kg)
Lifespan of brake disc A	2/35 E+06 (cycles)
Average temperature of brake disc A	75.463 °C
Weight of brake disc B	2.283 (kg)
Lifespan of brake disc B	3/58 E+06 (cycles)
Average temperature of brake disc B	67.386 °C

**Table 1.7** The quality index of the algorithms (lower values are better)

Algorithms	Criteria		
	Average temperature (%)	Weight (%)	Lifespan (%)
NSGA-II (brake disc A)	36.37	13.507	52.47
MOLCA (brake disc A)	28.15	7.93	39.33
NSGA-II (brake disc B)	38.79	7.62	44.21
MOLCA (brake disc B)	28.42	6.26	31.69

### 1.3.3 Using ELECTRE-I Multi-criteria Decision-Making Method

The Pareto fronts of the two algorithms are merged and prioritized by the ELECTRE-I method. The criteria of mass, life, and the average temperature of the surface are weighted by 0.2, 0.3, and 0.5, respectively. In Tables 1.8 and 1.9, the five best solutions obtained by this method for brake discs A and B are presented.

Given the feature values provided in Tables 1.8 and 1.9, the brake discs A and B are simulated using the Ansys finite element software. In Table 1.10, the simulation results are compared with the results of the optimization algorithms.

The optimal design for a brake disc is the B-type design (with rectangular-fin) with its geometric profile reported in Table 1.11. The performance gained by the optimized brake disc compared to the original rigid brake disc is shown in Fig. 1.14. In this figure, changes in the temperature for the optimized and rigid brake discs

**Table 1.8** Top 5 results for brake disc A determined by ELECTRE-I

No.	Mass (Kg)	Life (cycles)	Average temperature (°C)
1	2.4304	1.88E+06	86.8559
2	2.4419	1.70E+06	86.0854
3	2.4517	1.70E+06	85.9985
4	2.4200	1.61E+06	86.5555
5	2.4509	1.55E+06	85.6114

**Table 1.9** Top 5 results for brake disc B determined by ELECTRE-I

No.	Mass (Kg)	Life (cycles)	Average temperature (°C)
1	2.4475	2.41E+06	75.7487
2	2.4951	2.62E+06	75.1098
3	2.4482	2.54E+06	77.4284
4	2.4888	1.56E+06	71.4400
5	2.4997	1.43E+06	70.4615

**Table 1.10** Comparing simulation and optimization results

Brake discs	Objectives			
	Average temperature	Life (cycles)	Mass (kg)	Average error (%)
Brake disc A (fitted function)	86.8559	1.88E+06	2.4304	5.23
Brake disc A (simulated)	84.2415	2.08E+06	2.4816	
Brake disc B (fitted function)	75.7487	2.41E+06	2.4475	3.11
Brake disc B (simulated)	78.6046	2.39E+06	2.3705	

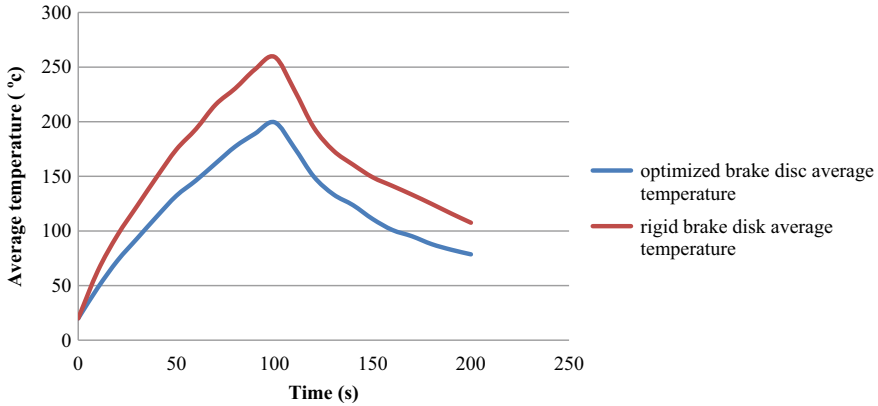
**Table 1.11** Geometric profile for optimized brake disc

	Fin width (mm)	Fin height (mm)	Ventilation radius (mm)	Ventilation holes number	Fin number
Dimensions	4	5.3504	3.1619	5.9533	17

**Table 1.12**  
Improvement gained by the optimized brake disc compared to the original rigid brake disc

	Average temperature (%)	Life (%)	Mass (%)
Improvement ratio	32	37	12

are shown. Table 1.12 reports the improvement gained by the optimized brake disc compared to the original rigid brake disc.



**Fig. 1.14** Changes in the average temperature of the optimized and rigid brake disc, during the braking process

## 1.4 Conclusion and Future Research

In this research, a disc brake has been designed that improves the weight, life, and heat transfer ratios by 12, 37 and 32% compared to the primary brake disc. The process mentioned in this study can also be used to optimize other mechanical components. Results show that the multi-objective league championship algorithm (MOLCA) has better performance than NSGA-II.

For future research, the following directions are recommended for considerations:

- Using different braking modes and different braking rates
- Considering the vibrations on the braking system and performing a modal analysis
- Investigating the effect of changing the material of the brake disc
- Testing the performance of the other metaheuristic algorithm on the problem, e.g., Optics Inspired Optimization (Husseinzadeh Kashan 2015; Jalili and Husseinzadeh Kashan 2018, 2019), Find-Fix-Finish-Exploit-Analyze metaheuristic algorithm (Husseinzadeh Kashan et al. 2019b), etc.

## Appendix 1

See Tables 1.13 and 1.14.

**Table 1.13** Mechanical and thermal properties of gray cast iron

Mechanical properties	Value (unit)
Density	7200 kg/m <sup>3</sup>
Elastic modulus	110,000 (Mpa)
Poisson ratio	0.28
Tensile ultimate strength	240 (Mpa)
Compressive ultimate strength	820 (Mpa)
Specific heat capacity	456 J/kg · K

**Table 1.14** Mechanical fatigue behavior of gray cast iron

Alternating ( <i>Pa</i> )	Cycles
3,999,000,000	10
2,827,000,000	20
1,896,000,000	50
1,413,000,000	100
1,069,000,000	200
441,000,000	2000
262,000,000	10,000
214,000,000	20,000
138,000,000	100,000
114,000,000	200,000
86,200,000	1,000,000

## Appendix 2

See Tables 1.15 and 1.16.

**Table 1.15** The number of 20 samples out of 135 results of simulation of brake disc A

Experiment no	Average temperature (°C)	Life (cycle)	Mass (Kg)	Ventilation hole's number	Fin's number	The radius of ventilation holes (mm)	Fin's height (mm)	Fin's radius (mm)	Std.
1	90.62259	824,170	2.5139	4	7	2.5	5.5	12	75
2	104.9052	581,630	2.4271	2	7	2.5	1	12	26
3	97.62401	12,900,000	2.7548	2	7	3.391905	8.175716	16.75683	23
4	86.26647	1,130,600	2.4902	2	8	1.608095	8.175716	7.243172	33
5	102.7141	12,900,000	2.7821	4	8	2.5	5.5	20	85
6	86.30192	254,850	2.4589	2	7	3.391905	8.175716	7.243172	22
7	78.15547	0	2.4182	2	7	2.5	5.5	4	24
8	86.47096	1,452,200	2.4645	2	8	3.391905	8.175716	7.243172	37
9	91.12425	729,010	2.5211	6	6	1	5.5	12	101
10	94.32059	12,900,000	2.8209	4	8	1.608095	8.175716	16.75683	79
11	91.72066	312,230	2.4929	2	6	4	5.5	12	10
12	91.09667	2,069,700	2.6571	6	6	3.391905	8.175716	16.75683	92
13	90.83313	721,410	2.5233	4	6	1	5.5	12	56
14	98.48795	3,448,200	2.6049	2	6	3.391905	8.175716	16.75683	8
15	103.6191	12,900,000	2.764	6	8	2.5	5.5	20	130
16	95.37752	12,900,000	2.7361	6	8	3.391905	8.175716	16.75683	128
17	95.9864	3,266,400	2.6626	2	8	2.5	10	12	42
18	101.6462	12,900,000	2.5165	2	7	3.391905	2.824284	16.75683	21
19	84.99149	996,850	2.4752	6	8	1.608095	8.175716	7.243172	123
20	85.91061	542,290	2.437	2	7	1.608095	2.824284	7.243172	16

**Table 1.16** The number of 20 samples out of 90 results of simulation of brake disc B

Experiment no	Average temperature (°C)	Life (cycle)	Mass (Kg)	Fin's number	Ventilation hole's number	The radius of ventilation holes (mm)	Fin's height (mm)	Fin's width (mm)	Std.
1	92.15	60,410	2.598	10	2	1.608095	8.175716	8.378414	67
2	72.1	474,100	2.579	15	2	2.5	10	6	36
3	83.27	72,630	2.465	10	4	2.5	5.5	6	45
4	78.58	21,740	2.459	10	2	3.391905	8.175716	3.621586	15
5	72.93	335,700	2.434	15	4	1.608095	8.175716	3.621586	26
6	100.72	12,900,000	2.5121	20	4	1.608095	2.824284	8.378414	88
7	88.04	1,146,000	2.392	15	4	3.391905	2.824284	8.378414	68
8	77.71	37,450	2.41	10	2	2.5	10	6	39
9	109.26	12,900,000	2.7575	20	4	1.608095	8.175716	8.378414	90
10	77.5	619,700	2.55	15	2	1	5.5	6	40
11	77.52	1,014,000	2.673	15	4	1.608095	8.175716	8.378414	84
12	90.15	1,220,000	2.489	15	4	1.608095	2.824284	8.378414	64
13	119.76	12,900,000	2.531	20	2	1.608095	2.824284	8.378414	76
14	98.96	53,490	2.364	10	4	1.608095	2.824284	3.621586	6
15	86.69	298,100	2.448	15	2	1.608095	2.824284	3.621586	24
16	88.91	12,900,000	2.555	20	2	2.5	5.5	6	60
17	118.22	12,900,000	2.466	20	2	3.391905	2.824284	8.378414	82 ara>
18	81.67	45,870	2.429	10	4	1.608095	8.175716	3.621586	4
19	71.54	537,500	2.535	15	4	2.5	10	6	54
20	109.12	111,200	2.466	10	4	1.608095	2.824284	8.378414	72

## References

- Adamowicz A, Grzes P (2011) Influence of convective cooling on a disc brake temperature distribution during repetitive braking. *Appl Therm Eng* 31(14–15):2177–2185
- Alimoradi MR, Husseinzadeh Kashan A (2018) A league championship algorithm equipped with network structure and backward Q-learning for extracting stock trading rules. *Appl Soft Comput* 68:478–493
- Alizadeh N, Husseinzadeh Kashan A (2019) Enhanced grouping league championship and optics inspired optimization algorithms for scheduling a batch processing machine with job conflicts and non-identical job sizes. *Appl Soft Comput* 83:105657
- Bagnoli F, Dolce F, Bernabei M (2009) Thermal fatigue cracks of fire fighting vehicles gray iron brake discs. *Eng Fail Anal* 16(1):152–163
- Belhocine A, Bouchetara M (2012) Thermal analysis of a solid brake disc. *Appl Therm Eng* 32:59–67
- Chopade MR, Valavade AP (2016) Experimental analysis and investigation for thermal performance of ventilated disc brake rotor using CFD. In: Heat transfer summer conference. American Society of Mechanical Engineers
- Galindo-Lopez C, Tirovic M (2008) Understanding and improving the convective cooling of brake discs with radial vanes. *Proc Inst Mech Eng Part D: J Autom Eng* 222(7):1211–1229
- Husseinzadeh Kashan A (2011) An efficient algorithm for constrained global optimization and application to mechanical engineering design: league championship algorithm (LCA). *Comput Aided Des* 43(12):1769–1792
- Husseinzadeh Kashan A (2014) League Championship Algorithm (LCA): an algorithm for global optimization inspired by sport championships. *Appl Soft Comput* 16:171–200
- Husseinzadeh Kashan A (2015) A new metaheuristic for optimization: optics inspired optimization (OIO). *Comput Oper Res* 55:99–125
- Husseinzadeh Kashan A, Karimi B (2010) A new algorithm for constrained optimization inspired by the sport league championships. In: IEEE congress on evolutionary computation. IEEE
- Husseinzadeh Kashan A, Abbasi-Poya A, Karimiyan S (2017). Mathematical formulation and a league championship algorithm for helicopter routing in offshore transportation. In: Second International Conference on Data Engineering and Communication Technology (ICDECT), Pune, India
- Husseinzadeh Kashan A, Jalili S, Karimiyan S (2018) Optimum structural design with discrete variables using league championship algorithm. *Civ Eng Infrastruct J* 51(2):253–275
- Husseinzadeh Kashan A, Jalili S, Karimiyan S (2019a) Premier league championship algorithm: a multi-population-based algorithm and its application on structural design optimization. In: *Socio-Cultural Inspired Metaheuristics*. Springer, Berlin, pp 215–240
- Husseinzadeh Kashan A, Eyvazi M, Abbasi-Pooya A (2020) An effective league championship algorithm for the stochastic multi-period portfolio optimization problem. *Sci Iran* 27(2):829–845
- Husseinzadeh Kashan A, Karimiyan S, Karimiyan M, Kashan MH (2012) A modified league championship algorithm for numerical function optimization via artificial modeling of the “between two halves analysis. In: The 6th international conference on soft computing and intelligent systems, and the 13th international symposium on advanced intelligence systems. IEEE
- Husseinzadeh Kashan A, Tavakkoli-Moghaddam R, Gen M (2019b) Find-Fix-Finish-Exploit-Analyze (F3EA) meta-heuristic algorithm: an effective algorithm with new evolutionary operators for global optimization. *Comput Ind Eng* 128:192–218
- Hwang P, Wu X (2010) Investigation of temperature and thermal stress in ventilated disc brake based on 3D thermo-mechanical coupling model. *J Mech Sci Technol* 24(1):81–84
- Jalili S, Husseinzadeh Kashan A (2018) Optimum discrete design of steel tower structures using optics inspired optimization method. *Struct Design Tall Spec Build* 27(9):e1466
- Jalili S, Husseinzadeh Kashan A (2019) An optics inspired optimization method for optimal design of truss structures. *Struct Design Tall Spec Build* 28(6):e1598



- Jalili S, Husseinzadeh Kashan A, Hosseinzadeh Y (2017) League championship algorithms for optimum design of pin-jointed structures. *J Comput Civ Eng* 31(2):04016048
- Kakandar E, Roy R, Mehnen J (2017) A simulation-based approach to model design influence on the fatigue life of a vented brake disc. *Procedia CIRP*. 59:41–46
- Kubota M, Hamabe T, Nakazono Y, Fukuda M, Doi K (2000) Development of a lightweight brake disc rotor: a design approach for achieving an optimum thermal, vibration and weight balance. *JSAE Rev* 21(3):349–355
- Mackin TJ, Noe SC, Ball K, Bedell B, Bim-Merle D, Bingaman M et al (2002) Thermal cracking in disc brakes. *Eng Fail Anal* 9(1):63–76
- Munisamy KM, Yusoff MZ, Thangaraju SK (2012) Ventilated brake disk air streamlining using curved vane. *Appl Mech Mater*. Trans Tech Publications
- Munisamy KM, Shuaib N, Yusoff MZ, Thangaraju SK (2013) Heat transfer enhancement on ventilated brake disk with blade inclination angle variation. *Int J Autom Technol* 14(4):569–577
- Saiz CB, Ingrassia T, Nigrelli V, Ricotta V (2015) Thermal stress analysis of different full and ventilated disc brakes. *Frattura Ed Integrita Strutturale* 9(34)
- Tauviqirrahman M, Jamari J, Bayuseno AP (2017) Thermo-mechanical investigation of ventilated disc brake with finite element. *Analysis* 8:3073–3081
- Yan H, Feng S, Yang X, Lu T (2015) Role of cross-drilled holes in enhanced cooling of ventilated brake discs. *Appl Therm Eng* 91:318–333

# Chapter 2

## Multi-response Optimization on Process Parameters of WEDM for Ti–6Al–4 V Alloy Using Grey Relational Approach



Ranjan Kumar and Kaushik Kumar

**Abstract** The present article produces an investigation of the material removal rate (MRR) and various surface roughness (SR) response parameters of the wire-cut electric discharge machining (WEDM) process. The paper also discusses the optimization of various machining control parameters using the grey relational analysis (GRA) technique. The investigation has obtained the optimized value of machining process parameters for maximized MRR and minimized surface roughness parameters. For carrying out the experimentation, the design of experiments (DOE) has been designed using the traditional Taguchi DOE approach and the  $L_{27}$  orthogonal array (OA) has been selected. In this regard, the four factors and three levels have been chosen for designing the variation control table for  $L_{27}$  OA, and discharge current ( $I_p$ ), voltage ( $V$ ), pulse-on time ( $T_{on}$ ) as well as the pulse-off time ( $T_{off}$ ) have been selected for variation control factors or variables. The response table based on the investigation and optimized data analysis “compares the relative magnitude of the effects,” including ranks on the basis of delta value. From the main effect plot, it can be clearly seen that the  $I_p$  is observed to be the most dominating significant factor over MRR and SR characteristics. The investigation suggests the most optimal process parameters for MRR and surface roughness performance characteristics of the aforementioned machining parameters.

**Keywords** Grey relational analysis (GRA) · Grey-Taguchi analysis · Machining parameters · Material removal rate (MRR) · Surface roughness parameters · Wire EDM machining · Discharge current ( $I_p$ ) · Pulse-on time ( $T_{on}$ ) · Pulse-off time ( $T_{off}$ )

---

R. Kumar · K. Kumar (✉)  
Birla Institute of Technology, Mesra, Ranchi, India  
e-mail: [kkumar@bitmesra.ac.in](mailto:kkumar@bitmesra.ac.in)

© The Author(s), under exclusive license to Springer Nature Singapore Pte Ltd. 2023  
A. J. Kulkarni (ed.), *Optimization Methods for Product and System Design*,  
Engineering Optimization: Methods and Applications,  
[https://doi.org/10.1007/978-981-99-1521-7\\_2](https://doi.org/10.1007/978-981-99-1521-7_2)

## 2.1 Introduction

In the last few decades, the inclination toward understanding the behavior of titanium alloy has grown drastically and the continuous growth in the study has made it possible to commercialize such an attractive alloy. Titanium alloy (Ti-alloy) i.e., Ti-6Al-4V is one of the toughest materials known for its characteristics of hard-to-machine using the ever-known non-conventional machining process (Gnanavelbabu et al. 2018). The said alloy is loaded with the remarkable mechanical properties of high corrosion resistance, lower thermal conductivity, comparatively higher mechanical strength as well as decent notable fatigue resistance characteristics. Owing to many other mechanical characteristics, it also possesses a lower modulus of elasticity, “high strength-to-weight ratio, and high elevating cutting temperature” (Barry et al. 2001; Hareesh et al. 2021). Titanium alloy (Ti-6Al-4V) carries many amazing characteristics that made this alloy suitable for a larger application arena such as aerospace and rocketry, automotive and marine applications. Also, constantly increasing demand has made this alloy a quite loving material that has also been incorporated into many other industrial and marine-based applications. These are being tremendously utilized in “petroleum refining, chemical processing, surgical implantation, pulp and paper pollution control, nuclear waste storage, food processing as well as electrochemical applications” (Ezugwu and Wang 1997; Myers et al. 1984). The extended applications of such titanium alloy are found in biomedical implants, jewelry, and chemical industries (Donachie 2000; Leyens and Peters 2003; Bodunrin et al. 2020). The Ti-alloy has been remarkably introduced in biomedical applications due to its “low elastic modulus comparable to human bones” (Rack and Qazi 2006; Niinomi 1998, 2019). The enormous utilization of titanium alloys (Ti-6Al-4V) can be estimated from the wide domain-wise utilization chart as shown in Fig. 2.1 (Web of Science 2021).

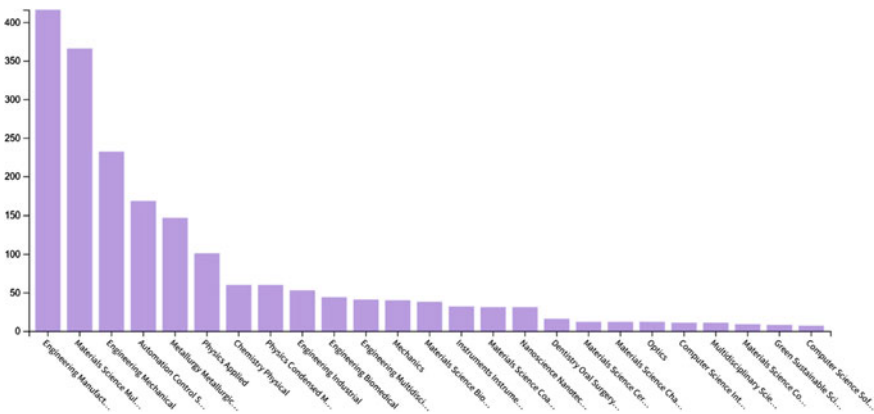
Despite having loving mechanical characteristics, the broader application arena, and attractive properties, the Ti-alloys also carry some shortcomings and challenges that restrict their demand and potential applications in many other domains. Firstly, The Ti itself is a costly material and possesses a high processing cost. Also, the Ti-alloys have a significant hindrance to their widespread utilization because the products manufactured using Ti or Ti-alloys are highly expensive and demand very complex and multistage traditional manufacturing processes (Froes et al. 2004; Esteban et al. 2008). Secondly, Ti-alloys used in biomedical implants have generally been found to have “poor tribological performance and low surface hardness (T. Frączek, M. Olejnik, and A. Tokarz 2009; Textor et al. 2001; Kustas and Misra 2017). Their tribological activity is characterized by high coefficients of friction (COF), severe adhesive wear, and low abrasion resistance” (Yerokhin et al. Aug. 2000). When in contact with surfaces, Ti and its alloys exhibit poor tribological characteristics, especially under mechanical sliding conditions. The mechanical sliding can cause surface wear by destroying the protective oxide layer (Kaur et al. 2019; Dong 2010; Dong and Bell 2000). The wide range of machining characteristics and



**Fig. 2.1** Domain-wise utilization of titanium alloy (Ti-6Al-4 V) (Web of Science 2021)

operations using Ti-6Al-4 V can be estimated by domain-wise published documents as delineated in Fig. 2.2 (Scopus.com 2021).

In the last few decades, “heat-resistant-super alloys (HRSA) like Ni and Ti-based alloys” earned exciting popularity and attention. The Ti-alloys possess unmatched mechanical and thermal properties that have found their potential applications in very much harsh and corrosive conditions (Devarajaiah and Muthumari 2018). “Generally, Ti alloyed with 6% Al and 4% vanadium, i.e., Ti-6Al-4 V is used in most of



**Fig. 2.2** Subject area-wise documents published for Ti-6Al-4 V machining operations (Scopus.com 2021)

the applications, and the incorporation of the traditional way of machining results in higher cutting forces, excessive tool wear,” and possess poor machinability characteristics. This is owing to the material’s lower heat conductivity, heightened “chemical reactivity, and great strength even at high temperatures.” There are several challenges that need to consider while machining Ti-alloys using traditional processes, these are as follows:

- i. *Higher strength of Ti-alloys at higher temperature resists the “plastic deformation” during machining.*
- ii. *During the machining process, the maximum amount of heat is generated which results in the welding of the tool to the tool face.*
- iii. *The Ti shows “chemical reactivity with almost all the tool materials” above 500 °C.*
- iv. *During machining, the issues of “deflection, rubbing and chatter occurs” result in the occurrence of a lower value of “modulus of elasticity.”*
- v. *Due to having an elevated temperature during the machining process, the risk of catching fire of Ti-alloy occurs.*

Hence, in order to avoid such machining issues that generally occur with the machining of hardened materials, we take the advantage of non-conventional machining (NCM) techniques. NCM is done by employing a variety of energy sources, including “mechanical, thermal, electrical, chemical, or a combination of the aforementioned energy sources,” and does not employ any cutting tools (Devarajaiah and Muthumari 2018; Singh 2015). The two most widely accepted non-conventional machining techniques are “electrical discharge machining (EDM) and wire-EDM.” Both of the prominent techniques are the electro-thermal machining method where the removal of materials is done by the “incessant sparks generated in a minute space available between the wire electrode and workpiece in the existence of dielectrics” (Sonawane et al. 2019). This generated spark affects the MRR. During the machining, wires made-up of different materials such as “brass, copper, tungsten, molybdenum” or some sort of coated wires are utilized as an electrode. WEDM is the best-suited machining operation for micro and macro machining of hardened and brittle materials and can be employed to develop any complex shaped products that help in finding their enormous industrial application such as aerospace, automotive, space, tool, and die making.

In this regard, many researchers have carried out very significant work, and employing optimization techniques using various heuristic and meta-heuristic algorithms has tremendously helped in achieving the most suitable and desired results. Devarasiddappa and coworkers (Devarasiddappa et al. 2020) have reported surface roughness during the WEDM machining operation of Ti–6Al–4V alloy by employing a modified TLBO algorithm. In this paper, the Taguchi L16 experimental was adopted in order to optimize the four process parameters, viz., pulse-on time ( $T_{on}$ ), pulse-off time ( $T_{off}$ ), current ( $I$ ), and wire speed (WS) at four different levels. The novelty occurs in this work in terms of minimization of surface roughness parameter in WEDM machining by employing the reusable wire technology during machining operation and the modified form of teaching–learning–based algorithm was employed

to optimize the process parameters. A similar kind of work was also carried out by Neeraj and coworkers (Sharma et al. 2019) in optimizing the multi-responses obtained during the WEDM machining process for titanium alloy. They proposed the employment of grey relational theory with consideration of Taguchi L9 orthogonal array-based experiments design. They tried optimizing only two machining parameters, viz, surface roughness (SR) and cutting speed (CS), and predicted for 95% of confidence level. A similar study was also carried out by Devarasiddappa and his coworkers (Devarajaiah and Muthumari 2018) in terms of optimizing the six machining parameters at four different levels. The experimental investigations carried out suggest that the current ( $I$ ) and ( $T_{\text{off}}$ ) are the most significant parameters that influence MRR and power consumption (PC). In this work, the process parameters were optimized using the desirability function analysis (DFA) showing the improvement in composite desirability (CD) by 7.88% at optimum parameters settings. Also, the obtained optimum parameters exhibit the improvement of 9.77 and 6.40% for the current ( $I$ ), and pulse-off-time ( $T_{\text{off}}$ ), respectively. Further, the response surface methodology (RSM) and analysis of variance (ANOVA) were employed and reported by Nitin and coworkers (Gupta et al. 2021) in order to obtain the optimal machining settings for determining the significance and contribution of input parameters to analyze the changes in output characteristics, viz., cutting speed and surface roughness. The study provides a comparative study on WEDM machining of annealed titanium alloy and quenched and hardened titanium alloy which shows that the cutting speed is quite large during the processing of annealed titanium alloy and is found to be 1.75 mm/min. in this way ahead, a predictive model of WEDM machining of titanium alloy was developed by Chandrasekaran and coworkers (Devarasiddappa and Chandrasekaran 2021) using soft computing-based fuzzy logic control. The proposed predictive model was developed using 180 sets of rule-base for optimizing the machining response of MRR providing the four input parameters. The proposed prediction showed better results with higher accuracy than the regression model along with an average percentage error of 5.44%. The study plots suggest that the higher levels of  $T_{\text{on}}$  coupled with lower levels of  $T_{\text{off}}$  results in increased values of MRR. This is attributed to the higher energy sparks produced due to the current supplied for a longer duration of time as well as the faster flushing off the molten material under the supplied dielectric fluid.

Recently, the manufacturing industries have experienced enormous growth and to meet the market demand, increasing productivity along with maintaining the component quality, the ecological and environmental concerns have been compromised which produced a very diverse effect. The environmental impact of sustainable manufacturing methods is concerned with energy efficiency, power consumption reduction, and carbon footprint is a significant issue that is needed to be addressed (Devarajaiah and Muthumari 2018). The tremendous rise in global warming and its negative consequences has driven manufacturers to adopt more sustainable means of manufacturing high-quality, cost-effective products that are also environmentally benign. Manufacturing sustainability is no more a choice but has become the necessity of today's demand. Apart from "quality and productivity, reducing power consumption, which leads to less energy loss and reduced machining costs, has gained importance"

(Tristo et al. 2015). In this regard, the present work has been carried out as a noble attempt of investigating the process parameters of multi-response optimization of Ti-6Al-4 V alloy. In the present work, the four factors such as  $I_p$ ,  $V$ ,  $T_{on}$ , and  $T_{off}$  have been considered to optimize the machining responses such as MRR and SR parameters like “Average surface roughness ( $R_a$ ), root mean square roughness ( $R_q$ ), skewness ( $R_{sk}$ ), kurtosis ( $R_{ku}$ ), and mean line peak spacing ( $R_{sm}$ )” through WEDM machining process and the corresponding process parameters have been optimized using the grey relational optimization process.

## 2.2 Machining Operation

In a machining operation, the material is removed from the workpiece and the final product is obtained with the desired level of accuracy and high-end surface finish. Hence the MRR and surface topography (ST) are important aspects and of great concern. The finished product at Less machining time is another important aspect that directly depends upon the MRR, “expressed in mass per unit time as well as volume per unit time,” of the process and needs to be considered. MRR is important in terms of industrial perspective whereas, surface roughness is important in terms of tribological operation. It influences “the mechanical properties, like fatigue behavior, corrosion resistance, creep life, etc., and also affects the functional attributes of machine components like friction, wear, reflection, heat transmission, lubrication, electrical conductivity, etc.”

### 2.2.1 Surface Parameters

Surface roughness is referred to as the “variations that occurred in the height of the surface relative to a reference plane. It is measured either along a single line profile or along with a set of parallel It is usually characterized by one of the two statistical height descriptors advocated by the American National Standards Institute (ANSI) and the International Standardization Organization (ISO)” (Sahoo 2005; Bhushan 2013) and generally categorized by “three different parameters, viz., amplitude, spacing, and hybrid parameters” as discussed below.

- (a) *Amplitude parameters: it is a measure of vertical characteristics of the occurred surface deviations. For example, “center line average roughness ( $R_a$ ), root mean square roughness ( $R_q$ ), skewness ( $R_{sk}$ ), kurtosis ( $R_{ku}$ ), peak-to-valley height, etc.”*
- (b) *Spacing parameters: it is the measurement of horizontal characteristics of surface deviations. For example, “mean line peak spacing, high spot count, peak count, etc.”*

- (c) *Hybrid parameters: it is the combination of both vertical and horizontal characteristics of surface deviations. For example, “root mean square slope of profile, root mean square wavelength, core roughness depth, reduced peak height, valley depth, peak area, valley area, etc.”*

Hence, the consideration of only one surface roughness parameter such as  $R_a$  is not sufficient to completely describe the surface quality.

## 2.3 Response Parameters

### 2.3.1 Material Removal Rate (MRR)

In the current study, the MRR has been selected as a response parameter that refers to the amount of materials that get removed in the unit interval of time and is generally defined as

$$\text{MRR} = \frac{W_i - W_f}{t_m} \quad (2.1)$$

where  $W_i$  and  $W_f$  are the initial (i.e., before machining) and final (i.e., after machining) weight of the workpiece samples and  $t_m$  is considered as the machining time, taken generally in seconds (s) or in minutes (min). For the sample weight calculation, the electronic weighing machine is utilized with accuracy of 0.01 mg.

### 2.3.2 Surface Roughness Parameters

There occur various surface roughness parameters which are utilized for specific reasons. In the current work, only five surface roughness parameters have been considered which have been discussed below.

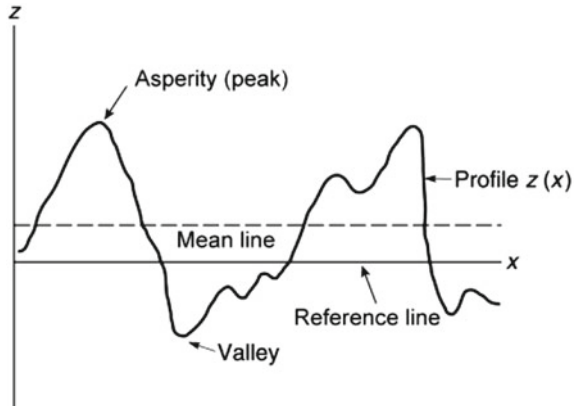
#### 2.3.2.1 Center Line Average or Average Surface Roughness ( $R_a$ )

It is the measure of the “mean of occurred deviations of the sample profile surface from the center-line along the profile length” and is calculated as

$$R_a = \frac{1}{L} \int_0^L |Z(x)| dx \quad (2.2)$$



**Fig. 2.3** Schematic surface profile showing the center-line average surface roughness (Bhushan 2013)



where  $L$  denotes the profile length and  $h(x)$  denotes the height of the deviated surface above the mean line measure from the origin along the  $x$  direction, and the  $R_a$  is generally expressed in  $\mu\text{m}$  as shown in Fig. 2.3.

### 2.3.2.2 Root Mean Square Roughness ( $R_q$ )

It is the measure of dispersion parameters for characterizing the surface roughness that is obtained by squaring the highest values of the available data and taking the square root of the mean. It is expressed in  $\mu\text{m}$ , and is given as

$$R_q = \sqrt{\frac{1}{L} \int_0^L [Z(x)]^2 dx} \quad (2.3)$$

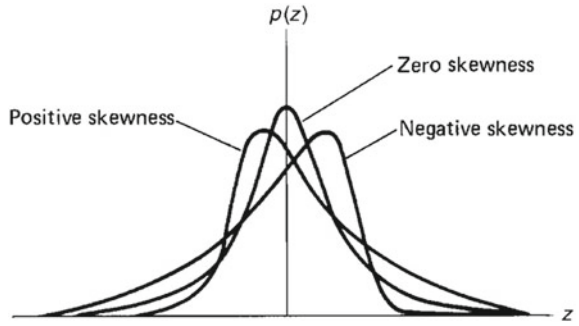
### 2.3.2.3 Skewness ( $R_{sk}$ )

It is the measure of “asymmetry of surface deviation about the mean plane”. The distribution curve from its symmetry as in Gaussian distribution and is given as

$$R_{sk} = \frac{1}{R_q^3} \int_0^L [Z(x)]^3 dx \quad (2.4)$$

It’s a “non-dimensional number, and for symmetrical distribution like Gaussian distribution curve,  $R_{sk} = 0$ . A surface having positive skewness has a wider range of peak heights that are higher than the mean (peak type profile)” as shown in Fig. 2.4.

**Fig. 2.4** Schematic showing the skewness of roughness profile (Bhushan 2013)



A surface having negative skewness possess more peaks with heights close to the “mean as compared to a gaussian distribution (valley type profile).”

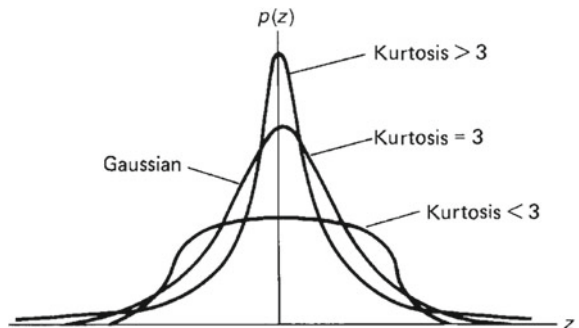
**2.3.2.4 Kurtosis ( $R_{ku}$ )**

It is the measure of the “sharpness of surface height distribution curve” and is expressed as

$$Rku = \frac{1}{R_q^4 L} \int_0^L [Z(x)]^4 dx \tag{2.5}$$

It characterizes “the spread of height distribution” and also possesses the non-dimensionality. The Gaussian distribution surface possesses the kurtosis value,  $R_{ku} = 3$ , and if  $R_{ku} > 3$  means that the surface is distributed centrally and has relatively sharper peaks than Gaussian and vice versa as shown in Fig. 2.5.

**Fig. 2.5** Schematic showing the kurtosis of roughness profile (Bhushan 2013)



### 2.3.2.5 Mean Line Peak Spacing ( $R_{sm}$ )

This is the measure of “mean spacing between the peaks, with a peak defined relative to the mean line “and is expressed as

$$R_{sm} = \frac{1}{L} \quad (2.6)$$

where  $n$  denotes the “number of peaks spacing” and  $S$  denotes the “spacing between the consecutive peaks.” This quantity is expressed in millimeters (mm).

Therefore, the surface roughness is a comparable factor, hence the absolute values of surface roughness needs to be considered.

## 2.4 GRA Optimization

Genichi Taguchi was the first to propose the Taguchi technique (Ghosh et al. 2012; Taguchi et al. 2005). This is a powerful technique utilized for designing high-quality systems at a relatively lower cost. It works on “orthogonal array” (OA) trials, which yield substantially lower variance for experiments with optimal parameters control. The Taguchi approach is appropriate for single-objective (SO) problems. However, the multi-objective (MO) optimization is not similar to single-objective problems and demands some better approach that can be employed to solve either the MO problems directly or one such approach that can convert the MO problems into SO problems and then the optimization can be done.

One factor that may require the higher-the-better (HB) features can affect the system performance and at the same time another component may also require the lower-the-better (LB) criterion for their effects and performance. Hence, the properties of multi-response optimization are complex. Keeping the things in context, the grey relational analysis (GRA) has been employed in the current study for multi-response optimization. Deng firstly proposes the “grey system theory” in the year of 1989. In a grey system, some part of the information is known and some information is hidden. Due to the associated uncertainties, grey system provides various available solution (Rao 2011). Based on this theoretical perspective, the GRA technique has been adapted effectively in solving many complicated problems (Jozić et al. 2015). The GRA algorithm is depicted in Fig. 2.6.

### 2.4.1 GRA Generation

The initial stage in GRA is initiated by normalizing the experimental results or numerical data in the range of 0–1. This is sometimes referred to as “grey relational generation.” In this stage, the data-pre-processing is done “in order to transfer original

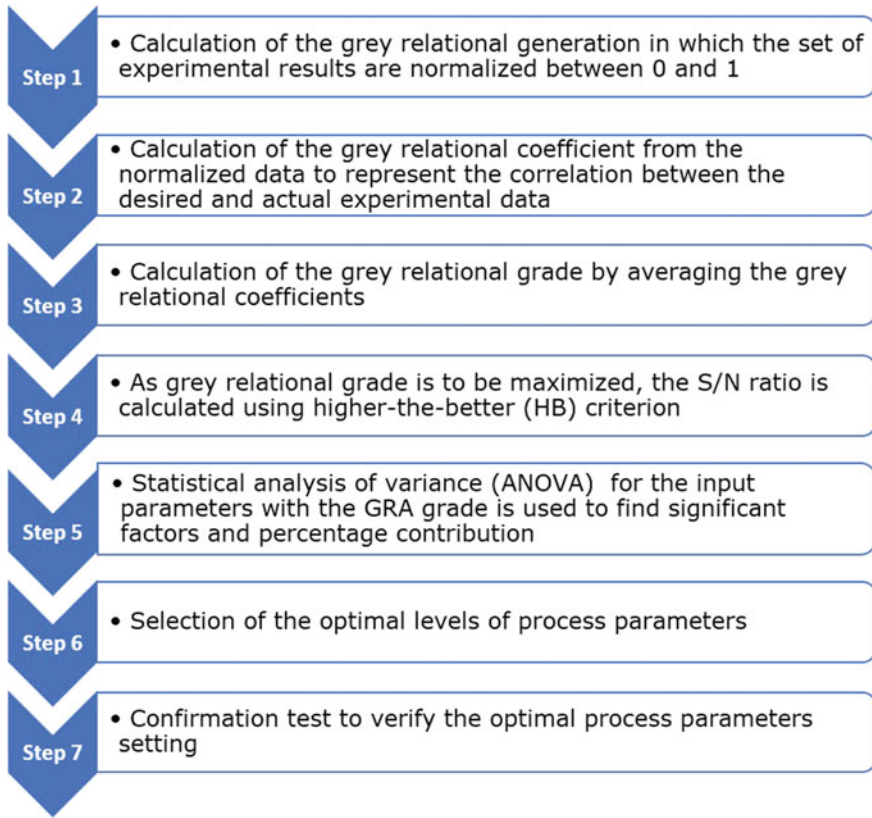


Fig. 2.6 Steps to employ the grey relational analysis optimization technique

sequence to a comparable sequence. However, depending on characteristics of data sequence, various methodologies of data pre-processing are available.” In this study, the normalization of various original data sequence for all the five surface roughness parameters have been done using lower-the-better performance characteristics and this performance characteristics of lower-the-better is given as

$$a_{ij} = \frac{\max(b_{ij}) - (b_{ij})}{\max(b_{ij}) - \min(b_{ij})} \tag{2.7}$$

where  $b_{ij}$  are the original individual data.

Further, the normalized data sequence for MRR is done using larger-the-better performance characteristics and is given as

$$a_{ij} = \frac{(b_{ij}) - \min(b_{ij})}{\max(b_{ij}) - \min(b_{ij})} \tag{2.8}$$

The normalized data sequence for MRR and other five SR parameters using the WEDM process of Ti–6Al–4 V alloy is provided in the below sections of this work.

### 2.4.2 Grey Relational Coefficient

For the  $j$ th response of  $i$ th experiment, if the value  $a_{ij}$  obtained from the “data pre-processing procedure is equal to or close to 1,” then the performance of  $i$ th experiment is regarded as best for the  $j$ th response. The reference sequence  $A_0$  is defined as  $(a_{01}, a_{02}, a_{0j}, \dots, a_{0n}) = (1, 1, \dots, 1, \dots, 1)$ , and it seeks to find the experiment “whose comparability sequence is the closest to the reference sequence”. In other, words, the GR coefficient determines how close the  $a_{ij}$  is to  $a_{0j}$ . The larger the GR coefficient, the closer it is. The GR coefficient is calculated as follows (Bhushan 2013):

$$\psi(a_{0j}, a_{ij}) = \frac{(\Delta_{\min} + \xi \Delta_{\max})}{(\Delta_{0j} + \xi \Delta_{\max})} \forall i = 1, 2, 3, \dots, m, \text{ and } j = 1, 2, 3, \dots, n \tag{2.9}$$

where  $\psi(a_{0j}, a_{ij})$  is referred to as the grey relational coefficient between  $a_{ij}$  and  $a_{0j}$ .

$$\Gamma(A_0, A_i) = \frac{1}{n} \sum_{j=1}^n w_j \psi(a_{0j}, a_{ij}) \forall i = 1, 2, 3, \dots, m \tag{2.10}$$

$\xi$  is ranging from 0 to 1, i.e., (0, 1] and is termed as distinguishing coefficient (DC). In present work,  $\xi$  is assumed to have a value of 0.5. This DC exhibits the index for distinguishability. This index of distinguishability is higher for smaller value of  $\xi$ .

### 2.4.3 Grey Relational Grade (GRG)

The grade values obtained in GRA depict the “relationship among the series.” It shows “measurement of quantification” in GR space. GRG is just the average of GR coefficients obtained in preceding phase that evaluates the overall response characteristics (Jozić et al. 2015; Das et al. 2015) and is given as

$$\Gamma(A_0, A_i) = \frac{1}{n} \sum_{j=1}^n w_j \psi(a_{0j}, a_{ij}) \forall i = 1, 2, 3, \dots, m \tag{2.10}$$

where  $\sum_{j=1}^n w_j = 1$ ,  $n$  denotes the number of process responses.  $\Gamma(A_0, A_i)$  represents the GRG between the comparability sequence  $A_i$  and reference sequence  $A_0$  “The grey relational grade indicates the degree of similarity between the comparability sequence

and the reference sequence. If an experiment gets the highest grey relational grade with the reference sequence, it means that comparability sequence is most similar to the reference sequence and that experiment would be the best choice” (Taylor and Ziegel 2012).

## 2.5 Ordering in GRA

The numerical values of GRG between items are not absolutely important GRA technique, but the ordering among the GRG values possesses more significant information. “The combination having the highest GRG value is given the highest order, whereas the combination having the lowest GRG value is given the lowest order.”

## 2.6 Experimentation

### 2.6.1 Experimentation Setup

The delineated Fig. 2.7 exhibits the complete experimental set-up. For carrying out the investigation procedure, the 5-axis CNC type WEDM machine (ELEKTRA, MAXICUT 434) has been utilized. A dielectric medium separates the workpiece from the electrode (i.e., deionized water). The regulated movement of “the wire through the workpiece causes spark discharges, which then erode the workpiece to produce the desired shape. Because evaporation of zinc promotes cooling at the interface of the workpiece and wire, a coating of zinc oxide on the wire helps to avoid the short-circuits and the high MRR in WEDM without wire breakage can be achieved by using zinc-coated copper wire (0.25 mm diameter).”

### 2.6.2 Selection of Process Parameters

However, there are numerous elements that might be investigated during the WEDM machining. But the literature suggests that the four machining parameters such as  $I_p$ ,  $V$ ,  $T_{on}$ , and  $T_{off}$  play a vital role in regulating the WEDM machining process. In the current study, the aforementioned design parameters have been chosen as design variables, whereas other parameters are considered to be “constant over the experimental domain.” Table 2.1 lists the variations in control machining variables with three different levels.



**Fig. 2.7** Experimental set-up

**Table 2.1** Variations on process control parameters

Process parameters	Units	Symbols	Level 1	Level 2	Level 3
			Code		
			1	2	3
Discharge current ( $I_p$ )	A	A	6	8	10
Voltage ( $V$ )	V	B	50	55	60
Pulse-on time ( $T_{on}$ )	$\mu s$	C	3	4	5
Pulse-off time ( $T_{off}$ )	$\mu s$	D	3	4	5

## 2.7 Design of Experiments

Design of experiments (DOE) is a technique that provides an organized way of getting the maximum possible conclusive information by conducting the minimum number of experimental runs, or from the minimum amount of energy, money, or other limited resources. Taguchi's design techniques (Taylor and Ziegel 2012) proposed an orthogonal array (OA) concept to employ to reduce the number of conducting experiments for determining the optimal machining parameters. To determine the main effects as well as the interaction effects of the considered factors simultaneously, an OA

requires the fewest number of experimental trials possible. The “total degrees of freedom (DOF) necessary to explore the main effects and interaction effects determines which OA design is best suited to conduct experiments.” The total number of degrees of freedom (DOFs) required is 20 ( $8 + 12$ ). In the present work,  $L_{27}$  OA was chosen because according to the Taguchi approach, “the total DOFs of the chosen OA must be greater than or equal to the total DOFs necessary for the experiments.” In the present work, the variations on process control parameters have been carried out and provided in Table 2.1. In Table 2.1,  $I_p$ ,  $V$ ,  $T_{on}$ , and  $T_{off}$  were selected as variables that are necessary to be optimized in three different levels. The corresponding varying parameters for the aforementioned process or machining control parameters have been tabulated with three different levels.

## 2.8 Response Factors and Their Measurements

In this study, the MRR and various SR factors have been considered as the response characteristics. MRR is defined as the ratio of the difference in weights before and after performing the machining operation of the workpiece to the total machining time taken as given in Eq. 2.1. In the current study, it is the measure of material’s weight loss and is given in gm/min. Further, for the current study, five different roughness parameters viz.  $R_a$ ,  $R_q$ ,  $R_{sk}$ ,  $R_{ku}$ , and  $R_{sm}$  have been selected. “Roughness measurement is done using a stylus-type profilometer, Talysurf (Taylor Hobson, Surtronic 3+). Roughness measurements in the transverse direction on the workpieces are repeated five times the average of five measurements of surface roughness parameter values are recorded”. The experimental data for the aforementioned response factors have been provided in tabulated form in Table 2.2.

## 2.9 Results and Discussions

### 2.9.1 Multi-objective Performance Characteristics

In determining the performance characteristics, the present study addresses various responses, namely MRR and SR characteristics in the WEDM process of titanium alloy Ti-6Al-4 V. Surface roughness is measured using “five surface roughness parameters:  $R_a$ ,  $R_q$ ,  $R_{sk}$ ,  $R_{ku}$ , and  $R_{sm}$ .” For determining the optimized machining or process parameters, the grey relational analysis (Julong 1989) and the Taguchi method maximize all six response parameters at the same time.



**Table 2.2** Experimental data based on the design of experiments

Runs	A	B	C	D	MRR	$R_a$ ( $\mu\text{m}$ )	$R_q$	$R_{sk}$	$R_{ku}$	$R_{sm}$
1	1	1	1	3	0.07763	2.9310	3.5915	0.0525	1.7700	0.0575
2	1	1	2	2	0.11992	2.7500	3.4250	0.2630	2.0565	0.0590
3	1	1	3	3	0.08295	2.5275	3.2115	0.0735	1.3405	0.0560
4	1	1	1	2	0.05877	2.8540	3.5490	0.1505	2.0115	0.0725
5	1	2	2	3	0.10997	2.6565	3.2775	0.1995	2.0025	0.0545
6	1	2	3	3	0.11814	2.4915	3.0965	0.0715	1.8200	0.0815
7	1	3	1	3	0.10120	2.6080	3.1910	0.1295	1.5715	0.0535
8	1	3	2	3	0.09141	3.0750	3.7940	0.0435	1.4265	0.0570
9	1	3	3	2	0.09745	2.6675	3.2790	0.0870	1.4500	0.0490
10	2	1	1	2	0.09587	1.2490	1.5975	0.1270	2.0575	0.0595
11	2	1	2	3	0.07830	2.3115	2.8400	0.0440	1.8690	0.0540
12	2	1	3	2	0.06575	2.7675	3.4300	0.1485	1.6250	0.0655
13	2	2	1	3	0.05356	2.8265	3.4415	0.0235	1.3215	0.0540
14	<b>2</b>	<b>2</b>	<b>2</b>	<b>1</b>	<b>1.01993</b>	<b>3.1765</b>	<b>3.9290</b>	<b>0.0430</b>	<b>1.5775</b>	<b>0.0625</b>
15	2	2	3	2	0.09435	1.6630	2.0665	0.0430	1.7890	0.0700
16	2	3	2	3	0.09216	2.4485	3.0085	0.0735	1.5250	0.0590
17	2	3	2	2	0.08007	1.5615	1.9400	0.0585	2.0240	0.0580
18	2	3	3	3	0.10554	2.7675	3.4215	0.1180	1.6075	0.0600
19	3	3	1	3	0.09546	2.8500	3.5065	0.0565	1.3865	0.0550
20	3	1	2	3	0.11854	2.7315	3.4000	0.0660	1.6950	0.0640
21	3	1	3	2	0.11634	2.6675	3.2965	0.0065	1.4500	0.0530
22	3	2	1	3	0.10765	3.3515	4.1805	0.0385	1.4925	0.0590
23	3	2	2	2	0.11579	3.2490	4.0000	0.0655	1.4085	0.0560
24	3	3	3	3	0.11042	2.7125	3.3490	0.0220	1.5515	0.0610
25	3	3	1	2	0.12930	2.8215	3.4550	0.0400	1.4575	0.0580
26	3	3	2	3	0.10510	3.0650	3.3265	0.0615	1.3565	0.0550
27	3	3	3	3	0.12369	10.8480	3.1715	0.0840	2.2955	0.0590

## 2.9.2 Grey Relational Approach

The experimental data obtained during the WEDM machining operation for “MRR” and “SR” parameters have been provided in Table 2.2. Since we require the maximum for the first and minimum for the second characteristics, so in this regard, the HB criterion is employed to get the maximized result of the first characteristics and at the same time, LB criterion has been employed to obtain the minimized values of the second characteristics. Here, for all five SR parameters, the LB criterion has been implemented. Using these HB and LB criteria of the aforementioned response characteristics, the normalization of data has been carried out according to the GRA

procedure. The normalized data sequence for the aforementioned response characteristics has been provided in tabulated form in Table 2.3. Further, using Eq. (2.10), the difference of the absolute value ( $\Delta o_j$ ) was determined and has been listed in Table 2.4. In the next step, the grey relational coefficient (GRC) has been determined using Eq. (2.9), and the results have been tabulated and shown in Table 2.5. Further, after averaging the GR coefficients, the grey relational grade (GRG) has been calculated using Eq. 2.10. “Here, it may be noted that the higher relational grade indicates that the corresponding parameter combination is closer to the optimal. The final values for the grey relational grade and their order are given in Table 2.6.”

**Table 2.3** Normalized data sequence for MRR and five surface roughness parameters

Normalization of data					
MRR	$R_a$	$R_q$	$R_{sk}$	$R_{ku}$	$R_{sm}$
0.02491	0.8248	0.2280	0.8207	0.5395	0.7385
0.06866	0.8436	0.2925	0.0000	0.2454	0.6923
0.03040	0.8668	0.3751	0.7388	0.9805	0.7846
0.00539	0.8328	0.2445	0.4386	0.2916	0.2769
0.05836	0.8534	0.3496	0.2476	0.3008	0.8308
0.06682	0.8706	0.4197	0.7466	0.4882	0.0000
0.04929	0.8584	0.3831	0.5205	0.7433	0.8615
0.03916	0.8098	0.1496	0.8558	0.8922	0.7538
0.04541	0.8522	0.3490	0.6862	0.8681	1.0000
0.04377	1.0000	1.0000	0.5302	0.2444	0.6769
0.02559	0.8893	0.5190	0.8538	0.4379	0.8462
0.01261	0.8418	0.2906	0.4464	0.6884	0.4923
0.00000	0.8357	0.2861	0.9337	1.0000	0.8462
1.00000	0.7992	0.0974	0.8577	0.7372	0.5846
0.04220	0.9569	0.8184	0.8577	0.5200	0.3538
0.03994	0.8750	0.4537	0.7388	0.7911	0.6923
0.02743	0.9674	0.8674	0.7973	0.2787	0.7231
0.05378	0.8418	0.2938	0.5653	0.7064	0.6615
0.04335	0.8332	0.2609	0.8051	0.9333	0.8154
0.06723	0.8456	0.3022	0.7680	0.6165	0.5385
0.06496	0.8522	0.3422	1.0000	0.8681	0.8769
0.05596	0.7810	0.0000	0.8752	0.8244	0.6923
0.06439	0.7916	0.0699	0.7700	0.9107	0.7846
0.05883	0.8475	0.3219	0.9396	0.7639	0.6308
0.07837	0.8362	0.2809	0.8694	0.8604	0.7231
0.05333	0.8108	0.3306	0.7856	0.9641	0.8154
0.07257	0.0000	0.3906	0.6979	0.0000	0.6923

**Table 2.4** Values of  $\Delta oj$  for calculating the GR coefficients

Values of $\Delta oj$					
MRR	$R_a$	$R_q$	$R_{sk}$	$R_{ku}$	$R_{sm}$
0.97509	0.1752	0.7720	0.1793	0.4605	0.2615
0.93134	0.1564	0.7075	1.0000	0.7546	0.3077
0.96960	0.1332	0.6249	0.2612	0.0195	0.2154
0.99461	0.1672	0.7555	0.5614	0.7084	0.7231
0.94164	0.1466	0.6504	0.7524	0.6992	0.1692
0.93318	0.1294	0.5803	0.2534	0.5118	1.0000
0.95071	0.1416	0.6169	0.4795	0.2567	0.1385
0.96084	0.1902	0.8504	0.1442	0.1078	0.2462
0.95459	0.1478	0.6510	0.3138	0.1319	0.0000
0.95623	0.0000	0.0000	0.4698	0.7556	0.3231
0.97441	0.1107	0.4810	0.1462	0.5621	0.1538
0.98739	0.1582	0.7094	0.5536	0.3116	0.5077
1.00000	0.1643	0.7139	0.0663	0.0000	0.1538
0.00000	0.2008	0.9026	0.1423	0.2628	0.4154
0.95780	0.0431	0.1816	0.1423	0.4800	0.6462
0.96006	0.1250	0.5463	0.2612	0.2089	0.3077
0.97257	0.0326	0.1326	0.2027	0.7213	0.2769
0.94622	0.1582	0.7062	0.4347	0.2936	0.3385
0.95665	0.1668	0.7391	0.1949	0.0667	0.1846
0.93277	0.1544	0.6978	0.2320	0.3835	0.4615
0.93504	0.1478	0.6578	0.0000	0.1319	0.1231
0.94404	0.2190	1.0000	0.1248	0.1756	0.3077
0.93561	0.2084	0.9301	0.2300	0.0893	0.2154
0.94117	0.1525	0.6781	0.0604	0.2361	0.3692
0.92163	0.1638	0.7191	0.1306	0.1396	0.2769
0.94667	0.1892	0.6694	0.2144	0.0359	0.1846
0.92743	1.0000	0.6094	0.3021	1.0000	0.3077

### 2.9.3 Signal-to-Noise (S/N) Ratio Analysis

Taguchi in the year 1990 proposed a Taguchi method for optimizing the single-objective optimization problems. There he proposed the S/N ratio formula that is utilized to convert the available dataset into the dataset of evolutionary characteristics. In this work, the S/N ratio analysis has been carried out with the GRG performance index. To carry out the maximization of grey relational grade, the S/N ratio has been calculated for the higher-the-better criterion using the following S/N ratio relation as

**Table 2.5** Grey relational coefficient

Grey relational coefficient					
MRR	$R_a$	$R_q$	$R_{sk}$	$R_{ku}$	$R_{sm}$
0.33896	0.7405	0.3931	0.7360	0.5206	0.6566
0.34932	0.7618	0.4141	0.3333	0.3985	0.6190
0.34023	0.7897	0.4445	0.6569	0.9625	0.6989
0.33453	0.7494	0.3982	0.4711	0.4138	0.4088
0.34683	0.7732	0.4346	0.3992	0.4170	0.7471
0.34887	0.7944	0.4628	0.6636	0.4942	0.3333
0.34466	0.7793	0.4477	0.5104	0.6608	0.7831
0.34227	0.7244	0.3703	0.7761	0.8226	0.6701
0.34374	0.7719	0.4344	0.6144	0.7912	1.0000
0.34335	1.0000	1.0000	0.5156	0.3982	0.6075
0.33912	0.8187	0.5097	0.7738	0.4708	0.7647
0.33616	0.7597	0.4134	0.4746	0.6161	0.4962
0.33333	0.7526	0.4119	0.8830	1.0000	0.7647
1.00000	0.7135	0.3565	0.7785	0.6555	0.5462
0.34298	0.9206	0.7336	0.7785	0.5102	0.4362
0.34245	0.8001	0.4779	0.6569	0.7053	0.6190
0.33954	0.9389	0.7904	0.7115	0.4094	0.6436
0.34573	0.7597	0.4145	0.5349	0.6300	0.5963
0.34325	0.7499	0.4035	0.7195	0.8822	0.7303
0.34898	0.7640	0.4174	0.6831	0.5660	0.5200
0.34842	0.7719	0.4319	1.0000	0.7912	0.8025
0.34625	0.6954	0.3333	0.8003	0.7401	0.6190
0.34828	0.7059	0.3496	0.6849	0.8484	0.6989
0.34694	0.7663	0.4244	0.8922	0.6792	0.5752
0.35171	0.7532	0.4101	0.7929	0.7817	0.6436
0.34562	0.7255	0.4276	0.6999	0.9330	0.7303
0.35028	0.3333	0.4507	0.6233	0.3333	0.6190

$$S/N \text{ ratio} = -10 \log \left( \frac{1}{n} \sum_{i=1}^n \frac{1}{y_i^2} \right) \tag{2.11}$$

where  $y$  is referred to as the GRG for the current maximization of grade and  $n$  indicates the number of trials or runs.

Further, the response table provided in Table 2.7 “compares the relative magnitude of the effects, including ranks based on the delta statistics.” The delta calculation is carried out by measuring the difference between the “highest average value and lowest average value” for each of the factors. Next, the ranks based on these delta values are

**Table 2.6** Grey relational grade (GRG) and rank

Grey relational grade and rank		
Runs	Grey relational grade	Rank
1	0.4742	19
2	0.4273	25
3	0.5254	5
4	0.4114	26
5	0.4505	22
6	0.4493	23
7	0.4905	18
8	0.5075	12
9	0.5331	4
10	0.5238	7
11	0.5033	14
12	0.4441	24
13	0.5479	3
<b>14</b>	<b>0.8050</b>	<b>1</b>
15	0.5094	11
16	0.4971	16
17	0.5191	9
18	0.4664	21
19	0.5202	8
20	0.4695	20
21	0.5540	2
22	0.4919	17
23	0.5029	15
24	0.5072	13
25	0.5140	10
26	0.5244	6
27	0.4111	27

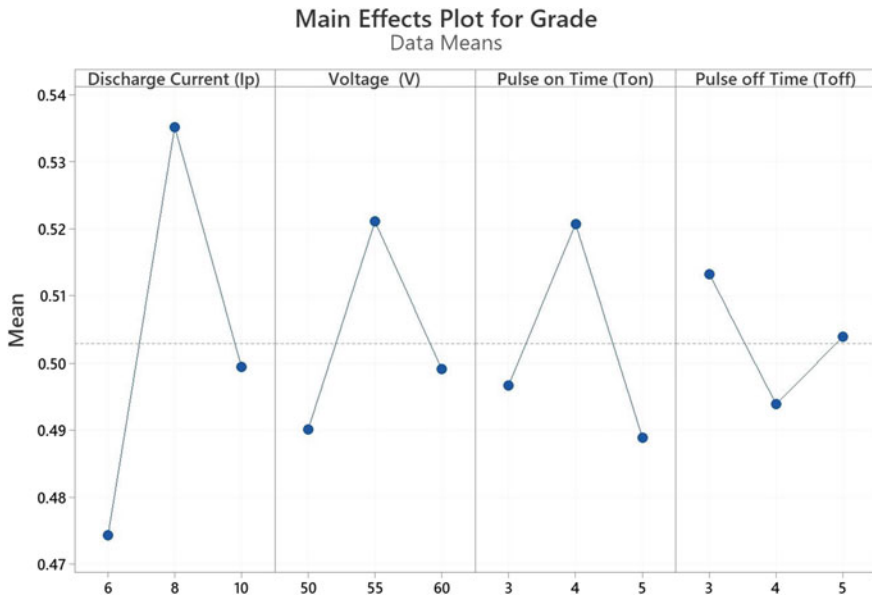
assigned. From the response table, it is evident that factor A, i.e., the discharge current ( $I_p$ ) got ranked 1 which means factor A plays a very significant role in controlling the response factors such as MRR and surface roughness characteristics during the WEDM machining process. For the GRG, the main effects plot, as well as interaction plots, has been drawn and delineated in Figs. 2.4 and 2.5.

If the line for a given parameter in the main effects plot is near horizontal, the parameter has no meaningful effect. A parameter for which the line has the greatest inclination, on the other hand, will have the most impact. From the given plot in Fig. 2.4, it is clear that parameter A, i.e., the discharge current ( $I_p$ ) is the most dominating factor, followed by factor D i.e., (pulse-on time). Further, estimating

**Table 2.7** Response table for grey relational analysis

Response table for GRA				
Level	A	B	C	D
1	0.474339	0.490191	0.496728	0.513206
2	0.535131	0.521044	0.520685	0.493908
3	0.499476	0.499149	0.488871	0.503976
Delta	0.060792	0.030853	0.031814	0.019298
Rank	1	3	2	4
Mean of the GRG = 0.5030				

an interaction plot helps in determining the existence of non-parallelism of parameter effects. “Thus, if the lines on the interaction plots are non-parallel, interaction occurs and if the lines cross, strong interactions occur between parameters.” From Fig. 2.5, it can be seen that there exists a strong interaction between the factors  $I_p$  and  $V$ , between  $V$  and  $T_{on}$ , and between  $T_{on}$  and  $T_{off}$  that shows an appreciable agreement with the previous works done in the literatures. On performing the GRA, we finally obtain the optimal machining or process parameters from the main effects plot as **A2B2C2D1**, i.e., the experimental combination number 14 possess the desired “optimal machining parameters obtained for maximum MRR and minimum surface roughness” performance characteristics (Figs. 2.8 and 2.9).



**Fig. 2.8** Main effects plot of weighted for GRA factors

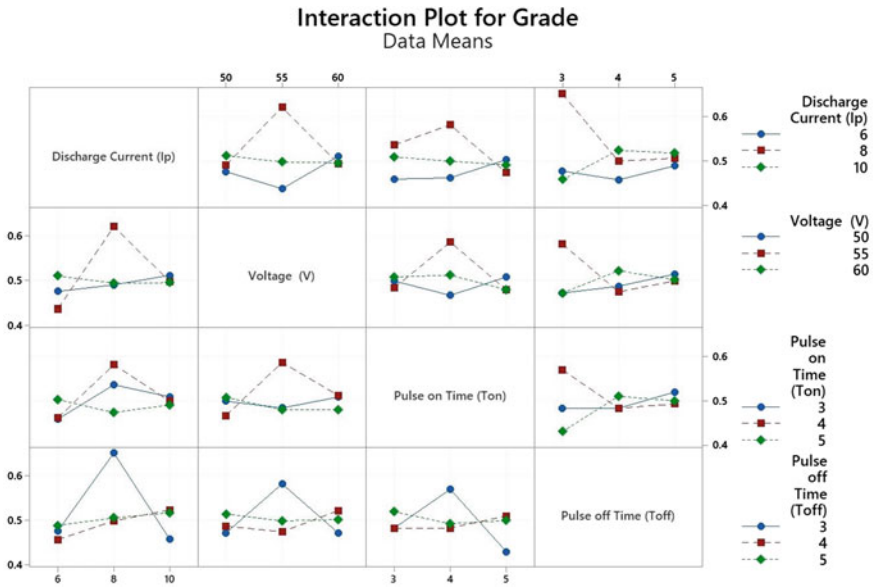


Fig. 2.9 Interaction plot of weighted grade among the GRA factors

## 2.10 Conclusion

In the current work, the study of various machining parameters optimization has been carried out for the titanium alloy (Ti–6Al–4 V) under WEDM machining operation. The GRA has been implemented to get the desired optimized values for the MRR and other SR performance characteristics. The DOE has been designed for four factors with three levels.  $I_p$ ,  $V$ ,  $T_{on}$ , and  $T_{off}$  have been taken into account for the four factors. The main effect plot results in the best optimal combination of process parameters. Current is the most dominating factor during the optimization results. The investigation suggests the most optimal process parameters for MRR and other SR performance characteristics are **A2B2C2D1**, i.e., level 2 of A, B, and C (i.e.,  $I_p$ ,  $V$ , and  $T_{on}$ ) and level 1 of D (i.e.,  $T_{off}$ ) being the optimal criterion of the aforementioned machining parameters.

## References

Barry J, Byrne G, Lennon D (2001) Observations on chip formation and acoustic emission in machining Ti-6Al-4V alloy. *Int J Mach Tools Manuf* 41(7):1055–1070. [https://doi.org/10.1016/S0890-6955\(00\)00096-1](https://doi.org/10.1016/S0890-6955(00)00096-1)

Bhushan B (2013) *An introduction to tribology*, vol 17, no 1, 2nd edn. John Wiley & Sons, Ltd

- Bodunrin MO et al (2020) Corrosion behavior of titanium alloys in acidic and saline media: role of alloy design, passivation integrity, and electrolyte modification. *Corros Rev* 38(1):25–47. <https://doi.org/10.1515/corrrev-2019-0029>
- Das MK, Kumar K, Barman TK, Sahoo P (2015) Optimization of WEDM process parameters for MRR and surface roughness using Taguchi-based grey relational analysis, vol 2, pp 1–25. <https://doi.org/10.4018/ijmfmp.2015010101>
- Devarajaiah D, Muthumari C (2018) Evaluation of power consumption and MRR in WEDM of Ti–6Al–4V alloy and its simultaneous optimization for sustainable production. *J Braz Soc Mech Sci Eng* 40(8):400. <https://doi.org/10.1007/s40430-018-1318-y>
- Devarasiddappa D, Chandrasekaran M (2021) Fuzzy logic modelling of sustainable performance measure (MRR) during WEDM of Ti/6Al/4V alloy. *Mater Today Proc* 46:3373–3378. <https://doi.org/10.1016/j.matpr.2020.11.487>
- Devarasiddappa D, Chandrasekaran M, Arunachalam R (2020) Experimental investigation and parametric optimization for minimizing surface roughness during WEDM of Ti6Al4V alloy using modified TLBO algorithm. *J Braz Soc Mech Sci Eng* 42(3):1–18. <https://doi.org/10.1007/s40430-020-2224-7>
- Donachie MJ (2000) Titanium: a technical guide. ASM International, Materials Park, Ohio
- Dong H (2010) Tribological properties of titanium-based alloys. In *Surface engineering of light alloys*. Elsevier, pp 58–80
- Dong H, Bell T (2000) Enhanced wear resistance of titanium surfaces by a new thermal oxidation treatment. *Wear* 238(2):131–137. [https://doi.org/10.1016/S0043-1648\(99\)00359-2](https://doi.org/10.1016/S0043-1648(99)00359-2)
- Esteban PG, Ruiz-Navas EM, Bolzoni L, Gordo E (2008) Low-cost titanium alloys? Iron may hold the answers. *Met Powder Rep* 63(4):24–27. [https://doi.org/10.1016/S0026-0657\(09\)70040-2](https://doi.org/10.1016/S0026-0657(09)70040-2)
- Ezugwu EO, Wang ZM (1997) Titanium alloys and their machinability—a review. *J Mater Process Technol* 68(3):262–274. [https://doi.org/10.1016/S0924-0136\(96\)00030-1](https://doi.org/10.1016/S0924-0136(96)00030-1)
- Frączek T, Olejnik M, Tokarz A (2009) Evaluation of plasma nitriding efficiency of titanium alloys for medical applications. *Metalurgija* 48(2):83–86
- Froes FH, Friedrich H, Kiese J, Bergoint D (2004) Titanium in the family automobile: the cost challenge. In: *Cost - Affordable Titanium, Symposium Dedication to Professor Harvey Flower, February 2004*, pp 159–166. <https://doi.org/10.1007/s11837-004-0144-0>
- Ghosh S, Sahoo P, Sutrardhar G (2012) Wear behaviour of Al-SiCp metal matrix composites and optimization using taguchi method and grey relational analysis. *J Miner Mater Charact Eng* 11(11):1085–1094. <https://doi.org/10.4236/jmmce.2012.1111115>
- Gnanavelbabu A, Saravanan P, Rajkumar K, Karthikeyan S, Baskaran R (2018) Optimization of WEDM process parameters on multiple responses in cutting of Ti-6Al-4V. *Mater Today Proc* 5(13):27072–27080. <https://doi.org/10.1016/j.matpr.2018.09.012>
- Gupta NK et al (2021) Revealing the WEDM process parameters for the machining of pure and heat-treated titanium (Ti-6Al-4V) alloy. *Materials (basel)* 14(9):2292. <https://doi.org/10.3390/ma14092292>
- Hareesh K, Nalina Pramod KV, Linu Husain NK, Binoy KB, Dipin Kumar R, Sreejith NK (2021) Influence of process parameters of wire EDM on surface finish of Ti6Al4V. *Mater. Today Proc.* 47:5017–5023. <https://doi.org/10.1016/j.matpr.2021.04.590>
- Jozić S, Bajić D, Celent L (2015) Application of compressed cold air cooling: achieving multiple performance characteristics in end milling process. *J Clean Prod* 100:325–332. <https://doi.org/10.1016/j.jclepro.2015.03.095>
- Julong D (1989) Introduction to grey systems theory. *J Grey Syst* 1(1):1–24. <https://doi.org/10.5555/90757.90758>
- Kaur S, Ghadirinejad K, Oskouei RH (2019) An overview on the tribological performance of titanium alloys with surface modifications for biomedical applications. *Lubricants* 7(8). <https://doi.org/10.3390/lubricants7080065>
- Kustas FM, Misra MS (2017) Friction and wear of titanium alloys. In: *Friction, lubrication, and wear technology*. ASM International, pp 502–508
- Leyens C, Peters M (2003) Titanium and titanium alloys: fundamental and applications. Wiley



- Myers JR, Bomberger HB, Froes FH (1984) Corrosion Behavior and Use of Titanium and Its Alloys. *JOM* 36(10):50–60. <https://doi.org/10.1007/BF03338589>
- Niinomi M (1998) Mechanical properties of biomedical titanium alloys. *Mater Sci Eng A* 243(1–2):231–236. [https://doi.org/10.1016/S0921-5093\(97\)00806-X](https://doi.org/10.1016/S0921-5093(97)00806-X)
- Niinomi M (2019) Titanium alloys. *Encycl Biomed Eng* 1–3:213–224. <https://doi.org/10.1016/B978-0-12-801238-3.99864-7>
- Rack HJ, Qazi JI (2006) Titanium alloys for biomedical applications. *Mater Sci Eng C* 26(8):1269–1277. <https://doi.org/10.1016/j.msec.2005.08.032>
- Rao RV (2011) *Advanced modeling and optimization of manufacturing processes*. Springer, London
- Sahoo P (2005) *Engineering tribology*. Prentice Hall, India
- Scopus.com (2021). <https://www.scopus.com/term/analyzer.uri?sid=9fc220e5bbbda8ab3dc35c99505569280&origin=resultslist&src=s&s=TITLE-ABS-KEY%28silk+composites%29&sort=plf-f&sdt=b&sot=b&sl=30&count=2728&analyzeResults=Analyze+results&txGid=1ce2651586f28a7ed0b3afcc9307eb7b>. Accessed 18 Apr 2021
- Sharma N, Khanna R, Sharma YK, Gupta RD (2019) Multi-quality characteristics optimisation on WEDM for Ti-6Al-4V using Taguchi-grey relational theory. *Int J Mach Mach Mater* 21(1/2):66. <https://doi.org/10.1504/IJMMM.2019.098067>
- Singh M (2015) Influence on kerf width in machining polystyrene by heating element profile maker using nichrome wire. *Int J Eng Res Technol (IJERT)* 4(4):135–140. <https://doi.org/10.17577/IJERTV4IS040275>
- Sonawane SA, Ronge BP, Pawar PM (2019) Multi-characteristic optimization of WEDM for Ti-6Al-4V by applying grey relational investigation during profile machining. *J Mech Eng Sci* 13(4):6059–6087. <https://doi.org/10.15282/jmes.13.4.2019.22.0478>
- Taguchi G, Chowdhary S, Wu Y (2005) *Taguchi's quality engineering handbook*. Wiley and Sons, America, US
- Taylor P, Ziegel ER (2012) *Taguchi techniques for quality engineering*
- Textor M, Sittig C, Frauchiger V, Tosatti S, Brunette DM (2001) Properties and biological significance of natural oxide films on titanium and its alloys, pp 171–230. [https://doi.org/10.1007/978-3-642-56486-4\\_7](https://doi.org/10.1007/978-3-642-56486-4_7)
- Tristo G, Bissacco G, Lebar A, Valentinčić J (2015) Real time power consumption monitoring for energy efficiency analysis in micro EDM milling. *Int J Adv Manuf Technol* 78(9–12):1511–1521. <https://doi.org/10.1007/s00170-014-6725-3>
- Web of Science. <https://www.webofscience.com/wos/woscc/analyze-results/4ee6a8cc-d967-4dbd-b420-bbb1e4e37451-1a28a043>. Accessed 18 Apr 2021
- Yerokhin AL, Nie X, Leyland A, Matthews A (2000) Characterisation of oxide films produced by plasma electrolytic oxidation of a Ti-6Al-4V alloy. *Surf Coat Technol* 130(2–3):195–206. [https://doi.org/10.1016/S0257-8972\(00\)00719-2](https://doi.org/10.1016/S0257-8972(00)00719-2)

# Chapter 3

## Tuning of Complex Coefficient Fractional Complex Order Controllers for a Generalized System Structure—An Optimisation Approach



P. Sathishkumar and N. Selvagesan

**Abstract** In general, controllers for integer, fractional and fractional complex order systems with dead time are tuned either analytically or through optimisation approaches. This is performed by accounting only the positive frequency data of the system. However, this way of controller tuning is applicable only for integer/fractional order systems containing real coefficients. These real-valued systems have an even symmetrical magnitude and odd symmetrical phase behaviour in frequency responses. Whereas for integer/fractional order systems containing complex coefficients and fractional complex order containing real/complex coefficients, an unsymmetrical behaviour is seen in its magnitude and phase responses. The conventional way of tuning controllers for such systems by considering only its positive frequency response results with reduced stability margins and in turn degrades its time response behaviour. Hence, controllers with complex coefficients are required for such systems to improve its time response and have a better stability margins. Hence, this chapter proposes complex coefficient fractional complex order controllers for such systems. An optimization approach is used to tune these controller parameters by considering both positive and negative frequency information of system with complex coefficients and complex order derivatives plus dead time. Numerical simulations are performed for a case study with the proposed and real-valued fractional order controllers.

**Keywords** Fractional order controllers · Complex coefficient controllers · Complex order derivatives · Positive and negative frequency · Frequency domain analysis

---

P. Sathishkumar · N. Selvagesan (✉)

Department of Avionics, Indian Institute of Space Science and Technology, Department of Space, Government of India, Trivandrum 695547, India  
e-mail: [n\\_selvag@iist.ac.in](mailto:n_selvag@iist.ac.in)

© The Author(s), under exclusive license to Springer Nature Singapore Pte Ltd. 2023  
A. J. Kulkarni (ed.), *Optimization Methods for Product and System Design*,  
Engineering Optimization: Methods and Applications,  
[https://doi.org/10.1007/978-981-99-1521-7\\_3](https://doi.org/10.1007/978-981-99-1521-7_3)

53

### 3.1 Introduction

In general, for physical system design and analysis, Integer Order (IO)/Fractional Order (FO) having real coefficients are taken into consideration. There are few literature study that present systems having coefficients in complex form. Few examples are asymmetric form of band pass and band rejection filters design (de Barros and Lind 1986), vibrational systems, whirling shaft and filters (Bose and Shi 1987), three-phase electrical systems model (Gatari and Garrigan 1999; Harnefors 2007), modelling of Coriolis forces (Henrion et al. 2002) and algorithms for mobile radio communications (Hromcik et al. 2002).

Generally, control theory has been evolved for practical systems having coefficients which are real. In literature, some authors have researched on systems having coefficients in complex form and are study of Routh's stability test for various systems with complex coefficients (Agashe 1985; Benidir and Picinbono 1990; Bodson and Kiselychnyk 2013; Bose 1989; Chen and Tsai 1993; Frank 1946); Kharitonov's stability conditions for interval systems having coefficients in complex form (Bose and Shi 1987) and it is also used in Bistriz (1988), Karl and Verghese (1993); Katbab et al. (1990) and Kogan (1993); Nyquist stability condition for complex coefficient models of three-phase system (Gatari and Garrigan 1999); Root locus in complex form is presented in Dòria-Cerezo and Bodson (2013) and are used for analysing three-phase rectifier's current control method in dq reference frame.

Design of controller for systems having complex coefficients is studied in the following: For rotational disc vibration system, state feedback controller is designed to have better transient response with minimal control effort and (Byun and Lee 1988); complex coefficient frequency domain stability analysis is studied for magnetically suspended flywheel rotor system (Ren et al. 2013) and cross coupled anti-symmetrical system (Ren and Fang 2014); controller design using Hurwitz test and complex root locus are proposed for doubly fed induction motor in Dòria-Cerezo et al. (2013) and Dòria-Cerezo and Bodson (2013) respectively; improvement of current quality in three-phase inverter by suppressing its harmonics with the help of complex coefficient controllers and filters designed via heuristic approach (Guo and Guerrero 2016); for cavity field control and Cartesian feedback linearisation of RF amplifiers, controller design is suggested (Troeng et al. 2017); sliding mode disturbance observer is designed with complex coefficient filters to suppress the higher order harmonics in the disturbance estimation (Yang et al. 2018).

Modelling and control design of system having derivatives in complex order form is the emerging research area. In Love (1971), derivatives in complex order form are introduced and later in Makris and Constantinou (1993) and Makris (1994), complex order derivatives with complex coefficients are proposed in Maxwell model to express the mechanical behaviour of the viscoelastic components. The proposed model helps in obtaining closer experimental results in the time domain characteristics. In Cois et al. (2001), for fractional order of commensurate type systems, complex state space representation is studied. In Guefrachi et al. (2012), frequency characteristics for models with fractional complex order derivatives are proposed. In Laurila and

Lahdelma (2014), detection of multiple faults in machines using complex order derivative. For differential equations having orders of fractional complex form, the existence and uniqueness of complex solutions are analysed in Abdolali et al. (2015).

In case of complex valued systems, the design of controllers is not well discussed in detail. In Sathishkumar and Selvagesan (2018), generalized system structure model is presented by introducing complex coefficients and derivatives of complex order. A unique expression for the parameters of the Fractional Order Controllers (FOCs) like  $PI^\alpha$ ,  $PD^\beta$ ,  $[PI]^\alpha$ ,  $[PD]^\beta$  and Fractional Complex Order Controller (FCOC) is derived for this generalized structure to meet the desired Wang et al. specifications defined in Wang et al. (2009), Luo et al. (2010) and Wang et al. (2009). Using only the positive frequency ( $\omega^+$ ) data, the parameters of FOCs/FCOC are tuned. Due to this, very large maximum values are observed in the negative frequency ( $\omega^-$ ) characteristics of the complementary sensitivity and sensitivity responses. This results in poor stability margins and degraded performance. It is due to not considering ( $\omega^-$ ) data in the design of controllers. Hence, real-valued IO/FO controllers are not suitable for complex valued systems.

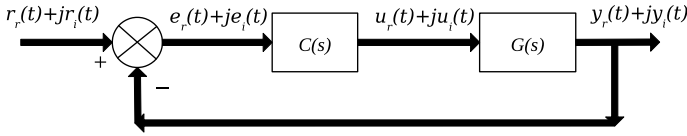
This problem is addressed by introducing complex valued controllers which are designed by accounting both ( $\omega^+$ ) and ( $\omega^-$ ) data. In this direction, complex coefficients are introduced in the Integer Order Controllers (IOCs) structure PI/PD/PID for such generalized systems (Sathishkumar and Selvagesan 2021). Recently, complex proportional resonant controllers are designed individually for filtering every harmonic signal seen in three-phase power converters (Serra et al. 2021) and complex coefficient active disturbance rejection controllers are designed to suppress the current harmonics observed in interior permanent magnet synchronous motor (Yang et al. 2022).

The above work motivates us to introduce Complex Coefficient Fractional Complex Order Controllers (CCFCOCs) (Sathishkumar 2019). The outcome of the chapter is described as follows:

- CCFCOCs are proposed for the generalized system structure.
- An optimization problem is formulated to tune the controller parameters of CCFCOCs to achieve the Wang-et-al specifications in ( $\omega^+$ ) and ( $\omega^-$ ).
- Numerical simulation is carried out to demonstrate the proposed CCFCOCs using a case study and observations are compared with real-valued FOCs.
- Analysis of time domain and frequency domain characteristics is studied for the FOCs of complex valued and its observations are compared with FOCs of real valued.

### 3.2 Generalized Closed-Loop Schematic Representation

The generalized system  $G(s)$  with controller  $C(s)$  shown in Fig. 3.1 is considered for the proposed controller design.



**Fig. 3.1** Schematic representation of generalized system with controller in closed loop

The structure of the generalized system  $G(s)$  is shown in (3.1) and it can accommodate any known class of IO/FO/Fractional Complex Order (FCO) with real and/or complex coefficient system Transfer Functions (TFs):

$$G(s) = e^{-Ls} K \frac{\sum_{i=0}^m (a_i + jb_i) s^{\alpha_i + j\beta_i}}{\sum_{k=0}^n (c_k + jd_k) s^{\gamma_k + j\delta_k}} \quad (3.1)$$

where  $a_i, b_i, c_k, d_k, \alpha_i, \beta_i, \gamma_k, \delta_k, K$  and  $L$  are real constants.  $L$  represents time delay or dead time of the system. The structure (3.1) can represent any given IO/FO/FCO system TF with appropriate choice of its parameters. Since  $G(s)$  is a complex system, input signal of the system  $u(t)$  and output signal of the system  $y(t)$  have both real and imaginary parts. Hence,  $r(t) = r_r(t) + jr_i(t)$  as the reference signal,  $e(t) = e_r(t) + je_i(t)$  as the error signal,  $u(t) = u_r(t) + ju_i(t)$  as system input signal and  $y(t) = y_r(t) + jy_i(t)$  as the system output signal are chosen in Fig. 3.1.

The controller  $C(s)$  can be three parameter FOCs or six parameter CCFCOCs and the structure of these controllers are defined in the below sub-sections.

### 3.2.1 Fractional Order Controllers

FOCs are the ones which possess dynamics that are governed by fractional calculus. Some of the popular linear time-invariant FOCs ( $C(s)$ ) are as follows:

#### 1. Fractional order proportional integral controller

It is of two types,

##### (a) $PI^\alpha$

$$C(s) = K_p + \frac{K_i}{s^\alpha} \quad (3.2)$$

The other form of  $PI^\alpha$  is

$$C(s) = K_1 \left( 1 + \frac{K_2}{s^\alpha} \right) \quad (3.3)$$

Equations (3.2) and (3.3) are related as  $K_p = K_1$ ,  $K_i = K_1 K_2$ .

(b)  $[PI]^\alpha$

$$C(s) = \left( K_p + \frac{K_i}{s} \right)^\alpha \quad (3.4)$$

The other form of  $[PI]^\alpha$  is

$$C(s) = K_1 \left( 1 + \frac{K_2}{s} \right)^\alpha \quad (3.5)$$

Equations (3.4) and (3.5) are related as  $K_p = K_1^{\frac{1}{\alpha}}$ ,  $K_i = K_1^{\frac{1}{\alpha}} K_2$ .

where  $\alpha > 0$ ;  $K_p, K_i, \in \mathbb{R}$ .

## 2. Fractional order proportional derivative controller

It is of two types,

(a)  $PD^\beta$

$$C(s) = K_p + K_d s^\beta \quad (3.6)$$

The other form of  $PD^\beta$  is

$$C(s) = K_1(1 + K_2 s^\beta) \quad (3.7)$$

Equations (3.6) and (3.7) are related as  $K_p = K_1$ ,  $K_i = K_1 K_2$ .

(b)  $[PD]^\beta$

$$C(s) = (K_p + K_d s)^\beta \quad (3.8)$$

The other form of  $[PD]^\beta$  is

$$C(s) = K_1(1 + K_2 s)^\beta \quad (3.9)$$

Equations (3.8) and (3.9) are related as  $K_p = K_1^{\frac{1}{\beta}}$ ,  $K_i = K_1^{\frac{1}{\beta}} K_2$ .

where  $\beta > 0$ ;  $K_p, K_d \in \mathbb{R}$ .

## 3.2.2 Complex Coefficient Controllers

CCFCOCs are proposed in this chapter and are as follows:

1. Complex Coefficient Fractional Complex Order  $PD^\gamma$  or  $PI^\gamma$  controller like structure:

$$C(s) = (K_{1r} + jK_{1i}) + \frac{(K_{2r} + jK_{2i})}{s^{\gamma_r + j\gamma_i}} \quad (3.10)$$

2. Complex Coefficient Fractional Complex Order  $[PI]^\alpha$  controller like structure:

$$C(s) = \left[ (K_{1r} + jK_{1i}) + \frac{(K_{2r} + jK_{2i})}{s} \right]^{\alpha_r + j\alpha_i} \quad (3.11)$$

3. Complex Coefficient Fractional Complex Order  $[PD]^\beta$  controller like structure:

$$C(s) = \left[ (K_{1r} + jK_{1i}) + (K_{2r} + jK_{2i})s \right]^{\beta_r + j\beta_i} \quad (3.12)$$

where  $K_{1r}, K_{1i}, K_{2r}, K_{2i}, \gamma_r, \gamma_i, \alpha_r, \alpha_i, \beta_r, \beta_i \in \mathbb{R}$ .

### 3.3 Tuning of Complex Coefficient *FCOCs*

To show the superiority of the fractional controllers, the proposed CCFOCs defined in (3.10), (3.11) and (3.12) are tuned to meet the Wang et al. specifications (3.13), (3.14) and (3.15) in  $\omega^+$  and (3.16), (3.17) and (3.18) in  $\omega^-$ . Obtaining a unified expressions of CCFOC parameters are tedious and hence, an optimization technique is used.

The following constrained optimization problem is proposed to tune the controller parameters by minimising the controller effort of the system shown in Fig. 3.1.

$$\begin{aligned} &\underset{\text{(Controller Parameters)}}{\text{Minimize}} \quad J = \int_0^\infty |u(t)|^2 dt \\ &\text{subject to:} \end{aligned}$$

1. In  $\omega^+$ :

(i) Gain cross over frequency ( $\omega_{gc}$ ):

$$|G_{\omega_{gc}}^+| |C_{\omega_{gc}}^+| = 1 \quad (3.13)$$

(ii) PM ( $\phi_m$ ):

$$\angle G_{\omega_{gc}}^+ + \angle C_{\omega_{gc}}^+ + \pi = \phi_m \quad (3.14)$$

(iii) Isodamping at  $\omega_{gc}$ :

$$\left. \frac{d\angle[G_{\omega^+}C_{\omega^+}]}{d\omega} \right|_{\omega=\omega_{gc}} = 0 \tag{3.15}$$

2. In  $\omega^-$ :

(a) Gain cross over frequency ( $\omega_{gc}$ ):

$$|G_{\omega_{gc}}^-||C_{\omega_{gc}}^-| = 1 \tag{3.16}$$

(b) PM ( $\phi_m$ ):

$$\angle G_{\omega_{gc}}^- + \angle C_{\omega_{gc}}^- - \pi = -\phi_m \tag{3.17}$$

(c) Isodamping at  $\omega_{gc}$ :

$$\left. \frac{d\angle[G_{\omega^-}C_{\omega^-}]}{d\omega} \right|_{\omega=\omega_{gc}} = 0 \tag{3.18}$$

### 3.4 Results and Discussions

To demonstrate the usage of CCFCOCs, the system and its specifications defined in Table 3.1 are used. The bounds for controller parameters are selected as  $K_{pr} \in [-10, 10]$ ,  $K_{pi} \in [-10, 10]$ ,  $K_{ir} \in [-10, 10]$ ,  $K_{ii} \in [-10, 10]$ ,  $K_{dr} \in [-10, 10]$ ,  $K_{di} \in [-10, 10]$ ,  $\alpha \in [-1, 1]$  and  $\beta \in [-1, 1]$ .

The `fmincon()` solver available in MATLAB (2010) is used to solve the optimization problem repeatedly with sufficiently large number of randomly selected initial guesses. For each controller case, 2000 random initial guesses are taken and the

**Table 3.1** System and its desired specifications

System	Specifications
$\frac{3+4j}{(0.8+0.2j)s^{1.9+0.4j}+(0.5+0.3j)s^{0.8+0.2j}}$	$\omega_{gc} = 5 \text{ rad/s}, \phi_m = 60^\circ$



**Table 3.2** Controller parameters for real and complex valued FOCs

System parameters	Controller	Parameters of the controller	Control effort ( $J = \int_0^\infty  u(t) ^2 dt$ )
$cK = 1, L = 0, a_0 = 3, b_0 = 4, c_0 = 0.8, d_0 = 0.2, c_1 = 0.5, d_1 = 0.3, \alpha_0 = 0, \beta_0 = 0, \gamma_0 = 1.9, \delta_0 = 0.4, \gamma_1 = 0.8, \delta_1 = 0.2,$	$CCPD^{\beta_r+j\beta_i}$	$K_{pr} = 0.4408; K_{pi} = -0.6003$ $K_{dr} = 1.1850; K_{di} = -0.5314$ $\beta_r = 0.6019; \beta_i = 0.3347$	6.9185
	$PD^\beta$	$K_p = 1.5735; K_d = 0.2066$ $\beta = 1.0807$	148.104
	$CC[PD]^{\beta_r+j\beta_i}$	$K_{pr} = 0.2644; K_{pi} = -0.7629$ $K_{dr} = 0.2945; K_{di} = -0.6107$ $\beta_r = 0.5793; \beta_i = 0.4616$	47.6554
	$[PD]^\beta$	$K_p = 1.360; K_d = 0.1420; \beta = 1.4269$	25676.274

corresponding converged values are found to be unique. The results of the proposed optimization problem are presented in Table 3.2 and these controllers are the only possible outcomes of the chosen case study. To show its superiority, the obtained results are compared with the corresponding real-valued FOCs obtained in Sathishkumar and Selvaganesan (2018) for the same case study are listed in Table 3.2.

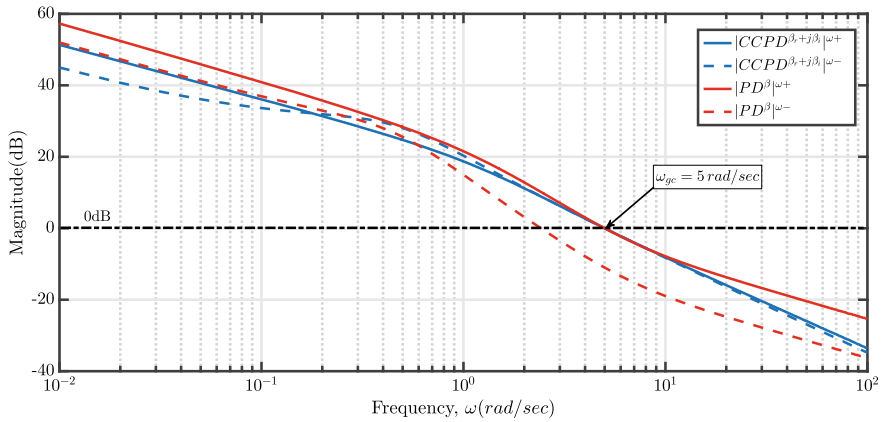
Figures 3.2 and 3.4 represent the  $\omega^+$  and  $\omega^-$  Bode magnitude response of system with the obtained controllers in the Table 3.2 respectively. Figures 3.3 and 3.5 represent the  $\omega^+$  and  $\omega^-$  Bode phase response of system with the obtained controllers in the Table 3.2 respectively.

It is noted that the Bode characteristics for system with real valued FOCs satisfy the desired closed-loop requirements in  $\omega^+$  only and not in  $\omega^-$ . The reason for not meeting the specifications in  $\omega^-$  is because of the unsymmetrical behaviour of the system not getting compensated by the real-valued FOCs. Hence, it is needed to design FOCs of complex valued form in order to meet the required constraints in both  $\omega^+$  and  $\omega^-$  simultaneously.

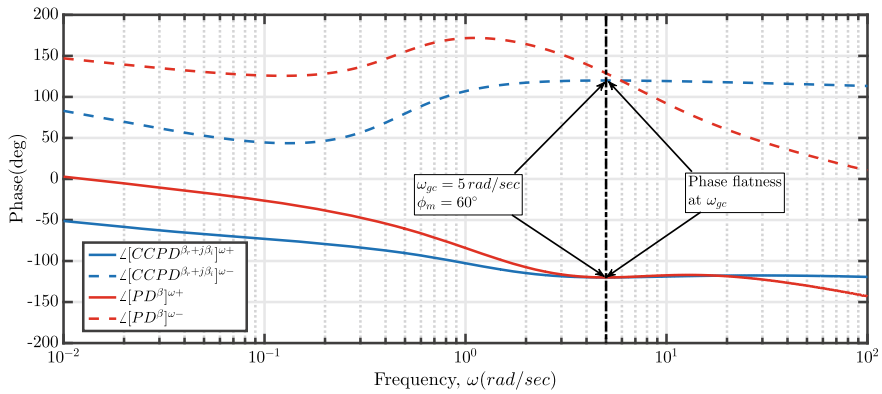
To study the robustness of parameter variation and stability of the selected example, complementary sensitivity ( $T$ ) and sensitivity ( $S$ ) (Aström and Murray 2010) are selected. The expressions of  $T$  and  $S$  are given as

$$T(j\omega) = \frac{G(j\omega)C(j\omega)}{1 + G(j\omega)C(j\omega)} \text{ and } S(j\omega) = \frac{1}{1 + G(j\omega)C(j\omega)}$$

$$M_T = \max_\omega |T(j\omega)| \text{ and } M_S = \max_\omega |S(j\omega)|$$



**Fig. 3.2** Open loop magnitude responses of system with  $CCPD^{\beta_r+j\beta_j}$  and  $PD^\beta$  controllers in  $\omega^+$  and  $\omega^-$

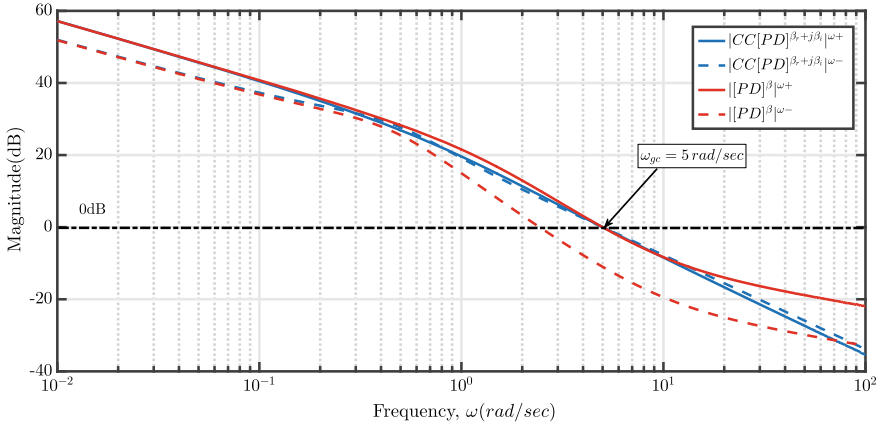


**Fig. 3.3** Open loop phase responses of system with  $CCPD^{\beta_r+j\beta_j}$  and  $PD^\beta$  controllers in  $\omega^+$  and  $\omega^-$

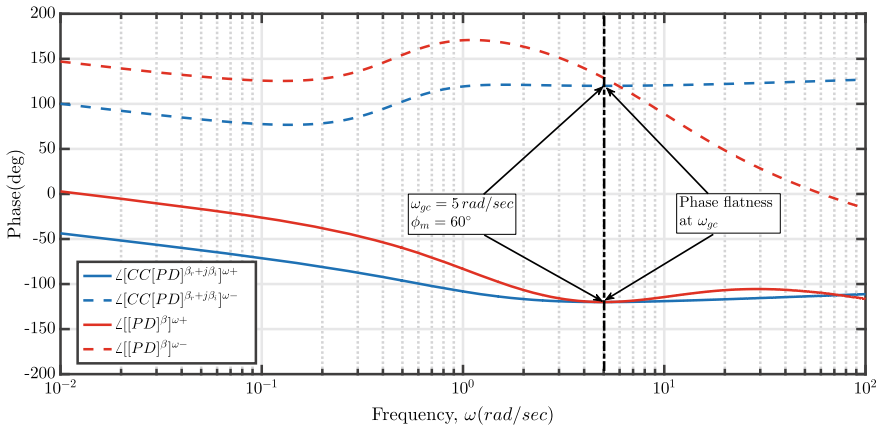
$$PM \geq 2 \sin^{-1} \left( \frac{1}{2M_S} \right) \text{ and } GM \geq \frac{M_S}{M_S - 1}$$

where  $M_T$  is the peak sensitivities of  $|T(jw)|$  and  $M_S$  is the peak sensitivities of  $|S(jw)|$  responses. Resonant peak is indicated by  $M_T$  and the maximum amplification gain of the load disturbance is indicated by  $M_S$ . Assured Phase Margin ( $PM$ ) and Gain Margin ( $GM$ ) are calculated from the maximum sensitivity ( $M_S$ ) and its expressions are given in Aström and Murray (2010).  $M_T$  and  $M_S$  should lie in the limits of 1–1.5 and 1.2–2.0 respectively for a good measure of robustness.

Sensitivity and complementary sensitivity responses for  $CCPD^{\beta_r+j\beta_j}$  and  $PD^\beta$  with system are shown in Figs. 3.6 and 3.7 respectively. Similarly, Sensitivity and



**Fig. 3.4** Open loop magnitude responses of system with  $CC[PD]^{\beta_r+j\beta_i}$  and  $[PD]^\beta$  controllers in  $\omega^+$  and  $\omega^-$

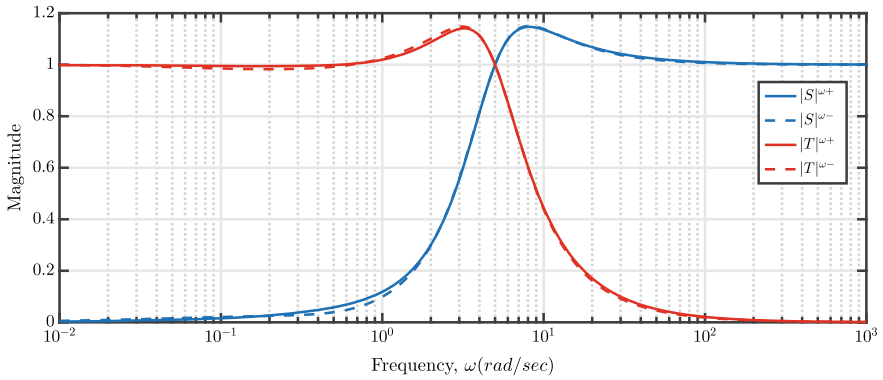


**Fig. 3.5** Open loop phase responses of system with  $CC[PD]^{\beta_r+j\beta_i}$  and  $[PD]^\beta$  controllers in  $\omega^+$  and  $\omega^-$

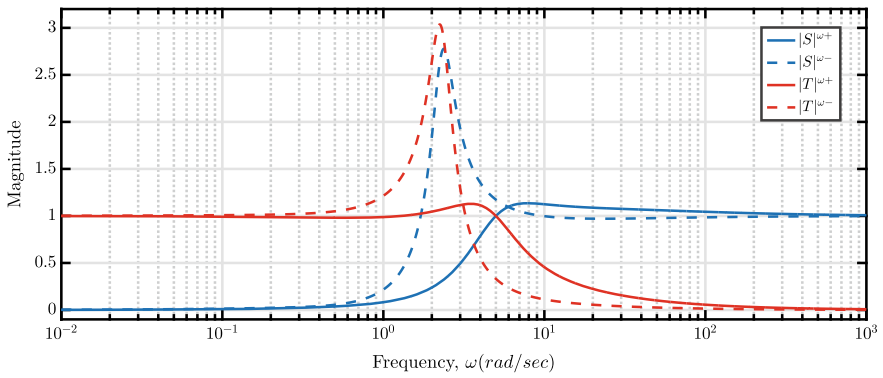
complementary sensitivity responses for  $CC[PD]^{\beta_r+j\beta_i}$  and  $[PD]^\beta$  with system are shown in Figs. 3.8 and 3.9 respectively.

From these sensitivity and complementary sensitivity responses,  $M_T$ ,  $M_S$ , guaranteed stability margins ( $GM$  and  $PM$ ) and bandwidth ( $\omega_{BW}$ ) metrics are listed in Table 3.3 which are obtained in both the  $\omega^+$  and  $\omega^-$  characteristics.

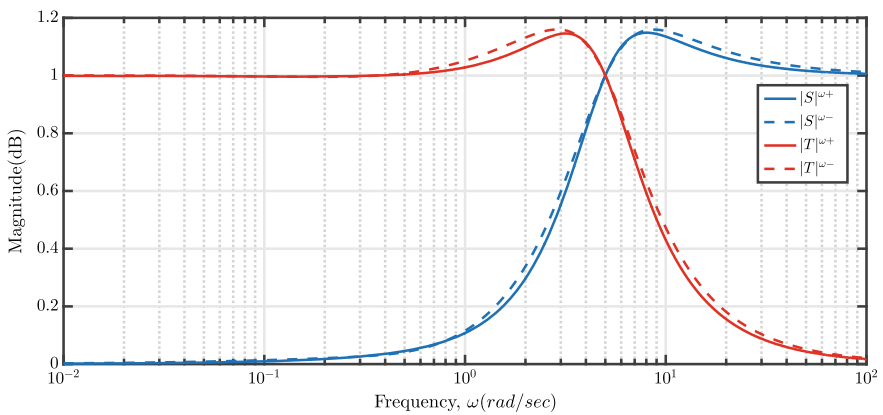
For time domain closed-loop simulation, an unit step command input  $r(t) = r_r(t) + jr_i(t) = 1 + j0$  is applied to the system shown in Fig. 3.1. To obtain the closed-loop response of the generalized system with the proposed controllers, Oustaloup approximation given in Valério and da Costa (2004) and Oustaloup et al. (2000) is used to approximate the fractional order terms in the system and the proposed controllers  $CCPD^{\beta_r+j\beta_i}$  and  $CC[PD]^{\beta_r+j\beta_i}$ . Frequency range of [0.001–



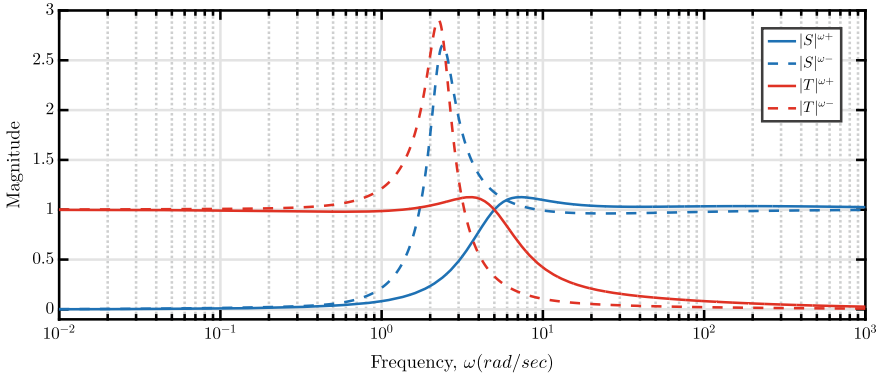
**Fig. 3.6** Sensitivity and complementary sensitivity responses of system with  $CCPD^{\beta_r + j\beta_j}$  in  $\omega^+$  and  $\omega^-$



**Fig. 3.7** Sensitivity and complementary sensitivity responses of system with  $PD^\beta$  in  $\omega^+$  and  $\omega^-$



**Fig. 3.8** Sensitivity and complementary sensitivity responses of system with  $CC[PD]^{\beta_r + j\beta_j}$  in  $\omega^+$  and  $\omega^-$



**Fig. 3.9** Sensitivity and complementary sensitivity responses of system with  $[PD]^\beta$  in  $\omega^+$  and  $\omega^-$

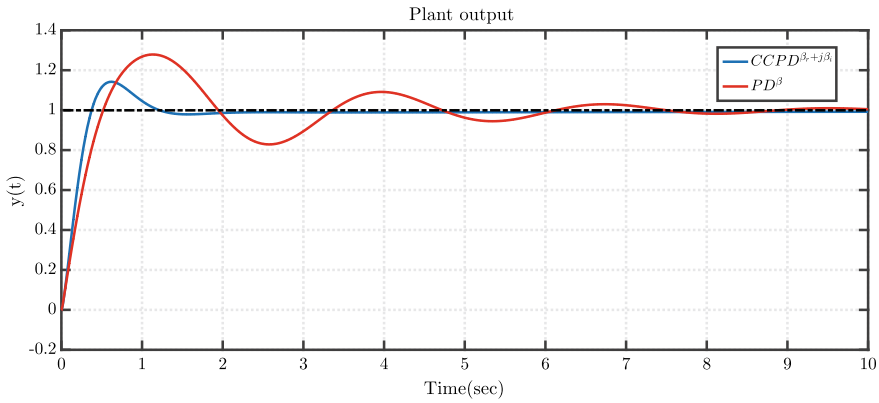
**Table 3.3** Observations from sensitivity and complementary sensitivity responses of complex and real-valued FOCs

Controllers	$\omega^+$	$\omega^-$
$CCPD^{\beta_r+j\beta_i}$	$M_S = 1.1469; M_T = 1.1412;$ $GM \geq 17.8507dB; PM \geq$ $51.6931^\circ \omega_{BW} = 7.0763 \text{ rad/s}$	$M_S = 1.1502; M_T = 1.1480;$ $GM \geq 17.6845dB; PM \geq$ $51.5356^\circ \omega_{BW} = 7.0684 \text{ rad/s}$
$PD^\beta$	$M_S = 1.1349; M_T = 1.1290;$ $GM \geq 18.4962dB; PM \geq$ $52.2778^\circ \omega_{BW} = 6.9699 \text{ rad/s}$	$M_S = 2.7770; M_T = 3.0362;$ $GM \geq 3.8778dB; PM \geq$ $20.7453^\circ \omega_{BW} = 3.6345 \text{ rad/s}$
$CC[PD]^{\beta_r+j\beta_i}$	$M_S = 1.1485; M_T = 1.1460;$ $GM \geq 17.7667dB; PM \geq$ $51.6139^\circ \omega_{BW} = 7.0183 \text{ rad/s}$	$M_S = 1.1594; M_T = 1.1598;$ $GM \geq 17.2344dB; PM \geq$ $51.0943^\circ \omega_{BW} = 7.2825 \text{ rad/s}$
$[PD]^\beta$	$M_S = 1.1261; M_T = 1.1264;$ $GM \geq 19.0147dB; PM \geq$ $52.7180^\circ \omega_{BW} = 6.8180 \text{ rad/s}$	$M_S = 2.6514; M_T = 2.9064;$ $GM \geq 4.1124dB; PM \geq$ $21.7394^\circ \omega_{BW} = 3.6536 \text{ rad/s}$

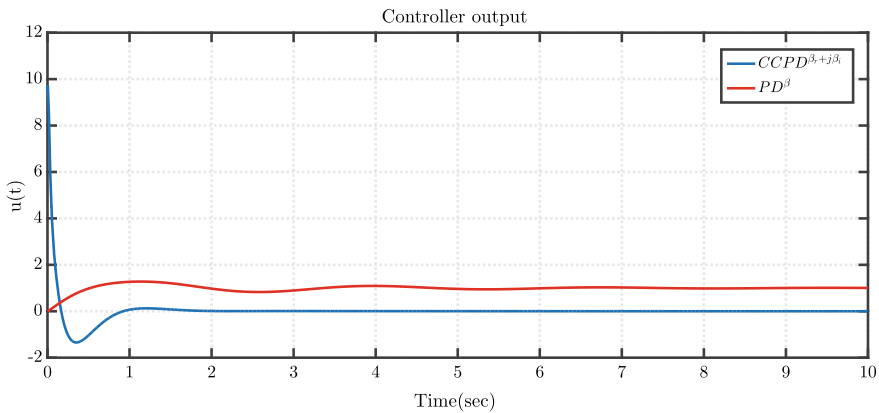
1,000]rad/s with order ( $N$ )10 is chosen for approximation. The real part of the system output responses is shown in Fig.3.10 for system with  $CCPD^{\beta_r+j\beta_i}$  and  $PD^\beta$  controllers. The real part of the system output responses is shown in Fig. 3.12 for system with  $CC[PD]^{\beta_r+j\beta_i}$  and  $[PD]^\beta$  controllers.

The real part of the controller output responses are shown in Fig.3.11 for system with  $CCPD^{\beta_r+j\beta_i}$  and  $PD^\beta$  controllers. The real part of the controller output responses are shown in Fig. 3.13 for system with  $CC[PD]^{\beta_r+j\beta_i}$  and  $[PD]^\beta$  controllers.

From the output responses shown in Figs. 3.10 and 3.12, it is seen that real-valued FOCs give deteriorated responses by introducing larger overshoot, larger settling time and oscillatory behaviour in comparison to CCFCOCs. This is because, real-valued FOCs are tuned by considering only the  $\omega^+$  information of the system. Hence,



**Fig. 3.10** System output responses of system with  $CCPD^{\beta_r+j\beta_i}$  and  $PD^\beta$

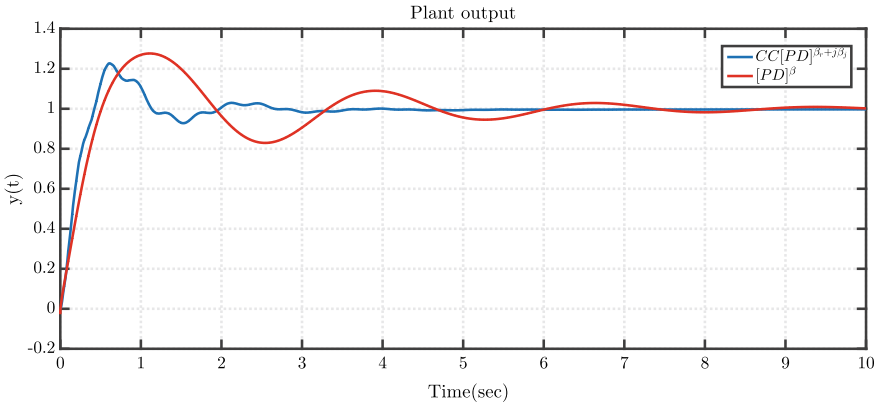


**Fig. 3.11** Controller output responses of system with  $CCPD^{\beta_r+j\beta_i}$  and  $PD^\beta$

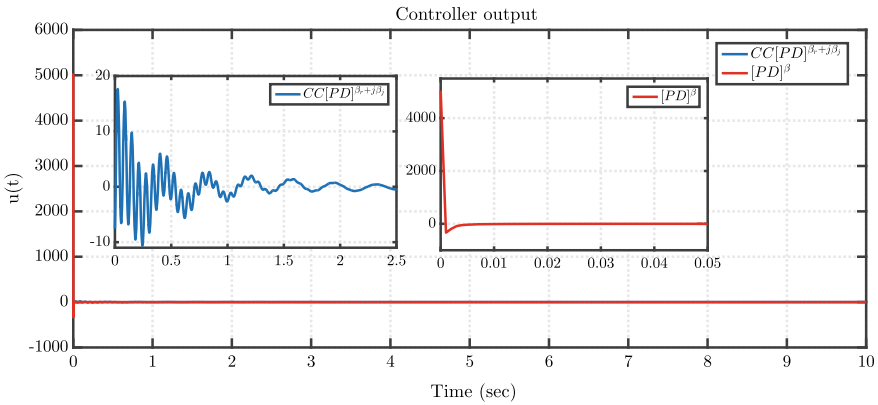
real-valued FOCs are selected only for real-valued systems and complex valued CCFCOCs are selected for complex valued systems.

For this case study, it is noted that both  $M_T$  and  $M_S$  measured for  $CCPD^{\beta_r+j\beta_i}$  are smaller in comparison to  $PD^\beta$  from  $\omega^+$  and  $\omega^-$  analysis. This ensures higher  $GM$  and  $PM$  for  $CCPD^{\beta_r+j\beta_i}$  which is observed as a reduced overshoot in Fig. 3.10. It is also noted that  $CCPD^{\beta_r+j\beta_i}$  has higher  $\omega_{BW}$  than  $PD^\beta$  which is seen as smaller rise time in Fig. 3.12. Similar behaviour is also seen for  $CC[PD]^{\beta_r+j\beta_i}$  in comparison to  $[PD]^\beta$ .

Table 3.2 shows the computed controller effort for system with proposed controllers. Since, only  $\omega^+$  characteristics are considered for tuning of real-valued FOCs and whereas in case of complex valued FOCS, both  $\omega^+$  and  $\omega^-$  characteristics are considered, their controller efforts comparisons are not discussed.



**Fig. 3.12** System output responses of system with  $CC[PD]^{\beta_r+j\beta_j}$  and  $[PD]^\beta$



**Fig. 3.13** Controller output responses of system with  $CC[PD]^{\beta_r+j\beta_j}$  and  $[PD]^\beta$

It is noted that  $CCPD^{\beta_r+j\beta_j}$  and  $CC[PD]^{\beta_r+j\beta_j}$  meet the desired specifications in both  $\omega^+$  and  $\omega^-$  simultaneously. FOCs of complex valued form also give better margins in stability metrics and improved time responses than FOCs of real-valued form. This indicates that only FOCs or IOC with complex valued form have to be chosen for such systems.

**Remarks:** The limitations of the CCFCOCs are: (i) Real time implementation of CCFCOCs is complex and a systematic approach need to be developed and (ii) Approximation of CCFCOCs need to be improved with any future approximation techniques.

### 3.5 Conclusion

In this chapter, CCFCOCs were proposed for the generalized system structure. An optimisation problem was formulated to tune the controller parameters of these complex valued controllers for the complex valued generalized system to attain the desired constraints in both  $\omega^+$  and  $\omega^-$ . The proposed controllers were also demonstrated using a case study and the results were compared with real-valued FOCs which are tuned to attain the desired constraints only in  $\omega^+$ . It was noted that only CCFCOCs with system had the capability to satisfy the required constraints both in  $\omega^+$  and  $\omega^-$ . Also, CCFCOCs have improved stability and robustness to parameter variations than real-valued FOCs. This was clearly seen from their sensitivity and complementary sensitivity characteristics. Hence, better time and frequency domain characteristics were achieved. Hence, CCFCOCs were recommended for controlling complex valued systems. Real time implementation and better approximation techniques of CCFCOCs could be the future direction.

### References

- Abdolali N, Yadollahzadeh M, Rahmat D (2015) On fractional differential equation with complex order. *Progr Fract Differ Appl* 1(3):223–227
- Agashe S (1985) A new general Routh-like algorithm to determine the number of RHP roots of a real or complex polynomial. *IEEE Trans Autom Control* 30(4):406–409
- Aström KJ, Murray RM (2010) *Feedback systems: an introduction for scientists and engineers*. Princeton University Press, Princeton, New Jersey
- Benidir M, Picinbono B (1990) Extended table for eliminating the singularities in Routh's array. *IEEE Trans Autom Control* 35(2):218–222
- Bistriz Y (1988) Stability criterion for continuous-time system polynomials with uncertain complex coefficients. *IEEE Trans Circuits Syst* 35(4):442–448
- Bodson M, Kiselychynk O (2013) The complex Hurwitz test for the analysis of spontaneous self-excitation in induction generators. *IEEE Trans Autom Control* 58(2):449–454
- Bose NK (1989) Tests for Hurwitz and Schur properties of convex combination of complex polynomials. *IEEE Trans Circuits Syst* 36(9):1245–1247
- Bose N, Shi Y (1987) A simple general proof of Kharitonov's generalized stability criterion. *IEEE Trans Circuits Syst* 34(10):1233–1237
- Bose N, Shi Y (1987) Network realizability theory approach to stability of complex polynomials. *IEEE Trans Circuits Syst* 34(2):216–218
- Byun SW, Lee CW (1988) Pole assignment in rotating disk vibration control using complex modal state feedback. *Mech Syst Signal Process* 2(3):225–241
- Chen SS, Tsai JSH (1993) A new tabular form for determining root distribution of a complex polynomial with respect to the imaginary axis. *IEEE Trans Autom Control* 38(10):1536–1541
- Cois O, Levron F, Oustaloup A (2001) Complex-fractional systems: modal decomposition and stability condition. In: *Proceedings of European control conference*, pp 1484–1489
- de Barros MP, Lind LF (1986) On the splitting of a complex-coefficient polynomial. *IEE Proc G Electron Circuits Syst* 133(2):95–98
- Dòria-Cerezo A, Bodson M, Batlle C, Ortega R (2013) Study of the stability of a direct stator current controller for a doubly fed induction machine using the complex Hurwitz test. *IEEE Trans Control Syst Technol* 21(6):2323–2331



- Dòria-Cerezo A, Bodson M (2013) Root locus rules for polynomials with complex coefficients. In: Proceedings of 21st Mediterranean conference on control and automation, pp 663–670
- Frank E (1946) On the zeros of polynomials with complex coefficients. *Bull Am Math Soc* 52(2):144–157
- Gataric S, Garrigan NR (1999) Modeling and design of three-phase systems using complex transfer functions. In: Proceedings of 30th annual IEEE power electronics specialists conference. Record. (Cat. No.99CH36321), pp 691–697
- Guefrachi A, Najar S, Amairi M, Abdelkrim M (2012) Frequency response of a fractional complex order transfer function. In: Proceedings of 13th international conference on sciences and techniques of automatic control and computer engineering, pp 765–773
- Guo X, Guerrero JM (2016) ABC-frame complex-coefficient filter and controller based current harmonic elimination strategy for three-phase grid connected inverter. *J Mod Power Syst Clean Energy* 4(1):87–93
- Harnefors L (2007) Modeling of three-phase dynamic systems using complex transfer functions and transfer matrices. *IEEE Trans Industr Electron* 54(4):2239–2248
- Henrion D, Ježek J, Sebek M (2002) Discrete-time symmetric polynomial equations with complex coefficients. *Kybernetika* 38:113–139
- Hromcik M, Sebek M, Ježek J (2002) Complex polynomials in communications: motivation, algorithms, software. In: Proceedings of IEEE international symposium on computer aided control system design, pp 291–296
- Karl WC, Verghese GC (1993) A sufficient condition for the stability of interval matrix polynomials. *IEEE Trans Autom Control* 38(7):1139–1143
- Katbab A, Kraus F, Jury EI (1990) Some Schur-stability criteria for uncertain systems with complex coefficients. *IEEE Trans Circuits Syst* 37(9):1171–1176
- Kogan J (1993) Robust Hurwitz  $l_p$  stability of polynomials with complex coefficients. *IEEE Trans Autom Control* 38(8):1304–1308
- Laurila J, Lahdelma S (2014) Advanced fault diagnosis by means of complex order derivatives. *Insight-Non-Destr Test Cond Monitor* 56(8):439–442
- Love ER (1971) Fractional derivatives of imaginary order. *J Lond Math Soc* 2(2):241–259
- Luo Y, Chen YQ, Wang CY, Pi YG (2010) Tuning fractional order proportional integral controllers for fractional order systems. *J Process Control* 20(7):823–831
- Makris N (1994) Complex-parameter Kelvin model for elastic foundations. *Earthquake Eng Struct Dynam* 23(3):251–264
- Makris N, Constantinou M (1993) Models of viscoelasticity with complex-order derivatives. *J Eng Mech* 119(7):1453–1464
- MATLAB. Version 7.10.0 (R2010a). The MathWorks Inc., Natick, Massachusetts
- Oustaloup A, Levron F, Mathieu B, Nanot FM (2000) Frequency-band complex noninteger differentiator: characterization and synthesis. *IEEE Trans Circuits Syst I: Fundam Theory Appl* 47(1):25–39
- Ren Y, Su D, Fang J (2013) Whirling modes stability criterion for a magnetically suspended fly-wheel rotor with significant gyroscopic effects and bending modes. *IEEE Trans Power Electron* 28(12):5890–5901
- Ren Y, Fang J (2014) Complex-coefficient frequency domain stability analysis method for a class of cross-coupled antisymmetrical systems and its extension in MSR systems. *Math Probl Eng*. Article ID 765858
- Sathishkumar P (2019) Fractional order controllers for complex valued systems and system with multiple nonlinearities. PhD thesis, Indian Institute of Space Science and Technology
- Sathishkumar P, Selvaganesan N (2018) Fractional controller tuning expressions for a universal plant structure. *IEEE Control Syst Lett* 2(3):345–350
- Sathishkumar P, Selvaganesan N (2021) Tuning of complex coefficient PI/PD/PID controllers for a universal plant structure. *Int J Control* 94(11):3190–3212
- Serra FM, Dòria-Cerezo A, Bodson M (2021) A multiple-reference complex-based controller for power converters. *IEEE Trans Power Electron* 36(12):14466–14477

- Troeng O, Bernhardsson B, Rivetta C (2017) Complex-coefficient systems in control. In: Proceedings of IEEE American control conference, pp 1721–1727
- Valério D, da Costa JS (2004) Ninteger: a non-integer control toolbox for matlab. In: Proceedings of the first IFAC workshop on fractional differentiation and applications, Bordeaux, France, pp 208–213
- Wang C, Luo Y, Chen YQ (2009) An analytical design of fractional order proportional integral and [proportional integral] controllers for robust velocity servo. In: Proceedings of 4th IEEE conference on industrial electronics and applications, pp 3448–3453
- Wang C, Luo Y, Chen YQ (2009) Fractional order proportional integral (FOPI) and [proportional integral] (FO[PI]) controller designs for first order plus time delay (FOPTD) systems. In: Proceedings of Chinese control and decision conference, pp 329–334
- Yang H, Zhang Y, Liang J, Xia B, Walker PD, Zhang N (2018) Deadbeat control based on a multipurpose disturbance observer for permanent magnet synchronous motors. *IET Electr Power Appl* 12(5):708–716
- Yang F, Jiang F, Xu Z, Qiu L, Xu B, Zhang Y, Yang K (2022) Complex coefficient active disturbance rejection controller for current harmonics suppression of IPMSM drives. *IEEE Trans Power Electron* 37(9):10443–10454

# Chapter 4

## A Review on Intelligent Optimization Techniques Based Fault Detection and Diagnosis in Power System Applications



**K. Vanchinathan and N. Selvaganesan**

**Abstract** This chapter presents a comprehensive review of computational intelligent optimization methods used for the Fault Detection and Diagnosis (FDD) purpose in power transmission lines. There have been several algorithms reported in literature for FDD optimization algorithms. These algorithms are developed and tested using the primary fault data obtained from power system simulated in matrix laboratory simulator. In real time simulation, the power system parameters are obtained through the sensors and hence the validity of FDD algorithms depends on the precision of the sensors. This is the inspiration to review various FDD optimization algorithms for transmission line in detail. The require performance improvement of power transmission line needs to be considered with the following factors (i) To improve the energy efficiency by reducing transmission losses and using efficient energy storage methods (ii) To improve the power quality and protection, hence to enhance the reliability and operational performance through power management. Based on above factors, this review considers the various FDD algorithms in power transmission line using computational intelligence techniques under varying load demands. Also, this review provides a valuable guidance and potential new research directions for selecting a suitable FDD method in the power transmission line.

**Keywords** Transmission line · Fault detection · Fault diagnosis · Power quality · Optimization techniques

---

K. Vanchinathan

Department of Electrical and Electronics Engineering, Velalar College of Engineering and Technology, Thindal, Erode, Tamil Nadu 638012, India

N. Selvaganesan (✉)

Department of Avionics, Indian Institute of Space Science and Technology, Thiruvananthapuram, Kerala 695547, India

e-mail: [n\\_selvag@iist.ac.in](mailto:n_selvag@iist.ac.in)

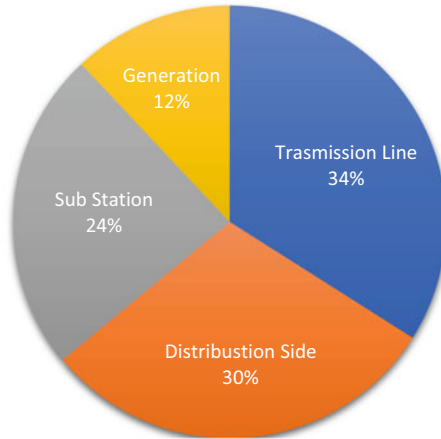
## 4.1 Introduction

Power systems are the most complicated man-made systems, with regular undesired voltage and current fluctuations. Because of growing concerns about Power Quality (PQ), this problem has been widely investigated in recent years (Mellit et al. 2018). The contemporary trend toward deregulation has pushed utilities to put additional stress on the system, bringing it closer to its stability limitations. As a result, power systems become more susceptible to microelectronic and nonlinear device disturbances. Electrical power is a requirement for residences, offices, industries, transportation, communication and almost all day-to-day works (Zhao et al. 2020). The present scenario of the power system in both developing and developed countries changed drastically to satisfy various new factors like increasing load demand, need for expansion of power system and introduction of electronics and computerized instrumentation, control and communication technologies (Chen et al. 2019). The power systems are growing immensely due to huge power flow into the system from generation plants to satisfy the ever rising load demand.

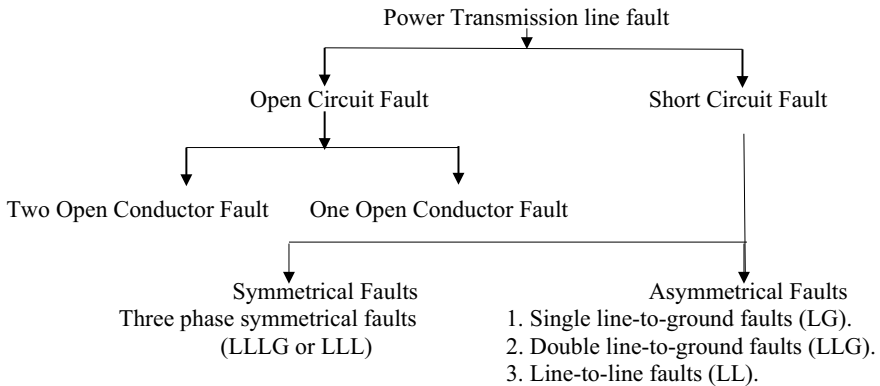
As a result, the system became huge and complex making centralised management a very difficult task. Hence in power sectors all over the world, de-regulation and unbundling are introduced to set down laws and rules for participation of private sector in generation, transmission and distribution of electric power (Vanchinathan and Valluvan 2018). De-regulation allowed public and private capital flow into the power industry, better management through recognition and support of electric utilities from the government (Mariano-Hernández et al. 2021). Though de-regulation allows better management through distribution of funds to all sectors of the power industry, and it introduces new problems like network congestion, deterioration in power quality, control and financial issues. Distributed generation is encouraged to reduce losses and improve voltage profile, but this increased the complexity of the distribution system calling for more attention towards operation, control, protection and improvement in power quality (He et al. 2009). The disturbances normally occur when a new source is interconnected to the grid systems (Vanchinathan et al. 2022). The percentage of fault detection and diagnosis in power systems is shown in Fig. 4.1.

This is depending on the type and the cause may persist for few milliseconds or extend to several minutes. Disturbances can be mainly of four categories: (i) voltage deviation like sag, swell (ii) momentary interruption (iii) current deviations like transformer inrush current and (iv) fault currents. The frequency deviation is the third category of disturbance which is due to excessive increase or decrease in load, and speed variation of synchronous generators. The fourth category is transients and impulses due to sudden change in load/generation, faults and lightning. However, only voltage deviations and transients are considered (Chen and Jiang 2019). The classification of power transmission line faults is shown in Fig. 4.2.

The basic requirement for secure and reliable operation of the power system is Fault Diagnosis (FD) and disturbance analysis. Both power system protection and Power Quality Assessment (PQA) need precise measurements (Gangsar and Tiwari 2020). However the iron cored Current Transformers (CTs) and Potential



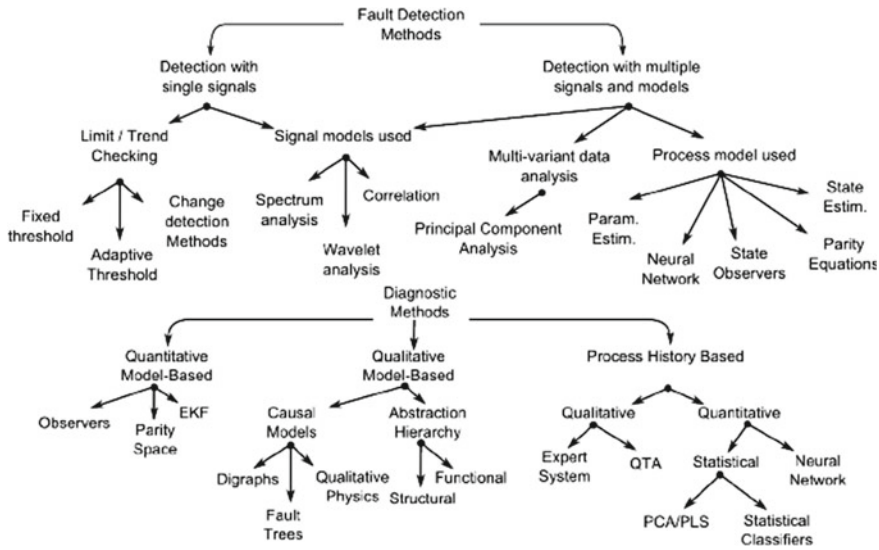
**Fig. 4.1** Percentage of fault detection and diagnosis in power systems



**Fig. 4.2** Classification of power transmission line faults

Transformers (PTs) have several limitations. CT saturation during faults due to higher than rated fault current and DC components results in distorted secondary current waveforms. This introduces error in measurements which leads to false tripping and unpredictable delays in relay operations. Also it limits the bandwidth of making them unsuitable for measurement in the event of high frequency transients and impulses (Harrou et al. 2018). Other issues like, temperature dependency, crosstalk, cost, weight and number of units required to cover all applications is also essential. Hence new sensors are to be identified and are suitable for the present digital technology (Vanchinathan et al. 2021). This problem is solved by Rogowski Coil (RC) as a current sensor which removes almost all shortcomings of iron cored CTs. The classification of FDD methods in the transmission line is shown in Fig. 4.3.

The contributions of this review paper are:



**Fig. 4.3** Classification of FDD Methods in Transmission Line (Isermann 2005a, b) and (Venkata Subramanian et al. 2003)

1. A detailed review on classification on FDD models such as model based, knowledge based, data-based analysis’s in power system applications.
2. A comprehensive review is presented to summarize the computational intelligence based FDD for power system.
3. This review aims the most important primary studies of FDD in power systems. Various methodologies of FDD utilizing intelligent optimization in power systems are discussed. This greatly helps the researchers to select best optimized FDD methodologies in power systems.

## 4.2 Preliminary Works

This work is influenced by research works carried out in the field of digitized power system operation, control and protection. In this section, detailed literature related to power quality assessment and fault diagnosis is presented. The details about the methodologies used in the related work are presented (Kim and Katipamula 2018). The issues and challenges in PQA and FDD of transmission lines and about how they are addressed in the presented method are discussed in Khalastchi and Kalech (2018). The methodology used for PQA and FDD uses MATLAB for fault and disturbance waveform generation, wavelet transform for feature extraction and fuzzy logic for algorithm implementation (Saxena et al. 2010).

**Table 4.1** Power system details

Power system quantity	Values
Voltage rating	350 kV
System frequency	50 Hz
Equivalent voltage $E_S$	$1 \angle 15^\circ$ p.u
Equivalent voltage $E_R$	$1 \angle 0^\circ$ p.u
Equivalent positive sequence source impedance $Z_{s1}$	$0.238 + 5.72 \Omega$
Equivalent zero sequence source impedance $Z_{s0}$	$2.738 + 10 \Omega$
Equivalent positive sequence source impedance $Z_{R1}$	$0.238 + 6.19 \Omega$
Equivalent zero sequence source impedance $Z_{R0}$	$0.833 + 5.12 \Omega$
Length of transmission line	90 km
Zero sequence line constants $R_0, L_0$ and $C_0$	$0.275 \Omega, 3.725 \text{ mH}, 6.71 \text{ nF}$
Positive sequence line constants $R_1, L_1$ and $C_1$	$0.0275 \Omega, 1.345 \text{ mH}, 9.483 \text{ nF}$

### 4.2.1 Fault Classification Using Power Frequency Components

In this method, a power system with two 345 kV generators is simulated in SIMULINK. The two generators are represented as S and R. The transmission line of 100 km is simulated as a uniformly distributed parameter model between the sending end bus A and the receiving end bus B with measurements performed at bus A. All types of asymmetrical and symmetrical faults are simulated for different fault distances, fault resistances and fault inception angles (AbdulMawjood et al. 2018). Further, the fault signal waveforms obtained are processed to determine the RMS values of fault currents (Pillai and Rajasekar 2018). The power system details and coding of fault types are listed in the Tables 4.1 and 4.2.

### 4.2.2 Effect of CT Saturation on Fault Data

During faults, the current increases by 4–12 times the normal value depending on the distance of fault from the CT location. Since CTs are iron-cored, their performance is limited based on the magnetization characteristics of the core. Hence the performance of CTs during fault conditions weaken due to magnetic saturation as discussed (Zhang et al. 2018). The FD algorithms are accordingly developed and tested on these waveforms, while in practical conditions power system data is derived from current

**Table 4.2** Coding of fault types

A-G	Phase A to ground fault
B-G	Phase B to ground fault
C-G	Phase C to ground fault
A-B	Phase-to-phase (AB type) fault
B-C	Phase-to-phase (BC type) fault
A-C	Phase-to-phase (AC type) fault
A-B-G	Phase-to-phase (AB type) to ground fault
B-C-G	Phase-to-phase (BC type) to ground fault
A-C-G	Phase-to-phase (AC type) to ground fault
A-B-C	Three phases (ABC type) fault
A-B-C-G	Three phases (ABC type) to ground fault

transformers and potential transformers. Hence, FD algorithms developed with simulated data fail to perform satisfactorily in practical conditions. However, the effect of CT saturation suggests no remedies. In this algorithm, the effect of CT saturation on the fault current waveform and hence on fault classification and location are determined (Li et al. 2021). RC is a linear sensor and has several advantages in power system protection and this algorithm is implemented with the RC model and the iron cored CT model. Subsequently the results of both the cases are compared. Clearly FD with RC produced good results with reduced errors without any major modification in the algorithm.

### 4.2.3 *Extraction of High Frequency Components from Fault Data Through Wavelet Transformation*

In FD based estimation of power frequency phasors, signals are subjected to high pass and low pass filters so that it will remove the DC and high frequency components. Then, by applying discrete Fourier transform techniques, the RMS values are estimated. In case of CT saturation, the signal sampling is delayed by one or two cycles from fault inception to estimate RMS values accurately and hence it will delay the FD process. On the other hand if FD uses Discrete Wavelet Transform (DWT), data from the first half cycle is enough as the high frequency components are highest during this period and decay as time progresses (Vanchinathan and Selvaganesan 2021).

FD in particular is simpler using multi resolution analysis of Wavelet Transformation (WT) and energy estimation of detailed components as presented. Hence this method is implemented using Multi-Resolution Analysis (MRA) of wavelet transformation technique. Three methods of FD are presented, one using RMS values while other two using WT. For comparison, the total time for FD includes time for data filtering, sampling and computation. It is found that the methods using WT are



faster and data sampling for half cycle from fault inception is adequate. However if RC is used instead of CT, the FD algorithm based on RMS values are equally good due to absence of attenuation in secondary waveform.

#### ***4.2.4 Time and Space Requirement for FD Algorithm Implementation***

FD algorithm is implemented using Artificial Neural Networks (ANN) in and fuzzy neural networks. FD using Probabilistic Neural Network (PNN) requires high training speed compared to back propagation networks. For more accurate results, NN require large samples of input and output data to train the network and hence design of ANN/PNN is more complex and time consuming making it unsuitable for real time applications. This method is implemented in fuzzy logic as it is very simple and most suitable for applications dealing with uncertain data and still come out with a fairly accurate result in less time.

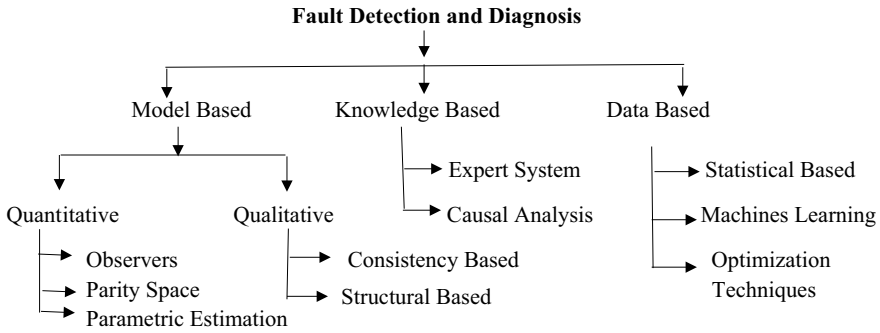
The summary of above-mentioned research has mostly been used in the operation of power systems. The creation of an analytical tool to confirm the integrated performance of the power system is similar to that of the current study. To evaluate the data, the raw interface data is converted into the interpreted data format using a message-description language. However, despite their practical contributions, they are unable to identify interface problems. Also this review focuses on optimization techniques-based failure detection and diagnosis in power system (Wang et al. 2021).

### **4.3 Methods for FDD in Power Systems**

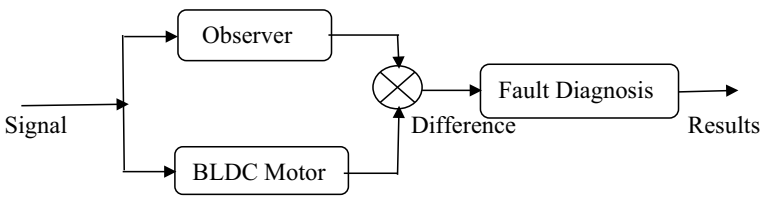
The detecting step necessitates the usage of FDDs information. This data is required to assist maintenance teams in decreasing the time it takes to restore the system. In order to determine the optimum way for making this data available to the detection system, the automation system architecture is considered. The current digital protection relays industry model entails combining sensor data processing, sample recording systems, time stamping techniques, and fault diagnostic methods into a single electronic device. The classification of fault detection and diagnosis is shown in Fig. 4.4.

#### ***4.3.1 Model-Based Fault Diagnosis***

The model-based defect diagnostics approach relies on state or parameter estimates and mathematical models of the PM machine should be available. The fault diagnostic



**Fig. 4.4** Classification of fault detection and diagnosis



**Fig. 4.5** Representation of model-based fault diagnosis

technique is built using the model and involves monitoring the difference between the measured output of the PM machine and the expected output from the model. The Fig. 4.5 shows the representation of model-based fault diagnosis.

### 4.3.2 Signal Based Fault Diagnosis

The signal-based approaches use the measured signals to diagnose faults without the need for machine models. Signal processing methods are used to extract fault characteristics from measured signals and then a diagnostic decision is made.

Figure 4.6 shows the signal-based fault diagnosis where there is multiplication of two sinusoidal waves with frequencies of 200 and 2000 Hz. The higher frequency component is called the carrier frequency and the lower one is the modulating frequency. Ideally, two peaks should appear in the spectrum at 200 and 2000 Hz. However, the spectrum only shows the carrier frequency at 2000 Hz with two symmetrical sidebands at 1800 and 2200 Hz.

Fault is one of the situations of power quality that demands greater attention and study since it is critical to the power system’s good functioning. For detection and categorization of transmission FDD has been a major problem. Three fault categorization algorithms have been suggested and tested. The general layout of FDD for the power systems is shown in Fig. 4.7.

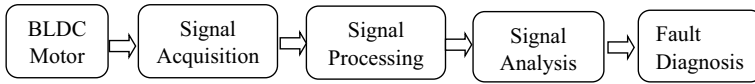


Fig. 4.6 Representation of signal based fault diagnosis

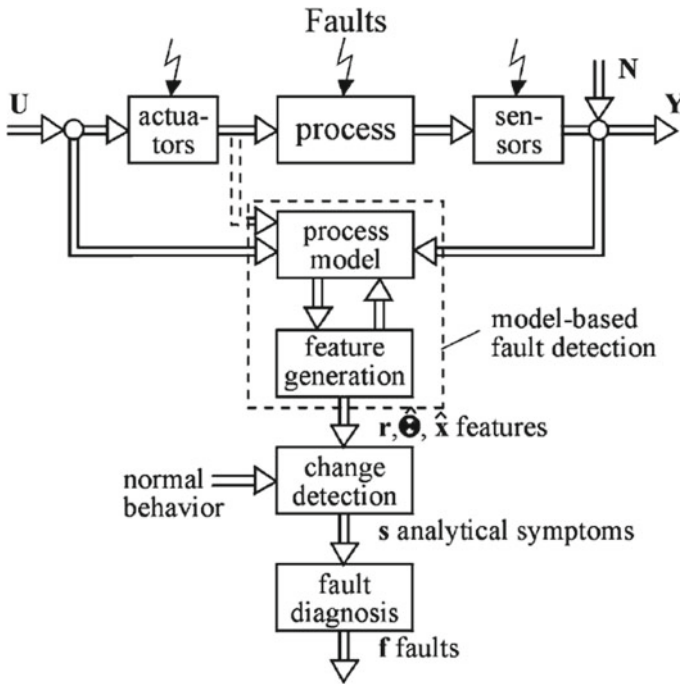


Fig. 4.7 General layout of FDD for power system (Isermann 2005a, b)

### 4.3.3 Fault Location Identification

The FD is about fault classification as well as determination of fault location. The precision of fault location would specify the time required for restoring the system. The Fault impedance calculation formula on different faults is shown in Table 4.3.

### 4.3.4 Errors in Fault Location for Various Faults

From the simulation data, the Actual Distance (AD) is known and the measured distance (MD) is computed from fault data. Then the % error is computed using Eq. (4.1) and listed as shown in Table 4.4a-c,

**Table 4.3** Fault impedance calculation formula on different faults

Fault type	Fault impedance $Z_f$ in $\Omega$
AG	$V_A/(I_A + kI_0)$
BG	$V_B/(I_B + kI_0)$
CG	$V_C/(I_C + kI_0)$
AB or ABG	$(V_A - V_B)/(I_A - I_B)$
BC or BCG	$(V_B - V_C)/(I_B - I_C)$
CA or CAG	$(V_C - V_A)/(I_C - I_A)$

$$\%Error = \frac{(AD - MD)}{AD} \times 100 \quad (4.1)$$

The above tables show that the %error ranges between  $-1.63$  and  $4.02$  with secondary values obtained from RC, while with CT it ranges between  $-5.62$  and  $-52.3$ . The error with CT is varying over a large range as it is dependent on two parameters (magnitude of fault current and the DC component). The fault current is determined by fault type and fault resistance while the DC component depends on Fault Inception Angle (FIA) with the faulty phase and is highest when fault occurs at zero current and minimum when fault occurs at maximum current. But with RC, the error is independent of FIA, as the DC component is eliminated in its output and hence the variation of error was less.

#### 4.4 Intelligent Optimization Techniques Based Fault Detection

This section provides the optimization algorithm used in FDD methods applied to a power system applications. This considers the technique employed, noise sensitivity, classification efficiency and disturbances which detects the normal condition, the outer race fault, the inner race fault, and the presence of both the inner and outer race faults. The vibration of the transformer is measured and optimization techniques are applied for the diagnosis of these faults (Jalayer et al. 2021). The classification of metaheuristic algorithms is shown in Fig. 4.8

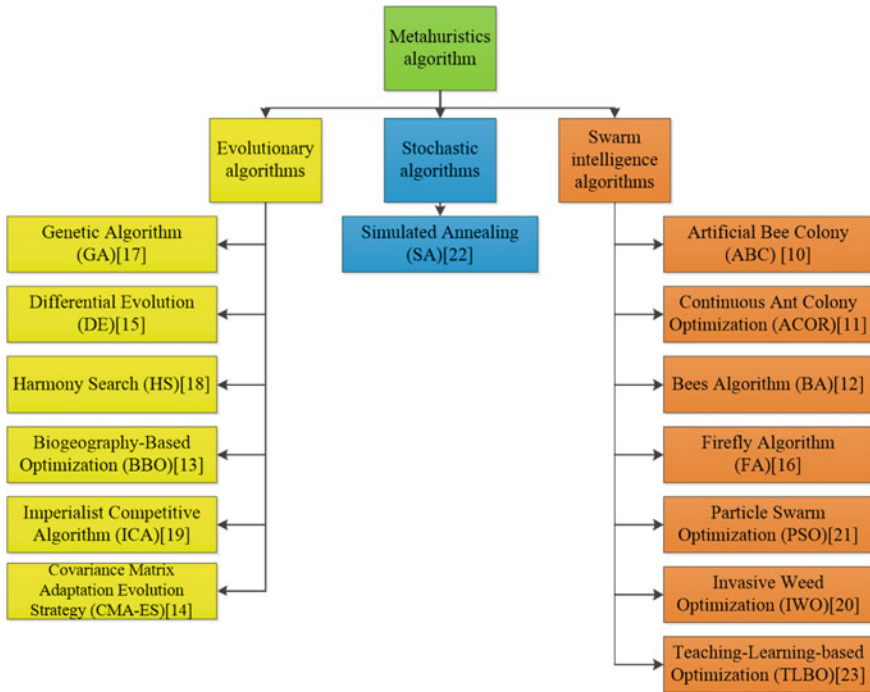
The pattern of these energy values is studied for different fault distances, fault resistances and fault inception angle to arrive at a logic for fault classification. The various techniques employed in power systems is shown in Table 4.5.

Intelligent optimization technique is one of the important data processing methods for solving complicated non-linear system problems and it plays a key role in defect detection and prediction. However, there have been few detailed assessments of computational intelligence's ongoing efforts in machinery status monitoring and problem diagnostics. This presents an overview of contemporary computational intelligence research and progress in defect detection, prediction, and optimal sensor

**Table 4.4** **a** Fault distances and error for LG fault. **b** Fault distances and error for LLG fault. **c** Fault distances and error for LL fault

Fault type	AD (Km)	MD with CT (Km)	% error with CT	MD with RC (Km)	% error with RC
<b>(a)</b>					
AG	30	33.63	-12.1	30.14	-0.48
	50	53.89	-7.78	50.12	-0.25
	80	86.32	-7.90	80.30	-0.37
BG	30	32.02	-6.76	29.81	0.60
	50	53.56	-7.13	49.65	0.69
	80	85.37	-6.72	80.03	-0.04
CG	30	31.68	-5.62	30.28	-0.93
	50	53.18	-6.37	50.27	-0.54
	80	84.72	-5.90	77.76	2.79
<b>(b)</b>					
ABG	30	45.41	-51.3	29.23	2.54
	50	70.29	-40.5	50.73	-1.47
	80	121.8	-52.3	79.80	0.23
BCG	30	32.23	-7.45	30.25	-0.71
	50	53.51	-7.03	49.95	0.18
	80	85.71	-7.14	80.10	-0.15
CAG	30	42.31	-41.0	30.49	-1.63
	50	70.12	-40.2	50.19	-0.38
	80	120.7	-50.9	76.77	4.02
<b>(c)</b>					
AB	30	41.90	-39.6	30.49	-1.66
	50	69.48	-38.9	51.65	-3.31
	80	112.2	-40.3	80.40	-0.51
BC	30	32.56	-8.55	29.97	0.08
	50	53.99	-7.98	50.05	-0.10
	80	85.89	-7.36	80.10	-0.13
CA	30	42.21	-40.7	30.05	-0.18
	50	73.56	-47.1	48.50	2.99
	80	121.7	-52.1	78.74	1.57

placement (Isermann 2005b). The benefits and drawbacks of computational intelligence approaches in real-world applications are explored. Different algorithms' features are contrasted, and application scenarios for these techniques are presented. The different methodologies of fault analysis and fault diagnosis techniques for power systems are shown in Table 4.6a, b.



**Fig. 4.8** Classification of metaheuristic algorithms

The development of computational intelligence has the following problems:

- i. There is a lack of an analytical foundation for computational intelligence approaches. Although NN has a theoretical base that is almost perfect, Evolutionary Algorithms (EA) do not yet have a mathematical foundation that is almost perfect. Theoretical investigations on stability, efficiency and convergence are still in the early stages of development. If researchers have a strong knowledge of the algorithm process and computational intelligence, these methods may be used correctly rather than impulsively for condition monitoring and defect diagnostics.
- ii. Fault Signals that have been identified and also utilized to validate the efficiency of intelligent optimization approaches are problematic to use in real time application. To FDD and intelligent optimization approaches should be further researched and developed.
- iii. These intelligent optimization algorithms require a long time to develop for FDD and its enhanced methodologies are based on an iterative process. As an outcome, future new research should focus on the implementation of intelligent optimization techniques-based on an online mode for power system monitoring and FDD.

**Table 4.5** Various techniques employed in power systems

Related papers	Technique employed	Noise sensitivity	Classification efficiency	Disturbances considered
He et al. (2009)	EDMRA	Not noise sensitive	Not specified	Swell, sag, with low frequency and high frequency distortion
Vanchinathan et al. (2022)	Energy spectrum	Noise sensitive	93%	Swell & sag
Saxena et al. (2010)	Multilevel wavelet transformation	Noise sensitive	Not specified	All disturbances
Kim and Katipamula (2018)	Energy deviation of disturbance signal	Noise sensitive	Not specified	Sag, swell, transient and harmonics
He et al. (2009)	DWT & PNN	Noise sensitive	94.6%	Sag, swell, capacitor switching, under and over voltage
Khalastchi and Kalech (2018)	MRA & ANN	Noise sensitive	Not specified	Swell for different time duration
Saxena et al. (2010)	Comparison b/w db4 & statistical computation	Noise sensitive	Not specified	Sag, swell, momentary interruption, transients
Abid et al. (2021)	MRA & statistical computation	Noise sensitive	Not specified	Sag, swell, momentary interruption, transients, notches
Isermann (2005a)	SVM	Noise sensitive	94% improvised to 97%	Sag, swell, outage, harmonics

An efficient organized FDD for transmission line in power systems using various intelligent optimization techniques such as ANN, WT, Hybrid—WT and RBFNN, Fuzzy inference system SVM, PCA for fault analysis and traveling wave-based, time frequency domain approaches for fault localization are presented. These methods are enhancing the reliability, robustness and transient characteristics of the transmission line in power systems.

## 4.5 Conclusion

This chapter presented a detailed review of various optimization algorithms for fault detection and diagnosis in power systems. From the detailed literature studies, it was found that the fault detection under overload conditions was highly challenging. The different optimization algorithms were developed for FDD to fault identification in

**Table 4.6 a** Different methodologies of fault analysis for power systems. **b** Different fault diagnosis techniques for power systems

Different methodologies of fault analysis	Models	Features	Average error of fault localization in %	Maximum error in %
(a)				
Artificial Neural Network (ANN) (Belagoune et al. 2021)	Input layer, hidden layer and output layer	Weight update and ANN structure development	1.427	7%
Wavelet transform (Fan et al. 2021)	The output waveform is analyzed and the frequency based fault transient signals is determined	Different levels of decomposition	0.217%	3%
Hybrid—WT and ANN (Aleem et al. 2015)	As modified, wavelet analysis was used in the development of a power system failure analyzer	Different transmission methods require an adjustable threshold level and no additional adjustments	0.6665%	0.35%
RBFNN for fault analysis (Chen et al. 2016)	Three layers similar to the ANN architecture	For fault location estimate, a distance relaying system is used	1.87%	0.51%
Fuzzy inference system applied in fault analysis (Raza et al. 2020)	Without the need for ANN or wavelet analysis	To obtain fast and accurate location outcomes	0.9842%	0.720%
Hybrid—WT, ANN, fuzzy logic inference and SVM (Isermann 2005b)	Fuzzy logic, WT, and ANN	For power transmission fault analysis, a wavelet fuzzy integrated methodology is used	0.76%	0.152%

(continued)

the power system under overload conditions resulting in small amount of average error. The hybrid WT and ANN algorithms are used to improve and accelerate future analysis of large multivariate data by reducing it to the most significant directions. The hybrid algorithms are primarily used to improve the accuracy in fault detection and minimizing the harmonic in fault locations. It is also evident that the error obtained with RC is very much lower in comparison with the error obtained with CT. Hence,



**Table 4.6** (continued)

Different methodologies of fault analysis	Models	Features	Average error of fault localization in %	Maximum error in %
SVM for fault analysis (Rafati et al. 2022)	Efficient and systematic	Both for training and testing, a wide and variety of data collection is required	0.7%	0.015%
Principal component analysis (Venkatasubramanian et al. 2003)	To determine the directions of variance in a collection of signals	To improve and accelerate future analysis of large multivariate data by reducing it to the most significant directions	2.7%	0.574%
Traveling wave-based analysis (Vanchinathan et al. 2021b)	The very first incident wave and subsequent reflections from the fault's occurrence location	For the planned 200 km line, the maximum localization error is even smaller than 270 m	0.65%	0.15%
Time–frequency domain approaches for fault localization (Taheri et al. 2021)	The most crucial details about the fault type and location	The first fault generated harmonic obtained	1.369%	0.64%

(b)

<i>Fault diagnosis techniques</i>	<i>Technique 1</i>	<i>Technique 2</i>	<i>Technique 3</i>	<i>Technique 4</i>
Prominent techniques (Kumarasamy et al. 2021)	Wavelet transformation-based analysis	Artificial neural network	Fuzzy logic approach	Artificial intelligence
Hybrid techniques (Belagoune et al. 2021)	Hybrid of ANN and fuzzy logic	Hybrid of BA and AI	Hybrid of GA and MGA	Hybrid of bat algorithm and AI

(continued)

the performance of FD is better with RC than with CT for all fault conditions. The presence of various optimization algorithms in FDD providing improved monitoring, operation, control and protection in the power system.

**Table 4.6** (continued)

Different methodologies of fault analysis	Models	Features	Average error of fault localization in %	Maximum error in %
Modern techniques (Vanchinathan et al. 2021a)	Support vector machine	Artificial intelligence	Phasor measurement unit	Principal component analysis

## References

- AbdulMawjood K, Refaat SS, Morsi WG (2018) Detection and prediction of faults in photovoltaic arrays: a review. In: 2018 IEEE 12th international conference on compatibility, power electronics and power engineering (CPE-POWERENG 2018), April 2018. IEEE, pp 1–8
- Abid A, Khan MT, Iqbal J (2021) A review on fault detection and diagnosis techniques: basics and beyond. *Artif Intell Rev* 54(5):3639–3664
- Aleem SA, Shahid N, Naqvi IH (2015) Methodologies in power systems fault detection and diagnosis. *Energy Syst* 6(1):85–108
- Belagoune S, Bali N, Bakdi A, Baadji B, Atif K (2021) Deep learning through LSTM classification and regression for transmission line fault detection, diagnosis and location in large-scale multi-machine power systems. *Measurement* 177:109330
- Chen H, Jiang B (2019) A review of fault detection and diagnosis for the traction system in high-speed trains. *IEEE Trans Intell Transp Syst* 21(2):450–465
- Chen K, Huang C, He J (2016) Fault detection, classification and location for transmission lines and distribution systems: a review on the methods. *High Volt* 1(1):25–33
- Chen Z, Chen Y, Wu L, Cheng S, Lin P (2019) Deep residual network based fault detection and diagnosis of photovoltaic arrays using current-voltage curves and ambient conditions. *Energy Convers Manage* 198:111793
- Fan C, Liu X, Xue P, Wang J (2021) Statistical characterization of semi-supervised neural networks for fault detection and diagnosis of air handling units. *Energy Build* 234:110733
- Gangsar P, Tiwari R (2020) Signal based condition monitoring techniques for fault detection and diagnosis of induction motors: a state-of-the-art review. *Mech Syst Signal Process* 144:106908
- Harrou F, Sun Y, Taghezouit B, Saidi A, Hamlati ME (2018) Reliable fault detection and diagnosis of photovoltaic systems based on statistical monitoring approaches. *Renew Energy* 116:22–37
- He H, Shen X, Starzyk JA (2009) Power quality disturbances analysis based on EDMRA method. *Int J Electr Power Energy Syst* 31(6):258–268
- Isermann R (2005a) *Fault-diagnosis systems: an introduction from fault detection to fault tolerance*. Springer Science & Business Media
- Isermann R (2005b) Model-based fault-detection and diagnosis—status and applications. *Annu Rev Control* 29(1):71–85
- Jalayer M, Orsenigo C, Vercellis C (2021) Fault detection and diagnosis for rotating machinery: a model based on convolutional LSTM, Fast Fourier and continuous wavelet transforms. *Comput Ind* 125:103378
- Khalastchi E, Kalech M (2018) On fault detection and diagnosis in robotic systems. *ACM Comput Surv (CSUR)* 51(1):1–24
- Kim W, Katipamula S (2018) A review of fault detection and diagnostics methods for building systems. *Sci Technol Built Environ* 24(1):3–21
- Kumarasamy V, Ramasamy VK, Chinnaraj G (2021) Systematic design of multi-objective enhanced genetic algorithm optimized fractional order PID controller for sensorless brushless DC motor drive. *Circuit World*

- Li B, Delpha C, Diallo D, Migan-Dubois A (2021) Application of artificial neural networks to photovoltaic fault detection and diagnosis: a review. *Renew Sustain Energy Rev* 138:110512
- Mariano-Hernández D, Hernández-Callejo L, Zorita-Lamadrid A, Duque-Pérez O, García FS (2021) A review of strategies for building energy management system: model predictive control, demand side management, optimization, and fault detect & diagnosis. *J Build Eng* 33:101692
- Mellit A, Tina GM, Kalogirou SA (2018) Fault detection and diagnosis methods for photovoltaic systems: a review. *Renew Sustain Energy Rev* 91:1–17
- Pillai DS, Rajasekar N (2018) A comprehensive review on protection challenges and fault diagnosis in PV systems. *Renew Sustain Energy Rev* 91:18–40
- Rafati A, Shaker HR, Ghahghahzadeh S (2022) Fault detection and efficiency assessment for HVAC systems using non-intrusive load monitoring: a review. *Energies* 15(1):341
- Raza A, Benrabah A, Alquthami T, Akmal M (2020) A review of fault diagnosing methods in power transmission systems. *Appl Sci* 10(4):1312
- Saxena D, Verma K, Singh S (2010) Power quality event classification: an overview and key issues. *Int J Eng Sci Technol* 2(3):186–199
- Taheri S, Ahmadi A, Mohammadi-Ivatloo B, Asadi S (2021) Fault detection diagnostic for HVAC systems via deep learning algorithms. *Energy Build* 250:111275
- Vanchinathan K, Valluvan KR, Gnanavel C, Gokul C, Renold RA (2021a). An improved incipient whale optimization algorithm based robust fault detection and diagnosis for sensorless brushless DC motor drive under external disturbances. *Int Trans Electr Energy Syst* e13251
- Vanchinathan K, Sathiskumar P, Selvaganesan N (2021b) A metaheuristic optimization algorithm-based speed controller for brushless DC motor: industrial case study. In: *Metaheuristic algorithms in industry 4.0*. CRC Press, pp 189–216
- Vanchinathan K, Valluvan KR, Gnanavel C, Gokul C (2021) Design methodology and experimental verification of intelligent speed controllers for sensorless permanent magnet Brushless DC motor. *Int Trans Electr Energy Syst* e12991. <https://doi.org/10.1002/2050-7038.12991>
- Vanchinathan K, Selvaganesan N (2021) Adaptive fractional order PID controller tuning for brushless DC motor using artificial bee colony algorithm. *Results Control Optim* 4:100032
- Vanchinathan K, Valluvan KR (2018) A metaheuristic optimization approach for tuning of fractional-order PID controller for speed control of sensorless BLDC motor. *J Circuits Syst Comput* 27(08):1850123
- Vanchinathan K, Valluvan KR, Gnanavel C, Gokul C (2022) Numerical simulation and experimental verification of fractional-order PI $\lambda$  controller for solar PV fed sensorless brushless DC motor using whale optimization algorithm. *Electric Power Components Syst* 50(1–2):64–80
- Venkatasubramanian V, Rengaswamy R, Yin K, Kavuri SN (2003) A review of process fault detection and diagnosis: part I: quantitative model-based methods. *Comput Chem Eng* 27(3):293–311
- Wang H, Peng MJ, Yu Y, Saeed H, Hao CM, Liu YK (2021) Fault identification and diagnosis based on KPCA and similarity clustering for nuclear power plants. *Ann Nucl Energy* 150:107786
- Zhang P, Shu S, Zhou M (2018) An online fault detection model and strategies based on SVM-grid in clouds. *IEEE/CAA J Autom Sinica* 5(2):445–456
- Zhao Y, Zhang C, Zhang Y, Wang Z, Li J (2020) A review of data mining technologies in building energy systems: load prediction, pattern identification, fault detection and diagnosis. *Energy Built Environ* 1(2):149–164

# Chapter 5

## Prediction of Surface Roughness Using Desirability Concept and Support Vector Machine for Fused Deposition Modeling Part



Vijaykumar Jatti, Vinaykumar Jatti, Pawandeep Dhall,  
and Akshaykumar Patel

**Abstract** Fused Deposition Modeling (FDM) technique involves the deposition of a fused layer of material according to the geometry designed in the software. The quality of parts produced by FDM is greatly affected by several parameters. This study investigates the effect of printing speed, layer thickness, extrusion temperature and infill percentage on the surface roughness of parts. An approach based on Response Surface Methodology (RSM) and Design of Experiments (DOE) will lead to a reduction in the significant number of experimental runs. Specimens are prepared for surface roughness test. Optimum values of process parameters are determined using desirability concept and which gives the minimum surface roughness of the FDM printed part. Support vector machine predicted almost the same actual surface roughness value with a mean squared error of 7.186.

**Keywords** Additive manufacturing · Response surface methodology · Surface roughness · Desirability concept · Support vector machine

### 5.1 Introduction

Fused deposition modelling is an additive manufacturing technology in which the mechanical and surface properties obtained should be as comparable to the conventional injection moulding process. Torres et al. employed the Taguchi method, regression analysis and ANOVA during PLA parts printing by considering input

---

V. Jatti (✉) · V. Jatti  
Symbiosis Institute of Technology, Pune, Maharashtra, India  
e-mail: [vijaykumar.jatti@sitpune.edu.in](mailto:vijaykumar.jatti@sitpune.edu.in)

V. Jatti  
e-mail: [vinay.jatti@sitpune.edu.in](mailto:vinay.jatti@sitpune.edu.in)

P. Dhall · A. Patel  
D.Y. Patil College of Engineering, Akurdi, Pune, Maharashtra, India

parameters as layer thickness, post-processing (heat treating) time and infill density. Responses considered in the study are yield strength, shear strength, fracture strain, shear modulus and proportional limit (Torres et al. 2015). Laeng et al. used Taguchi Method, ANOVA and S/N ratio to optimize the throwing distance of a FDM printed Bow with input parameters as layer thickness, raster width and print velocity during ABS part printing (Laeng et al. 2006). Liu et al. used Taguchi method, ANOVA, Gray relation analysis, S/N ratio to optimize the flexural strength, impact strength and tensile strength while PLA parts printing considers process parameters as layer thickness, raster width, air gap, raster angle (raster orientation) and build orientation (Liu et al. 2017). Numerous studies have been conducted to study the effect of process parameters on the fused deposition modelling parts mechanical and surface properties (Masood et al. 2010; Hossain et al. 2013; Lanzotti et al. 2015; Rodríguez-Panes et al. 2018; Wang et al. 2017; Tymrak et al. 2014). Equbal et al. optimize the raster orientation and layer thickness using the Taguchi method during FDM parts printing (Equbal et al. 2017).

Literature depicts that a close control over process parameters results into comparable mechanical and surface properties with injection moulded parts. There is a scatter of process parameters over a large range which results into best mechanical and surface properties. This requires significant experimentation to identify the influencing parameters. Hence, in this study desirability concept and support vector machine have been employed. The experimental layout has been designed using response surface methodology of design of experiments concept. The optimal value of surface roughness was obtained based on the desirability concept. Additionally, a predictive model was developed to determine and check the surface roughness values using support vector machines. This chapter is organized as with Sect. 5.2 on materials and methods, Sect. 5.3 on results and discussion, Sect. 5.4 on conclusion.

## 5.2 Materials and Methods

With FDM printing, a model is generated on CAD software, which is then converted into STL files for stereolithography. Three-dimensional surfaces are represented in this file as an assembly of planar triangles. A greater number of triangles will ensure better accuracy. Once the STL file has been converted, the slicing process involves steps such as describing the part 3D, dividing the parts into slices, and determining the support material and path as well as the angle of the tool. Various parameters are set in the STL file to specify how the machines, such as the nozzle, heater, etc., will operate in various layers. A Creality Ender 3 machine with a bed size of  $220 \times 220 \times 250$  mm was used to create the FDM samples. The part was designed using CATIA software and converted into an STL file, which was sliced into machine-readable g-code files using the Cura engine of the Repetier software. The material used to create the specimen is Polylactic Acid (PLA) which is commonly used for FDM processed parts. The DOE factors considered are shown in Table 5.1.

**Table 5.1** Input parameters and its level

Input parameters	Levels of input parameters
Layer thickness (mm)	0.08, 0.16, 0.24, 0.32 and 0.4
Print speed (mm/s)	20, 35, 50, 65 and 80
Extrusion temperature (°C)	190, 200, 210, 220, and 230
Infill percentage (%)	10, 33, 55, 78 and 100

### 5.3 Results and Discussion

Table 5.2 depicts the 31 trial conditions for conduction of experiments as per response surface methodology along with observed surface roughness values.

Figure 5.1 depicts the effect of input parameters on surface roughness of FDM printed parts, and it can be seen that layer height and print speed largely influence the surface roughness. 3D printing is a layer-by-layer process and hence it produces a step like effect on the finished parts. Various post processing techniques need to be used to improve the overall quality of the part. This step like effect results in surface roughness. Increase in layer height increases the step effect and thus increases the surface roughness. Surface roughness also increases the surface roughness as at greater speed, and improper distribution of material causes a wavy surface and also results in change of cross sections. If the parameters are set such as the layer thickness and printing speed both are kept at its maximum, the part will be printed faster than ever but it will give the worst surface finish. Also, with lowest layer height and print speed, the layer will completely solidify before the second layer could be deposited and hence there will be inadequate adhesion resulting in moderate surface finish and this also increases the printing time. Hence, to get better quality of the product, one can use moderate layer thickness and printing speed and hence combination of process parameters is needed to balance the surface roughness, printing time as well cost of part. Surface roughness almost remains constant with increase in Extrusion temperature. But higher value of extrusion temperature along with the moderate value of layer thickness reduces the surface roughness drastically. There is almost a negligible effect of infill percentage on surface roughness of parts fabricated. Using RSM desirability approach, the combination of process parameters is been found out where we get the optimum value of surface roughness, refer Fig. 5.2. FDM processed parts are again fabricated using these parameters for surface roughness test that were carried out to validate the results obtained. The validations readings are shown in Table 5.3.

A heat map is created to understand the effect of FDM input parameters on surface roughness, as seen from Fig. 5.3. In a heat map, colours represent the values in data, and on a two-dimensional representation, the values are shown as lines. The heatmap provides an immediate visual summary of information about the nature of the relation between the target and features, so we can easily refer to the relationships between the targets and features using the heatmap. Heatmaps with more elaborate graphical capabilities can be used to present complex data sets in a more engaging way. It is

**Table 5.2** Trail conditions and observed values

Experiments	Infill percentage	Layer height (mm)	Print speed	Extrusion temp (°C)	Surface roughness (µm)
1	78	0.32	35	220	14.96
2	10.5	0.24	50	210	19.86
3	33	0.16	35	220	5.45
4	33	0.32	35	200	18.95
5	33	0.16	65	200	15.30
6	100.5	0.24	50	210	15.27
7	78	0.16	35	200	15.48
8	33	0.32	65	200	19.91
9	78	0.32	65	200	23.30
10	33	0.16	65	220	15.46
11	78	0.16	35	220	16.74
12	55.5	0.24	50	210	8.60
13	33	0.32	35	220	22.00
14	55.5	0.24	50	190	9.44
15	55.5	0.24	50	210	13.71
16	78	0.32	65	220	20.60
17	55.5	0.24	50	210	10.84
18	55.5	0.24	50	210	10.53
19	55.5	0.24	50	230	8.87
20	33	0.32	65	220	22.5
21	55.5	0.24	50	210	12.93
22	55.5	0.24	80	210	9.52
23	78	0.16	65	200	15.99
24	55.5	0.24	20	210	14.80
25	55.5	0.08	50	210	14.51
26	55.5	0.4	50	210	19.65
27	55.5	0.24	50	210	14.96
28	78	0.32	35	200	12.7
29	55.5	0.24	50	210	12.00
30	78	0.16	65	220	15.9
31	33	0.16	35	200	15.48

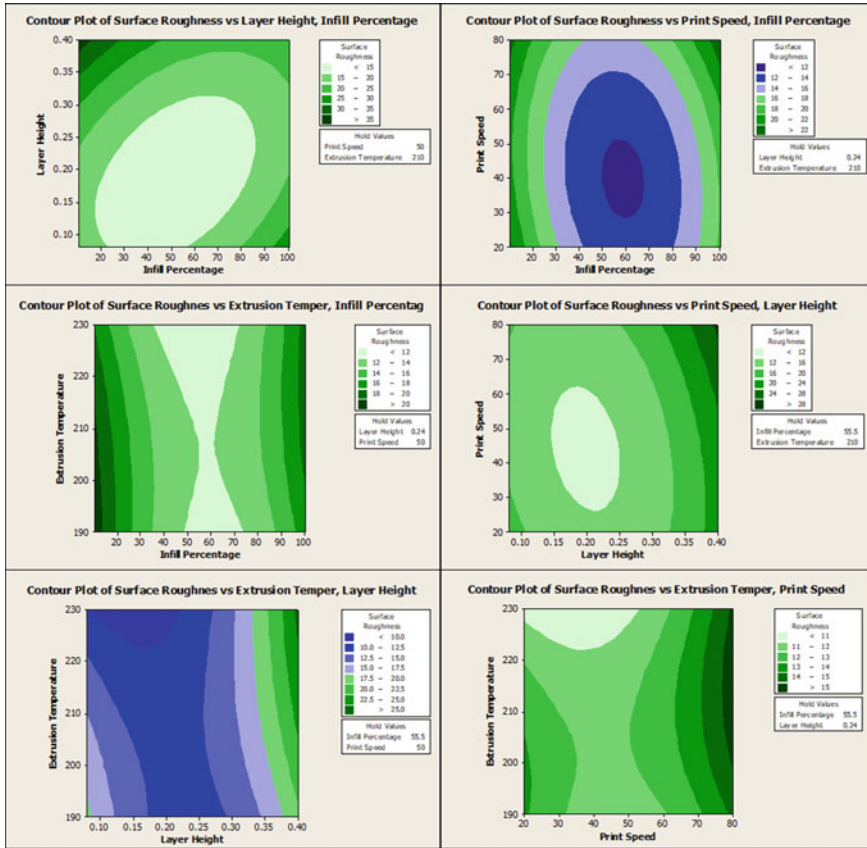


Fig. 5.1 Effect of process parameters on surface roughness

worth noting that the values seen on a heatmap refer to coefficients of correlation between two variables, which represents the relationship between them directly. For an explanation of the direction of the relation, refer Table 5.4. According to the data gathered from one source, a heatmap will be created and plotted according to that data.

For using support vector machine firstly data is divided into the training set and testing set manually. In the data set for the training process, there are twenty data points. In addition, there are eleven data points which was used for testing purposes.

From training data it is visible that all the values for surface roughness fluctuate around 15. Since we are applying Support vector regression to predict the values of surface roughness, the hyperplane for SVR also lie near 15. Hence after prediction it is clear that the values of hyperplane is around the net value of 15, which can be seen in the array given below. This array includes the predicted values of surface roughness using support vector regression for the features in testing dataset.



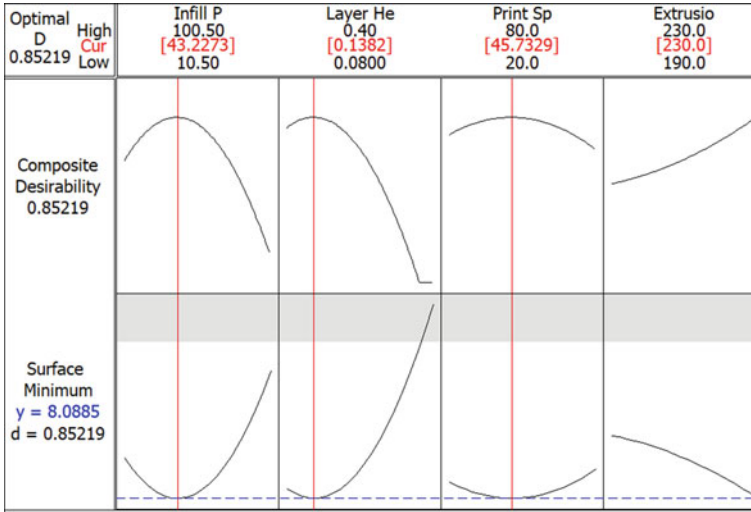


Fig. 5.2 Values of process parameters to obtain optimum surface roughness

Table 5.3 Validation experiments

Property	RSM desirability approach	Experimental
Surface roughness ( $\mu\text{m}$ )	8.0885	8.954

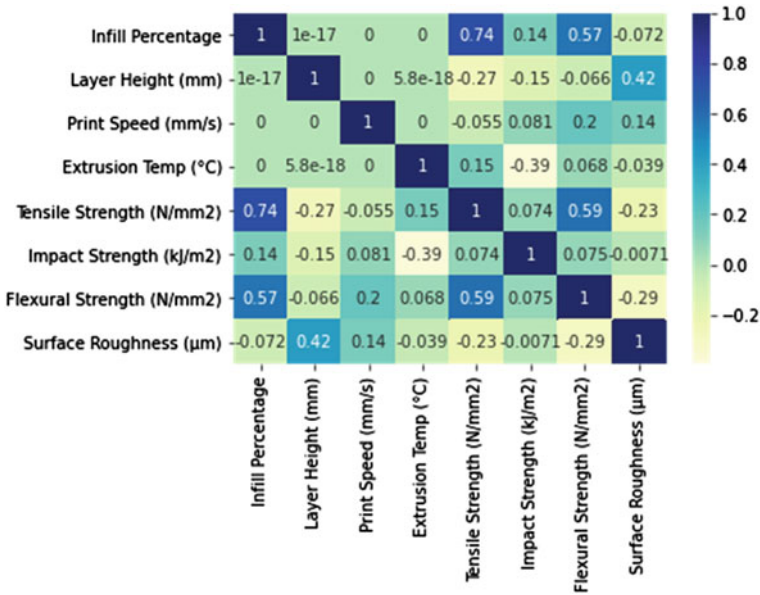


Fig. 5.3 Heat map using the experimental values

**Table 5.4** Correlation coefficient value and meaning

Correlation coefficient value	Correlation type	Meaning
1	Perfect positive correlation	When one variable changes, the others change in the same direction
0	Zero correlation	There is no relationship between the variables
-1	Perfect negative correlation	When one variable changes, the other variables change in the opposite direction

Array ([15.36282615, 15.40514157, 15.36688051, 15.34004093, 15.36282156, 15.36283114, 15.36282615, 15.33369683, 15.36282615, 15.35254443, 15.40131848]).

These values are then compared with the actual values from the testing dataset and we got mean squared error up to 7.186 which is quite acceptable.

### 5.4 Conclusions

In this study, surface roughness properties of 3D printed specimens are presented. Process parameters such as extrusion temperature, print speed, infill percentage and layer height have been examined for their effect on surface roughness. It has been found that greater layer height and print speed results in greater surface roughness. Eventually, optimum values of surface roughness were found out using the desirability approach and were validated experimentally. Optimum surface roughness can be obtained at infill percentage, layer height, print speed and extrusion temperature that are set at 43.22%, 0.0962 mm, 20 mm/s and 230 °C, respectively. A mean squared error of 7.186 was obtained by the support vector machine during prediction of the surface roughness value.

### References

Eqbal A, Sood AK, Ansari AR, Eqbal MA (2017) Optimization of process parameters of FDM part for minimizing its Dimensional inaccuracy. *Int J Mech Prod Eng Res Dev* 7:57–66

Hossain MS, Ramos J, Espalin D, Perez M, Wicker R (2013) Improving tensile mechanical properties of FDM-manufactured specimens via modifying build parameters. *Solid Free Fabr Proc* 380–392

Laeng J, Khan ZA, Khu S (2006) Optimizing flexible behaviour of bow prototype using Taguchi approach. *J Appl Sci* 6:622–630

Lanzotti A, Grasso M, Staiano G, Martorelli M (2015) The impact of process parameters on mechanical properties of parts fabricated in PLA with an open-source 3-D printer. *Rapid Prototyp J* 221:604–617

- Liu X, Zhang M, Li S, Si L, Peng J, Hu Y (2017) Mechanical property parametric appraisal of fused deposition modeling parts based on the gray Taguchi method. *Int J Adv Manuf Technol* 89:2387–2397
- Masood S, Mau K, Song W (2010) Tensile properties of processed FDM polycarbonate material. *Mater Sci Forum* 654–656:2556–2559
- Rodríguez-Panes A, Claver J, Camacho AM (2018) The influence of manufacturing parameters on the mechanical behaviour of PLA and ABS pieces manufactured by FDM: a comparative analysis. *Materials* 11:1333–1353
- Torres J, Cotelo J, Karl J, Gordon AP (2015) Mechanical property optimization of FDM PLA in shear with multiple objectives. *JOM* 67:1183–1193
- Tymrak BM, Kreiger M, Pearce JM (2014) Mechanical properties of components fabricated with open-source 3-D printers under realistic environmental conditions. *Mater Des* 58:242–246
- Wang L, Gramlich WM, Gardner DJ (2017) Improving the impact strength of Poly(lactic acid) (PLA) in fused layer modeling (FLM). *Polymer* 114:242–248

# Chapter 6

## An Extremum Model for the Performance Analysis of a Loop Heat Pipe Using Nano-fluids



Jobin Jose and Tapano Kumar Hotta

**Abstract** Steady-state experiments are carried out to predict the thermal performance of a loop heat pipe using the Copper–Water Nano-fluid with 1% concentration. Deionised water is considered as the baseline case for the comparison. The studies are performed for varied heat loads of 30–270 W. The cooling water is supplied at 20 °C with a flow rate of 40 L/h. A parametric study is carried out for the thermal resistance, evaporator temperature and interface temperature of the heat pipe that affects its performance. The results highlight a notable enhancement in the thermal characteristics of the heat pipe using the Nano-fluids in comparison to the baseline case. The evaporator temperature and the thermal resistance of the heat pipe are reduced by 30% and 17%, respectively using the Nano-fluids. An extremum model is used to predict the minimum evaporator temperature of the heat pipe at the optimal power (heat) input.

**Keywords** Deionised water · Interface temperature · Heat pipe · Nano-fluid · Extremum model

### 6.1 Introduction

Effective cooling is an important parameter for the reliable functioning of electronic equipment. Conventional methods like air and water cooling are incapable of providing sufficient cooling capacity; hence passive cooling techniques like heat pipes are gaining significant importance in recent times. A heat pipe exchanges the heat between two solid contacts through the phase transition. These act as effective thermal conductors due to their increased heat transfer coefficient value for condensation and boiling. The effectual thermal conductivity of the heat pipes varies with the

---

J. Jose · T. K. Hotta (✉)

School of Mechanical Engineering, Vellore Institute of Technology, Vellore 632014, Tamil Nadu, India

e-mail: [tapano.hotta@vit.ac.in](mailto:tapano.hotta@vit.ac.in)

length of the heat pipes, it may reach up to 100 kW/(m. K) compared to 0.4 kW/(m. K) for Copper.

Several studies were performed to analyse the loop heat pipe thermal performance. The experimental studies to predict the thermal characteristics of the wicked heat pipes using Copper Nano-particles of the size of 80–90 nm at different heat inputs of 100, 150 and 200 W were carried out by Solomon et al. (2012). The thermal resistance of these heat pipes is found to be lower than the conventional one (without the wick). Asirvatham et al. (2013) analysed experimentally the thermal characteristics of the heat pipes using Silver-Water Nano-fluid with Silver Nano-particles at three different volume concentrations. They carried out a parameter study for the heat transfer coefficient, thermal resistance, axial temperature, and thermal conductivity of the heat pipes. They concluded that there is a significant reduction in the thermal resistance by 76.2% and the heat transfer coefficient is enhanced to a maximum limit of 52.7% for the 0.009% concentration of Silver Nano-particles. Kumaresan et al. (2014) conducted experiments to compare the thermal characteristics of the heat pipes with sintered wick using CuO-deionized water. They found a maximum drop in the surface temperature for the heat pipe using a sintered wick. It was also observed that the heat pipe evaporator temperature using the Nano-enhanced phase change material (PCM) was reduced by 25.75% than the conventional one. Tharayil et al. (2016) performed experiments on the thermal performance of a loop heat pipe using graphene-water Nano-fluid. The heat load varied between 20 and 380 W and the Nano-particle concentration was between 0.003%, 0.006% and 0.009%. They found that the thermal resistance was reduced by 21.6% and the evaporator interface temperature by 10.3% than the distilled water at the optimum Nano-particle concentration. Krishna et al. (2017) conducted experiments on a heat pipe using Nano-enhanced PCM (Ne-PCM) for electronic cooling. They considered Water, Tricosane and  $\text{Al}_2\text{O}_3$  as the working fluid, PCM and Nano-particle, respectively. The Nano-enhanced PCM was prepared by mixing Tricosane with different volume % of Nano-particles and found that the PCM thermal conductivity was improved by 32% using the Nano-particle as compared to the pure Tricosane. Chernysheva et al. (2014) developed a loop heat pipe for the effective cooling of the supercomputers using the Copper–Water as the working fluid. The parameters considered for the analysis are the condenser cooling temperature that affects the thermal characteristics of the loop heat pipe. The results indicated that the operating temperature doesn't vary significantly with the change in cooling temperature of the condenser below 40 °C; hence these heat pipes are to be used only above 50 °C. Xu et al. (2014) manufactured a loop heat pipe with a disc-shaped evaporator having a transparent cover for observing the flow motion. Three types of Cu-Ni composite wicks were considered for the analysis, i.e.,  $\text{Cu}_5\text{Ni}_{10}$ ,  $\text{Cu}_3\text{Ni}_2$  and  $\text{Cu}_1\text{Ni}_4$ . It was found that the loop heat pipe with  $\text{Cu}_3\text{Ni}_2$  wick was having low evaporator temperature among the three wicks. Wang and Wei (2016) analysed experimentally the characteristics of a novel heat pipe under various conditions. They observed that the major driving force for the heat pipe was the capillary force and vapour pressure. Zhao et al. (2021) carried out experiments on loop heat pipes using cupric oxide Nano-fluids. The evaporator was provided with a porous wick sintered with nickel powder. The results indicated that

there was a significant enhancement in the thermal performance of the heat pipes using the Nano-fluid. The evaporator thermal resistance and wall temperature were also reduced by 17.6% and 12.7 °C, respectively.

The present study uses the Copper–Water Nano-fluid in the loop heat pipe. The goal is to study its thermal performance and compare it with the baseline case. The heat input is varied between 30 and 270 W with a 1% Nano-particle concentration. The schematic layout of the experimental facility, detailed experimental procedure, results and discussion (variation of interface temperature, evaporator temperature and thermal resistance with heat input) along with the development of the extremum model is highlighted in the subsequent sections.

### 6.2 Experimental Setup

The schematic layout of the experimental facility used for the present study is depicted in Fig. 6.1. It consists of a heat pipe, heater assembly, data acquisition system, thermocouples, rotameter and cooling water supply.

The heater assembly is arranged in such a way that a uniform temperature is provided at the evaporator surface. The evaporator is covered by a thick insulation layer to prevent any amount of heat loss from it. For maintaining the required power input, the heater is connected to a dimmerstat. The required current and voltage are measured using a voltmeter and an ammeter, respectively. The cooling water is supplied to the condenser and a chilling unit is provided to maintain the temperature

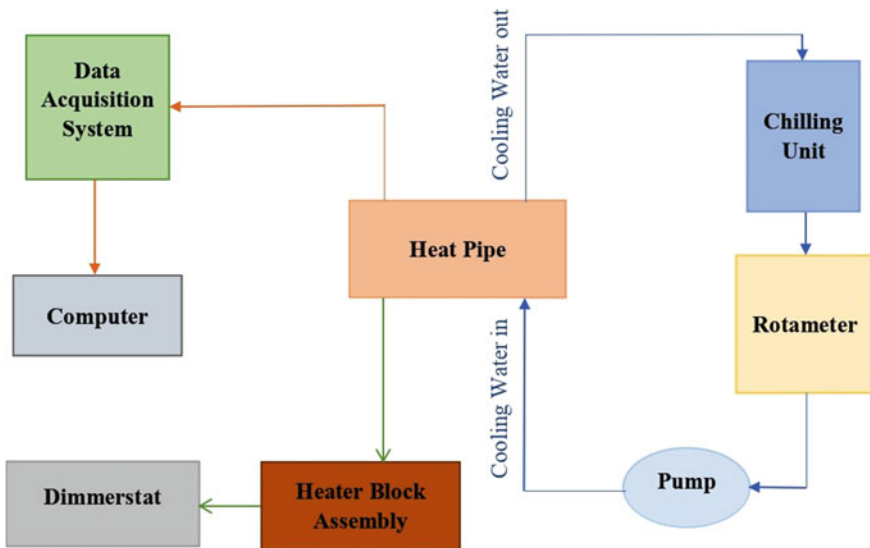


Fig. 6.1 Schematic layout of the experimental facility

**Table 6.1** Specifications of the heat pipe

Component	Specifications (mm)
Evaporator	Length: 35; Width: 35; Height: 12
Condenser	Length: 235; Width:75; Height: 50
Liquid line/Vapor line	Outer diameter: 13; Inner diameter: 11; Length: 475

of the cooling water. A Rotameter is used to regulate the cooling water flow rate supplied to the condenser. Twelve thermocouples are used to measure the temperature at various heat pipe locations. These are connected to the data logger which records the temperature of the heat pipe. A computer is also connected to the data logger to store all the data.

### 6.3 Experimental Procedure

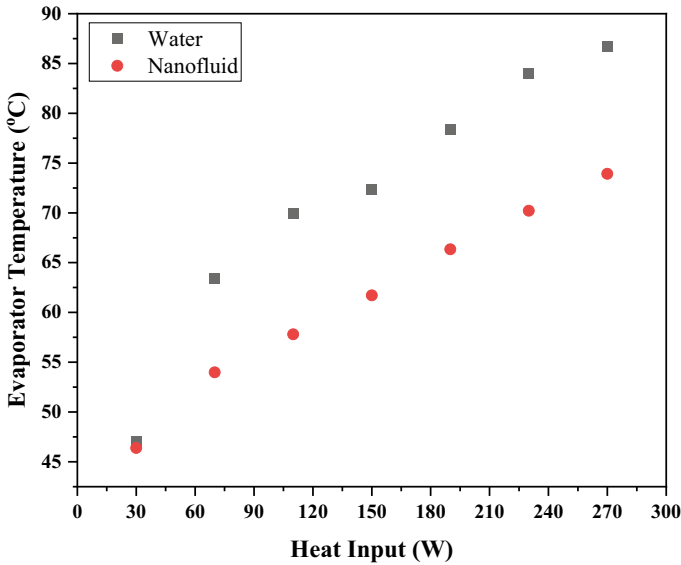
The heat pipe is fabricated as per the specifications mentioned in Table 6.1 and then it is filled with the working fluids (Water/Nano-fluid). The evaporator is connected to the heater and is covered by a thick glass wool insulation layer. Two sets of experiments are conducted; one using water and the other using the Nano-fluid. For both experiments, the heat pipe is positioned in such a way that the condenser will be above the evaporator.

Initially, the cooling water is supplied to the condenser at a flow rate of 40 L/hr and a temperature of 20 °C. The flow rate and temperature are regulated using a rotameter and a chilling unit, respectively. The heat input is then varied between 30 and 270 W. Initially, a heat load of 30 W is supplied to the evaporator using the heater and by adjusting the dimmerstat. Once the steady-state condition has been reached the heat load is then raised in steps of 40 W to reach 270 W. The thermocouples measure the temperature at different heat pipe locations. The data logger is used to record and store the data on the computer.

### 6.4 Results and Discussions

#### 6.4.1 Variation of Evaporator Temperature with Heat Input

The evaporator temperature variation with the heat inputs for two different working fluids (Water and Nano-fluids) is depicted in Fig. 6.2. It is clear that the evaporator temperature of the heat pipe increases with a rise in the heat input for both the working fluids. The maximum evaporator temperatures of the heat pipe using Water and Copper–Water Nano-fluid are found to be 86.68 °C and 73.92 °C, respectively at 280 W. The Nano-fluids help to reduce the evaporator temperature of the heat pipe



**Fig. 6.2** Variation of the evaporator temperature with heat input

for all the heat inputs and a maximum reduction of 17% is achieved at 110 W. This is because, the thermal conductivity of the Nano-fluid is higher than water, which helps to dissipate more heat from the heat pipe. This makes it suitable for the thermal management of electronic devices.

#### **6.4.2 Variation of Interface Temperature with Heat Input**

The variation of interface temperature at the evaporator under the various heat inputs for two different working fluids is shown in Fig. 6.3. It is clear from the Figure that, the interface temperature increases with the rise in heat input. The heat pipe with Copper–Water Nano-fluid is found to have a lower interface temperature value for all the heat loads. The maximum interface temperature of the heat pipe using Water and Nano-fluid is found to be 111.73 °C and 94.13 °C, respectively at 270 W. Due to the increased thermal conductivity value, Nano-fluid helps to reduce the interface temperature of the heat pipe leading to better thermal management.

#### **6.4.3 Variation of Thermal Resistance with Heat Input**

The effect of thermal resistance on the performance of the heat pipe under different heat inputs for two different working fluids is shown in Fig. 6.4.



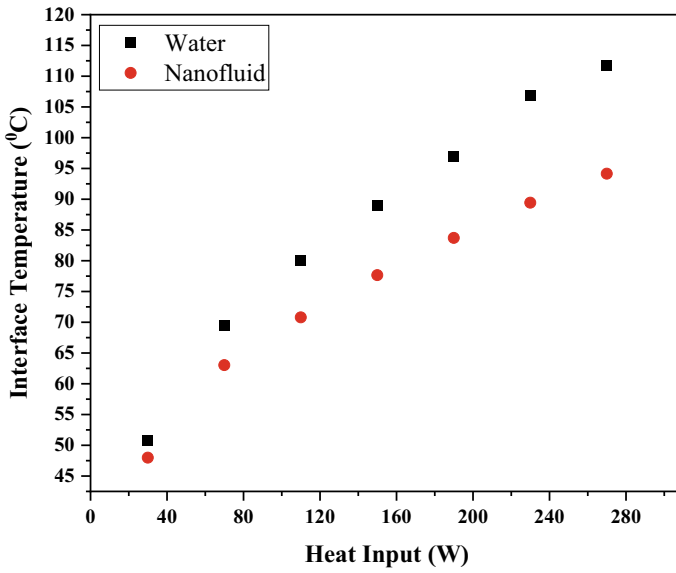


Fig. 6.3 Variation of the interface temperature with heat input

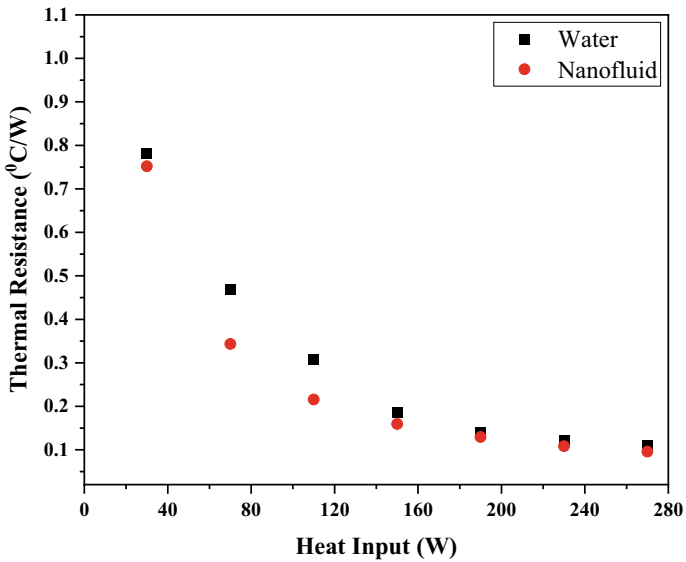


Fig. 6.4 Variation of the thermal resistance with heat input

It is seen that the thermal resistance of the heat pipe falls with an increase in heat input for both working fluids. The Nano-fluid is found to have a lower thermal resistance (a maximum reduction of 30% is obtained at 110 W) than that of Water. It is observed that at the initial heat loads, the thermal resistance is high, as there will be more working fluid in the evaporator and the vapour formation takes place at a lower rate. After a heat load of 70 W, there is a significant drop in thermal resistance due to the higher rate of vapour formation.

#### 6.4.4 Effect of Evaporator and Condenser Temperature Difference on the Heat Input

The temperature variation between the evaporator and condenser ( $T_e - T_c$ ) under various heat inputs for two working fluids is shown in Fig. 6.5. It is seen that the temperature difference between the evaporator and condenser for the loop heat pipe increases for both the working fluids with an increase in heat input. It is observed that the use of Nano-fluid reduces the  $T_e - T_c$  value of the heat pipe for all the heat inputs as compared to the baseline case. A maximum reduction of about 32% is obtained at 110 W.

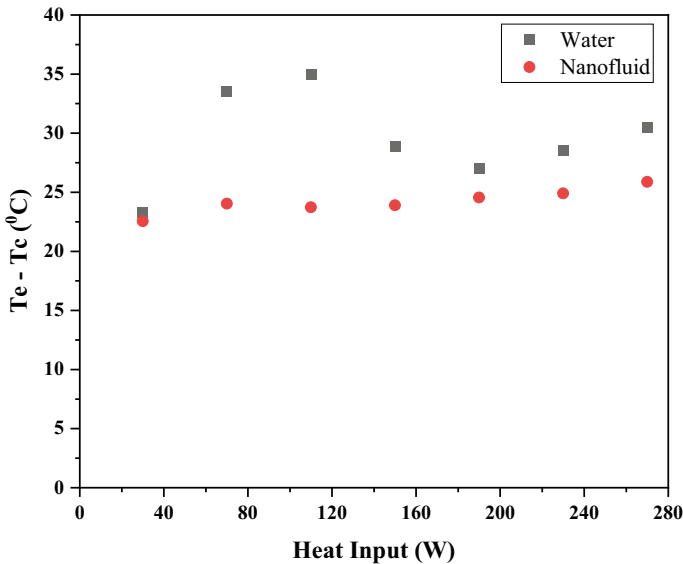


Fig. 6.5 Effect of the evaporator and condenser temperature with heat input

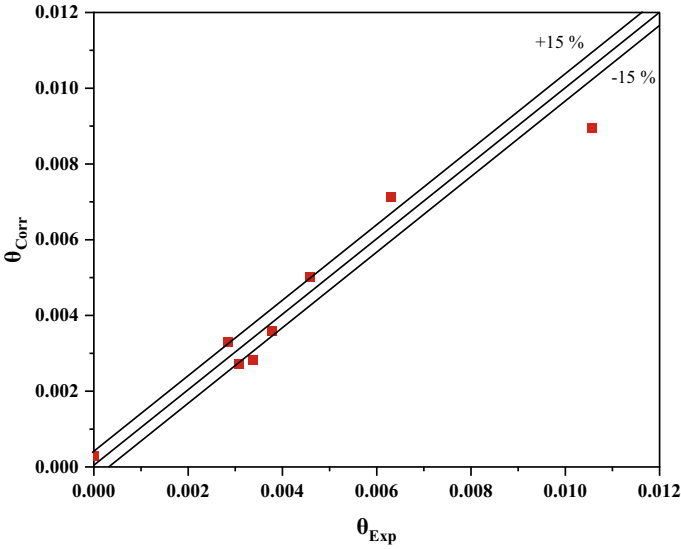


Fig. 6.6 Parity plot

### 6.4.5 Correlation

For the use of the wide heat transfer community and to generalise the results, a correlation is put forth for the non-dimensional evaporator temperature of the heat pipe,  $\theta$  ( $\theta = \frac{T_e - T_\infty}{\Delta T_{ref}}$ , where  $\Delta T_{ref} = \frac{qL}{k}$ ;  $T_e$  is the evaporator temperature, °C;  $T_\infty$  is the ambient temperature, °C;  $\Delta T_{ref}$  is the reference temperature difference, °C;  $q$  is the heat flux, W/m<sup>2</sup>;  $L$  is the heat pipe length, m;  $k$  is the thermal conductivity of the working fluid, W/(m. K)) and non-dimensional heat input,  $Q^*$  ( $Q^* = \frac{Q_{actual}}{Q_{max}}$ , where  $Q_{actual}$  and  $Q_{max}$  are the actual and maximum heat transfer, respectively) for the Nano-fluid. The correlation is valid for 7 data points and has a regression coefficient of 95% with an RMS error of 10%. The correlation is given in Eq. 6.1.

$$\theta = 0.00152(Q^*)^2 - 0.00243(Q^*) + 0.00124 \tag{6.1}$$

A parity plot between the actual and correlated  $\theta$  values shown in Fig. 6.6 suggests that both results agree with an error band of 15%.

### 6.4.6 Extremum Model

An extremum strategy (minima-maxima) is developed to determine the optimal heat load of the heat pipe at which the evaporator temperature is found to be a minimum. It is seen that at a non-dimensional heat load of 0.799, the evaporator temperature is

the minimum. This is converted to the actual value and the actual (optimal) heat load to the heat pipe is found to be 215.73 W at which the minimum obtained evaporator temperature is 29.58 °C.

## 6.5 Conclusion

Steady-state experiments are carried out for the performance analysis of the loop heat pipe under variable heat loads using two different working fluids (Water and Nano-fluid). The following conclusions are obtained from the study.

- The Nano-fluids have enhanced the heat pipe thermal performance.
- The evaporator temperature and the thermal resistance of the heat pipe are reduced by 17% and 30%, respectively by using the Nano-fluid. There is also a significant drop in its interface temperature.
- The maximum interface temperature of the heat pipe is 111.73 °C and 94.13 °C, respectively using Water and Nano-fluid at a heat load of 270 W.
- The difference between the evaporator and condenser temperature is reduced by 32% as compared to the baseline case.
- The extremum model is found to be useful to minimize the evaporator temperature at the optimal heat load.
- The whole idea suggests the thermal management aspects of the heat pipe using the Nano-fluid.

### Scope for Future Studies

- The study can be extended further using the Artificial Intelligence and Machine Learning approach toward the thermal performance of electronic devices.
- Conventional heat pipes can be replaced with wickless ones for better performance.

## References

- Asirvatham LG, Nimmagadda R, Wongwises S (2013) Heat transfer performance of screen mesh wick heat pipes using silver-water nano-fluid. *Int J Heat Mass Transf* 60(1):201–209
- Chernysheva MA, Yushakova SI, Maydanik YF (2014) Copper-water loop heat pipes for energy-efficient cooling systems of supercomputers. *Energy* 69:534–542
- Krishna J, Kishore PS, Solomon AB (2017) Heat pipe with nano enhanced-PCM for electronic cooling application. *Exp Therm Fluid Sci* 81:84–92
- Kumaresan G, Venkatachalapathy S, Asirvatham LG, Wongwises S (2014) Comparative study on heat transfer characteristics of sintered and mesh wick heat pipes using cuo nano-fluids. *Int Commun Heat Mass Transf* 57:208–215
- Solomon AB, Ramachandran K, Pillai BC (2012) Thermal performance of a heat pipe with nanoparticles coated wick. *Appl Therm Eng* 36(1):106–112

- Tharayil T, Asirvatham LG, Ravindran V, Wongwises S (2016) Thermal performance of miniature loop heat pipe with graphene-water nano-fluid. *Int J Heat Mass Transf* 93:957–968
- Wang X, Wei J (2016) Visual investigation on startup characteristics of a novel loop heat pipe. *Appl Therm Eng* 105:198–208
- Xu J, Zhang L, Xu H, Zhong J, Xuan J (2014) Experimental investigation and visual observation of loop heat pipes with two-layer composite wicks. *Int J Heat Mass Transf* 72:378–387
- Zhao T, Ma Z, Zhang Z, Deng W, Long R, Liu W, Ma L, Liu Z (2021) Experimental investigation of a loop heat pipe with a flat evaporator and cupric oxide nano-fluids as working fluid. *Energy Rep* 7:7693–7703

# Chapter 7

## Selected Multi-criteria Decision-Making Methods and Their Applications to Product and System Design



Zhiyuan Wang, Seyed Reza Nabavi, and Gade Pandu Rangaiah

**Abstract** Optimization problems in design and engineering often involve multiple conflicting objectives, and their solution requires multi-objective optimization (MOO). The solution of MOO problems is a set of equally good optimal solutions, known as Pareto-optimal solutions (front). One more critical step is therefore required to choose one solution from the Pareto-optimal front, for implementation; this step is known as multi-criteria decision-making (MCDM). In this chapter, MCDM procedure, 4 normalization methods, 4 weighting methods and 5 MCDM methods are described. Then, MS Excel program, developed by our group, for these chosen methods is presented. Finally, several MCDM applications involving product and system design are used to demonstrate the applicability and effectiveness of the MS Excel program and the selected MCDM methods.

**Keywords** Multi-objective optimization · Multi-criteria decision making · Normalization methods · Weighting methods · MS Excel program · Product design · System design

---

Z. Wang · G. P. Rangaiah (✉)  
Department of Chemical and Biomolecular Engineering, National University of Singapore,  
Singapore 117585, Singapore  
e-mail: [chegpr@nus.edu.sg](mailto:chegpr@nus.edu.sg)

Z. Wang  
e-mail: [wangzhiyuan@u.nus.edu](mailto:wangzhiyuan@u.nus.edu)

Z. Wang  
Department of Continuing Education, DigiPen Institute of Technology Singapore,  
Singapore 139660, Singapore

S. R. Nabavi  
Department of Applied Chemistry, Faculty of Chemistry, University of Mazandaran, Babolsar,  
Iran

G. P. Rangaiah  
School of Chemical Engineering, Vellore Institute of Technology, Vellore 632014, India

## 7.1 Introduction

Optimization has found numerous applications in engineering, particularly since 1960's. Many optimization applications in engineering have more than one objective (or performance criterion). Such applications require multi-objective (or multi-criteria) optimization (MOO or MCO). Spurred by this and development of techniques for handling multiple objectives, MOO has found many applications in engineering in the last two decades. Recent reviews of these MOO applications are by Gunantara (2018), Rangaiah et al. (2020) and Liu et al. (2020).

Optimization of an application for more than one objective gives a set of optimal solutions (known as non-dominated solutions or Pareto-optimal front/solutions), which are equally good in the sense that no objective can be further improved without resulting in the deterioration of at least one other objective. MOO in engineering has mainly focused on the development of a model for the application, formulation of the MOO problem and solution of the formulated problem to find Pareto-optimal front. However, for completion of MOO, one more crucial step is required to choose one of these Pareto-optimal solutions for implementation.

The methods that can be used to select one solution from the Pareto-optimal front are known as multi-criteria decision making or analysis (MCDM or MCDA) methods. This step of using MCDM methods has not received much attention in engineering applications of MOO until recently. For instance, Gidde et al. (2018) applied the gray relational analysis (GRA) method in the design optimization of a rectangular wave passive micromixer. Parhi et al. (2019, 2020) employed the technique for order of preference by similarity to ideal solution (TOPSIS) method in the optimization of batch distillation process. Zhou et al. (2021) proposed an MOO-based TOPSIS method for sustainable product design under epistemic uncertainty. Wang et al. (2021) proposed a preference ranking on the basis of ideal-average distance (PROBID) method and applied it to the design of the volatile organic component (VOC) recovery process. Park et al. (2023) utilized the PROBID method in the design of zero energy building by taking into account the needs for supporting electric vehicles. Several new MCDM methods and applications are reported by different research groups in Kulkarni (2022). Wang et al. (2022) applied selected MCDM methods in the design and operation of supercritical water gasification process and combustion process in a power plant.

As noted above, the step of MCDM is receiving attention in some engineering applications only recently. Hence, the purpose of this chapter is to describe MCDM procedure, selected MCDM methods and their use for applications in product and system design. Results of these applications highlight the effect of the chosen weighting and MCDM method on the selected solution. In addition, a MS Excel program for selected MCDM methods is developed as part of this work, and it is available to interested researchers and practitioners. All these will be useful for the increased application of MCDM for selecting one of the (Pareto-optimal) solutions.

Rest of this chapter is organized as follows. First, generic procedure of MCDM is presented in Sect. 7.2. Normalization and weighting methods, required for many

MCDM methods, are described in Sect. 7.3. Then, selected MCDM methods are explained in Sect. 7.4. A Microsoft Excel program, EMCDM445, for these methods and its use are outlined in Sect. 7.5. Application of selected MCDM methods to example datasets on product and system design and discussion of its results are covered in Sect. 7.6. Finally, this chapter ends with a summary in Sect. 7.7.

From the education perspective, the learning outcomes of this chapter on MCDM methods are:

1. State the need for MCDM methods
2. Outline the generic procedure of MCDM methods
3. Explain normalization and weighting methods
4. Describe selected MCDM methods
5. Apply MCDM methods to the given dataset of Pareto-optimal solutions
6. Interpret the results from the application of MCDM methods

This chapter will be useful to those readers new to MCDM whereas the EMCDM445 program for selected MCDM methods will be handy to all readers in their study of MOO and MCDM.

## 7.2 Procedure of MCDM

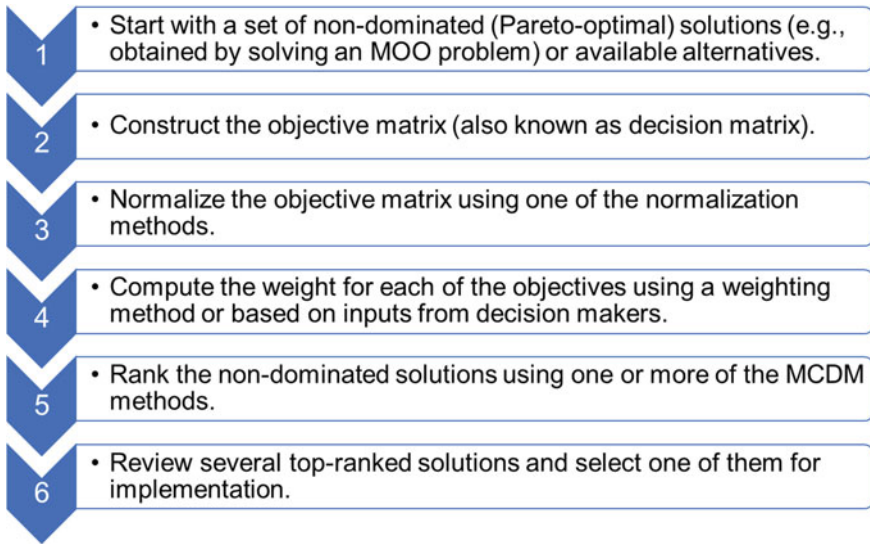
The **five steps** of MCDM are presented in Fig. 7.1. The **first step** is to start with a set of non-dominated solutions, which are found by formulating and solving the MOO problem under study. In the MOO problem, each objective/criterion can be for either maximization (also referred to as the benefit objective) or minimization (also referred to as the cost objective). Instead of solving the MOO problem, available alternatives (or solutions) and their performance criteria can be compiled and used in MCDM.

The **second step** is to construct an objective matrix, which is also called as decision matrix in some publications. This matrix consists of  $m$  rows (with one row for each non-dominated solution or alternative) and  $n$  columns (with one column for each objective or criterion). Hence, the objective/decision matrix does not contain values of decision variables or constraints in the MOO problem.

In the **third step**, the objective values are normalized using one of the normalization methods, such as vector and max–min normalization methods. One can choose to skip the normalization step (e.g., when values of all objectives are comparable). However, normalization is recommended to avoid domination of MCDM computations by those objectives with relatively large values compared to other objectives, which is the situation in many engineering applications.

In the **fourth step**, the weight for each of the objectives is provided (e.g., by decision makers) or computed using one of the weighting methods such as the entropy method. Equal weights for all objectives, if appropriate, can be given. The **fifth step** is to rank the non-dominated solutions using one or several MCDM methods, which may rank the solutions differently. In the **sixth and final** step, review the 3 or 4





**Fig. 7.1** General steps of MCDM

top-ranked solutions by one or more MCDM methods, for selecting one of them for implementation. In this selection, optimal values of decision variables in the MOO problem, if available, or other considerations may be used.

### 7.3 Normalization and Weighting Methods

For describing the popular normalization, weighting methods and MCDM methods (which are all implemented in the Excel-based MCDM program, described in Sect. 7.5), together with their mathematical equations in this and next sections, the following symbols are introduced, and they are used throughout this chapter. The objective matrix is a matrix of  $m$  rows (with one row for each non-dominated solution or alternative) and  $n$  columns (with one column for each objective or criterion).  $f_{ij}$  represents the value of the  $j$  th objective at the  $i$  th non-dominated (Pareto-optimal) solution,  $F_{ij}$  represents the normalized  $f_{ij}$  after applying one of the normalization methods, and  $w_j$  is the weight of the  $j$  th objective. Besides, note that the range of integers  $i$  and  $j$  are  $i \in [1, m]$  and  $j \in [1, n]$ , respectively.

Normalization is an important step in bringing all values in the objective matrix to a common scale (e.g., between 0 and 1). This is effective to prevent objectives with relatively large values dominating the calculations in MCDM. Table 7.1 presents the four normalization methods, namely, sum, vector, max–min and max normalization, and their mathematical equations. For the range of normalized values, assuming all  $f_{ij}$  values are greater than 0, two cases may be used to examine the normalized values,

**Table 7.1** Normalization methods and their mathematical equations

Method	Equations, where $i \in [1, m]$ and $j \in [1, n]$
Sum normalization	$F_{ij} = \frac{f_{ij}}{\sum_{k=1}^m f_{kj}}$ for both benefit and cost objectives
Vector normalization	$F_{ij} = \frac{f_{ij}}{\sqrt{\sum_{k=1}^m f_{kj}^2}}$ for both benefit and cost objectives
Max–min normalization	$F_{ij} = \frac{f_{ij} - \min_{k \in [1, m]} f_{kj}}{\max_{k \in [1, m]} f_{kj} - \min_{k \in [1, m]} f_{kj}}$ for benefit objectives $F_{ij} = \frac{\max_{k \in [1, m]} f_{kj} - f_{ij}}{\max_{k \in [1, m]} f_{kj} - \min_{k \in [1, m]} f_{kj}}$ for cost objectives
Max normalization	$F_{ij} = \frac{f_{ij}}{\max_{k \in [1, m]} f_{kj}}$ for benefit objectives $F_{ij} = \frac{\min_{k \in [1, m]} f_{kj}}{f_{ij}}$ for cost objectives

$F_{ij}$ : (i) range of values of an objective is narrow, e.g., within 5%, and (ii) ratio of maximum to minimum of an objective is  $\mu$ . In case (i), normalized values by sum and vector normalizations will be approximately  $1/m$  and  $1/\sqrt{m}$ , and normalized values by max normalization will be close to 1.0. In case (ii), on the other hand, normalized values by sum normalization will be  $\left[ \frac{1}{1+\mu(m-1)}, \frac{\mu}{\mu+(m-1)} \right]$ , by vector normalizations will be  $\left[ \frac{1}{\sqrt{1+\mu^2(m-1)}}, \frac{\mu}{\sqrt{\mu^2+(m-1)}} \right]$ , and by max normalization will be  $\left[ \frac{1}{\mu}, 1.0 \right]$ . In both cases (i) and (ii), normalized values by max–min normalization will be between 0.0 and 1.0.

After normalization by either max–min or max method, normalized values of a cost objective will be like those of a benefit objective (i.e., higher values are preferred). Note that division by zero may occur while using sum and max normalizations (Table 7.1): in sum normalization, when an objective has some positive and some negative values, and their sum is zero; and in max normalization, when the maximum value of a benefit objective is zero or any value of a cost objective is zero. Further, all values of a cost objective by max normalization become zero if the minimum of that cost objective is zero. Although these situations are not common, care should be exercised if the value of an objective is zero or values of an objective include both positive and negative values.

There are many methods for calculating the weight of each of  $m$  objectives. Some of them compute weights using the values in the objective matrix and do not require any inputs from the user or decision maker, and they are known as objective weighting methods; in this phrase, objective is the adjective, and it means that not influenced by personal feelings or opinions in considering and representing facts. Some other weighting methods require inputs from the user or decision maker (and not the objective matrix) for calculating weights, and they are known as subjective weighting methods. Inputs can vary from one decision maker to another, and consequently the computed weights are subjective. In the following, two objective weighting methods and two subjective weighting methods are described. See Wang et al. (2020) for some more objective and subjective weighting methods.

**Entropy weighting method** (Hwang and Yoon, 1981) relies on a probability-theoretic formulation of a measure of informational uncertainty to decide the weights for objectives. An objective is allocated a relatively higher weight if there is a more significant difference in the values of that objective among the non-dominated solutions. According to the review by Hafezalkotob et al. (2019), entropy method is the most frequently used weighting method in MCDM applications. It consists of the following three steps.

**Step <1>:** Normalize the objective matrix using the sum normalization (Table 7.1), as in Hwang and Yoon (1981).

**Step <2>:** Compute the entropy value of each objective in the normalized objective matrix:

$$E_j = -\frac{1}{\ln(m)} \sum_{i=1}^m (F_{ij} \ln F_{ij}) \quad \text{for } j \in [1, n] \quad (7.1)$$

Note that the above equation uses normalized objective values.

**Step <3>:** Find the weight of each objective based on computed entropy values:

$$w_j = \frac{1 - E_j}{\sum_{j=1}^n (1 - E_j)} \quad \text{for } j \in [1, n] \quad (7.2)$$

Although sum normalization is used in Step 1 as per Hwang and Yoon (1981), the normalization method employed affects weights calculated by the entropy method; see Wang et al. (2020) for some examples.

Another weighting method, namely, **Criteria Importance Through Intercriteria Correlation (CRITIC)** is based on the correlation between any two objectives and the standard deviation of each individual objective. The original study by Diakoulaki et al. (1995) reveals that this method produces more evenly distributed weights that consider the information offered by all objectives and enable a better resolution of trade-offs among the objectives. It also has three steps as follows. Like the entropy method, weights given by the CRITIC method depend on the normalization method used in Step 1 (Wang et al., 2020).

**Step <1>:** Normalize the objective matrix using the max–min normalization method (Table 7.1), as in Diakoulaki et al. (1995).

**Step <2>:** Calculate the Pearson product moment correlation between any 2 objectives:

$$\rho_{jk} = \frac{\sum_{i=1}^m (F_{ij} - \bar{F}_j)(F_{ik} - \bar{F}_k)}{\sqrt{\sum_{i=1}^m (F_{ij} - \bar{F}_j)^2} \sqrt{\sum_{i=1}^m (F_{ik} - \bar{F}_k)^2}} \quad \text{for } j, k \in [1, n] \quad (7.3)$$

Here,  $\bar{F}_j = \frac{1}{m} \sum_{i=1}^m F_{ij}$  and  $\bar{F}_k = \frac{1}{m} \sum_{i=1}^m F_{ik}$  represent the arithmetic mean of  $j$  th and  $k$  th normalized objective, respectively.

**Step <3>.** Compute the standard deviation of each individual normalized objective and then determine the weight for each objective as follows:

$$\sigma_j = \sqrt{\frac{\sum_{i=1}^m (F_{ij} - \bar{F}_j)^2}{m}} \quad \text{for } j \in [1, n] \tag{7.4}$$

$$c_j = \sigma_j \sum_{k=1}^n (1 - \rho_{jk}) \quad \text{for } j \in [1, n] \tag{7.5}$$

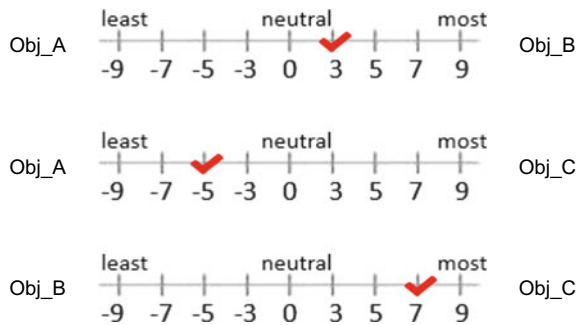
$$w_j = \frac{c_j}{\sum_{k=1}^n c_k} \quad \text{for } j \in [1, n] \tag{7.6}$$

**Analytical Hierarchy Process (AHP)**, developed by Saaty (1990), is a popular subjective weighting method in MCDM applications (Hafezalkotob et al., 2019). It involves a sequence of pair-wise comparisons among the objectives for generating the objective weights. It does not require any values from the objective matrix; instead, it solely leverages the decision makers’ subjective preferences to determine the weights for objectives. AHP is conveniently described in three steps, using a simple example.

**Step <1>**: Consider an objective matrix with 3 objectives, namely, Obj\_A, Obj\_B, and Obj\_C (i.e.,  $n = 3$ ). The first pair-wise comparison given by decision makers in the top row of Fig. 7.2 shows that the favor (preference) level of Obj\_B over Obj\_A is 3 on the scale of from  $-9$  to  $+9$  (where  $-9$  indicates the Obj\_B is least favored,  $+9$  indicates Obj\_B is most favored, and  $0$  indicates equally favoring of Obj\_A and Obj\_B). Likewise, for the second pair-wise comparison of Obj\_C over Obj\_A, decision makers consider that Obj\_C is less favored than Obj\_A and hence give a  $-5$ . For the third pair-wise comparison of Obj\_C over Obj\_B, decision makers consider that Obj\_C is more favored than Obj\_B and hence give a  $7$ . Note that decision makers are not confined to choose from only the 9 integer values on the scale; they can choose any other values within the range of  $[-9, 9]$ , such as  $+2.5$ ,  $+4.7$  and  $-3.4$ . For  $n$  objectives, there will be  $\frac{n(n-1)}{2}$  pair-wise comparisons; hence, decision makers may have to provide many inputs.

**Step <2>**: Construct the pair-wise comparison matrix illustrated in Table 7.2. All values on the leading diagonal of the matrix are set as 1. For all values above the leading diagonal, if the corresponding favor level given by the decision maker is positive ( $>0$ ), then take its reciprocal value in the matrix; if the corresponding favor level given by the decision maker is negative ( $<0$ ), then use its absolute value

**Fig. 7.2** Pair-wise comparisons of 3 objectives in AHP method; each tick symbol shows the favor (preference) level given by decision makers for the comparison of the right-side objective over the left-side objective



**Table 7.2** Pair-wise comparison matrix of 3 objectives, for AHP method

	Obj_A	Obj_B	Obj_C
Obj_A	1	1/3	5
Obj_B	3	1	1/7
Obj_C	1/5	7	1

in the matrix. If the corresponding favor level given by the decision maker is zero (i.e., neutral), it will be taken as 1, which is same as the unity value on the diagonal. Values below the leading diagonal are reciprocal of the corresponding values above the leading diagonal (i.e.,  $a_{gj} = \frac{1}{a_{jg}}$  for  $j \in [1, n - 1]$  and  $g \in [j + 1, n]$ ; here,  $a_{gj}$  is the value at the  $g$  th row and  $j$  th column of the matrix. For the simple example, the complete pair-wise comparison matrix based on inputs in Fig. 7.2 is presented in Table 7.2.

**Step <3>**: Apply sum normalization to the pair-wise comparison matrix constructed in the previous step. Here, sum is based on each column.

$$A_{gj} = \frac{a_{gj}}{\sum_{h=1}^n a_{hj}} \text{ for } g, j \in [1, n] \tag{7.7}$$

Then, weights for the objectives are computed as

$$w_g = \frac{\sum_{j=1}^n A_{gj}}{n} \text{ for } g \in [1, n] \tag{7.8}$$

Table 7.3 shows the normalized pair-wise comparison matrix (computed by Eq. 7.7) and weights for the objectives (computed by Eq. 7.8), for example.

**Best–Worst (BW) Method** is another subjective weighting method, introduced by Rezaei (2016) using two vectors of pair-wise comparisons to derive weights of objectives, which has been receiving much attention in recent years. It calculates the weight for each objective based on only the decision makers’ subjective inputs, like AHP. The three steps in the BW method are as follows.

**Step <1>**: Decision makers are to Identify the best objective (i.e., their most favored objective) and the worst objective (i.e., their least favored objective).

**Step <2>**: Decision makers are to decide the distances from the best objective that they identified in the prior step to all the remaining objectives, on the integer

**Table 7.3** Normalized pair-wise comparison matrix and weights for the example, by AHP method

	Pair-wise comparison matrix			Weight
	Obj_A	Obj_B	Obj_C	
Obj_A	0.238095	0.040000	0.813953	0.364016
Obj_B	0.714286	0.120000	0.023256	0.285847
Obj_C	0.047619	0.840000	0.162791	0.350137

scale between 1 and 9. The Best-to-Others (BO) vector is then constructed as:

$$A_B = \{a_{B1}, a_{B2}, \dots, a_{Bn}\} \tag{7.9}$$

Here,  $a_{Bj}$ , , within the range of [1, 9], is the distance from the best objective  $B$  to objective  $j$ . The larger the  $a_{Bj}$  value, the further the objective  $j$  is from the best objective (i.e., in terms of priority). Note that  $a_{BB}$  (i.e., best-to-best) is always 1, and  $a_{Bj}$  need not be different for different objectives. Similarly, decision makers need to decide the distances of all objectives to the worst objective that they identified. The Others-to-Worst (OW) vector is then constructed as

$$A_W = \{a_{1W}, a_{2W}, \dots, a_{nW}\} \tag{7.10}$$

Here,  $a_{jW}$ , , within the range of [1, 9], is the distance from objective  $j$  to the worst objective  $W$ .  $a_{WW}$  (i.e., worst-to-worst) is set as 1, and  $a_{jW}$  need not be different for different objectives.

**Step <3>:** The final step of BW method is to formulate and solve the linear optimization problem, whose solution generates the weights for the objectives.

$$\text{Minimize } \xi \tag{7.11a}$$

$$\text{with respect to } w_1, w_2, \dots, w_n \tag{7.11b}$$

$$\text{subject to } \sum_{j=1}^n w_j = 1 \tag{7.11c}$$

$$|w_B - a_{Bj}w_j| \leq \xi \text{ where } j \in [1, n] \tag{7.11d}$$

$$|w_j - a_{jW}w_W| \leq \xi \text{ where } j \in [1, n] \tag{7.11e}$$

Here,  $w_B$  and  $w_W$  are the weight of the best and worst objectives, respectively.

### 7.4 Selected MCDM Methods

Our recent studies (Wang and Rangaiah, 2017; Wang et al., 2020) analyzed many MCDM methods for many mathematical problems and engineering applications. Considering the simplicity of the principle, user inputs required, ability to handle objective values of different magnitudes and popularity, we recommended the following MCDM methods: TOPSIS, Simple Additive Weighting (SAW), GRA and Multi-Attributive Border Approximation Area Comparison (MABAC) and PROBID. These 5 MCDM methods are described in the following sub-sections.

### 7.4.1 Gray Relational Analysis

Normalization of the objective matrix, identification of ideal reference network and computation of the gray relational coefficient (GRC) are the three key steps in the GRA method. The non-dominated solution (or alternative) with the highest GRC value is ranked as the top optimal solution and recommended. The GRA method has the unique feature of not requiring any user inputs, such as weights for the objectives. A numerical example illustrating the GRA method can be found in Song and Jamalipour (2005).

**Step <1>:** Normalize the objective matrix using the max–min normalization (Table 7.1), as in Song and Jamalipour (2005). Recall that normalized values of a cost objective by this normalization will be like those of a benefit objective.

**Step <2>:** Identify the ideal reference network having the best value for each of all the objectives.

$$F_j^+ = \max_{i \in [1, m]} F_{ij} \text{ where } j \in [1, n] \quad (7.12)$$

**Step <3>:** Compute GRC value for each non-dominated solution by the following equations.

$$\Delta I_{ij} = \left| F_j^+ - F_{ij} \right| \text{ where } i \in [1, m] \text{ and } j \in [1, n] \quad (7.13)$$

$$GRC_i = \frac{1}{m} \sum_{j=1}^n \frac{\Delta \min + \Delta \max}{\Delta I_{ij} + \Delta \max} \text{ where } i \in [1, m] \quad (7.14)$$

Here,  $\Delta \max = \max_{i \in [1, m], j \in [1, n]} (\Delta I_{ij})$  and  $\Delta \min = \min_{i \in [1, m], j \in [1, n]} (\Delta I_{ij})$ . The solution having the highest GRC value is top ranked and recommended.

#### 7.4.1.1 Multi-attributive Border Approximation Area Comparison

Pamučar and Čirović (2015) proposed the MABAC method and illustrated it with a numerical example. The main idea behind it is to calculate the distance between each non-dominated solution and the boundary approximation area that is based on the product of weighted normalized values of each objective. The top ranked optimal solution is that with the greatest distance. The steps of MABAC are as follows.

**Step <1>:** Normalize the objective matrix using the max–min normalization (Table 7.1), as in Pamučar and Čirović (2015). Recall that normalized values of a cost objective by this normalization will be like those of a benefit objective.

**Step <2>:** Apply weight to each objective; in this,  $F_{ij}$  is offset by 1 to avoid any value becoming 0 in the next step.

$$v_{ij} = (1 + F_{ij}) \times w_j \text{ for } i \in [1, m] \text{ and } j \in [1, n] \quad (7.15)$$

**Step <3>:** Determine the boundary approximation area (by Eq. 7.16), and then calculate the distance of each non-dominated solution to the boundary approximation area (by Eq. 7.17).

$$b_j = \left( \prod_{i=1}^m v_{ij} \right)^{1/m} \quad \text{for } j \in [1, n] \quad (7.16)$$

$$Q_i = \sum_{j=1}^n (v_{ij} - b_j) \quad \text{for } i \in [1, m] \quad (7.17)$$

The solution/alternative with the greatest distance ( $Q_i$ ) is top ranked and recommended.

#### 7.4.1.2 Preference Ranking on the Basis of Ideal-Average Distance

The primary benefit of the PROBID method proposed by Wang et al. (2021) is that it provides a thorough coverage of the mean solution and many tiers of ideal solutions for ranking non-dominated solutions. See Wang et al. (2021) for detailed discussion about this method and a numerical example. The steps of PROBID are as follows:

**Step <1>:** Normalize the objective matrix using vector normalization (Table 7.1), as in Wang et al. (2021).

**Step <2>:** Apply weight to each objective.

$$v_{ij} = F_{ij} \times w_j \quad \text{for } i \in [1, m] \text{ and } j \in [1, n] \quad (7.18)$$

**Step <3>:** Determine the most positive ideal solution, abbreviated as PIS ( $A_{(1)}$ ), 2nd PIS ( $A_{(2)}$ ), 3rd PIS ( $A_{(3)}$ ), ..., and  $m$ th PIS ( $A_{(m)}$ ) (i.e., negative ideal solution).

$$\begin{aligned} A_{(k)} &= \{(\text{Large}(v_j, k) | j \in J), (\text{Small}(v_j, k) | j \in J')\} \\ &= \{v_{(k)1}, v_{(k)2}, v_{(k)3}, \dots, v_{(k)j}, \dots, v_{(k)n}\} \end{aligned} \quad (7.19)$$

Here,  $k \in [1, m]$ ,  $J$  is the set of maximization objectives from  $[1, n]$ ,  $J'$  is the set of minimization objectives from  $[1, n]$ ,  $\text{Large}(v_j, k)$  represents the  $k$ th largest value in the  $j$ th weighted normalized objective,  $\text{Small}(v_j, k)$  represents the  $k$ th smallest value in the  $j$ th weighted normalized objective, and  $v_{(k)j}$  is the  $k$ th best value (i.e., the  $k$ th largest value for a benefit objective or the  $k$ th smallest value for a cost objective) in the  $j$ th weighted normalized objective. The average value of each weighted normalized objective is calculated as:

$$\bar{v}_j = \frac{\sum_{k=1}^m v_{(k)j}}{m} \quad \text{for } j \in [1, n] \quad (7.20)$$

$$\bar{A} = \{\bar{v}_1, \bar{v}_2, \bar{v}_3, \dots, \bar{v}_j, \dots, \bar{v}_n\} \quad (7.21)$$



**Step <4>:** Compute the Euclidean distance of each non-dominated solution to each of the  $m$  ideal solutions.

$$S_{i(k)} = \sqrt{\sum_{j=1}^n (v_{ij} - v_{(k)j})^2} \quad i, k \in [1, m] \quad (7.22)$$

The distance of each non-dominated solution to the average solution is computed as:

$$S_{i(\text{avg})} = \sqrt{\sum_{j=1}^n (v_{ij} - \bar{v}_j)^2} \quad i \in [1, m] \quad (7.23)$$

**Step <5>:** Find the overall positive-ideal distance as well as the overall negative-ideal distance.

$$S_{i(\text{pos-ideal})} = \begin{cases} \sum_{k=1}^{\frac{m+1}{2}} \frac{1}{k} S_{i(k)} & i \in [1, m] \text{ when } m \text{ is an odd number} \\ \sum_{k=1}^{\frac{m}{2}} \frac{1}{k} S_{i(k)} & i \in [1, m] \text{ when } m \text{ is an even number} \end{cases} \quad (7.24)$$

$$S_{i(\text{neg-ideal})} = \begin{cases} \sum_{k=\frac{m+1}{2}}^m \frac{1}{m-k+1} S_{i(k)} & i \in [1, m] \text{ when } m \text{ is an odd number} \\ \sum_{k=\frac{m}{2}+1}^m \frac{1}{m-k+1} S_{i(k)} & i \in [1, m] \text{ when } m \text{ is an even number} \end{cases} \quad (7.25)$$

**Step <6>:** Compute the ratio of pos-ideal distance to neg-ideal distance ( $R_i$ ) and then performance score ( $P_i$ ) of each non-dominated solution.

$$R_i = \frac{S_{i(\text{pos-ideal})}}{S_{i(\text{neg-ideal})}} \quad i \in [1, m] \quad (7.26)$$

$$P_i = \frac{1}{1 + R_i^2} + S_{i(\text{avg})} \quad i \in [1, m] \quad (7.27)$$

The solution/alternative with the largest performance score is top ranked and recommended.

## 7.4.2 Simple Additive Weighting (SAW)

The SAW method, possibly the simplest MCDM methods, was first presented in Fishburn (1967) and MacCrimmon (1968). It begins by utilizing the max normalization to create the normalized objective matrix and applying weights. Then, objective values of each non-dominated solution (or alternative) are simply summed up. The

top ranked solution is the one with the highest value in this summation and recommended. A numerical example about using the SAW method can be found in Afshari et al., (2010).

**Step <1>:** Normalize the objective matrix using max normalization (Table 7.1), as in MacCrimmon (1968). Recall that normalized values of a cost objective by this normalization will be like those of a benefit objective. Owing to max normalization, one limitation of SAW method is that, in the original objective matrix, maximum value of a maximization (benefit) objective and any value of a minimization (cost) objective cannot be 0, in order to avoid division by zero.

**Step <2>:** Apply weight to each objective.

$$v_{ij} = F_{ij} \times w_j \quad i \in [1, m] \text{ and } j \in [1, n] \quad (7.28)$$

**Step <3>:** Sum up the weighted normalized value for each non-dominated solution.

$$A_i = \sum_{j=1}^n v_{ij} \quad i \in [1, m] \quad (7.29)$$

The solution/alternative with the largest value for the sum is top ranked and recommended.

### 7.4.3 *Technique for Order of Preference by Similarity to Ideal Solution*

Hwang and Yoon (1981) created TOPSIS method and illustrated it using a numerical example. The top ranked non-dominated solution chosen in this method is the solution that is furthest to the negative ideal solution while also being the closest to the positive ideal solution. The best value of each objective, that is, the maximal value of the maximization objective and the minimal value of the minimization objective, makes up the ideal positive solution. On the other hand, the worst value of each objective, that is, the minimal value of the maximization objective and the maximal value of the minimization objective, constitute the negative ideal solution. The steps in TOPSIS method are as follows.

**Step <1>:** Normalize the objective matrix using vector normalization (Table 7.1), as in Hwang and Yoon (1981).

**Step <2>:** Apply weight to each objective.

$$v_{ij} = F_{ij} \times w_j \quad i \in [1, m] \text{ and } j \in [1, n] \quad (7.30)$$

**Step <3>:** Determine the positive ideal solution  $A^+$  and negative ideal solution  $A^-$  as follows

$$\begin{aligned}
A^+ &= \{(\max_{i \in [1, m]}(v_{ij}) | j \in J), (\min_{i \in [1, m]}(v_{ij}) | j \in J')\} \\
&= \{v_1^+, v_2^+, v_3^+, \dots, v_j^+, \dots, v_n^+\}
\end{aligned} \tag{7.31}$$

$$\begin{aligned}
A^- &= \{(\min_{i \in [1, m]}(v_{ij}) | j \in J), (\max_{i \in [1, m]}(v_{ij}) | j \in J')\} \\
&= \{v_1^-, v_2^-, v_3^-, \dots, v_j^-, \dots, v_n^-\}
\end{aligned} \tag{7.32}$$

Here,  $J$  is the set of maximization objectives from  $[1, n]$  and  $J'$  is the set of minimization objectives from  $[1, n]$ .

**Step <4>:** Compute the Euclidean distance of each non-dominated solution to the positive ideal and negative ideal solutions, respectively, as follows:

$$S_{i+} = \sqrt{\sum_{j=1}^n (v_{ij} - v_j^+)^2} \quad i \in [1, m] \tag{7.33}$$

$$S_{i-} = \sqrt{\sum_{j=1}^n (v_{ij} - v_j^-)^2} \quad i \in [1, m] \tag{7.34}$$

**Step <5>:** Quantify the closeness ( $C_i$ ) of each non-dominated solution.

$$C_i = \frac{S_{i-}}{S_{i-} + S_{i+}} \quad i \in [1, m] \tag{7.35}$$

The solution with the largest  $C_i$  is top ranked and recommended.

## 7.5 Microsoft Excel Program for MCDM

Calculations for the 4 normalization methods, 4 weighting methods and 5 MCDM methods described in the above sections can be performed using a calculator or a spreadsheet. However, a validated and easy-to-use program for them will be very useful for correct and quick computations. Hence, the 4 normalization, 4 weighting and 5 MCDM methods are implemented in a Microsoft Excel program: EMCDM445, whose Overview worksheet is in Fig. 7.3. Interested readers can obtain a copy of it by sending an email request to [chegpr@nus.edu.sg](mailto:chegpr@nus.edu.sg) and [wangzhiyuan@u.nus.edu](mailto:wangzhiyuan@u.nus.edu). A more extensive Microsoft Excel program with 8 weighting methods and 15 MCDM methods (Wang et al. 2020, 2021) is also available via an email request. Both the programs have a friendly user interface and are easy to use for MCDM.

The EMCDM445 has the following features.

Methods for Ranking Pareto-Optimal (Non-Dominated) Solutions to Select One Optimal Solution	
Department of Chemical and Biomolecular Engineering, National University of Singapore <a href="https://blog.nus.edu.sg/rangajiah/">(https://blog.nus.edu.sg/rangajiah/)</a>	
For more details, see Wang Z., Nabavi S.R. and Rangaiah G.P., "Selected Multi-Criteria Decision Making Methods and their Applications to Product and System Designs" in the book by A.J. Kulkarni (editor), 'Optimization Methods for Product and System Design', Springer (2022).	
Hope you can use this program in your work. Please cite the above reference in your publications.	
Worksheet	Description
Overview	1. The overview serves to provide brief description and instructions for using this program. 2. Carefully read and follow them.
Results From MOO	1. This worksheet is for the user to provide Pareto-optimal (i.e., non-dominated) solutions for his/her application. 2. This program requires non-dominated solutions, which should be copied to this worksheet. 3. Number of non-dominated solutions can be few (e.g., 4 or 9) and many (e.g., 78, 105 or 164). 4. There are no limits on number of objectives, decision variables, constraints and non-dominated/optimal solutions. 5. Data on decision variables and constraints are optional for using this program. 6. Names of Decision Variables (X1, X2, X3 etc.), Objectives (F1, F2 etc.) and Constraints (C1, C2, C3 etc.), if available, should be pasted in row 3 of worksheet "Results From MOO". 7. All values should be pasted in rows starting from row 5. <b>Closely and strictly</b> follow the format in the current sheet "Results from MOO".
Main Interface	1. In this main interface of the program, user needs to provide essential information such as Number of Objectives, Decision Variables, Constraints etc. 2. Number of Decision Variables and Constraints should be given as 0 (zero) if user does not have those data. 3. User can choose any weighting method or ranking/election method; s/he can also enter their own inputs (i.e., without using any of the weighting methods). 4. If user wishes to try all rankin/selection methods, click 'Run all Methods' and then click 'Show all Charts' to have results of all methods in the form of plots for comparison. 5. All created worksheets can be deleted by clicking 'Delete Worksheets of All Methods'. Use this as and when required before trying a different weighting and/or ranking/selection method.
Results of Each Method	Results of each method or all methods chosen by the user from the Main Interface are given on newly created worksheets (e.g. TOPSIS Results). Scroll down and/or to right to see the plots.
All Charts	This worksheet will be created if 'Show All Charts' is clicked.

Fig. 7.3 Overview worksheet of the EMCDM445 Program

- Objective matrix data are provided by the user in the worksheet “Results from MOO” (Fig. 7.4).
- It can compute weights of objectives by one of the objective or subjective weighting methods, as per user’s choice. Alternatively, user can give her/his preferred weights. Further, the program has the option to combine the weights found by a weighting method with those given by the user, via the formula:  $\text{combinedweightofjthobjective} = \frac{W_{uj}W_{wj}}{\sum_{j=1}^n W_{uj}W_{wj}}$ , where  $W_{uj}$  is the user-provided weight and  $W_{wj}$  is the weight found by the chosen weighting method, both for the  $j$ th objective.
- The user can choose to run any one of the 5 MCDM methods by clicking it. Alternatively, she/he can run all 5 MCDM methods by clicking “Run all Methods” (at the bottom left in Fig. 7.5).
- The default normalization for each MCDM method is as per its original reference; see the description in Sect. 7.3. However, the program allows the user to change the normalization method (to another that is feasible with the MCDM method) or choose not to use normalization (i.e., apply MCDM method on the original dataset).
- The “Show All Charts” button (at the bottom left in Fig. 7.5) is to consolidate and present all the charts/results of 5 MCDM methods that were run, in one worksheet.

Objective Names →	CC (Min)	SS (Max)	TC (Max)	TX (Min)	TZ (Min)	MD (Max)	ML (Max)
Leave this row 4 as blank.							
1	1200000	5590	8	24	24	205	350
2	1550000	3465	8	20	20	280	520
3	1400000	5950	12	15	20	250	469
4	1100000	5940	12	12	15	230	600
5	1200000	5940	12	12	16	150	330
6	1500000	3465	12	6	12	260	420
7	2600000	3960	12	12	16	300	625
8	1320000	4950	12	24	30	240	340
9	1180000	4480	8	24	24	250	330
10	1550000	3950	12	15	20	280	460
11	1600000	3450	12	15	20	280	460
12	1200000	3465	8	20	24	264	400
13	1350000	2970	8	20	24	264	400
14	1400000	2970	12	24	30	300	600
15	1350000	3465	12	30	30	264	350
16	1450000	2970	12	20	24	300	400
17	1520000	2475	12	20	24	300	400
18	1376000	4752	12	20	24	235	350
19	1440000	4752	12	20	24	235	600
20	1824000	3790	10	12	20	300	530
21	1920000	3790	10	12	20	300	1030

Fig. 7.4 Worksheet for providing the objective matrix data to the EMCDM445 Program

**Main Interface**

Plot Needed?  Yes  No

Step 1: Provide Pareto-optimal solutions in the previous worksheet "Results from MOO".

No. of Objectives	7
No. of Decision Variables	0
No. of Constraints	0
No. of Solutions	21

Step 2: Enter values in cells D5 to D8 (if no decision variables or constraint, input value 0)

Step 3: Choose type of objective

Objectives	Types (Max or Min)	Weightage used (Entropy)
CC (Min)	Min	0.105624
SS (Max)	Max	0.157762
TC (Max)	Max	0.065165
TX (Min)	Min	0.261056
TZ (Min)	Min	0.119718
MD (Max)	Max	0.054169
ML(Max)	Max	0.236506

Step 4: Weight can be chosen by user or found by one or more methods on the right. If required, scroll to right and/or down

- Entropy Weight
- CRITIC Weight
- AHP Weight
- BWM Weight

Step 5: Choose one or all MCDM methods on the left side.

- GRA
- MABAC
- PROBID
- SAW
- TOPSIS

Buttons: Run all Methods, Show All Charts, Delete All Results

Navigation: Overview, Results from MOO, Main Interface, All Charts, GRA Results, MABAC Results, PROBID Results, SAW Results, TC

Fig. 7.5 Main Interface of the EMCDM445 program

To succinctly present objective values of different magnitude in one plot, fractional objective values are calculated using:  $\text{FractionalJthObjective} = \frac{F_j - F_{j,\min}}{F_{j,\max} - F_{j,\min}}$ .

- The program allows the user to decide whether to plot or not.
- The “Delete All Results” button (at the bottom left in Fig. 7.5) is to safely delete all the MCDM worksheets containing the charts/results of previous runs. Use this button before a new trial or run.

Before using the program for MCDM, study the important points in the Overview worksheet (Fig. 7.3). This is essential for correct use of the program. As shown in Fig. 7.5, there are 5 steps for performing MCDM.

**Step <1>:** Provide the objective matrix (i.e., values of all objectives for the various alternatives) in the worksheet: “Results from MOO”. Figure 7.4 presents this worksheet with values for 7 objectives and 21 alternatives, for the machine tool selection problem. Alternatively, Pareto-optimal solutions found by multi-objective optimization can be provided in the “Results from MOO” worksheet; these can include values of decision variables and constraints besides the objective values. In either case, values of the first alternative/solution must be in row 5; this is important. Names of objectives can be given in columns B, C, ... of row 3 (Fig. 7.4).

**Step <2>:** Enter number of objectives (must be 2 or more), number of decision variables (zero if none), number of constraints (zero if none) and number of alternatives/solutions (must be 2 or more) in cells D5 to D8 (Fig. 7.5).

**Step <3>:** Choose the type (either Max or Min) of each objective.

**Step <4>:** Weight can be given by the user or found by one of the 4 methods on the right side in Fig. 7.5.

**Step <5>:** Perform MCDM by choosing one or all 5 MCDM methods on the left side in Fig. 7.5.

Results of each MCDM method are presented in a separate worksheet, as can be seen by different worksheets in the bottom of Fig. 7.5. If “Show All Charts” is executed, selected solution/alternative by the 5 methods are presented in the “All Charts” worksheet, which includes objective values of the selected alternatives in the form of a bar chart, a radar chart and a table (Fig. 7.6) as well as 2D plots (one for each MCDM method, not shown in Fig. 7.6) of the first and last objectives. These enable the user to assess, both qualitatively and quantitatively, the alternatives (Pareto-optimal solutions) recommended by different MCDM methods.

## 7.6 Results and Discussion

For illustrating the 4 weighting methods and 5 MCDM methods as well as EMC445 program, 4 applications from product and system designs are carefully chosen and discussed. Brief details of these applications are given in Table 7.4 whereas their objective matrices (datasets) are in the Appendix. As can be seen from Table 7.4, the selected 4 applications are diverse in the area/domain of the application, number of objectives from 2 to 10, and number of alternatives from 6 to 74.

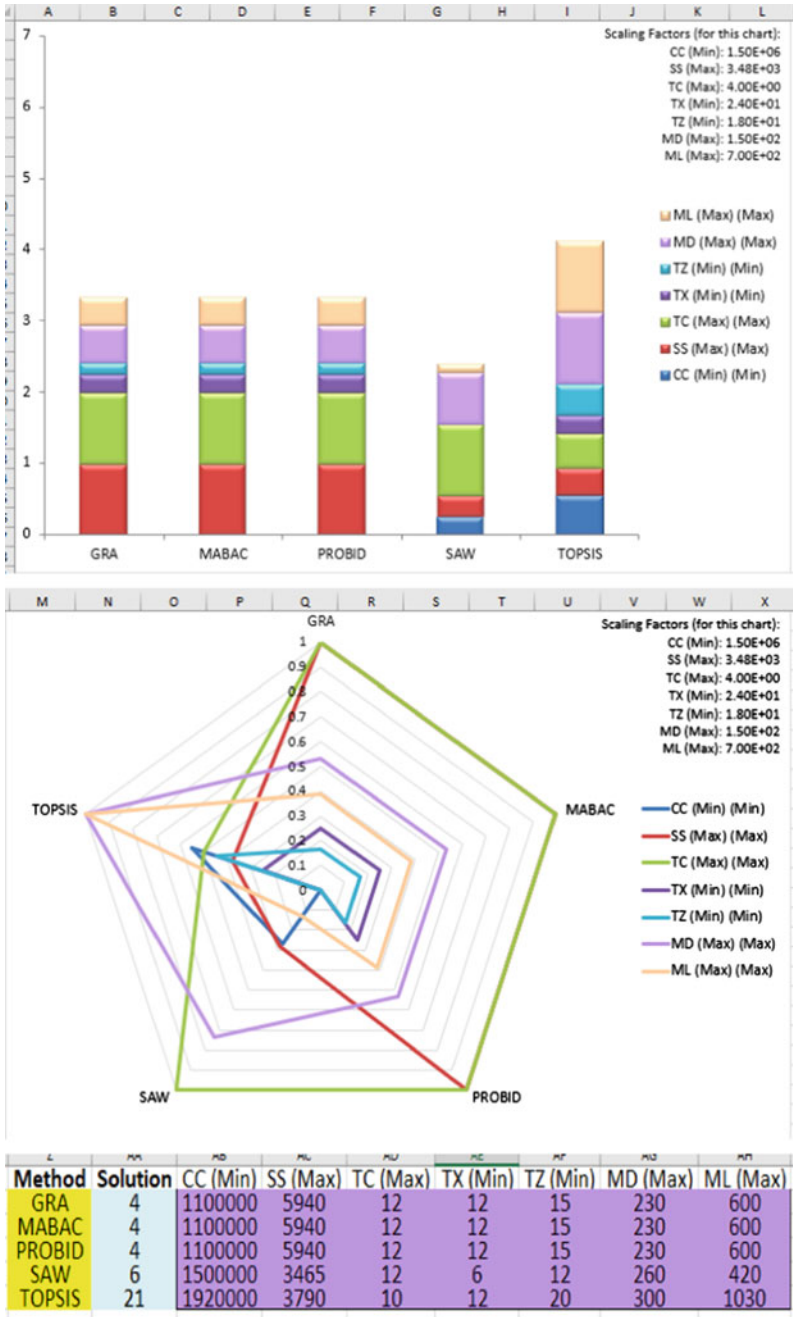


Fig. 7.6 Bar chart, radar chart and list of selected solutions by GRA, MABAC, PROBID, SAW and TOPSIS, in the “all charts” worksheet of the EMCDM445 program

**Table 7.4** Brief details of selected MCDM applications from product and system design; See Tables 7.5, 7.6, 7.7, 7.7, and 7.8 for the objectives/criteria in each application

Application: brief details	No. of objectives	No. of alternatives	Reference(s)
<b>Fruit Supply Chain:</b> This supply chain was optimized for simultaneous minimization of total cost and maximization of satisfying demand (quantified as responsiveness)	2	16 from the Pareto-optimal front	Cheraghalipour et al. (2018)
<b>VOC Recovery:</b> Design of a process system for recovery of volatile organic compounds (VOC) considering both economic and environmental objectives	5	74 from the Pareto-optimal front	Lee and Rangaiah (2009)
<b>Machine Tool Selection:</b> This application is on selecting one from many alternatives for a computerized numerical control machine	7	16 non-dominated alternatives	Sun (2002); Chakraborty (2011)
<b>Non-Traditional Machining (NTM) Process Selection:</b> This application is on the selection of one from various machining processes for the treatment of advanced engineering materials	10	8 non-dominated alternatives	Chakraborty (2011)

Moreover, the objective matrix for fruit supply chain and VOC recovery applications was obtained in the cited reference, by solving the related multi-objective optimization problem. On the other hand, the objective matrix for machine tool selection and non-traditional machining (NTM) process selection were probably compiled from the available alternatives and their values for the performance criteria (objectives). However, in all these applications, ranking and selection of one alternative (Pareto-optimal solution) requires MCDM. Here, each application was analyzed using 5 MCDM methods; for conciseness, only 2 of the 4 weighting methods were used in each application. The results of these trials are sufficient to illustrate the weighting and MCDM methods that are described in the previous sections.

Results from the application of 5 MCDM methods with the chosen weighting methods are presented in Tables 7.5, 7.6, 7.7 and 7.8. The recommended alternative/solution by GRA is unaffected by the weighting method (as it does not require



**Table 7.5** Recommended alternatives by 5 MCDM methods with 2 different weighting methods: fruit supply chain dataset

Objective	Weight	GRA	MABAC	PROBID	SAW	TOPSIS
<i>Using weights by the entropy method</i>						
Min. TC	0.886324	5,356,513	5,272,345	5,324,449	5,272,345	5,272,345
Max. RS	0.113676	0.776971	0.745228	0.764647	0.745228	0.745228
AAFD		Nil	0.028772	0.010996	0.028772	0.028772
<i>Using weights by AHP method*</i>						
Min. TC	0.125	5,356,513	6,755,311	5,941,683	5,941,683	5,941,683
Max. RS	0.875	0.776971	0.822531	0.812448	0.812448	0.812448
AAFD		Nil	0.143974	0.074114	0.074114	0.074114

Notes TC—Total Cost; RS—Responsiveness

\* In AHP method, favor level of C2 (RS) over C1 (TC) was chosen as 7

any weights). Recommended alternative by an MCDM method may be same or different from that by GRA because of different weights and/or MCDM method. The differences, if any, between the alternative recommended by an MCDM method and that by GRA are quantified by the average of absolute fractional differences (AAFD) between the values of criteria in the two recommended alternatives; it is given by:

$$AAFD = \frac{1}{n} \sum_1^n \frac{|C_{i,MCD} - C_{i,GRA}|}{|C_{i,MCD} + C_{i,GRA}|/2} \tag{7.36}$$

Here,  $n$  is the number of criteria/objectives,  $C_{i,GRA}$  is the value of the  $i$ th criterion in the alternative recommended by GRA, and  $C_{i,MCDM}$  is the value of the  $i$ th criterion in the alternative recommended by another MCDM. The value of AAFD indicates the closeness of the alternative recommended by another MCDM with that by GRA; zero or small value of AAFD means the two recommended alternatives are same or comparable.

For the fruit supply chain dataset, recommended alternatives by 5 MCDM methods with entropy and AHP weights are presented in Table 7.5. As evident from this table, weights of objectives (column 2) by the entropy and AHP methods are very different. One reason for this is the chosen favor level of 7 for RS over TC. Weights by AHP method would be equal if the favor level of RS over TC is zero. Recall that AHP method is a subjective method, and its weights depend on the favor level selected by the user.

In the case of weights by the entropy method, the recommended alternatives for fruit supply chain application by 5 MCDM methods are comparable (Table 7.5). On the other hand, use of weights by AHP method leads to recommendation of a different alternative by MABAC, PROBID, SAW and TOPSIS compared to that by GRA. Interestingly, PROBID, SAW and TOPSIS recommend the same alternative.

**Table 7.6** Recommended alternatives by 5 MCDM methods with 2 different weighting methods: VOC recovery process design

Objective	Weight	GRA	MABAC	PROBID	SAW	TOPSIS
<i>Using weights by the CRITIC method</i>						
Max. NPW	0.176857	5.698,102.8	4,115,691.5	3,557,449.5	3,528,699	3,557,449.5
Min. HTP	0.222063	1.732E-07	1.388E-07	1.584E-07	1.552E-07	1.584E-07
Min. ETP	0.164652	3.024E-05	3.148E-05	4.276E-05	4.31E-05	4.276E-05
Min. ATPM	0.163876	0.2026962	0.2111912	0.2869329	0.2892404	0.2869329
Min. PCOP	0.272552	13.631483	7.4598343	0.5780334	0.5259401	0.5780334
AAFD		Nil	0.241892	0.615242	0.626762	0.615242
<i>Using weights by BW method*</i>						
Max. NPW	0.188679	5.698,102.8	5,698,102.8	3,091,184.1	3,528,699	3,091,184.1
Min. HTP	0.05283	1.732E-07	1.732E-07	1.531E-07	1.552E-07	1.531E-07
Min. ETP	0.362264	3.024E-05	3.024E-05	3.902E-05	4.31E-05	3.902E-05
Min. ATPM	0.113208	0.2026962	0.2026962	0.2617941	0.2892404	0.2617941
Min. PCOP	0.283019	13.631483	13.631483	1.6027706	0.5259401	1.6027706
AAFD		Nil	0.0	0.560661	0.626689	0.560661

Notes NPT—Net Present Worth; HTP—Human Toxicity Potential; ETP—Ecotoxicity Potential; Atmospheric Potential; PCOP—Photochemical Oxidation Potential

\* Inputs given for BW method are as follows: Best Objective is ETP (C3), Worst Objective is HTP (C2), Best-to-Others (BO) vector (Eq. 7.9) is (3, 4, 1, 5, 2) and Worst-to-Others (WO) vector (Eq. 7.10) is (4, 1, 3, 6, 2)

**Table 7.7** Recommended alternatives by 5 MCDM methods with 2 different weighting methods: machine tool selection

Objective	Weight	GRA	MABAC	PROBID	SAW	TOPSIS
<i>Using weights by the entropy method</i>						
Min. CC	0.120161	1,100,000	1,100,000	1,100,000	1,500,000	1,920,000
Max. SS	0.114203	5940	5940	5940	3465	3790
Max. TC	0.055164	12	12	12	12	10
Min. TX	0.298785	12	12	12	6	12
Min. TZ	0.137903	15	15	15	12	20
Max. MD	0.023069	230	230	230	260	300
Max. ML	0.250715	600	600	600	420	1030
AAFD		<i>Nil</i>	<i>0</i>	<i>0</i>	<i>0.314041</i>	<i>0.32061</i>
<i>Using weights by BW method*</i>						
Min. CC	0.336328	1,100,000	1,100,000	1,100,000	1,100,000	1,100,000
Max. SS	0.164063	5940	5940	5940	5940	5940
Max. TC	0.098438	12	12	12	12	12
Min. TX	0.030078	12	12	12	12	12
Min. TZ	0.246094	15	15	15	15	15
Max. MD	0.054688	230	230	230	230	230
Max. ML	0.070313	600	600	600	600	600
AAFD		<i>Nil</i>	<i>0.0</i>	<i>0.0</i>	<i>0.0</i>	<i>0.0</i>

Notes CC—Capital Cost; SS—Spindle Speed Range; TC—Total Capacity; TX—Rapid Traverse Rate of X-axis; TZ—Rapid Traverse Rate of Z-Axis; MD—Maximum Machining Diameter; ML—Maximum Machining Length

\* Inputs given for BW method are as follows: Best Objective is CC (C1), Worst Objective is TX (C4), Best-to-Others (BO) vector (Eq. 7.9) is (1, 3, 5, 6, 2, 9, 7) and Worst-to-Others (WO) vector (Eq. 7.10) is (6, 2, 8, 1, 4, 7, 6)

This may not always occur for two reasons: weights by AHP method depend on user's inputs and different application (i.e., objective matrix). Results in Table 7.5 indicate that the recommended alternative by a MCDM method can be different depending on the weights.

For VOC recovery process design, recommended alternatives by the 5 MCDM methods with weights by CRITIC and BW methods are given in Table 7.6. Weights of two objectives (namely, NPW and PCOP) are comparable by both CRITIC and BW methods whereas those of the remaining objectives (namely, HTP, ETP and ATMP) are different. Recall that the BW method is based on user's inputs given in the footnote of Table 7.6. In the case of CRITIC weights, the 5 MCDM methods recommend different alternatives; however, PROBID and TOPSIS recommend the same alternative. Using weights by BW method, the recommended alternative by MABAC is the same as that of GRA, PROBID and TOPSIS select the same alternative, and top-ranked alternative by SAW is the same as that using CRITIC weights.

**Table 7.8** Recommended alternatives by 5 MCDM methods with 2 different weighting methods: NTM process selection

Objective	Weight	GRA	MABAC	PROBID	SAW	TOPSIS
<i>Using weights by the CRITIC method</i>						
Min.TSF	0.076097	2	2	1	2.5	1
Min. PR	0.07372	1.4	1.4	10	0.2	10
Max. MRR	0.156419	0.1	0.1	500	1.6	500
Min. C	0.068471	3	3	2	4	2
Max. E	0.065112	5	5	4	5	4
Min.TF	0.104739	2	2	2	2	2
Min.TC	0.134625	1	1	3	1	3
Max. S	0.123594	3	3	1	3	1
Max. M	0.09471	5	5	5	5	5
Max. F	0.102514	5	5	5	5	5
AAFD		<i>Nil</i>	<i>0.0</i>	<i>0.679686</i>	<i>0.377264</i>	<i>0.679686</i>
<i>Using weights by AHP method</i>						
Min. TSF	0.07352	2	2	2	2.5	2
Min. PR	0.07185	1.4	1.4	1.4	0.2	1.4
Max. MRR	0.071435	0.1	0.1	0.1	1.6	0.1
Min. C	0.119381	3	3	3	4	3
Max. E	0.119695	5	5	5	5	5
Min.TF	0.060787	2	2	2	2	2
Min.TC	0.126612	1	1	1	1	1
Max. S	0.11549	3	3	3	3	3
Max. M	0.098725	5	5	5	5	5
Max. F	0.142505	5	5	5	5	5
AAFD		<i>Nil</i>	<i>0.0</i>	<i>0.0</i>	<i>0.377264</i>	<i>0.0</i>

*Notes* TSF—Tolerance and Surface Finish; PR—Power Requirement; MRR—Material Removal Rate; C—Cost; E—Efficiency, TF—Tooling and Fixtures; TC—Tool Consumption; S—Safety; M—Work Material, F—Shape Feature

These observations are likely to be different if the user gives different inputs to BW method.

For the machine tool selection, Table 7.7 summarizes the recommended alternatives by 5 MCDM methods with weights by the entropy and BW methods, which give different weights for the objectives in this application. Using the entropy method, GRA, MABAC and PROBID recommend the same alternative whereas SAW and TOPSIS recommend a different alternative. In the case of weights by BW method, all 5 MCDM methods lead to the same alternative; however, this may not occur with other preferences of the user provided to BW method. Recall that alternatives

recommended by 5 MCDM methods with weights by BM method are not the same for the VOC recovery application in Table 7.6.

For NTM process selection, recommended alternatives by 5 MCDM methods in conjunction with 2 different methods for weights are presented in Table 7.8 whereas favor level given for objective functions for AHP method (like in Fig. 7.2) are given in Table 7.9. In this application with 10 objectives, number of favor levels required for AHP method is  $10 \times 9/2 = 45$ . For NTM process selection, weights by CRITIC method are different from those by AHP method for some objectives, and they are comparable for other objectives. If weights by the CRITIC method are used, there are 3 recommended alternatives: one is given by both GRA and MABAC, another is given by PROBID and TOPSIS, and yet another is given by SAW. Using AHP weights, 4 of 5 MCDM methods give the same recommended solution. However, SAW gives a different alternative that is same as that recommended by it with CRITIC weights. Like BW method, the user may get different recommended alternatives with different inputs for AHP method.

In summary, results for 4 applications in Tables 7.5, 7.6, 7.7 and 7.8 by 5 MCDM methods and different weighting methods clearly show that weights can affect the recommended alternative by a MCDM method (except for GRA that does not require weights) and the recommended alternatives by 5 MCDM methods can be different or similar. Given these, the user can choose a particular weighting method and MCDM method, and then perform MCDM for the application. Here, the selection of a weighting method and MCDM method is subjective and not easy. Alternatively, the user can try several weighting and MCDM methods for the application and then review the recommended alternatives for choosing one of them. The recommended alternatives will not be many, and so their review is easier compared to reviewing all alternatives in the objective matrix. For this approach, we suggest the entropy

**Table 7.9** AHP parameters (favor level of objective functions) used for NTM dataset presented in Table 7.8

	C1 (TSF)	C2 (PR)	C3 (MRR)	C4 (C)	C5 (E)	C6 (TF)	C7 (TC)	C8 (S)	C9 (M)	C10 (IF)
C1 (TSF)										
C2 (PR)	9									
C3 (MRR)	7	5								
C4 (C)	-3	-7	9							
C5 (E)	5	3	-5	-7						
C6 (TF)	0	9	-3	3	-9					
C7 (TC)	-7	0	7	0	-5	5				
C8 (S)	-3	9	0	5	7	9	-7			
C9 (M)	5	7	9	-5	-7	0	3	3		
C10 (IF)	9	3	5	-3	5	0	-5	9	5	

and CRITIC methods (since they do not require inputs from the user) and 5 MCDM methods described in this chapter.

## 7.7 Conclusion

In conclusion, this chapter described the MCDM procedure and its many details including 4 normalization methods, 4 weighting methods and 5 MCDM methods, one MS Excel program for these methods and their use for 4 diverse applications in product and system design. Main points of this chapter are as follows.

- MCDM is required for choosing one of the alternatives (from the available choices, or Pareto-optimal solutions found by solving a MOO problem). It generally involves several steps: normalization of the objective matrix, use of a weighting method and MCDM method for ranking the alternatives.
- Four normalization methods are summarized in Table 7.1). Principles and equations of the entropy, CRITIC, AHP and BW weighting methods are presented in Sect. 7.3 whereas those of 5 MCDM methods (namely, GRA, MABAC, PROBID, SAW and TOPSIS) in Sect. 7.4.
- MS Excel-based program: EMCDM445 can be employed for MCDM. It has 4 normalization methods, 4 weighting methods and 5 MCDM methods; the user can choose any one of them for her/his application.
- EMCDM445 was successfully employed for 4 diverse objective matrices (datasets) in Table 7.4. The results on weights of objectives and recommended alternatives are in Tables 7.5, 7.6, 7.7 and 7.8.
- The recommended solution for an application depends on both the chosen weighting method and MCDM method employed.
- For an application, it is not easy to choose one of the available weighting methods and one of many MCDM methods. Hence, use several MCDM methods in conjunction with a few weighting methods, and then analyze the recommended alternatives for choosing one of them for implementation. This analysis is easier compared to analyzing all alternatives in the objective matrix.
- Further studies are required for establishing the appropriate weighting and MCDM methods for an application.

### Exercises

1. Perform normalization of the objective matrix for the fruit supply chain dataset in Table 7.10 in the Appendix, by sum, vector, max–min and max methods, whose equations are in Table 7.1. Compare the range of each normalized objective by each of the four normalization methods. (Answer: ranges are summarized in the following table.)

Objective	Sum method	Vector method	Max–min method	Max method
Cost	0.0565 to 0.0724	0.225 to 0.289	0.0 to 1.0	0.780 to 1.0
Responsiveness	0.0588 to 0.0649	0.235 to 0.259	0.0 to 1.0	0.906 to 1.0

2. An objective matrix with 5 objectives (A, B, C, D and E) and 4 alternatives, is shown in the table below. The following parts can be answered using manual calculations or EMCDDM445 program.

Objective names →	A (Min)	B (Max)	C (Max)	D (Min)	E (Min)
Alternatives ↓					
1	20	8	13	4	9
2	5	2	8	17	10
3	4	17	6	2	1
4	6	6	9	15	3

- (a) Apply entropy weighting method to calculate the weights of the objectives. (Answer: weights for A, B, C, D and E are respectively 0.233374, 0.216633, 0.03823, 0.262035 and 0.249728)
  - (b) Use the weights calculated in part (a) and apply TOPSIS method to compute the closeness value for each alternative. Which alternative does TOPSIS recommend? (Answer for closeness of alternatives 1, 2, 3 and 4 are respectively 0.398895, 0.358287, 0.958917, 0.508982; TOPSIS recommends the alternative 3 with the largest closeness value)
  - (c) Use the weights you calculated in part (a) and apply the PROBID method to compute the performance score for each alternative. Which alternative does PROBID recommend? (Answer for performance score of alternatives 1, 2, 3 and 4 are respectively 0.515521, 0.326647, 1.140223, 0.584214; PROBID recommends the alternative 3 with the largest performance score)
  - (d) Do TOPSIS and PROBID recommend the same alternative? Try other weighting and MCDM methods, and compare your results obtained in parts (b) and (c).
3. Use dataset given in the previous exercise question and apply the following modifications to one or two objective functions.
- (a) Linear transformation using  $y = 4x + 5$ . Then, perform MCDM on the modified dataset using entropy and CRITIC weighting methods (i.e., in two separate trials) and 5 MCDM methods. Compare the recommended alternatives with those based on the original dataset.
  - (b) Objective reformulation using  $y = 1/x$ , where  $x$  is the value of objective B. Then, perform MCDM on the modified dataset using entropy and CRITIC weighting methods (i.e., in two separate trials) and 5 MCDM methods. Compare the recommended alternatives with those based on the original dataset.

4. Using the EMCDM445 program, perform MCDM on fruit supply chain dataset in Table 7.10 in the Appendix, by all 5 MCDM methods with CRITIC weights and compare the recommended alternatives with those in Table 7.5. Repeat this with weights by BW method.
5. Using the EMCDM445 program, perform MCDM on VOC recovery dataset in Table 7.11 in the Appendix, by all 5 MCDM methods with the entropy weights and compare the recommended alternatives with those in Table 7.6. Repeat this with weights by AHP method.
6. Using the EMCDM445 program, perform MCDM on machine tool selection dataset in Table 7.12 in the Appendix, by all 5 MCDM methods with CRITIC weights and compare the recommended alternatives with those in Table 7.7. Repeat this with weights by AHP method.
7. Using the EMCDM445 program, perform MCDM on NTM process selection dataset in Table 7.13 in the Appendix, by all 5 MCDM methods with the entropy weights and compare the recommended alternatives with those in Table 7.8. Repeat this with weights by the BW method.

## Appendix

See Tables 7.10, 7.11, 7.12 and 7.13.

**Table 7.10** Fruit supply chain dataset

Alternatives	Cost (Min)	Responsiveness (Max)
1	6,755,310.62	0.82253112
2	5,272,344.69	0.745228216
3	5,356,513.03	0.776970954
4	6,290,380.76	0.814688797
5	5,941,683.37	0.812448133
6	5,789,378.76	0.800497925
7	5,536,873.75	0.788174274
8	6,611,022.04	0.816182573
9	5,304,408.82	0.752697095
10	6,077,955.91	0.814315353
11	5,324,448.90	0.764647303
12	5,689,178.36	0.791908714
13	5,336,472.95	0.768008299
14	6,663,126.25	0.819170124
15	5,713,226.45	0.799004149
16	5,601,002.00	0.788921162



**Table 7.11** VOC recovery dataset

Alternatives	NPW (Max)	HTP (Min)	ETP (Min)	ATMP (Min)	PCOP (Min)
1	6,281,790.929	7.30988E-07	3.00506E-05	0.19937244	21.03959542
2	6,229,166.687	6.84412E-07	3.00814E-05	0.199751359	20.41826937
3	5,922,622.11	6.22614E-07	3.05126E-05	0.202878371	19.50919131
4	5,750,640.75	4.65311E-07	3.01689E-05	0.201146474	17.51728608
5	5,698,102.756	1.73162E-07	3.02393E-05	0.202696164	13.63148329
6	5,693,883.702	7.10462E-07	3.00838E-05	0.19967136	20.75485036
7	5,659,683.09	7.21214E-07	3.00848E-05	0.199638818	20.90722464
8	5,597,224.184	7.15728E-07	3.00829E-05	0.199645904	20.81855419
9	5,566,530.954	6.5288E-07	3.01385E-05	0.200251419	19.73823207
10	5,515,474.577	2.81644E-07	3.02528E-05	0.202387141	14.96397377
11	5,497,221.833	5.70282E-07	3.01166E-05	0.200408165	18.9177645
12	5,469,174.673	5.39636E-07	3.01247E-05	0.200575944	18.51884853
13	5,378,025.227	4.60758E-07	3.01775E-05	0.201221118	17.45760844
14	5,351,461.97	1.90471E-07	3.03431E-05	0.203330524	13.61091338
15	5,256,490.899	3.79832E-07	3.01838E-05	0.201561748	16.41466406
16	5,094,515.829	1.4562E-07	3.07972E-05	0.206548796	11.61647499
17	4,996,388.001	1.75383E-07	3.05412E-05	0.204718042	12.16176942
18	4,988,224.302	1.69023E-07	3.76726E-05	0.252694105	8.458640946
19	4,812,629.31	4.0948E-07	3.01596E-05	0.201289875	16.77191543
20	4,788,595.762	4.73031E-07	3.01377E-05	0.200908588	17.61107706
21	4,786,718.805	4.72134E-07	3.01428E-05	0.200945765	17.60629691
22	4,644,816.883	2.91281E-07	3.0223E-05	0.202151528	15.22202555
23	4,631,389.663	1.59444E-07	3.19886E-05	0.21450879	11.04862378
24	4,489,600.117	4.08188E-07	3.0161E-05	0.201304089	16.75923021
25	4,382,953.547	1.29189E-07	3.14197E-05	0.210795469	9.929168929
26	4,356,142.616	2.50723E-07	3.04739E-05	0.203987862	13.39663506
27	4,355,250.034	2.49254E-07	3.04727E-05	0.203985337	13.3809039
28	4,335,487.967	6.41115E-07	3.01108E-05	0.20010822	19.81656894
29	4,226,762.574	1.49214E-07	3.0556E-05	0.204913454	11.90770844
30	4,115,691.505	1.38846E-07	3.14839E-05	0.211191222	7.459834321
31	4,072,679.228	3.04457E-07	3.02154E-05	0.202051564	15.3793287
32	3,932,372.704	1.97705E-07	3.12901E-05	0.20967163	11.38121286

(continued)

**Table 7.11** (continued)

Alternatives	NPW (Max)	HTP (Min)	ETP (Min)	ATMP (Min)	PCOP (Min)
33	3,864,611.051	1.44803E-07	3.29215E-05	0.220835671	6.410976901
34	3,750,612.443	7.61273E-07	3.00531E-05	0.199277731	21.383684
35	3,722,327.172	1.45592E-07	3.28916E-05	0.220632017	6.897671194
36	3,684,853.908	2.15771E-07	3.07912E-05	0.206250338	11.69551341
37	3,656,307.745	1.3168E-07	3.3055E-05	0.221781772	6.156119184
38	3,581,084.462	1.45417E-07	3.29013E-05	0.220697725	6.420691259
39	3,574,102.037	1.46871E-07	3.29737E-05	0.221179676	6.37781606
40	3,557,449.533	1.58372E-07	4.27587E-05	0.286932892	0.578033365
41	3,528,699.024	1.55227E-07	4.31002E-05	0.289240448	0.525940059
42	3,438,917.589	1.41936E-07	3.09542E-05	0.207618275	10.12600856
43	3,395,880.46	3.46861E-07	3.02316E-05	0.202004487	15.84964087
44	3,297,992.633	3.60964E-07	3.02096E-05	0.201804876	16.00653593
45	3,180,446.649	1.49063E-07	3.09164E-05	0.207337895	10.14735474
46	3,106,722.218	1.52235E-07	3.77857E-05	0.253516331	2.904691725
47	3,105,496.908	1.52329E-07	3.77937E-05	0.253570016	2.898102931
48	3,091,881.862	1.53203E-07	3.90273E-05	0.261861129	1.603918416
49	3,091,184.09	1.531E-07	3.90172E-05	0.261794146	1.602770585
50	3,021,738.327	1.53389E-07	3.98348E-05	0.267290729	1.558477405
51	2,885,339.472	1.24338E-07	3.10629E-05	0.208414042	9.890222128
52	2,874,645.853	1.53621E-07	3.95888E-05	0.265635628	1.599423732
53	2,854,310.334	1.53972E-07	3.97016E-05	0.266392578	1.597202194
54	2,847,066.093	1.27112E-07	3.21436E-05	0.215670227	9.060510461
55	2,630,861.514	1.55004E-07	3.89627E-05	0.261420543	1.648844281
56	2,628,666.98	1.55845E-07	4.11665E-05	0.276236039	0.939751461
57	2,564,768.745	1.54999E-07	3.98216E-05	0.267195862	1.595499441
58	2,526,834.695	1.47958E-07	3.59066E-05	0.240896445	4.608506307
59	2,504,530.035	1.98914E-07	3.08089E-05	0.20643128	11.16119865
60	2,460,826.784	1.44548E-07	3.85403E-05	0.258618562	0.55303372
61	2,439,790.788	1.51158E-07	3.59447E-05	0.241141129	4.408199018
62	2,414,450.868	1.47132E-07	3.62487E-05	0.243200187	3.780157227
63	2,411,669.526	1.53714E-07	3.61916E-05	0.242792138	3.891025685
64	2,387,196.685	1.49959E-07	3.58956E-05	0.240815222	3.88391907
65	2,351,119.409	1.50929E-07	3.84824E-05	0.258205951	2.303531269

(continued)

**Table 7.11** (continued)

Alternatives	NPW (Max)	HTP (Min)	ETP (Min)	ATMP (Min)	PCOP (Min)
66	2,268,835.002	1.40145E-07	3.39013E-05	0.227441202	6.011963607
67	2,213,268.819	1.30379E-07	3.25004E-05	0.218057497	6.633146689
68	1,946,556.668	1.48144E-07	3.42886E-05	0.230016548	5.347714099
69	1,920,519.321	1.47141E-07	3.48246E-05	0.233623946	5.511532054
70	1,862,154.541	1.30472E-07	3.13628E-05	0.210408006	7.562302191
71	1,837,622.413	1.49263E-07	3.76746E-05	0.252780066	2.877145575
72	1,827,261.668	1.51106E-07	3.72667E-05	0.250030386	3.010138495
73	1,797,392.538	1.51307E-07	3.74982E-05	0.251586181	2.963300627
74	1,678,950.743	1.52483E-07	3.7474E-05	0.251419743	2.916741545

**Table 7.12** Machine tool selection dataset

	Alternatives	CC	SS	TC	TX	TZ	MD	ML
		Min	Max	Max	Min	Min	Max	Max
1	YANG ML-25A	1,550,000	3,465	8	20	20	280	520
2	YCM TC-15	1,400,000	5,950	12	15	20	250	469
3	VTURN 16	1,100,000	5,940	12	12	15	230	600
4	FEMCO WNCL-20	1,500,000	3,465	12	6	12	260	420
5	FEMCO WNCL-30	2,600,000	3,960	12	12	16	300	625
6	EX-106	1,320,000	4,950	12	24	30	240	340
7	ECOCA SJ20	1,180,000	4,480	8	24	24	250	330
8	ECOCA SJ25	1,550,000	3,950	12	15	20	280	460
9	TOPPER TNL-85A	1,200,000	3,465	8	20	24	264	400
10	TOPPER TNL-100AL	1,400,000	2,970	12	24	30	300	600
11	TOPPER TNL-85 T	1,350,000	3,465	12	30	30	264	350
12	TOPPER TNL-100 T	1,450,000	2,970	12	20	24	300	400
13	ATECH MT-52S	1,376,000	4,752	12	20	24	235	350
14	ATECH MT-52L	1,440,000	4,752	12	20	24	235	600
15	ATECH MT-75S	1,824,000	3,790	10	12	20	300	530
16	ATECH MT-75L	1,920,000	3,790	10	12	20	300	1030

**Table 7.13** Non-Traditional Machining (NTM) process selection dataset

	Alternatives	TSF	PR	MRR	Cost	E	TF	TC	S	M	F
		Min	Min	Max	Min	Max	Min	Min	Max	Max	Max
1	Ultrasonic machining	1	10	500	2	4	2	3	1	5	5
2	Water jet machining	2.5	0.22	0.8	1	4	2	2	3	5	4
3	Electrochemical machining	3	100	400	5	2	3	1	3	1	1
4	Chemical machining	3	0.4	15	3	3	2	1	3	3	1
5	Electric discharge machining	3.5	2.7	800	3	4	4	4	3	1	5
6	Wire electrical discharge machining	3.5	2.5	600	3	4	4	4	3	1	5
7	Electron beam machining	2.5	0.2	1.6	4	5	2	1	3	5	5
8	Laser beam machining	2	1.4	0.1	3	5	2	1	3	5	5

## References

Afshari A, Mojahed M, Yusuff RM (2010) Simple additive weighting approach to personnel selection problem. *Int J Innov Manag Technol* 1(5):511–515

Chakraborty S (2011) Applications of the MOORA method for decision making in manufacturing environment. *Int J Adv Manuf Technol* 54(9):1155–1166

Cheraghali-pour A, Paydar MM, Hajiaghaei-Keshteli M (2018) A bi-objective optimization for citrus closed-loop supply chain using Pareto-based algorithms. *Appl Soft Comput* 69:33–59

Diakoulaki D, Mavrotas G, Papayannakis L (1995) Determining objective weights in multiple criteria problems: the CRITIC method. *Comput Oper Res* 22(7):763–770

Fishburn PC (1967) A problem-based selection of multi-attribute decision making methods. Blackwell Publishing, New Jersey

Gidde RR, Shinde AB, Pawar PM, Ronge BP (2018) Design optimization of a rectangular wave micromixer (RWM) using Taguchi based grey relational analysis (GRA). *Microsystem Technol: Sens Actuators Syst Integr* 24(9):3651–3666

Gunantara N (2018) A review of multi-objective optimization: methods and its applications. *Cogent Eng* 5(1):1502242

Hafezalkotob A, Hafezalkotob A, Liao H, Herrera F (2019) An overview of MULTIMOORA for multi-criteria decision-making: theory developments, applications and challenges. *Inf Fusion* 51:145–177

Hwang C-L, Yoon K (1981) Multiple attribute decision making: methods and applications a state-of-the-art survey. Springer

Kulkarni AJ (ed) (2022) Multiple criteria decision making: techniques, analysis and applications, 1st edn. Springer

Lee ESQ, Rangaiah GP (2009) Optimization of recovery processes for multiple economic and environmental objectives. *Ind Eng Chem Res* 48(16):7662–7681

Liu H, Li Y, Duan Z, Chen C (2020) A review on multi-objective optimization framework in wind energy forecasting techniques and applications. *Energy Convers Manage* 224:113324

MacCrimmon KR (1968) Decision making among multiple-attribute alternatives: a survey and consolidated approach. Rand Corp, Santa Monica CA

Park M, Wang Z, Li L, Wang X (2023) Multi-objective building energy system optimization considering EV infrastructure. *Applied Energy* 332:120504

- Pamučar D, Čirović G (2015) The selection of transport and handling resources in logistics centers using Multi-Attributive Border Approximation Area Comparison (MABAC). *Expert Syst Appl* 42(6):3016–3028
- Parhi SS, Pramanik A, Rangaiah GP, Jana AK (2020) Evolutionary algorithm based multiobjective optimization of vapor recompressed batch extractive distillation: assessing economic potential and environmental impact. *Ind Eng Chem Res* 59(11):5032–5046
- Parhi SS, Rangaiah GP, Jana AK (2019) Vapor recompressed batch distillation: optimizing reflux ratio at variable mode. *Comput Chem Eng* 124:184–196
- Rangaiah GP, Feng Z, Hoadley AF (2020) Multi-objective optimization applications in chemical process engineering: tutorial and review. *Processes (basel, Switzerland)* 8(5):508
- Rezaei J (2016) Best-worst multi-criteria decision-making method: some properties and a linear model. *Omega* 64:126–130
- Saaty TL (1990) How to make a decision: the analytic hierarchy process. *Eur J Oper Res* 48:9–26
- Song Q, Jamalipour A (2005) Network selection in an integrated wireless LAN and UMTS environment using mathematical modeling and computing techniques. *IEEE Commun* 12(3):42–48
- Sun S (2002) Assessing computer numerical control machines using data envelopment analysis. *Int J Prod Res* 40(9):2011–2039
- Wang Z, Rangaiah GP (2017) Application and analysis of methods for selecting an optimal solution from the Pareto-optimal front obtained by multiobjective optimization. *Ind Eng Chem Res* 56(2):560–574
- Wang Z, Parhi SS, Rangaiah GP, Jana AK (2020) Analysis of weighting and selection methods for Pareto-optimal solutions of multiobjective optimization in chemical engineering applications. *Ind Eng Chem Res* 59(33):14850–14867
- Wang Z, Rangaiah GP, Wang X (2021) Preference ranking on the basis of ideal-average distance method for multi-criteria decision-making. *Ind Eng Chem Res* 60(30):11216–11230
- Wang Z, Li J, Rangaiah GP, Wu Z (2022) Machine learning aided multi-objective optimization and multi-criteria decision making: framework and two applications in chemical engineering. *Comput Chem Eng* 165:107945
- Zhou J, Xiahou T, Liu Y (2021) Multi-objective optimization-based TOPSIS method for sustainable product design under epistemic uncertainty. *Appl Soft Comput* 98:106850

**Part II**  
**Optimization for Financial Systems**

# Chapter 8

## Cohort Intelligence Solution to Bank Asset Liability Management



**Pranav Kulkarni, Aniket Nargundkar, Anand J. Kulkarni, and Apoorva Shastri**

**Abstract** An organization's financial management must be sound if it is to grow. Setting prioritised goals that need to be optimised is one technique to have successful financial management. These objectives could include profit maximisation, loss minimization, asset maximising, etc. These issues are categorised as multi-objective problems because they involve numerous factors that are at odds. Cohort Intelligence (CI) and the Goal Programming (GP) technique have been used in this publication to address a financial issue. The effectiveness of this strategy was demonstrated by the optimal results.

**Keywords** Cohort intelligence · Goal programming · Optimization · Asset-liability management

---

P. Kulkarni (✉)  
Marathwada Mitramandal's College of Engineering, Pune 411052, India  
e-mail: [pranav.kulkarni1337@gmail.com](mailto:pranav.kulkarni1337@gmail.com)

A. Nargundkar  
Symbiosis International (Deemed University), Symbiosis Institute of Technology, Lavale,  
Pune 412115, India  
e-mail: [aniket.nargundkar@sitpune.edu.in](mailto:aniket.nargundkar@sitpune.edu.in)

A. J. Kulkarni · A. Shastri  
Dr. Vishwanath Karad, MIT World Peace University, Pune 411038, India  
e-mail: [anand.j.kulkarni@mitwpu.edu.in](mailto:anand.j.kulkarni@mitwpu.edu.in)

A. Shastri  
e-mail: [apoorva.shastri@mitwpu.edu.in](mailto:apoorva.shastri@mitwpu.edu.in)

## 8.1 Introduction

In today's fast-moving world, all entities need to exhibit certain levels of financial strength to cope with the velocity of progress and to be dominant in their respective sectors. This financial strength in turn can be achieved by apt management of assets and liabilities, while keeping a close eye on the risk factors and making an effort for the reduction of the same.

The ratio of the assets to the liabilities is extremely important in the determination of the metrics for success and failure for any financial/non-financial entity or organization. The multidimensionality of asset and liability management as a process was demonstrated by Tektas et al. (2005). Furthermore, they also demonstrated the impact of different managerial strategies on the financial wellbeing of banks during crisis.

However, as demonstrated by Halim et al. (2015); the optimization of financial structures requires an optimization technique that goes beyond linear programming (LP), as any kind of financial optimization is classified as a multi-dimensional & multi-objective optimization problem, where various goals and constraints are considered varying from profit maximization to interest rate increase and risk reduction. Handling of these multiple objectives and constraints requires techniques that are able to consider multiple input parameters with different emphasis factors and weights for each of them.

Goal Programming (GP) is an extension of the Linear Programming Paradigm put forth by Charnes and Cooper (1957). Priorities and weights are assigned to every goal according to the hard constraints, where goals with higher weights are prioritized and set to be achieved first, while goals with lower priority are slotted after the completion of the higher priority goals. Examples of priority in goals are Solvency over Deposit Growth & Liquidity over Net Asset increase. Once these goals are completed, the lower priority goal completion is done to the best extent.

Moreover, the financial sector is not just limited to entities such as banks and funds, it also includes Stock Markets, Foreign Exchange, Cryptocurrency markets etc., which demand the forecasting of prices and commodity costs in real-time for the maximization of portfolios and minimization of various risk factors. This is a sector where optimization algorithms are preferred as they prove to be robust and provide the best results possible. The usefulness of GP models in the optimization of the financial structure was critically examined by Lin and O'Leary in 1993. A GP model was created by Siew et al in 2017 to compare and improve the financial management of Malaysian banks based on benchmark target values for each aim. Investigations have been done into six different goals, including total assets, total liabilities, equity, profitability, earnings, and total goal accomplishments.

The AI-based metaheuristics known as "socio-inspired optimization approaches" are based on the rivalry and social interaction of society's members. The most well-known socio-inspired algorithms include the Ideology Algorithm (Huan et al.



2017), Election Algorithm (Emami and Derakhshan 2015), The League Championship Algorithm (Kashan 2009), Soccer League Competition Algorithm (Moosavian 2015), Teaching Learning Based Optimization (Rao 2016), Cultural Evolution Algorithm (Kuo and Lin 2013), Social Learning Optimization (Liu et al. 2016; Ahmadi-Javid and Hooshangi Tabrizi 2017).

Kulkarni et al. created the Cohort intelligence (CI), an optimization strategy based on societal artificial intelligence (2013). Furthermore, Patankar and Kulkarni (2018) have also suggested CI variants. A cohort is a collection of learners. Through engagement and competition with other candidates in the cohort, these candidates try to exhibit their best individual behaviour. The candidates change as a result of this learning. When the majority of the candidates display similar behaviour and further learning from one another is not possible, it is assumed that the entire cohort has reached saturation.

In the past, the CI algorithm has been used to solve problems involving discrete and mixed variables (Kale and Kulkarni 2018), the 0–1 Knapsack problem (Kulkarni and Shabir 2016), data clustering applications (Krishnasamy et al. 2014), shell and tube heat exchanger optimization (Dhavle et al. 2018), healthcare (Aladeemy et al. 2020), feature selection (Aladeemy et al. 2017) as well as manufacturing process parameter optimization problems (Shastri et al. 2020, Shastri et al. 2021, Gulia and Nargundkar 2019, Pansari et al. 2019, Kulkarni et al. 2016, Kulkarni et al. 2018).

Of all the problems regarding Asset & Liability Management, the original authors of the manuscript (Kosmidou and Zopounidis 2004) have tried to solve one such problem of a specific Greek Bank by studying the ALM strategy of the year 1999 and trying to predict a future course of ALM strategy for the year 2000 using Goal Programming along with Simulation Analysis.

In this manuscript, the CI algorithm is used to solve an asset-liability management problem as defined by Kosmidou et al. 2016. The manuscript is divided as follows:

Section 8.2 describes the methodology adopted to solve the GP Asset & Liability management problem.

Section 8.3 provides the detailed mathematical formulations and the constraints for the problem.

Section 8.4 comprises of the results along with detailed illustrations for comparison of solutions obtained.

Section 8.5 includes the conclusion along with the future directions for the problem.

## 8.2 Methodology

Kulkarni et al. (2013) created Cohort Intelligence (CI); a socio-inspired optimization system based on Artificial Intelligence (AI) ideas. Candidates in a cohort communicate and compete with one another in order to attain common goals. The CI Algorithm tries to model this behaviour specifically. Each candidate observes the conduct of other candidates in the cohort in order to enhance its own behaviour. Each candidate in the cohort exhibits a specific conduct that may lead to an improvement in their own behaviour. When a candidate tries to emulate a specific behaviour marked by certain characteristics, it frequently adopts those characteristics in ways that benefit its own purpose. This leads to the entire group's overall behavioural evolution throughout time.

Multi-objective optimization is a subset of multi-criteria decision analysis, and Goal Programming (GP) is a subset of that. By reducing the variances between the target aim and the realised results, GP focuses on managing several, normally conflicting objectives. The production of set constraints with target values in GP is the result of re-formulating the original objectives. The variations from the intended goal are represented by two deviational variables,  $d^+$  (positive deviation) and  $d^-$  (negative deviation). GP prioritises goals in a hierarchical manner, with higher-priority goals being achieved first and lower-priority goals being completed after the higher-priority goals have been completed.

The Penalty Function is in charge of adding the target value to the objective function by multiplying the penalty parameter by the violation (deviation in the case of the problems discussed in this paper).

As a result, a new objective function known as the pseudo-objective function emerges. When the deviational variables have a value of 0, there is no violation of the constraints, resulting in the achievement of the objective goal. Static penalty functions, dynamic penalty functions, and adaptive penalty functions are the three basic types of penalty functions. The static penalty function approach is discussed in this manuscript, which penalises non-feasible solutions by imposing a constant penalty for violating the constraints (Table 8.1).

Further discussion is about the problem of managing assets and liabilities of a particular Greek bank are thoroughly discussed. The problem formulations in terms of decision variables, goal constraints and objective functions are presented in detail.

The problem is adopted from Kosmidou et al. 2016. In the problem, the balance sheet of a bank for the year of 2000 is determined using a Goal Programming model along with Simulation Analysis by the original authors, and this manuscript intends

**Table 8.1** Control parameters and stopping criteria of CI

Algorithm	Parameter	Stopping criteria
CI	Number of candidates = 5	1000 iterations
	Value of reduction factor = 0.9	
	Penalty parameter = 1000	

to do the same by using a different method, namely the nexus of Goal Programming and Cohort Intelligence Algorithm. The problem contains 42 independent variables, which are categorized into Assets (X) and Liabilities (Y) respectively. The details of the variables are described in the Table 8.2.

**Table 8.2** The decision variables of the goal programming function

Assets	Liabilities
X <sub>1</sub> : Cash	Y <sub>1</sub> : Due to credit institutions
X <sub>2</sub> : Cheques receivable	Y <sub>2</sub> : Due to credit institutions with agreed maturity
X <sub>3</sub> : Deposits to the Bank of Greece	Y <sub>3</sub> : Commitments arising out of sale and repurchase transactions
X <sub>4</sub> : Treasury bills and other securities issued by the Greek State	Y <sub>4</sub> : Deposits repayable on demand
X <sub>5</sub> : Other Treasury bills and securities	Y <sub>5</sub> : Saving deposits
X <sub>6</sub> : Interbank deposits and loans repayable on demand	Y <sub>6</sub> : Deposits with agreed maturity
X <sub>7</sub> : Other interbank deposits and loans	Y <sub>7</sub> : Cheques and orders payable
X <sub>8</sub> : Loans and advances to customers maturing within one year	Y <sub>8</sub> : Commitments arising out of sale and repurchase transactions(customer amounts)
X <sub>9</sub> : Loans and advances to customers maturing after one year	Y <sub>9</sub> : Dividends payable
X <sub>10</sub> : Other receivables	Y <sub>10</sub> : Income tax and other taxes payable
X <sub>11</sub> : Securities issued by Greek State	Y <sub>11</sub> : Withholdings in favour of social security funds and other third parties
X <sub>12</sub> : Other securities	Y <sub>12</sub> : Other liabilities
X <sub>13</sub> : Shares and other variable-yield securities	Y <sub>13</sub> : Accruals and deferred income
X <sub>14</sub> : Investments in non-affiliates	Y <sub>14</sub> : Accrued interest on time deposits
X <sub>15</sub> : Investments in affiliates	Y <sub>15</sub> : Other accrued expenses of the year
X <sub>16</sub> : Other assets	Y <sub>16</sub> : Provisions for staff retirement indemnities
X <sub>17</sub> : Deferred charges	Y <sub>17</sub> : Other provisions for liabilities and charges
X <sub>18</sub> : Accrued income state bonds	Y <sub>18</sub> : Loans of reduced indemnity
X <sub>19</sub> : Accrued income other bonds	Y <sub>19</sub> : Share capital
X <sub>20</sub> : Accrued income loans and advances	Y <sub>20</sub> : Retained earnings
X <sub>21</sub> : Other accrued income	
X <sub>22</sub> : Fixed assets	

### 8.2.1 Constraints & Goals

Before proceeding to the goal programming formulation, it would be appropriate to describe the constraints and goals that were used. The formulation of the problem has been adopted as specified in Kosmidou et al. 2016; with some modifications such as the addition of the penalty function.

Banking regulations place restrictions on some types of accounts. For example, total loans ( $X_8 + X_9 + X_{10}$ ) given are expected to remain stable at least at last year's levels (7,632,392) and cannot increase by more than 38% in comparison to these levels, as shown below:

$$X_8 + X_9 + X_{10} \geq 7,632,392 \quad (8.1)$$

$$X_8 + X_9 + X_{10} \leq 1.38 * 7,632,392 \quad (8.2)$$

Similarly, the following limits stipulate that total deposits must not increase by more than 28% over the previous year's levels (12,348,981) and must not fall below that level:

$$Y_4 + Y_5 + Y_6 + Y_7 + Y_8 \geq 12,348,981 \quad (8.3)$$

$$Y_4 + Y_5 + Y_6 + Y_7 + Y_8 \leq 1.28 * 12,348,981 \quad (8.4)$$

Because the share capital of commercial banks makes up the majority of their capital, the variable  $Y_{19}$  is chosen for the creation of the asset liability management model:

$$Y_{19} \geq 1,052,384 \quad (8.5)$$

Furthermore, the retained earnings to total assets  $Y_{20}$  ratio demonstrates the overall asset profitability. This ratio is set to 2.27% in this paper, which is the average growth rate of the retained earnings to total assets ratio:

$$Y_{20} \geq 2.27\% * \sum_{i=1}^{22} X_i \quad (8.6)$$

The bank's duty to reserve a certain amount of its deposits in a special interest-bearing account at the Bank of Greece, as well as in interest-bearing government bonds, results in the following constraints. Furthermore, a portion of private deposits is used to fund loans to public-sector companies:

$$Y_4 + Y_5 + Y_6 + Y_7 + Y_8 - 1.99(X_8 + X_9 + X_{10}) = 0 \quad (8.7)$$

$$Y4 + Y5 + Y6 + Y7 + Y8 - 2.29(X4 + X5 + X11 + X12 + X13) = 0 \quad (8.8)$$

$$Y4 + Y5 + Y6 + Y7 + Y8 - 5.67X3 = 0 \quad (8.9)$$

The equality relationship between assets and liabilities, as well as net worth, is defined by the constraint below (the amount 653,116 € refers to the amount of capital that is expected to be stable):

$$\sum_{i=1}^{22} X_i - \sum_{j=1}^{20} Y_j = 653116 \quad (8.10)$$

The following constraint assumes that the total assets are expected to increase not more than 30% above the previous year's levels:

$$\sum_{i=1}^{22} x_i \leq 1.30 * 17327046 \quad (8.11)$$

The solvency goal, which is linked to the bank's risk exposure, is the next goal constraint. The solvency ratio is a risk indicator that is calculated by dividing the bank's equity capital by its total weighted assets. The asset weighting reflects their proportional risk, with larger weights indicating a higher level of risk. According to the European Communities Commission's recommendation, this ratio must be larger than or equal to 8% in order to ensure the required solvency:

$$Y19 - 0.3349Y20 - 0.08(0.2X4 - 0.5X8 - 0.7X9 - 0.5X10 - 0.2X11 - 0.4X12 - X13) - d_1^+ + d_1^- = 0 \quad (8.12)$$

The liquidity target is described as the ratio of liquid assets to current obligations, which is utilised as a liquidity risk measure in the following constraint. This ratio, according to Bank policy, should be around 0.60 and not more than 0.60, suggesting that at least half of the total capital of the bank should be drawn from liquid current data rather than deposits in order to prevent liquidity risk:

$$\sum_{i=1}^{21} X_i - 0.6 \sum_{j=1}^{18} Y_j - d_2^+ + d_2^- = 0 \quad (8.13)$$

The next constraint establishes a target for deposit growth (28% greater than the previous year's deposits), indicating the management's choice to sustain the broader economy's deposit growth estimate:

$$Y4 + Y5 + Y6 + Y7 + Y8 - d_4^+ + d_4^- = 1.28 * 12,348,981 \quad (8.14)$$

Considering the historical data of the bank's prior fiscal years, it is assumed that the average growth rate of the ratio deposits to total assets should be at least 73.31%:

$$Y4 + Y5 + Y6 - d_{10}^+ + d_{10}^- = 73.31\% * 17,327,046 \quad (8.15)$$

Similarly, the following constraint specifies the goal for the increase of the loans granted which is set at 38% above the previous year's level:

$$X8 + X9 + X10 - d_3^+ + d_3^- = 1.38 * 7,632,392 \quad (8.16)$$

Finally, it should be noted that the aforementioned goal programming model includes goals requiring that variables such as cash, receivables, deposits with the Bank of Greece, and fixed assets maintain their previous year's levels:

$$X1 - 0.01 * 17,327,046 + d_6^- - d_6^+ = 0 \quad (8.17)$$

$$X2 - 0.004 * 17,327,046 + d_7^- - d_7^+ = 0 \quad (8.18)$$

$$X3 - 0.14 * 17,327,046 + d_8^- - d_8^+ = 0 \quad (8.19)$$

$$X22 - 0.015 * 17,327,046 + d_9^- - d_9^+ = 0 \quad (8.20)$$

For ease of comprehension, the decision/hard constraints are abbreviated as shown in the Table 8.3.

**Table 8.3** Abbreviations for various constraints

Hard constraint	Abbreviation
Negative deviation of share capital	$SC^-$
Negative deviation of retained earnings	$RE^-$
Positive deviation of first deposits & cheques constraint	$DC_1^-$
Negative deviation of first deposits & cheques constraint	$DC_1^+$
Positive deviation of second deposits & cheques constraint	$DC_2^+$
Negative deviation of second deposits & cheques constraint	$DC_2^-$
Positive deviation of third deposits & cheques constraint	$DC_3^+$
Negative deviation of third deposits & cheques constraint	$DC_3^-$
Positive deviation of equality between assets, liabilities & net worth	$E^+$
Negative deviation of equality between assets, liabilities & net worth	$E^-$
Positive deviation of total asset increase	$TA^+$

### 8.3 Mathematical Formulation

As previously said, the main benefit of goal programming is its flexibility, which allows the decision maker to simply incorporate different variants of constraints and goals.

The proposed goal programming formulation can be written as follows, taking into account the limitations and goals described above, as well as the preferences of the banking managers:

$$Minz = \sum_{k=3}^{10} d_k^+ + \sum_{k=3}^{10} d_k^- + 2d_2^+ + 3d_1^- \tag{8.21}$$

Subject to:

$$X8 + X9 + X10 \geq 7,632,392 \tag{8.22}$$

$$X8 + X9 + X10 \leq 1.38 * 7,632,392 \tag{8.23}$$

$$Y4 + Y5 + Y6 + Y7 + Y8 \geq 12,348,981 \tag{8.24}$$

$$Y4 + Y5 + Y6 + Y7 + Y8 \leq 1.28 * 12,348,981 \tag{8.25}$$

$$Y19 \geq 1,052,364 \tag{8.26}$$

$$Y20 \geq 2.27\% * \sum_{i=1}^{22} Xi \tag{8.27}$$

$$Y4 + Y5 + Y6 + Y7 + Y8 - 1.99(X8 + X9 + X10) = 0 \tag{8.28}$$

$$Y4 + Y5 + Y6 + Y7 + Y8 - 2.29(X4 + X5 + X11 + X12 + X13) = 0 \tag{8.29}$$

$$Y4 + Y5 + Y6 + Y7 + Y8 - 5.67X3 = 0 \tag{8.30}$$

$$\sum_{i=1}^{22} Xi - \sum_{j=1}^{20} Yj = 653116 \tag{8.31}$$

$$\sum_{i=1}^{22} xi \leq 1.30 * 17327046 \tag{8.32}$$

$$Y_{19} - 0.3349Y_{20} - 0.08(0.2X_4 - 0.5X_8 - 0.7X_9 - 0.5X_{10} - 0.2X_{11} - 0.4X_{12} - X_{13}) - d_1^+ + d_1^- = 0 \tag{8.33}$$

$$\sum_{i=1}^{21} X_i - 0.6 \sum_{j=1}^{18} Y_j - d_2^+ + d_2^- = 0 \tag{8.34}$$

$$X_8 + X_9 + X_{10} - d_3^+ + d_3^- = 1.38 * 7,632,392 \tag{8.35}$$

$$Y_4 + Y_5 + Y_6 + Y_7 + Y_8 - d_4^+ + d_4^- = 1.28 * 12,348,981 \tag{8.36}$$

$$X_1 - 0.01 * 17,327,046 + d_6^- - d_6^+ = 0 \tag{8.37}$$

$$X_2 - 0.004 * 17,327,046 + d_7^- - d_7^+ = 0 \tag{8.38}$$

$$X_3 - 0.14 * 17,327,046 + d_8^- - d_8^+ = 0 \tag{8.39}$$

$$X_{22} - 0.015 * 17,327,046 + d_9^- - d_9^+ = 0 \tag{8.40}$$

$$Y_4 + Y_5 + Y_6 - d_{10}^+ + d_{10}^- = 73.31\% * 17,327,046 \tag{8.41}$$

$$X_i \geq 0, Y_j \geq 0, d_k^- \geq 0, d_k^+ \geq 0, \forall i = 1, 2, \dots, 22; j = 1, 2, \dots, 20; k = 1, 2, \dots, 10 \tag{8.42}$$

On application of Goal Programming to the said problem, a pseudo-objective function is obtained which contains the penalty variable as shown below

$$\begin{aligned} \text{Minz} = & \sum_{k=3}^{10} d_k^+ + \sum_{k=3}^{10} d_k^- + 2d_2^+ + 3d_1^- + p[(SC^-)^2 + (RE^-)^2 \\ & + (DC_1^+)^2 + (DC_1^-)^2 + (DC_2^+)^2 + (DC_2^-)^2 + (DC_3^-)^2 \\ & + (DC_3^+)^2 + (E^+)^2 + (E^-)^2 + (TA^+)^2] \end{aligned} \tag{8.43}$$

where ‘p’ is the penalty variable that is determined prior to execution according to the constraints and goals.

In this problem, the value of penalty is set at **1000**.



### 8.4 Results

On application of the Cohort Intelligence method to the bank in question, satisfactory and comparable results are obtained when compared to the results obtained by usage of Simulation Analysis.

When compared with the actual strategy (AS) of the bank, it is evident that the values output by the CI algorithm are comparable and are better for some variables when compared with the results of the previous work, where the values are output in a large range and with high variance.

Figure 8.1 represents the convergence plot of the pseudo-objective function. For ease of visualization and to differentiate between candidates, the graph for 50 iterations is shown.

Figure 8.2 shows the plot of the various deviations for 1000 iterations that have been considered In the Goal Programming formulation.

Table 8.4 shows the solutions obtained using Cohort Intelligence & Goal Programming on the Pseudo-Objective Function (Table 8.5).

From Table 8.6, it is evident that the CI algorithm provides with comparable values when compared with the previous approach and the Actual Strategy of the bank, and the values where variance is high can be attributed to the stochastic nature of the bank’s variables, such as the rates of interest which fluctuate according to the market.

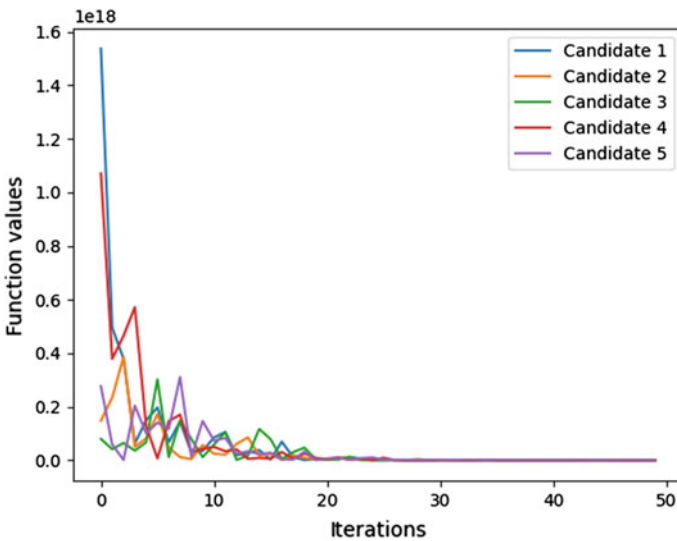


Fig. 8.1 Pseudo objective function convergence

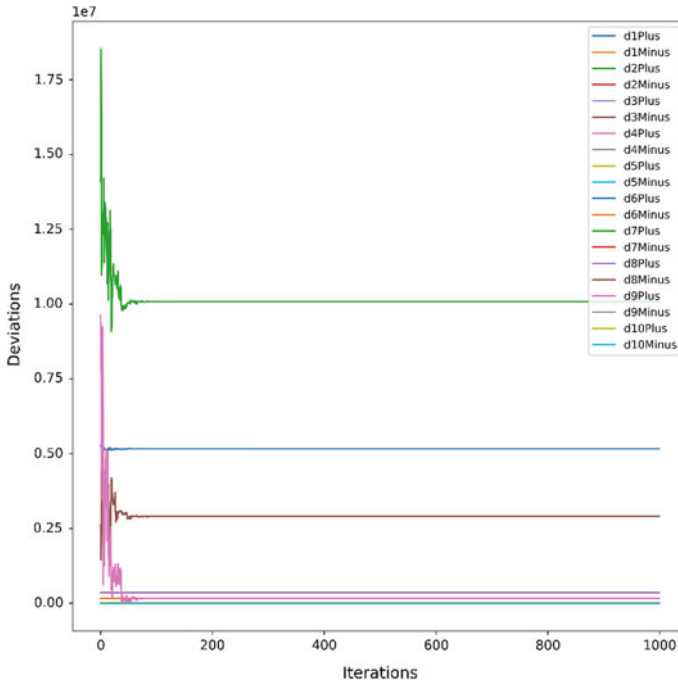


Fig. 8.2 Plot of deviations

Table 8.4 Best solution values for problem using CI

Solution methodology	CI (best version)	
Variables		
Best optimal result (lowest value of pseudo objective function)	X <sub>2</sub>	71,031.756
	X <sub>3</sub>	2,786,596.718
	X <sub>4</sub>	1,501,441.377
	X <sub>8</sub>	3,123,309.843
	X <sub>9</sub>	88,626.39721
	X <sub>10</sub>	4,724,506.883
	Y <sub>1</sub>	24,507.21165
	Y <sub>2</sub>	24,047.67432
	Y <sub>3</sub>	76,767.6659
	Y <sub>4</sub>	12,087,469.23
	Y <sub>5</sub>	308,420.4472
	Y <sub>6</sub>	309,118.5694
	Y <sub>7</sub>	3,011,661.599
	Y <sub>8</sub>	83,436.75098
	Y <sub>19</sub>	5,078,460.52
	Y <sub>20</sub>	528,683.8379

**Table 8.5** Mean of 30 solution values using CI

Solution methodology	CI (best version)	
Variables		
Mean of 30 optimal solutions	X <sub>2</sub>	70,853.25486
	X <sub>3</sub>	2,786,606.108
	X <sub>4</sub>	1,565,795.334
	X <sub>8</sub>	3,833,822.133
	X <sub>9</sub>	100,031.1494
	X <sub>10</sub>	3,944,133.206
	Y <sub>1</sub>	26,045.74366
	Y <sub>2</sub>	24,861.85964
	Y <sub>3</sub>	113,377.8983
	Y <sub>4</sub>	12,087,418.06
	Y <sub>5</sub>	307,391.4306
	Y <sub>6</sub>	307,622.0316
	Y <sub>7</sub>	3,013,765.246
	Y <sub>8</sub>	83,366.9969
Y <sub>19</sub>	5,070,027.457	
Y <sub>20</sub>	528,043.0941	
Runtime (s)	0.9025	

**Table 8.6** Comparison of solution values

Variable values	Simulation analysis	Cohort intelligence	Actual strategy of bank
X <sub>2</sub>	71,153.30	71,031.756	79,079.94
X <sub>3</sub>	2,786,231.92	2,786,596.718	1,883,999.81
X <sub>4</sub>	3,779,185.45	1,501,441.377	6,976,945.44
X <sub>8</sub>	189,120.55	3,123,309.843	8,262,491.89
X <sub>9</sub>	144,370.52	88,626.39721	3,610,828.97
X <sub>10</sub>	7,605,169.72	4,724,506.883	19,372.98
Y <sub>1</sub>	27,912.73	24,507.21165	851,488.71
Y <sub>2</sub>	27,125.26	24,047.67432	3,205,814.06
Y <sub>3</sub>	172,567.99	76,767.6659	986,568.61
Y <sub>4</sub>	12,087,289.46	12,087,469.23	3,070,110.44
Y <sub>5</sub>	309,248.10	308,420.4472	6,712,749.03
Y <sub>6</sub>	306,890.03	309,118.5694	5,637,741.45
Y <sub>7</sub>	3,011,042.54	3,011,661.599	189,980.40
Y <sub>8</sub>	83,464.84	83,436.75098	4,515,094.38
Y <sub>19</sub>	5,018,383.78	5,078,460.52	744,576.73
Y <sub>20</sub>	529,219.80	528,683.8379	337,545.89

## 8.5 Conclusion

Real world problems in the financial domain are solved using Cohort Intelligence algorithm along with Goal Programming. The problem solved consists of Asset-Liability Management with Solvency & Liquidity being at the top of the preference order for a bank in Greece. The results highlight that the CI approach generates equally good and comparable results as compared to the previous approached used by the authors which is Simulation Analysis (Kosmidou et al. 2016).

The robustness of the CI algorithm is also demonstrated by the Standard Deviation of the function values, that comes out to  $2.7792E^{15}$ , which is optimal when the gigantic ranges of the variable values are considered. The computational time for 1000 iterations of the algorithm was 0.9 s in Python which is reasonable. Further reduction in time complexity can be achieved by tuning the reduction factor and the number of candidates present in the cohort, as well as converting the code into a compiled version using JIT or Numba, or completely writing it in a compiled language such as C++.

Various real-time financial issues including the stock market, bitcoin market, FX, etc. can be solved via cohort intelligence. The algorithm's quick computation speed is useful when handling time-limited problems. Cohort intelligence has the capacity to improve prediction model accuracy while balancing the goals that need to be attained.

## References

- Aladeemy M, Tutun S, Khasawneh MT (2017) A new hybrid approach for feature selection and support vector machine model selection based on self-adaptive cohort intelligence. *Expert Syst Appl* 88:118–131
- Aladeemy M, Adwan L, Booth A, Khasawneh MT, Poranki S (2020) New feature selection methods based on opposition-based learning and self-adaptive cohort intelligence for predicting patient no-shows. *Appl Soft Comput* 86:105866
- Charnes A, Cooper WW (1957) Management models and industrial applications of linear programming. *Manage Sci* 4(1):38–91
- Dhavle SV, Kulkarni AJ, Shastri A, Kale IR (2018) Design and economic optimization of shell-and-tube heat exchanger using cohort intelligence algorithm. *Neural Comput Appl* 30(1):111–125
- Halim BA, Abd Karim H, Fahami NA, Mahad NF, Nordin SKS, Hassan N (2015) Bank financial statement management using a goal programming model. *Procedia Soc Behav Sci* 211:498–504
- Huan TT, Kulkarni AJ, Kanesan J, Huang CJ, Abraham A (2017) Ideology algorithm: a socio-inspired optimization methodology. *Neural Comput Appl* 28(1):845–876
- Kale IR, Kulkarni AJ (2018) Cohort intelligence algorithm for discrete and mixed variable engineering problems. *Int J Parallel Emergent Distrib Syst* 33(6):627–662
- Kashan AH (2009) League championship algorithm: a new algorithm for numerical function optimization. In: 2009 international conference of soft computing and pattern recognition, December 2009. IEEE, pp 43–48
- Kosmidou K, Zopounidis C (2004) Combining goal programming model with simulation analysis for bank asset liability management. *INFOR: Inf Syst Oper Res* 42(3):175–187

- Krishnasamy G, Kulkarni AJ, Paramesran R (2014) A hybrid approach for data clustering based on modified cohort intelligence and K-means. *Expert Syst Appl* 41(13):6009–6016
- Kulkarni AJ, Shabir H (2016) Solving 0–1 knapsack problem using cohort intelligence algorithm. *Int J Mach Learn Cybern* 7(3):427–441
- Kulkarni AJ, Baki MF, Chaouch BA (2016) Application of the cohort-intelligence optimization method to three selected combinatorial optimization problems. *Eur J Oper Res* 250(2):427–447
- Kulkarni O, Kulkarni N, Kulkarni AJ, Kakandikar G (2018) Constrained cohort intelligence using static and dynamic penalty function approach for mechanical components design. *Int J Parallel Emergent Distrib Syst* 33(6):570–588
- Kulkarni AJ, Durugkar IP, Kumar M (2013) Cohort intelligence: a self supervised learning behavior. In: 2013 IEEE international conference on systems, man, and cybernetics, October 2013. IEEE, pp 1396–1400
- Lin TW, O’Leary DE (1993) Goal programming applications in financial management. *Adv Math Programm Financ Plan* 3(1):211–230
- Liu ZZ, Chu DH, Song C, Xue X, Lu BY (2016) Social learning optimization (SLO) algorithm paradigm and its application in QoS-aware cloud service composition. *Inf Sci* 326:315–333
- Patankar NS, Kulkarni AJ (2018) Variations of cohort intelligence. *Soft Comput* 22(6):1731–1747
- Rao RV (2016) Teaching-learning-based optimization algorithm. In: Teaching learning based optimization algorithm. Springer, Cham, pp 9–39
- Shastri AS, Nargundkar A, Kulkarni AJ, Sharma KK (2020) Multi-cohort intelligence algorithm for solving advanced manufacturing process problems. *Neural Comput Appl* 32(18):15055–15075
- Shastri A, Nargundkar A, Kulkarni AJ, Benedicenti L (2021) Optimization of process parameters for turning of titanium alloy (grade II) in MQL environment using multi-CI algorithm. *SN Appl Sci* 3(2):1–12
- Siew LW, Wai CJ, Hoe LW (2017) Data driven decision analysis in bank financial management with goal programming model. In: International visual informatics conference, November 2017. Springer, Cham, pp 681–689
- Tektas A, Ozkan-Gunay EN, Gunay G (2005) Asset and liability management in financial crisis. *J Risk Financ*

# Chapter 9

## Cohort Intelligence Solution to Goal Programming Problems from Financial Management Domain



**Aayush P. Khandekar, Aniket Nargundkar, Anand J. Kulkarni, and Apoorva Shastri**

**Abstract** A good financial management plays a critical role for the growth of any organization. The prevalent approach of achieving this is by setting priority-based goals which need to be optimized. These goals can be maximization of profit, loss reduction, asset maximization, etc. Such problems are classified as Multi-Objective problems which involve multiple conflicting objectives. Goal Programming (GP) has been a popular approach for solving such problems. In this chapter, Cohort Intelligence (CI), a socio-inspired optimization algorithm is applied to solve four financial real-world GP problems. A Static Penalty Function approach is adopted to achieve goals as constraints. The problems are referred to as Bank Financial Statement Optimization, Financial Structure Optimization, Financial Analysis of Non-Life Insurance Sector and Technical Analysis of Non-Life Insurance Sector. The results obtained with CI approach could satisfy all the goals and constraints successfully.

**Keywords** Cohort intelligence · Goal programming · Optimization · Financial management

---

A. P. Khandekar (✉)  
Vishwakarma Institute of Technology, Pune 411037, India  
e-mail: [akhandekar582@gmail.com](mailto:akhandekar582@gmail.com)

A. Nargundkar  
Symbiosis Institute of Technology, Symbiosis International (Deemed University), Lavale,  
Pune 412115, India  
e-mail: [aniket.nargundkar@sitpune.edu.in](mailto:aniket.nargundkar@sitpune.edu.in)

A. J. Kulkarni · A. Shastri  
Dr Vishwanath Karad, MIT World Peace University, Pune 411038, India  
e-mail: [anand.j.kulkarni@mitwpu.edu.in](mailto:anand.j.kulkarni@mitwpu.edu.in)

A. Shastri  
e-mail: [apoorva.shastri@mitwpu.edu.in](mailto:apoorva.shastri@mitwpu.edu.in)

## 9.1 Introduction

In today's era, any economy or an organization needs to be financially strong to mark its dominance in the respective sector. Financial strength can be achieved by managing the assets and liabilities while monitoring and reducing the risk factors. Tektas et al. (2005) highlighted that asset and liability management is a multidimensional process. The ratio of asset to liability determines the success or failure of an organization. The financial structure of an economy or an organization plays a vital role in deciding the future of the organization which makes it necessary for the organization to prioritize certain goals/targets over others. These goals may include profit maximization, risk reduction, asset maximization, etc. Financial structure optimization is a multi-objective problem requiring an optimization technique beyond Linear Programming (LP) (Halim et al. 2015). Goal Programming (GP), an extension of Linear Programming introduced by Charnes and Cooper (1957) is capable of handling multi-objective problems. In case Goals Priorities, goals with higher priorities are set to be achieved first while goals with lower priorities are set to be achieved after the achievement of the higher priority goals. These priorities may include profit maximization over risk management, increasing the liquidity ratio over shareholder equity, etc. This ensures the achievement of higher priority goals. Once they are achieved, the model tries to achieve as many low priority goals as possible. Hence, GP is adopted to solve such financial management problems.

The financial sector is not limited to economies and organizations. It also comprises the Stock Markets, Foreign Exchange, etc. In the Stock Market, real world predictions are made on the stock price, stock selection for portfolios, etc. Fernández-Blanco et al. (2008) proposed appropriate indicating parameters for trading using Evolutionary Algorithms. Predictions using optimization algorithms are also performed on Financial Crisis Prediction. Uthayakumar et al. (2020) put forward a two-phase model based on Ant Colony Optimization (ACO). Phase one focuses on ACO based Feature Selection (ACO-FS) and the second phase focuses on ACO based Data Classification (ACO-DC). Abdel-Basset et al. (2020) presented a Multi-Criteria Decision-Making (MCDM) model based on neutrosophic Analytic Hierarchy Process(AHP), Vlse Kriterijumska Optimizacija Kompromisno Resenje (VIKOR) method, and Technique Order of Preference bi Similarity to Ideal Solution(TOPSIS) methods for optimizing the financial ratios of manufacturing companies. Lin and O'Leary (1993) critically reviewed the applicability of GP models in the financial structure optimization. Siew et al. (2017) developed a GP model to optimize and compare the financial management of the banks in Malaysia based on the benchmark target value for each goal. In total six goals such as total assets, total liability, equity, profitability, earnings and total goal achievements have been investigated.

The socio-inspired optimization methods are the type of the AI based metaheuristics which are based on the competition and interaction of the societal individuals.

The notable socio-inspired methods are Ideology Algorithm (Huan et al. 2017), Election Algorithm (Emami and Derakhshan 2015), The League Championship Algorithm (Kashan 2009), Soccer League Competition Algorithm (Moosavian 2015), Teaching Learning Based Optimization (Rao et al. 2016), Cultural Evolution Algorithm (Kuo and Lin 2013), Social Learning Optimization (Liu et al. 2016), Anarchic Society Optimization (Ahmadi-Javid and Hooshangi-Tabrizi 2017). An optimization approach—Cohort intelligence (CI) based on societal artificial intelligence is developed by Kulkarni et al. (2013). Further, the variation of CI has also been proposed by Patankar and Kulkarni (2018). A cohort is a group of learning candidates. These candidates attempt to achieve the best possible individual behavior through interaction and competition with other candidates in the cohort. This learning drives the candidates to evolve. The entire cohort is assumed to have saturated when most of the candidates exhibit similar behavior and further learning from one another is not possible. So far applications of CI algorithm include solutions to discrete and mixed variables problems (Kale and Kulkarni 2018; Kulkarni et al. 2016, 2018), 0–1 Knapsack problem (Kulkarni and Shabir 2016), data clustering application (Krishnasamy et al. 2014), shell and tube heat exchanger optimization (Dhavle et al. 2018), healthcare (Aladeemy et al. 2020), feature selection (Aladeemy et al. 2017), manufacturing process parameters optimization problems (Gulia and Nargundkar 2019; Pansari et al. 2019; Shastri et al. 2020, 2021). Recently, the Pareto based Multi-Objective Cohort Intelligence (MOCI) algorithm was proposed by Patil and Kulkarni (2020).

From this literature review it is evident that the CI algorithm can solve discrete, continuous, and mixed variable problems. It is successfully applied to solve several problems from variegated domains such as design, manufacturing, supply chain, healthcare, etc. In the current work, goals are considered as constraints and Penalty Function (PF) based constraint handling approach is adopted with CI for solving GP problems.

In this paper, CI algorithm is applied to solve four problems from the financial management domain. The remainder of the paper is organized as follows: Section 9.2 describes the methodology adopted to solve the GP finance management problems. Section 9.3 provides the detailed mathematical problem formulations. The results obtained with the comparison of solutions are illustrated in Sect. 9.3. A conclusion along with the future direction is discussed in Sect. 9.4.

## 9.2 Methodology

Cohort Intelligence (CI), a socio-inspired optimization algorithm developed by Kulkarni et al. (2013), is based on Artificial Intelligence (AI) concepts. To achieve shared goals, the candidates present in a cohort interact and compete with one another. The CI Algorithm specifically attempts to model this behavior. To improve its behavior, each candidate observes the behavior of other candidates present in the cohort. Each candidate in the cohort follows certain behavior which may result in the improvement of its own behavior. When a candidate attempts to follow a given



**Table 9.1** Control parameters and stopping criteria of CI

Algorithm	Parameter	Stopping criteria
CI	Number of candidates = 5	Objective function value is less than $10e-16$
	Value of reduction factor = 0.9	
	Penalty parameter = 10	

behavior characterized by certain qualities, it often adopts such qualities in a manner that may improve its own goal. This Leads To the overall behavioral development of the entire group overtime. The control parameters used in the experimentation with CI Algorithm is presented in Table 9.1.

GP is a branch of multi-objective optimization which itself is a branch of multi-criteria decision analysis. GP focuses on managing multiple, normally conflicting objectives by minimizing the deviations between the target goal and the realized results. In GP, re-formulation of the original objectives leads to the generation of set constraints with target values. Two deviational variables,  $d^+$  (positive deviation) and  $d^-$  (negative deviation) are formed, representing the deviations from target goal. GP focuses on the goals hierarchically; the goals with the higher priority are set to be achieved first and the goals with lower priorities are set to be achieved after the accomplishment of the higher priority goals.

The objective function is integrated with the concept of Penalty Function where the Penalty Function is responsible for adding the product of penalty parameters and the violation (deviation in the case of the problems solved in this paper) from the target value to the objective function. Hence, for every deviation exceeding the set goal for an objective, a penalty is enforced. This leads to the formation of a new objective function known as the pseudo-objective function. When the value of the deviational variables is 0, the violation of the constraints does not take place resulting in the achievement of the target goal. The Main Types of penalty functions are static penalty function, dynamic penalty function and adaptive penalty function. This paper focuses on the static penalty function approach which acts on penalizing the non-feasible solutions by applying a constant penalty for the violation of the constraints.

The penalty-based methods convert the constrained problem into unconstrained problem by penalizing the objective function when constraints are violated, and then minimize this penalized objective function using unconstrained optimization methods (Arora 2004). The conversion of constrained problem into unconstrained problem by adopting the Penalty Function based approach is shown below. The pseudo-objective function would be:

$$\text{Minimize : } d_i^+ + \text{penalty}_1 + \text{penalty}_2$$

Based on the violation of the constraints the penalty is calculated as shown:

$$\text{iff}(x) > t$$

*then penalty*<sub>1</sub> =  $f(x) - t$

*else penalty*<sub>1</sub> = 0

*end*

*if*  $g(x) > 0$

*then penalty*<sub>2</sub> =  $g(x)$

*else penalty*<sub>2</sub> = 0

*end*

In the above formulation,  $f(x)$  is an objective function,  $t$  is the set goal value and  $g(x)$  are an inequality constraint. If the problem involves an equality constraint, that could be converted to the inequality constraint by considering the limits on both sides.

### 9.3 CI Solutions to GP Problems from Financial Domains

In this section, the four Financial Problems are thoroughly discussed. The problem formulations in terms of decision variables, goal constraints and objective function are presented in detail.

#### 9.3.1 Bank Financial Statement Optimization

The problem is adopted from Halim et al. (2015). In the problem, five goals of one of the premier banks in Malaysia, viz. asset accumulation, liability reduction, equity wealth, profitability and earnings in the financial statement have been modelled with GP and optimized with CI. The details are presented in Table 9.2. The priorities for this particular problem are (from highest priority to lowest priority) maximization of the total assets, minimization of the liabilities, maximization of the equity wealth, maximization of the total earnings and maximization of profitability.

**Table 9.2** Maybank coded financial statements from 2010 to 2014 (RM' million)

Item	2010	2011	2012	2013	2014	Total
Asset	0.3367	0.4516	0.4948	0.5603	0.6403	2.4837
Liability	0.3080	0.4157	0.4509	0.5126	0.5856	2.2729
Equity	0.0287	0.0325	0.0438	0.0477	0.0547	0.2074
Profit	0.0038	0.0026	0.0057	0.0066	0.0067	0.0254
Earnings	0.2908	0.3766	0.4256	0.4792	0.5518	2.1241
Total	0.9680	1.2790	1.4209	1.6064	1.8391	7.1135

**Decision Variables:**

$x_1, x_2, x_3, x_4, x_5$  represent the number of financial statements in the years 2010, 2011, 2012, 2013 and 2014.

**Goal Constraints:**

$$0.3367x_1 + 0.4516x_2 + 0.4948x_3 + 0.5603x_4 + 0.6403x_5 + d_1^- \geq 2.4837 \quad (9.1)$$

$$0.3080x_1 + 0.4157x_2 + 0.4509x_3 + 0.5126x_4 + 0.5856x_5 + d_2^+ \leq 2.2729 \quad (9.2)$$

$$0.0287x_1 + 0.0325x_2 + 0.0438x_3 + 0.0477x_4 + 0.0547x_5 + d_3^- \geq 0.2074 \quad (9.3)$$

$$0.0038x_1 + 0.0026x_2 + 0.0057x_3 + 0.0066x_4 + 0.0067x_5 + d_4^- \geq 0.0254 \quad (9.4)$$

$$0.2908x_1 + 0.3766x_2 + 0.4256x_3 + 0.4792x_4 + 0.5518x_5 + d_5^- \geq 2.1241 \quad (9.5)$$

$$0.9680x_1 + 1.2790x_2 + 1.4209x_3 + 1.6064x_4 + 1.8391x_5 + d_6^- \geq 7.1135 \quad (9.6)$$

$$x_1 \geq 0.9 \quad (9.7)$$

$$x_2 \geq 1.279 \quad (9.8)$$

$$x_3 \geq 1.4209 \quad (9.9)$$

$$x_4 \geq 1.6064 \quad (9.10)$$

$$x_5 \geq 1.8391 \quad (9.11)$$

$$d_1^- + d_2^+ + d_3^- + d_4^- + d_5^- + d_6^- \geq 0 \tag{9.12}$$

**Objective Function:**

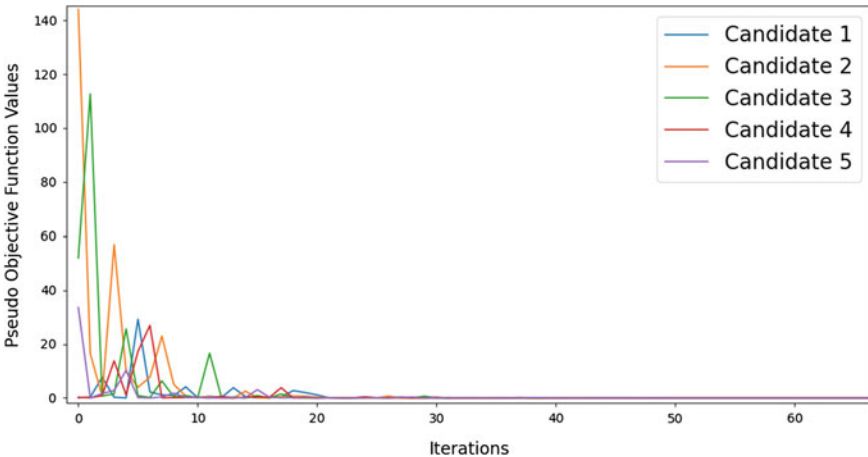
$$\text{Minimize : } d_1^- + d_2^+ + d_3^- + d_4^- + d_5^- + 2d_6^- \text{ w.r.t the goal constraints } \tag{9.13}$$

Penalty is added to the objective function that will result in a new function known as the pseudo-objective function.

**Pseudo Objective Function:**

$$\begin{aligned} \text{Minimize : } & d_1^- + d_2^+ + d_3^- + d_4^- + d_5^- + 2d_6^- + \\ & \text{penalty}(d_1^{-2} + d_2^{+2} + d_3^{-2} + d_4^{-2} + d_5^{-2} + d_6^{-2}) \end{aligned} \tag{9.14}$$

Figure 9.1 represents the convergence plot of the Bank Financial Statement Optimization problem. It shows that the convergence of the pseudo-objective function takes place successfully. The plot converges to a value of  $6 \times 10^{-5}$ . Figure 9.2 represents the line graph of the deviational variables. Table 9.3 represents the best version of solutions of deviation values, variables, standard deviation and runtime obtained while generating the optimal solution. It is evident from Table 9.4 that the CI algorithm generates excellent outcome, resulting in all the values of the deviation variables converging to zero. All The goals are achieved and the optimal solutions are generated. The comparison of solutions is also represented in Table 9.4.



**Fig. 9.1** Convergence plot of bank financial statement optimization problem

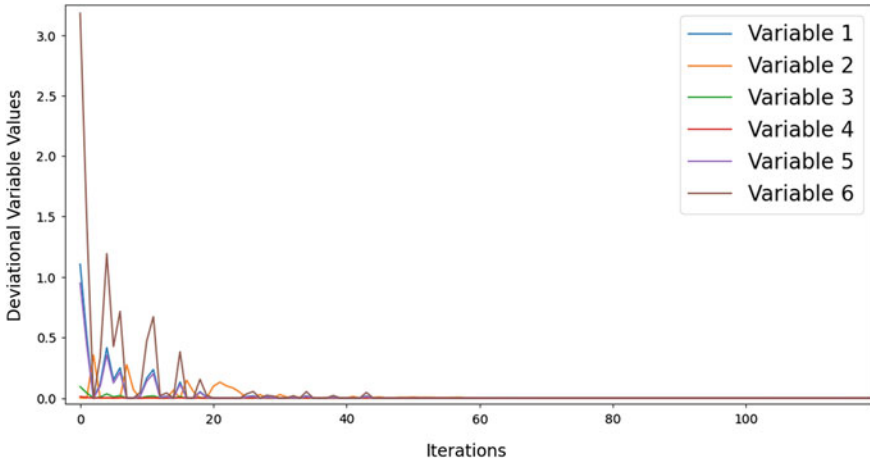


Fig. 9.2 Deviation plot of bank financial statement optimization problem

### 9.3.2 Financial Structure Optimization

The problem is adopted from Perić and Babić (2012). The considered problem is from the domain of financial structure optimization problems. The problem has eight variables representing current assets, fixed assets, current liabilities, long term liabilities, shareholder equity and retained earnings, four goals viz. current ratio, debt ratio, turnover ratio and profitability ratio and two hard constraints. The variables along with their expected ranges are given in Table 9.5. The priorities for this particular problem are minimization of the current ratio, minimization of the debt ratio, maximization of the turnover ratio and maximization of the profitability ratio.

The goals are as follows:

Current Ratio:

$$MinZ_1(x) = \frac{x_1}{x_2} \tag{9.15}$$

Debt Ratio:

$$MinZ_2(x) = \frac{x_4 + x_5}{x_6 + x_7} \tag{9.16}$$

Turnover Ratio:

$$MaxZ_3(x) = \frac{60}{x_1 + x_2} \tag{9.17}$$

Profitability Ratio:

**Table 9.3** Solutions for bank financial statement optimization using CI

Solution methodology	CI (best version)	
Variables/Goal values		
Best optimal result (lowest value of pseudo objective function)	$x_1$	0.8604
	$x_2$	0.8839
	$x_3$	1.1199
	$x_4$	0.5449
	$x_5$	1.4615
	Goal 1	2.4841
	Goal 2	2.2726
	Goal 3	0.2084
	Goal 4	0.0254
	Goal 5	2.1273
	Goal 6	7.1178
	Deviation from goal 1	0.0000
	Deviation from goal 2	0.0000
	Deviation from goal 3	0.0000
	Deviation from goal 4	0.0000
	Deviation from goal 5	0.0000
Deviation from goal 6	0.0000	
Mean of 30 optimal solutions	$x_1$	0.539
	$x_2$	9.79E-01
	$x_3$	0.69
	$x_4$	1.047
	$x_5$	1.459
	Goal 1	2.4858
	Goal 2	2.2752
	Goal 3	0.2073
	Goal 4	0.0252
	Goal 5	2.1259
	Goal 6	7.1195
	Deviation from goal 1	0.0000
	Deviation from goal 2	0.0023
	Deviation from goal 3	0.0001
	Deviation from goal 4	0.0002
	Deviation from goal 5	0.0000
Deviation from goal 6	0.0000	
Standard deviation of variables	0.2868	
Runtime (s)	0.19	

**Table 9.4** Comparison of solutions to bank financial statement optimization using CI

Goal priority	Deviation variable	Lingo software version-11 (Halim et al. 2015)	Cohort intelligence
P1	$d_1^-$	0	0
P2	$d_2^+$	0	0
P3	$d_3^-$	0	0
P4	$d_4^-$	0	$1 \times 10^{-4}$
P5	$d_5^-$	0	0
P6	$d_6^-$	0	0

**Table 9.5** Variable definitions

Parameter	Variable	Upper limit	Lower limit
Current asset	$x_1$	250	150
Fixed asset	$x_2$	300	–
Total assets	$x_3 = x_1 + x_2$	–	350
Current liabilities	$x_4$	300	75
Long-term liabilities	$x_5$	300	100
Shareholders' equity	$x_6$	125	75
Retained earnings added	$x_7$	140	100
Total liabilities and equity	$x_8 = x_4 + x_5 + x_6 + x_7$	–	–

$$Min Z_4(x) = \frac{x_7}{60} \tag{9.18}$$

S.t.

$$x_1 + x_2 + d_3^- + d_3^+ = x_4 + x_5 + x_6 + x_7 \tag{9.19}$$

$$x_1 + x_2 + d_1^- \geq 350$$

$$x_4 + x_5 + d_2^- \geq 250 \tag{9.20}$$

and

$$x_1, x_2, x_4, x_5, x_6, x_7 \geq 0 \tag{9.21}$$

**Objective Function:**

$$\text{Minimize} : d_1^- + d_2^- + d_3^- + d_3^+ \tag{9.22}$$

**Pseudo Objective Function:**

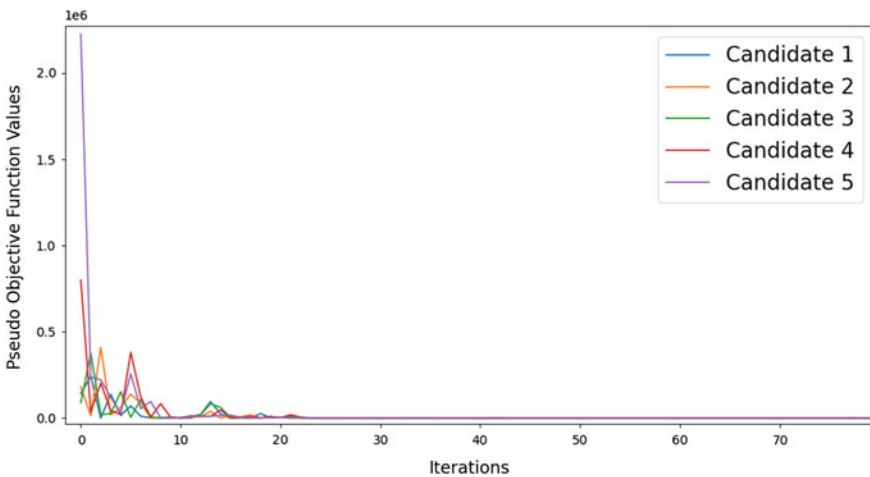
The pseudo-objective function is obtained after converting the hard constraint into soft constraints using the penalty function. The constant static penalty used is  $p = 10$ .

$$\text{Minimize} : d_1^- + d_2^- + d_3^- + d_3^+ + \text{penalty}(d_1^{-2} + d_2^{-2} + d_3^{-2} + d_3^{+2}) \tag{9.23}$$

Figure 9.3 represents the Convergence Plot of the Financial Structure Optimization Problem. It shows that the convergence of the pseudo-objective function takes place successfully. The best value (lowest) of the pseudo-objective function obtained during this convergence is  $5.68E-14$ . Figure 9.4 represents the Deviation Plot of this particular problem. It displays the values of the deviational variables tending to zero.

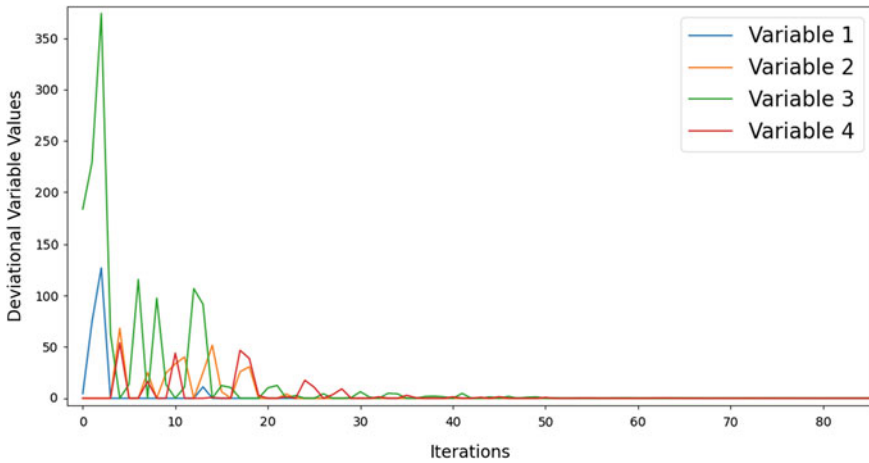
Table 9.6 represents the statistics of the solutions obtained. Along with deviation variables, variable values have also been provided for which the optimal solutions are obtained.  $z_1, z_2, z_3,$  and  $z_4$  values are also mentioned in Table 9.7. These values represent the goal ratios. All deviational variable values obtained for the best optimal solution are zero stating that the convergence of the pseudo-objective function has taken place successfully. The goal variable values i.e.,  $z_1, z_2, z_3,$  and  $z_4$  are calculated from their respective ratios and are displayed in Table 9.7. These values have been successfully optimized resulting in the achievement of the goals.

The result comparison displayed in Table 9.7 shows that the solutions obtained for the goal variables  $z_1, z_2$  and  $z_3$  are better as compared to the previous results. On



**Fig. 9.3** Convergence plot of financial structure optimization problem





**Fig. 9.4** Deviation plot of financial structure optimization problem

the contrary, the solution for  $z_4$  is slightly less than the previous obtained value. But regardless, it is an acceptable optimal solution.

### 9.3.3 *Financial and Technical Analysis of Non-Life Insurance Sector*

#### 9.3.3.1 **Financial Analysis**

This problem is adopted from Karagül (2018). This problem considers the financial analysis and the problem 4 refers to the technical analysis of non-life insurance sectors. In case of non-life insurance sectors, profit maximization and risk reduction are not the only objectives that need to be considered. Multiple goals which are set need to be achieved in order to be financially strong. These goals have a relative priority associated with them which clarifies the goals that are important and the goals that are not. Goals with less priority can be given less importance and can be achieved once the high priority goals have been achieved. In some specific cases, less priority goals can be compromised after the high priority goals have been achieved since there might not be a feasible solution which satisfies and provides an optimal solution for both the high priority goals as well as the low priority goals. For the financial analysis of the non-life insurance sector, five different goals have been considered which are mentioned in Table 9.8. The decision variables represent the financial ratios for the years 2011, 2012, ..., 2015 respectively.

**Table 9.6** Solutions for financial structure optimization using CI

Solution methodology		CI
Variables/Goal values		
Best optimal result (lowest value of pseudo objective function)	$x_1$	228.18
	$x_2$	281.18
	$x_4$	128.36
	$x_5$	135.97
	$x_6$	115.92
	$x_7$	129.10
	Goal 1	0.8115
	Goal 2	1.0788
	Goal 3	0.1178
	Goal 4	2.1518
Mean of 30 optimal solutions	$x_1$	214.66
	$x_2$	267.64
	$x_4$	1.24E+02
	$x_5$	143.78
	$x_6$	96.440
	$x_7$	117.91
	Goal 1	0.8126
	Goal 2	1.26E+00
Standard deviation of variables		19.934
Runtime (s)		0.16

**Table 9.7** Result comparison

Goal variable	Previous results (Perić and Babić 2012)	Cohort intelligence
$z_1$	1.0905	0.8115
$z_2$	1.2529	1.0788
$z_3$	0.1335	0.1178
$z_4$	2.0755	2.1518

**Goal Constraints:**

$$0.4x_1 - 3.38x_2 + 4.198x_3 + 3.36x_4 - 1.46x_5 + d_1^- \geq 0.622 \tag{9.24}$$

$$67.57x_1 + 68.61x_2 + 77.21x_3 + 81.92x_4 + 76.06x_5 + d_2^- \geq 74.274 \tag{9.25}$$

**Table 9.8** Financial ratios

Financial ratios	Year					Priority
	2011	2012	2013	2014	2015	
Return on assets	0.4	-3.38	4.19	3.36	-1.46	P1
Liquidity ratio	67.57	68.61	77.21	81.92	76.06	P2
Capital adequacy ratio	128.46	107.63	125.01	136.4	106.2	P3
Shareholders' equity/technical reserves	59.73	47.9	52.51	52.23	38.75	P4
Premium	246.68	285.24	251.38	232.09	285.65	P5

$$128.46x_1 + 107.63x_2 + 125.01x_3 + 136.4x_4 + 106.2x_5 + d_3^- \geq 120.74 \quad (9.26)$$

$$59.73x_1 + 47.9x_2 + 52.51x_3 + 52.23x_4 + 38.75x_5 + d_4^- \geq 50.22 \quad (9.27)$$

$$246.68x_1 + 285.24x_2 + 251.38x_3 + 232.09x_4 + 285.65x_5 + d_5^- \geq 260.208 \quad (9.28)$$

$$x_1, x_2, x_3, x_4, x_5 \geq 0 \quad (9.29)$$

$$x_1 \leq 502.84 \quad (9.30)$$

$$x_2 \leq 506.04 \quad (9.31)$$

$$x_3 \leq 510.3 \quad (9.32)$$

$$x_4 \leq 506 \quad (9.33)$$

$$x_5 \leq 505.2 \quad (9.34)$$

The above goal constraints are constructed from the data mentioned in Table 9.8. From the goal constraints, an objective function is formulated depending upon the identified set goals.

**Objective Function:**

$$Minimize : d_1^- + d_2^- + d_3^- + d_4^- + d_5^- \quad (9.35)$$

To obtain the pseudo-objective function, a penalty is added to the objective function.

**Table 9.9** Technical ratios

Technical ratios	Year					Priority
	2011	2012	2013	2014	2015	
Premium growth rate	21.57	19.1	21.65	8.43	20.43	P1
Technical profitability ratio	0.42	-3.53	4.1	4.68	-1.79	P2
Loss ratio	69.76	74.54	68.57	69.37	79.57	P3
Expenses ratio	26.24	25.12	24.26	23.17	22.56	P4

**Pseudo Objective Function:**

$$Minimize : d_1^- + d_2^- + d_3^- + d_4^- + d_5^- + penalty(d_1^{-2} + d_2^{-2} + d_3^{-2} + d_4^{-2} + d_5^{-2}) \tag{9.36}$$

**9.3.3.2 Technical Analysis**

This problem is adopted from Karagül (2018). For the technical analysis of the non-life insurance sector, four different ratios are considered viz. Premium growth rate, technical profitability ratio, Loss ratio and Expenses ratio. The priorities of these ratios are provided in Table 9.9. The decision variables represent the technical ratios for the years 2011, 2012, ..., 2015 respectively. Table 9.9 provides the values of the technical ratios for the years 2011–2015.

**Goal Constraints:**

$$21.57x_1 + 19.1x_2 + 21.65x_3 + 8.43x_4 + 20.43x_5 + d_1^- \geq 18.236 \tag{9.37}$$

$$0.42x_1 - 3.53x_2 + 4.1x_3 + 4.68x_4 - 1.79x_5 + d_2^- \geq 0.776 \tag{9.38}$$

$$69.76x_1 + 74.54x_2 + 68.57x_3 + 69.37x_4 + 79.57x_5 + d_3^+ \leq 72.362 \tag{9.39}$$

$$26.24x_1 + 25.12x_2 + 24.26x_3 + 23.17x_4 + 22.56x_5 + d_4^+ \leq 24.27 \tag{9.40}$$

$$x_1, x_2, x_3, x_4, x_5 \geq 0 \tag{9.41}$$

$$x_1 \leq 117.98 \tag{9.42}$$

$$x_2 \leq 115.23 \tag{9.43}$$

$$x_3 \leq 118.58 \quad (9.44)$$

$$x_4 \leq 105.65 \quad (9.45)$$

$$x_5 \leq 120.77 \quad (9.46)$$

### Objective Function:

$$\text{Minimize} : d_1^- + d_2^- + d_3^+ + d_4^+ \quad (9.47)$$

### Pseudo Objective Function:

$$\text{Minimize} : d_1^- + d_2^- + d_3^+ + d_4^+ + \text{penalty}(d_1^{-2} + d_2^{-2} + d_3^{+2} + d_4^{+2}) \quad (9.48)$$

Tables 9.10 and 9.11 present the statistical data of the solutions obtained for Financial and Technical Analysis of Non-Life Insurance Sectors respectively. These statistics include the best optimal values for variables, goals and deviational variables. It is evident from Tables 9.10 and 9.11 that values of the deviational variables for both the problems are zero, indicating that the solutions obtained successfully satisfies the set goals. The function values obtained are precise up to  $10^{-9}$  indicating that the function values eventually converge to zero. For variable values, it should be noted that the algorithm does not violate the bounds set for each variable.

## 9.4 Conclusion

Real-world applications of CI algorithm in the financial domain are solved in this paper. The problems solved are Bank Financial Statement Optimization, Financial Structure Optimization, Financial and Technical Analysis of the Non-Life Insurance Sector. The results highlight that the CI approach has generated optimal results which satisfy all constraints set for the pseudo-objective function. Additionally, the standard deviation obtained for each pseudo-objective function is less than  $1 \times 10^{-3}$  indicating the robustness of the CI algorithm. The computational time for all the problems was less than 0.3 s which is reasonable. The computational time can be further reduced by tuning the reduction factor and number of candidates present in the cohort. In the near future, Cohort Intelligence can be applied to various real-time financial problems related to the stock market, cryptocurrency market, forex, etc. Low computation time of the algorithm proves beneficial while solving time bound problems. Cohort Intelligence has the potential to optimize prediction models to improve the accuracy while balancing the targets that are set to achieve.

**Table 9.10** Solutions for financial analysis of non-life insurance sector using CI

Solution methodology	CI	
Variables/Goal values		
Best optimal result (lowest value of pseudo objective function)	$x_1$	114.06
	$x_2$	358.75
	$x_3$	411.60
	$x_4$	248.71
	$x_5$	437.81
	Goal 1	757.41
	Goal 2	117776
	Goal 3	185140
	Goal 4	75566.3
	Goal 5	416722
	Deviation from goal 1	0
	Deviation from goal 2	0
	Deviation from goal 3	0
	Deviation from goal 4	0
	Deviation from goal 5	0
Mean of 30 optimal solutions	$x_1$	244.64
	$x_2$	233.51
	$x_3$	267.95
	$x_4$	341.89
	$x_5$	238.18
	Goal 1	1234.46
	Goal 2	9.94E+04
	Goal 3	161987
	Goal 4	66955.1
	Goal 5	341703
	Deviation from goal 1	0
	Deviation from goal 2	0
	Deviation from goal 3	0
	Deviation from goal 4	0
	Deviation from goal 5	0
Average standard deviation of variables	131.02	
Runtime (s)	0.27	

**Table 9.11** Solutions for technical analysis of non-life insurance sector using CI

Solution methodology	CI	
Variables/Goal values		
Best optimal result (lowest value of pseudo objective function)	$x_1$	80.964
	$x_2$	16.438
	$x_3$	52.679
	$x_4$	54.582
	$x_5$	105.61
	Goal 1	5818.6
	Goal 2	258.35
	Goal 3	22,675
	Goal 4	7462.7
	Deviation from goal 1	0
	Deviation from goal 2	0
	Deviation from goal 3	0
	Deviation from goal 4	0
	Mean of 30 optimal solutions	$x_1$
$x_2$		51.664
$x_3$		67.841
$x_4$		70.897
$x_5$		48.531
Goal 1		5401.4
Goal 2		3.67E+02
Goal 3		21,670
Goal 4		7331.6
Deviation from goal 1		0
Deviation from goal 2		0
Deviation from goal 3		0
Deviation from goal 4		0
Average standard deviation of variables		31.287
Runtime (s)	0.26	

## References

Abdel-Basset M, Ding W, Mohamed R, Metawa N (2020) An integrated plithogenic MCDM approach for financial performance evaluation of manufacturing industries. *Risk Manag* 22(3):192–218

Ahmadi-Javid A, Hooshangi-Tabrizi P (2017) Integrating employee timetabling with scheduling of machines and transporters in a job-shop environment: a mathematical formulation and an anarchic society optimization algorithm. *Comput Oper Res* 84:73–91

- Aladeemy M, Adwan L, Booth A, Khasawneh MT, Poranki S (2020) New feature selection methods based on opposition-based learning and self-adaptive cohort intelligence for predicting patient no-shows. *Appl Soft Comput* 86:105866
- Aladeemy M, Tutun S, Khasawneh MT (2017) A new hybrid approach for feature selection and support vector machine model selection based on self-adaptive cohort intelligence. *Expert Syst Appl* 88:118–131
- Arora JS (2004) *Introduction to optimum design*. Elsevier Academic Press, San Diego, California, USA
- Charnes A, Cooper WW (1957) Management models and industrial applications of linear programming. *Manag Sci* 4(1):38–91
- Dhavle SV, Kulkarni AJ, Shastri A, Kale IR (2018) Design and economic optimization of shell-and-tube heat exchanger using cohort intelligence algorithm. *Neural Comput Appl* 30(1):111–125
- Emami H, Derakhshan F (2015) Election algorithm: a new socio-politically inspired strategy. *AI Commun* 28(3):591–603
- Fernández-Blanco P, Bodas-Sagi DJ, Soltero FJ, Hidalgo JI (2008) Technical market indicators optimization using evolutionary algorithms. In: *Proceedings of the 10th annual conference companion on Genetic and evolutionary computation*, July 2008, pp 1851–1858
- Gulia V, Nargundkar A (2019) Optimization of process parameters of abrasive water jet Machining using variations of Cohort Intelligence (CI). In: Malik H, Srivastava S, Sood Y, Ahmad A (eds) *Applications of Artificial Intelligence Techniques in Engineering*. *Advances in Intelligent Systems and Computing*, vol 697. Springer, Singapore
- Halim BA, Abd Karim H, Fahami NA, Mahad NF, Nordin SKS, Hassan N (2015) Bank financial statement management using a goal programming model. *Procedia Soc Behav Sci* 211:498–504
- Huan TT, Kulkarni AJ, Kanesan J, Huang CJ, Abraham A (2017) Ideology algorithm: a socio-inspired optimization methodology. *Neural Comput Appl* 28(1):845–876
- Kale IR, Kulkarni AJ (2018) Cohort intelligence algorithm for discrete and mixed variable engineering problems. *Int J Parallel Emergent Distrib Syst* 33(6):627–662
- Karagül BZ (2018) Financial and technical analysis of insurance sector with goal programming model. *Sigma J Eng Nat Sci* 36(2):553–561
- Kashan AH (2009) League championship algorithm: a new algorithm for numerical function optimization. In: *2009 international conference of soft computing and pattern recognition*, December 2009. IEEE, pp 43–48
- Krishnasamy G, Kulkarni AJ, Paramesran R (2014) A hybrid approach for data clustering based on modified cohort intelligence and K-means. *Expert Syst Appl* 41(13):6009–6016
- Kulkarni AJ, Shabir H (2016) Solving 0–1 knapsack problem using cohort intelligence algorithm. *Int J Mach Learn Cybern* 7(3):427–441
- Kulkarni AJ, Baki MF, Chaouch BA (2016) Application of the cohort-intelligence optimization method to three selected combinatorial optimization problems. *Eur J Oper Res* 250(2):427–447
- Kulkarni AJ, Durugkar IP, Kumar M (2013) Cohort intelligence: a self supervised learning behavior. In: *2013 IEEE international conference on systems, man, and cybernetics*, October 2013. IEEE, pp 1396–1400
- Kulkarni O, Kulkarni N, Kulkarni AJ, Kakandikar G (2018) Constrained cohort intelligence using static and dynamic penalty function approach for mechanical components design. *Int J Parallel Emerg Distrib Syst* 33(6):570–588
- Kuo HC, Lin CH (2013) Cultural evolution algorithm for global optimizations and its applications. *J Appl Res Technol* 11(4):510–522
- Lin TW, O’Leary DE (1993) Goal programming applications in financial management. *Adv Math Program Financ Plan* 3(1):211–230
- Liu ZZ, Chu DH, Song C, Xue X, Lu BY (2016) Social learning optimization (SLO) algorithm paradigm and its application in QoS-aware cloud service composition. *Inf Sci* 326:315–333
- Moosavian N (2015) Soccer league competition algorithm for solving knapsack problems. *Swarm Evol Comput* 20:14–22



- Pansari S, Mathew A, Nargundkar A (2019) An investigation of burr formation and cutting parameter optimization in micro-drilling of brass C-360 using image processing. In: Proceedings of the 2nd international conference on data engineering and communication technology. Springer, Singapore, pp 289–302
- Patankar NS, Kulkarni AJ (2018) Variations of cohort intelligence. *Soft Comput* 22(6):1731–1747
- Patil MV, Kulkarni AJ (2020) Pareto dominance based multiobjective cohort intelligence algorithm. *Inf Sci* 538:69–118
- Perić T, Babić Z (2012) Financial structure optimization by using a goal programming approach. *Croat Oper Res Rev* 3(1):150–162
- Rao RV (2016) Teaching-learning-based optimization algorithm. *Teaching learning based optimization algorithm*. Springer, Cham, pp 9–39
- Shastri AS, Nargundkar A, Kulkarni AJ, Sharma KK (2020) Multi-cohort intelligence algorithm for solving advanced manufacturing process problems. *Neural Comput Appl* 32(18):15055–15075
- Shastri A, Nargundkar A, Kulkarni AJ, Benedicenti L (2021) Optimization of process parameters for turning of titanium alloy (Grade II) in MQL environment using multi-CI algorithm. *SN Appl Sci* 3(2):1–12
- Siew LW, Wai CJ, Hoe LW (2017) Data driven decision analysis in bank financial management with goal programming model. In: International visual informatics conference, November 2017. Springer, Cham, pp 681–689
- Tektas A, Ozkan-Gunay EN, Gunay G (2005) Asset and liability management in financial crisis. *J Risk Financ*
- Uthayakumar J, Metawa N, Shankar K, Lakshmanaprabu SK (2020) Financial crisis prediction model using ant colony optimization. *Int J Inf Manag* 50:538–556

# Chapter 10

## Solving Asset and Liability Management Problem Using Cohort Intelligence and Goal Programming



Ishan G. Gala, Aniket Nargundkar, Anand J. Kulkarni, and Apoorva Shastri

**Abstract** An organization's growth is dependent on proper financial management; this needs to be done in the most optimal way possible. One possible approach is to set priority-based goals and optimize them based on these goals. The goals can be maximizing net profit, reducing non-performing assets, reducing loss, etc. This is a multi-objective problem in which there are multiple conflicting variables and goals with different priorities. Cohort Intelligence (CI) along with Goal Programming (GP) approach is used in this paper to solve asset and liability management problems. Varied results are obtained compared to the previous method used to solve this problem.

**Keywords** Cohort intelligence · Goal programming · Optimization · Asset and liability

### 10.1 Introduction

In today's finance-driven world managing your finances optimally is one of the top priorities. Managing finances at a personal level is very easy compared to managing

---

I. G. Gala (✉)  
Marathwada Mitramandal's College of Engineering, Pune 411052, India  
e-mail: [ishangala16@gmail.com](mailto:ishangala16@gmail.com)

A. Nargundkar  
Symbiosis International (Deemed University), Symbiosis Institute of Technology, Lavale,  
Pune 412115, India  
e-mail: [aniket.nargundkar@sitpune.edu.in](mailto:aniket.nargundkar@sitpune.edu.in)

A. J. Kulkarni · A. Shastri  
Dr. Vishwanath Karad, MIT World Peace University, Pune 411038, India  
e-mail: [anand.j.kulkarni@mitwpu.edu.in](mailto:anand.j.kulkarni@mitwpu.edu.in)

A. Shastri  
e-mail: [apoorva.shastri@mitwpu.edu.in](mailto:apoorva.shastri@mitwpu.edu.in)

finances at an organizational level. Assets and Liabilities are the two main aspects when it comes to managing finances.

An asset is a resource with monetary value that an individual, corporation or country owns or controls with the expectation of future benefit. A company's assets are reported on its balance sheet. They are divided into four categories: current, fixed, financial and intangible. They are purchased or created to increase a company's value or benefit its operations. An asset is anything that can generate cash flow, reduce expenses or increase sales in the future, whether it's manufacturing equipment or a patent. A liability is something that a person or company owes, usually a monetary amount. Liabilities are settled over time by transferring economic benefits such as money, goods or services. Liabilities on the balance sheet include loans, accounts payable, mortgages, deferred revenues, bonds, warranties and accrued expenses. Liabilities and assets can be contrasted. Liabilities are things you owe or have borrowed, whereas assets are things you own or are owed.

Any organization's success or failure is determined by its asset-to-liability ratio. The financial structure of an economy or an organization is critical in determining the organization's future, requiring the organization to prioritize certain goals/targets over others. Profit maximization, risk reduction, asset maximization and so on are examples of such objectives. Managing the assets and liabilities of an organization is the main goal of this paper. Financial structure optimization is a multi-objective problem that requires a technique other than Linear Programming (LP) (Halim et al. 2015). Goal Programming (GP), a Linear Programming extension introduced by Charnes and Cooper in 1961, can handle multi-objective problems. When it comes to goal priorities, higher priority goals are set to be completed first, while lower priority goals are set to be completed after the higher priority goals are completed. Profit maximization over risk management, increasing the liquidity ratio over shareholder equity and so on are examples of such priorities. This ensures that higher priority goals are met. After they are completed, the model attempts to complete as many low priority goals as possible. As a result, GP is used to solve such financial problems. Lin and O'Leary (1993) conducted a critical review of the applicability of GP models in financial structure optimization. Siew et al. (2017) created a GP model to optimize and compare bank financial management.

AI-based metaheuristics such as socio-inspired optimization methods are based on competition and interaction of the individuals in that environment. The notable socio-inspired methods are Ideology Algorithm (Huan et al. 2017), Election Algorithm (Emami and Derakhshan 2015), The League Championship Algorithm (Kashan, 2009), Teaching Learning Based Optimization (Rao, 2016), Soccer League Competition Algorithm (Moosavian, 2015), Cultural Evolution Algorithm (Kuo and Lin, 2013), Social Learning Optimization (Liu et al., 2016), Anarchic Society Optimization (Ahmadi-Javid and Hooshangi-Tabrizi, 2017). Cohort Intelligence (CI) based on artificial intelligence is developed by Kulkarni et al. (2013). Further, the variations of CI have also been proposed by Patankar and Kulkarni (2018). A cohort is a group of candidates who learn. Through interaction and competition with other candidates in the cohort, these candidates attempt to achieve the best possible individual behaviour. This learning helps the candidates to evolve. When the majority

of the candidates exhibit similar behaviour and further learning from one another is impossible, the entire cohort is assumed to have saturated. So far applications of the CI algorithm include solutions to discrete and mixed variables problems (Kale and Kulkarni 2018), 0–1 Knapsack problem (Kulkarni and Shabir 2016).

In this paper, the CI algorithm is applied to solve asset and liability management problem adopted by Tanwar et al. (2020). The paper is organized as follows: Sect. 10.2 describes the methodology adopted to solve the problem using CI and GP. Section 10.3 provides detailed mathematical problem formulations. The results obtained with the comparison of solutions are illustrated in Sect. 10.4. A conclusion along with the future direction is discussed in Sect. 10.5.

## 10.2 Methodology

Cohort Intelligence (CI) is an optimization algorithm developed by Kulkarni et al. in 2013. CI is based on artificial intelligence (AI) concepts. It attempts to model the behavior often observed in a self-organizing system in which candidates in a cohort interact and compete with one another in order to achieve shared goals. Each candidate attempts to improve his/her own behaviour by observing the behaviour of all other candidates in the cohort. Each candidate in the cohort exhibits a specific behaviour, which may improve their own behaviour.

When a candidate attempts to follow a specific behaviour characterized by certain qualities, it frequently adopts such qualities in a way that may help it achieve its own goal. As a result, candidates in the cohort learn from one another, which helps to improve the behaviour of the entire group over time. The cohort's behaviour is said to have reached saturation (convergence) if, after a significant number of learning attempts, the individual behaviour of all candidates does not improve significantly, making differentiation difficult. In other words, the differences in the candidates' individual behaviours become insignificant.

GP focuses on dealing with several, often conflicting objectives that have been assigned a target value that must be achieved. It's a branch of multi-objective optimization, which is itself a branch of multi-criteria decision analysis. Divergence variables ( $d+$  and  $d-$ ) are used in GP equations to indicate the amount of deviation from the objective goal.

The penalty function is responsible for the correction measure/penalty given for the deviation in decision constraints. It is the product of the penalty parameter multiplied by the square of deviation. This generates a new objective function known as the pseudo function. When the value of deviation variables is 0, there is no penalty given to the objective function which results in the achievement of the goal. The main types of penalty functions are static penalty function, dynamic penalty function and adaptive penalty function. The static penalty function approach is used in this paper which penalizes the non-feasible solutions by applying a constant penalty for the constraint violation (Table 10.1).

**Table 10.1** Control parameters and stopping criteria of CI

Algorithm	Parameter	Stopping criteria
CI	Number of candidates = 5	1000 iterations
	Value of reduction factor = 0.9	
	Penalty parameter = 1000	

The main objective of this paper is to design a model that can optimize the assets and liabilities of a bank using Cohort Intelligence (CI) and Goal Programming. The data we are referring to in this paper to formulate and solve the problem is from the Oriental Bank of Commerce (OBC Bank). The problem is taken from the research paper published in the Indian Journal of Finance and Banking by Tanwar et al. (2020).

The goals for the banks, as suggested by experts, we have taken the same goals as mentioned in the paper.

Table 10.2 contains all the goals that need to be achieved.

These goals need to be achieved based on priorities. Each goal has a different priority. The formulation of equations is done based on the goals. There are different decision variables segregated as assets and liabilities. This is the main aim of the paper of manage assets and liabilities.

**Table 10.2** Goals to be achieved based on priority

Goals	Definition
Liquidity risk	Liquidity risk is the inability of a bank to meet its obligation when it arises. Banks manage their liquidity risk through ALM
Capital adequacy	The Capital Adequacy ratio determines the extent of capital a bank requires against its risk-weighted credit exposure to protect it against losses before the risk of insolvency
Market share of deposit	It shows the bank's share of customer deposits in an aggregate deposit of scheduled commercial banks in India
Market share of credit	It shows the credit available to banks from the aggregate credit facility available to all scheduled commercial banks in India
Return on asset	It shows the profit-generating capacity of a bank from its total asset available. The higher the ratio better it is for the bank
Return on equity	It measures the return on investment invested by shareholders. The higher the ratio the better it is for the company
Non-performing asset	The banks want to reduce their non-performing asset. It is calculated by dividing Gross NPA by Gross Advances. The lower the ratio, the better it is for the bank

### 10.3 Mathematical Formulation

#### 10.3.1 Decision Variables

Identification of the decision variables.

The Indian bank balance sheet has assets and liabilities. These assets and liabilities are the decision variables.

Table 10.3 contains all the decision variables used to formulate the decision constraints, goal constraints and objective function.

**Table 10.3** Decision variables

<b>Assets</b>
<i>Cash and bank balance</i>
Cash in hand
Balance with RBI
Balance with banks and money at call and short notice in India
Balance with banks and money at call and short notice outside India
<i>Investments</i>
Investment in government securities
Investment in approved securities
Shares
Debentures
Investment in subsidiaries/joint ventures
Others (commercial papers, mutual funds, etc.)
<i>Advances</i>
Bills purchased and discounted
Cash credit, overdrafts, loans repayable on demand
Term loans
Advances in priority sector
Advances in banks in India
Fixed assets and intangible assets
Other assets
<b>Liabilities</b>
<i>Shareholders fund</i>
Capital
Reserves and surplus
<i>Deposits</i>

(continued)

**Table 10.3** (continued)

<b>Assets</b>
Demand deposit
Saving deposits
Term deposits
<i>Borrowings</i>
Borrowings from India
Borrowings from RBI
Borrowings from banks and other institutions and agencies
Borrowings outside India
Other liabilities
Others (including provisions)

### 10.3.2 Decision Constraints and Goal Constraints

The equations for decision constraints and goal constraints are adopted from the original manuscript Mathematical modelling of asset liability management in banks using goal programming and AHP (Tanwar et al. 2020) please refer to the main paper for equations.

**Goal Constraints:**

1. Market Share of Credit

$$\begin{aligned}
 & \textit{Bills Purchased \& discounted} \\
 & + \textit{Cash Credit, Overdrafts, Loans repayable on demand} \quad (10.1) \\
 & + \textit{Term Loans} + d_1^- - d_1^+ = 1758137400
 \end{aligned}$$

2. Market Share of Deposit

$$\textit{Demand Deposit} + \textit{Saving Deposits} + \textit{Term Deposits} + d_2^- - d_2^+ = 2325928410 \quad (10.2)$$

3. Return on equity

$$0.0046(\textit{Capital} + \textit{Reserves\&Surplus}) + d_3^- - d_3^+ = 549938 \quad (10.3)$$

4. Return on Asset

$$\begin{aligned}
 & 0.0004(\textit{Sum of first 13 asset variables} + \textit{Fixed Assets} + \textit{Other Assets}) \\
 & + d_4^- - d_4^+ = 549938 \quad (10.4)
 \end{aligned}$$

5. Capital adequacy ratio

$$x1 = \textit{Investment in government securities}$$

- x2 = Investment in approved securities
- x3 = Shares
- x4 = Debentures
- x5 = Investment in Subsidiaries/Joint Ventures
- x6 = Others (Commercial papers, Mutual funds, etc.)
- x7 = Bills Purchased & discounted
- x8 = Cash Credit, Overdrafts, Loans repayable on demand
- x9 = Term Loans

$$\begin{aligned}
 & \text{Capital} + \text{Reserves \& Surplus} + d_5^- - d_5^+ \\
 & = 0.115 * (0.5 * (x1 + x2) + \\
 & \quad 1.25 * (x3 + x4 + x5 + x6) + x7 + x8 + 1.25 * (x9))
 \end{aligned} \tag{10.5}$$

6. Liquidity risk

NTDL = Demand Deposit + Saving Deposits + Term Deposits + Borrowings from RBI + (Borrowings from Banks and other institutions and Agencies) + Other Liabilities – (Balance with Banks and Money at call and short notice in India) – (Advances in Banks in India)

EXCASH = Balance with RBI – 0.04\*(NTDL)

HQLA = Cash in hand + EXCASH + Investment in government securities – 0.195\*(NTDL) + 0.15\*(NTDL)

$$\text{HQLA} + d_6^- - d_6^+ = 374319700 \tag{10.6}$$

7. Gross NPA

$$\begin{aligned}
 & \text{NPA} + d_7^- - d_7^+ \\
 & = 0.10 * (\text{Bills Purchased \& discounted} + \text{Term Loans} \\
 & \quad + \text{Cash Credit, Overdrafts, Loans repayable on demand})
 \end{aligned} \tag{10.7}$$

Table 10.4 contains deviation variables which would be used in the objective for minimization. Every goal has a different deviation variable based on the type of deviation (positive or negative).

While formulating the objective function weights have been assigned to each goal based on their priority. The deviation variables are multiplied by weights in the objective function.

Objective Function:



**Table 10.4** Deviation variables for objective function

Goal	Deviation variable
Market share of credit	$d_1^-$
Market share of the deposit	$d_2^-$
Return on equity	$d_3^-$
Return on asset	$d_4^-$
Capital adequacy	$d_5^-$
Liquidity risk	$d_6^-$
NPA	$d_7^+$

$$Z = 0.0504 * d_1^- + 0.0446 * d_2^- + 0.138 * d_3^- + 0.133 * d_4^- + 0.229 * d_5^- + 0.208 * d_6^- + 0.107 * d_7^+ \quad (10.8)$$

## 10.4 Results

Assets and liabilities play a significant role in the growth of a company, if managed properly they can boost profits and reduce the risk of a company losing money. The CI model developed can be applied to any bank by modifying the multiplier in each expression as per their balance sheet structure.

Solving the asset and liability problem for the above bank data using Cohort Intelligence, varied results are obtained when compared to the method used previously.

Figure 10.1 represents the convergence plot of the pseudo-objective function. The below graph is shown for 100 interactions to understand the convergence curve.

Figure 10.2 shows the plot of deviations of goal constraints for 100 iterations that have been considered in formulation using Goal Programming.

Table 10.5 shows the solutions obtained using Cohort Intelligence and Goal Programming on the Pseudo-Objective Function.

Table 10.6 shows the mean of 30 optimal solutions obtained using Cohort Intelligence and Goal Programming on the Pseudo-Objective Function.

Out of the 7 goals mentioned in Table 10.2, 10.6 goals are successfully achieved such as Market share of credit, Market share of deposits, Return on assets, Return on equity, Capital adequacy ratio and Non-performing asset, however, the goal for Liquidity risk is not achieved and hence it is not considered while calculating standard deviation in Table 10.5.

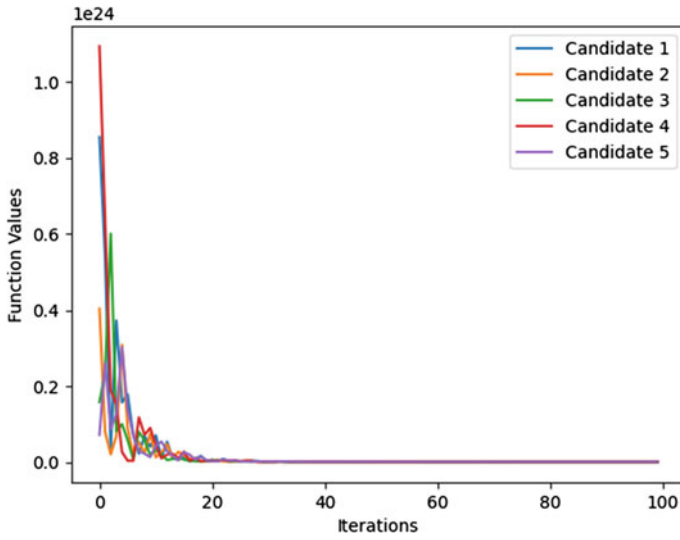


Fig. 10.1 Pseudo-objective function convergence

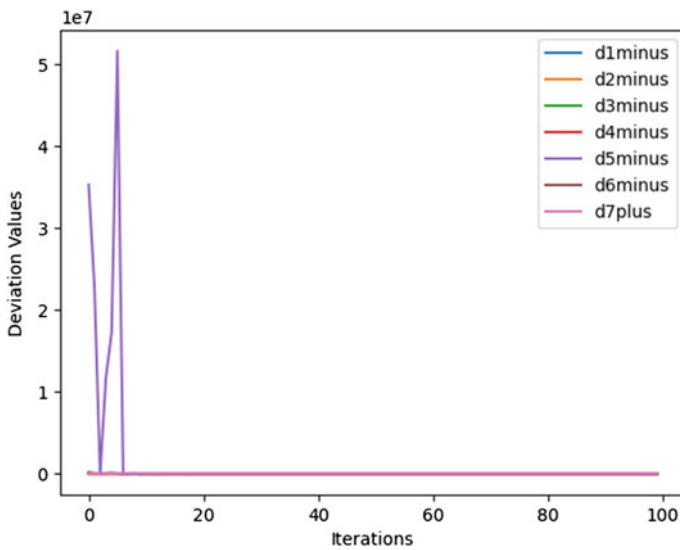


Fig. 10.2 Plot of deviations

Table 10.7 shows the deviation values for each deviation variable corresponding to the goal. Out of 7 goals, 6 have been achieved and have a deviation value equal to 0. The deviation is seen for one goal which is not achieved.

**Table 10.5** Best solution values for the problem using CI

Solution methodology		CI (best version)
Variables		
Best optimal result (lowest value of pseudo-objective function)	Cash in hand	65,813,141
	Balance with RBI	0
	Balance with banks and money at call and short notice in India	10,764,311
	Balance with banks and money at call and short notice outside India	5,197,539
	Investment in government securities	131,000,000
	Investment in approved securities	1321.068
	Shares	8,830,526
	Debentures	69,088,046
	Investment in subsidiaries/joint ventures	1,170,144
	Others (commercial papers, mutual funds, etc.)	26,643,555
	Bills purchased and discounted	18,356,445
	Cash credit, overdrafts, loans repayable on demand	337,000,000
	Term loans	166,000,000
	Advances in priority sector	149,000,000
	Advances in banks in India	73,586,090
	Fixed assets and intangible assets	17,657,033
	Other assets	69,500,000
	Capital	0
	Reserves and surplus	98,541,818
	Demand deposit	41,185,480
	Saving deposits	50,185,487
	Term deposits	187,000,000
	Borrowings from RBI	4,632,384
Borrowings from banks and other institutions and agencies	25,520,393	
Borrowings outside India	0	
Other liabilities	2,993,294	
Others (including provisions)	35,579,537	
Runtime (s)		1.408 s

**Table 10.6** Mean of 30 solutions using CI

Solution methodology		CI (best version)
Variables		
Mean of 30 optimal solutions	Cash in hand	61,623,843.830
	Balance with RBI	0
	Balance with banks and money at call and short notice in India	19,862,186.900
	Balance with banks and money at call and short notice outside India	5,422,220.358
	Investment in government securities	255,000,000
	Investment in approved securities	705.7985383
	Shares	5,757,244.515
	Debentures	72,009,139.900
	Investment in subsidiaries/joint ventures	1,107,459.991
	Others (commercial papers, mutual funds, etc.)	12,047,083.680
	Bills purchased and discounted	17,129,958.110
	Cash credit, overdrafts, loans repayable on demand	311,000,000
	Term loans	367,000,000
	Advances in priority sector	299,000,000
	Advances in banks in India	65,541,279.300
	Fixed assets and intangible assets	13,957,480.150
	Other assets	70,124,646.280
	Capital	0
	Reserves and surplus	72,136,970.530
	Demand deposit	54,777,454.710
	Saving deposits	76,525,411.300
	Term deposits	157,000,000
	Borrowings from RBI	28,562,725.230
Borrowings from banks and other institutions and agencies	28,050,355.780	
Borrowings outside India	0	
Other liabilities	8,794,049.775	
Others (including provisions)	24,282,386.730	
Standard deviation of function values		0.000

**Table 10.7** Deviation values of deviation variables for each goal

Goal	Deviation variable	Deviation value
Market share of credit	$d_1^-$	0
Market share of the deposit	$d_2^-$	0
Return on equity	$d_3^-$	0
Return on asset	$d_4^-$	0
Capital adequacy	$d_5^-$	0
Liquidity risk	$d_6^-$	24,136,030.050
NPA	$d_7^+$	0

Table 10.8 shows the comparison between the results obtained using Cohort Intelligence and Goal Programming and the previous approach on the Pseudo-Objective Function.

**Table 10.8** Result comparison

Variables	AHP+GP	Cohort intelligence	Real
Cash in hand and balance with RBI	122,359,300	65,813,141	111,938,820
Balance with banks and money at call and short notice in India and outside India	2,719,096	15,961,850	52,822,048
Investment in government securities and approved securities	600,920,200	131,000,000	583,275,898
Shares, debentures, investment in subsidiaries/joint ventures and others	106,044,700	105,732,271	209,402,321
Bills purchased and discounted, cash credit, overdrafts, loans repayable on demand, term loans	1,758,137,410	521,000,000	1,592,848,135
Fixed assets and intangible assets	33,746,640	17,657,033	25,892,722
Other assets	95,168,350	69,500,000	142,915,717
Total assets	2,719,095,696	927,000,000	2,719,095,661
Capital and reserves and surplus	277,877,600	98,541,818	189,012,435
Demand deposit	209,333,600	41,185,480	142,610,850
Saving deposits	534,963,500	50,185,487	541,258,880
Term deposits	1,581,631,000	187,000,000	1,642,584,046
Borrowings from RBI, banks and other institutions and Agencies	67,977,388	30,152,777	141,193,671
Borrowings outside India	0	0	0
Other liabilities	9,245,268	2,993,294	16,850,484
Others (including provisions)	38,067,340	35,579,537	45,585,295
Total liabilities	2,719,095,696	445,638,393	2,719,095,661

## 10.5 Conclusion

Real-world problem in the financial domain is solved in this paper. The problem of asset and liability management of an Indian bank is solved using Cohort Intelligence and Goal Programming. The results show that the CI approach has generated varied results as compared to the previous approach. The standard deviation obtained for the pseudo-objective function is 0.000. Six of the seven goals mentioned have been met, including the market share of credit, market share of deposits, return on assets, return on equity, capital adequacy ratio and non-performing asset, but the goal for liquidity risk is not met, so it is not taken into account when calculating standard deviation. This indicates the robustness of the CI algorithm considering the gigantic range of input values. The computational time for the problem was 1.408 s for the best iteration which is reasonable considering the complexity of the problem and the number equations. The time required for computation can be further reduced by tuning some parameters such as the reduction factor and the number of candidates present in the cohort. In the future, Cohort Intelligence can be applied to various real-world financial problems. Robustness and the low computation time of the algorithm prove to be beneficial while solving complex and time bound problems. Cohort Intelligence has the potential to optimize prediction models in order to improve accuracy while balancing the goals that are set.

## References

- Ahmadi-Javid A, Hooshangi-Tabrizi P (2017) Integrating employee timetabling with scheduling of machines and transporters in a job-shop environment: a mathematical formulation and an anarchic society optimization algorithm. *Comput Oper Res* 84:73–91
- Emami H, Derakhshan F (2015) Election algorithm: a new socio-politically inspired strategy. *AI Commun* 28(3):591–603
- Halim BA, Abd Karim H, Fahami NA, Mahad NF, Nordin SKS, Hassan N (2015) Bank financial statement management using a goal programming model. *Procedia Soc Behav Sci* 211:498–504
- Huan TT, Kulkarni AJ, Kanesan J, Huang CJ, Abraham A (2017) Ideology algorithm: a socio-inspired optimization methodology. *Neural Comput Appl* 28(1):845–876
- Kale IR, Kulkarni AJ (2018) Cohort intelligence algorithm for discrete and mixed variable engineering problems. *Int J Parallel Emergent Distrib Syst* 33(6):627–662
- Kashan AH (2009) League championship algorithm: a new algorithm for numerical function optimization. In: 2009 international conference of soft computing and pattern recognition, December 2009. IEEE, pp 43–48
- Kulkarni AJ, Durugkar IP, Kumar M (2013) Cohort intelligence: a self supervised learning behavior. In: 2013 IEEE international conference on systems, man, and cybernetics, October 2013. IEEE, pp 1396–1400
- Kulkarni AJ, Shabir H (2016) Solving 0–1 knapsack problem using cohort intelligence algorithm. *Int J Mach Learn Cybern* 7(3):427–441
- Kuo HC, Lin CH (2013) Cultural evolution algorithm for global optimizations and its applications. *J Appl Res Technol* 11(4):510–522
- Lin TW, O’Leary DE (1993) Goal programming applications in financial management. *Adv Math Program Financ Plan* 3(1):211–230

- Liu ZZ, Chu DH, Song C, Xue X, Lu BY (2016) Social learning optimization (SLO) algorithm paradigm and its application in QoS-aware cloud service composition. *Inf Sci* 326:315–333
- Moosavian N (2015) Soccer league competition algorithm for solving knapsack problems. *Swarm Evol Comput* 20:14–22
- Patankar NS, Kulkarni AJ (2018) Variations of cohort intelligence. *Soft Comput* 22(6):1731–1747
- Rao RV (2016) Teaching-learning-based optimization algorithm. In: *Teaching learning based optimization algorithm*. Springer, Cham, pp 9–39
- Siew LW, Wai CJ, Hoe LW (2017) Data driven decision analysis in bank financial management with goal programming model. In: *International visual informatics conference*, November 2017. Springer, Cham, pp 681–689
- Tanwar J, Vaish AK, Rao NVM (2020) Mathematical modeling of asset liability management in banks using goal programming and AHP. *Indian J Financ Bank* 4(4):1–19

**Part III**  
**Optimization for Image Processing**



# Chapter 11

## Proposing a New Feature Clustering Method in Order to the Binary Classification of COVID-19 in Computed Tomography Images



Alireza Balavand and Soheyla Pahlevani

**Abstract** Since the outbreak of coronavirus (COVID-19), different image classification algorithms have been proposed to detect suspected cases based on computed tomography scan (CT) images. Due to the lack of a valid database and the lack of CT scan images, the results of most of these algorithms have not been reliable and they have not been trained with the standard number of CT images. So, in this paper, a new classification algorithm is proposed in which a valid database of CT scans with 6322 images is used in order to train the proposed algorithm. This algorithm includes three main steps: In the first step, the features are extracted using two pre-trained convolutional neural networks called ResNet18 and GoogleNet. Due to generating many features using the ResNet18 and GoogleNet, a new dimension reduction method is proposed in which a new metaheuristic algorithm called Curling Optimization Algorithm (COA) is proposed as a part of the dimension reduction process. The main idea of the new dimension reduction algorithm is the combination of COA and DBSCAN algorithms. In the third step, binary classification is done by the Support Vector Machine (SVM). According to the results of the classification of the CT images, the proposed algorithm has achieved high accuracy more than 93% in ResNet18 features and more than 91% in GoogleNet features.

**Keywords** CT images · ResNet18 · Google-Net · Curling Optimization Algorithm (COA) · DBSCAN · Support Vector Machine (SVM) · Covid-19

---

A. Balavand (✉)

Department of Industrial Engineering, Science and Research Branch, Islamic Azad University, Tehran, Iran

e-mail: [a.balavand@srbiau.ac.ir](mailto:a.balavand@srbiau.ac.ir)

S. Pahlevani

Department of Industrial Engineering, Electronic Branch, Islamic Azad University, Tehran, Iran

© The Author(s), under exclusive license to Springer Nature Singapore Pte Ltd. 2023

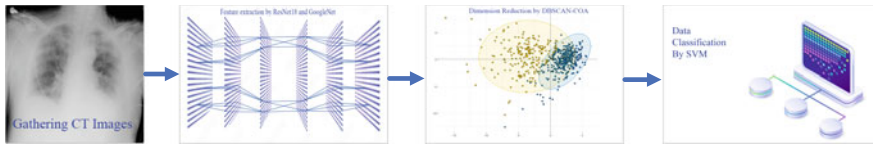
193

A. J. Kulkarni (ed.), *Optimization Methods for Product and System Design*,

Engineering Optimization: Methods and Applications,

[https://doi.org/10.1007/978-981-99-1521-7\\_11](https://doi.org/10.1007/978-981-99-1521-7_11)

## Graphical Abstract



COVID-19 binary classification algorithm with four steps of gathering CT Images, feature extraction, dimension reduction, and classification

## 11.1 Introduction

Since the outbreak of the coronavirus (COVID-19), several medical aid systems have been developed to identify suspected cases in the entire world. Among these methods, computer-aided design (CAD) and machine vision (MV) (Steger et al. 2018) have had a major effect to identify suspected cases in the absence of experienced specialists. Image classification is one of the main methods that many algorithms with different performances have proposed in the field of image processing (Balaji and Lavanya 2019). Diagnosis with the help of classification algorithms in computed tomography scan (CT) images has been used widely in different studies (Gao et al. 2017; Zhang, et al. 2020). Each of these algorithms has had different accuracy and speed. Therefore, the competitive advantage of algorithms is based on two factors the accuracy of the classification and the speed of the classification algorithm. Using of classification algorithms in diagnosing COVID-19 cases has been developed after the outbreak of coronavirus. In most of these algorithms, there has not been a standard dataset of previous coronavirus cases and the classification algorithm is trained with unreliable data. So, the results of most classification algorithms have not been reliable. Whatever the training dataset includes more cases, the accuracy of classification will be reliable. These classification algorithms can be used as a coronavirus diagnosis system along with specialists and reduce human errors. Classification algorithms include five main phases pre-processing, image segmentation, feature extraction, dimension reduction, and classification. It is possible that some algorithms have not used one or two mentioned stages. Pre-processing involves methods such as noise reduction and intensity values correction. Image segmentation categorizes pixels into similar groups and helps to highlight the lesion. A series of features are extracted from the image in the feature extraction methods. These features usually include static features such as entropy, skewness, mean, energy, torque, and correlation. Some other feature extraction methods have been derived from the pre-trained deep neural networks which are based on convolutional neural networks. In dimension reduction methods, the important features are selected from the features and uncorrelated features have been removed from datasets. Usually, in the balanced classification method, data

is usually divided into two sections train and test data by k-fold-cross-validation method. The classification algorithms are trained using the training features, and the prediction is done in the test data.

The rest of this paper is organized as the following. In Sect. 11.2, the related works will be reviewed. In Sect. 11.3, the proposed method is presented. The results of the proposed method are presented in Sects. 11.4, and 11.5 includes discussions and conclusions.

## 11.2 Related Works

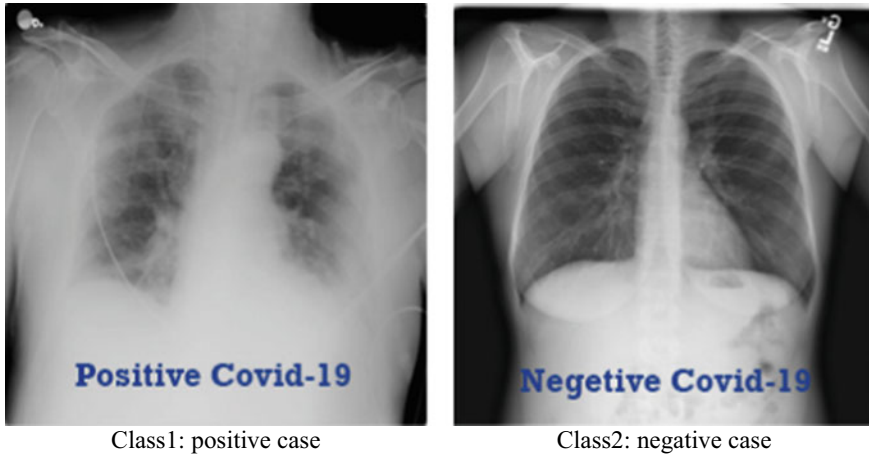
Medical Image Classification (Balavand and Husseinzadeh 2020) techniques are known as prominent methods for the prediction and diagnosis of many diseases based on CT images. But classification algorithms have not had a good performance when there are not been high-quality features. Many methods have been developed to create proper features. In recent years, deep learning methods have been widely used for feature extraction (Balavand et al. 2019; Zouch 2022). Pre-trained convolutional neural networks are one of them that have known as transfer deep learning methods (Pathak 2020). These methods have been used for the diagnosis of COVID-19 in CT images in many papers due to generating high-quality features (Aggarwal et al. 2022). Rahimzadeh and Attar (2020) proposed new training techniques to help better learning in unbalancing data. They used their method on X-ray images of COVID-19 and their proposed neural network is based on the concatenation of the Xception and ResNet50V2 networks. In (Li et al. 2020) used deep learning methods in the diagnosis of coronavirus in CT images. This study classified images into two classes negative and positive. In Toğaçar et al. (2020) with the use of MobileNetV2 and SqueezeNet features, a features dataset was created. In this study, the fuzzy color technique and SVM were used for pre-processing and classification, respectively. In Wallis (2020), a scoring tool was developed for the diagnosis of COVID-19 severity. In this study, the patients were classified into three sections. Some patients had high respiratory interventions and need ventilation. Other patients need oxygen and some patients did not need oxygen and were classified into the moderate stage. In Ucar and Korkmaz (2019), a COVID-19 diagnosis system was introduced in which SqueezeNet and Bayes were used for feature extraction and classification, respectively. The hybrid method in Loey et al. (2020) included feature extraction and classification of COVID-19 using a real dataset. In this study, feature extraction was done by ResNet50, and SVM was used for classification. In Minaee et al. (2004), four popular convolutional neural networks including ResNet18, ResNet50, SqueezeNet, and DenseNet-121 were used to identify COVID-19 disease in the chest X-ray images. A DenseNet201 was used for binary classification in COVID-19 according to chest CT images in Jaiswal (2020). The study of Yoo et al. (2020) investigated the feasibility of using three binary decision-tree classifiers based on deep learning for detecting COVID-19 from CXR images. In Ko et al. (2020) a simple 2D deep learning framework named the fast-track COVID-19 classification

network (FCONet) was proposed. They used VGG16, ResNet50, Inception-v3, or Xception as the backbone. Also, 3993 chest CT images of patients with COVID-19 pneumonia, other pneumonia, and non-pneumonia diseases were used as datasets. The study of Shibly et al. (2020) proposed a VGG16 Network-based Faster Regions with Convolutional Neural Networks framework to detect COVID-19 patients from chest X-Ray images. Optimization algorithms (Balavand 2022; Kashan et al. 2021) have been used widely in classification of medical images. In Apostolopoulos and Mpesiana (2020), VGG19 and the MobileNet v2 were used to classify a dataset with X-ray images that included patients with common bacterial pneumonia, confirmed COVID-19 disease, and normal incidents. In Murugan et al. (2021) that the backpropagation algorithm and Whale Optimization Algorithm (WOA) combines to optimize such Deep Learning networks. CovH2SD algorithm has been proposed to detect COVID-19 in CT images in Balaha et al. (2021) in which Harris Hawks Optimization (HHO) has been used to optimize the hyperparameters. Genetic algorithm has been used to optimize the hyperparameters of novel convolutional neural network in Carvalho et al. (2021). In Gopatoti et al. (2022), optimal feature selection technique using enhanced grey-wolf optimizer with genetic algorithm (EGWO-GA) has been proposed to classify COVID-19 images.

In this paper, a new framework for classification of COVID-19 is proposed in which 6322 CT images as a valid database are used. This framework covers the weakness of other algorithms in which there was not been a valid database and the results were not reliable. This framework includes three main steps feature extraction, dimension reduction, and classification. In the feature extraction section, pre-trained deep convolutional neural network models are used. Among these models, ResNet18 and GoogleNet are used to feature extraction. In dimension reduction step, a new algorithm is proposed in which a new metaheuristic algorithm called Curling Optimization Algorithm (COA) is presented. COA inspires by Curling game and its strategies. Finally, in the classification step, binary Support Vector Machine (SVM) is used.

### 11.3 Proposed Method

In this section, the proposed method will be described in detail. Accordingly, at first, COVID-19 images will be explained then the features will be extracted by ResNet18 and GoogleNet. The dimension reduction method algorithm along with pseudo-code will be represented. Finally, the binary classification using the SVM algorithm will be explained.



**Fig. 11.1** COVID-19 images with different classes

### ***11.3.1 Images***

One of the methods that are being used for identifying COVID-19 is medical imaging especially the type of Computed Tomography scan (CT scan) of the lung. In this paper, CT images have been used for classification. These images have two classes in which some images show positive cases of COVID-19 and vice-versa. These images have been gathered from (Chowdhury et al. 2020; Rahman et al. 2021). There are 6322 slices of CT images of which 3161 out of the total of 6322 slices have been evaluated by a radiologist as positive cases and the rest of the images have been considered negative cases. The images are 224 by 224 in PNG format and are imaged by a 0.8 thickness configuration. Two samples of images are shown in Fig. 11.1 where the left image from positive cases and the right one from negative cases have been selected, respectively.

### ***11.3.2 Features Extraction***

Pre-trained Deep Neural Networks have been used for classification, feature extraction, and transfer learning (Russakovsky et al. 2015; Zhou et al. 2016). One of the steps for decreasing the number of data is feature extraction in classification methods. Deep learning methods have been used due to creation of high-quality features from images (Tian 2013). Pre-trained convolution neural networks are one of the best tools for feature extraction. Most of these methods are trained on subsets of images (Challenge 2012). AlexNet, vgg16, vgg19, SqueezeNet, GoogleNet, and Resnet are the famous model of pre-trained convolutional neural networks. Most of these methods have included convolution layer, pooling layer, and fully connected layer in terms

of structure and they are different from each other in terms of accuracy, speed, and size. Pre-trained convolutional neural networks are most used for feature extraction from images. Weights and biases are in the convolution layer such as some filters that are applied to images with different sizes and dimensions. In the convolution layer, images convert to a feature map with shape (number of images)  $\times$  (feature map height)  $\times$  (feature map width)  $\times$  (feature map channels). In the pooling layer, the size of images is decreased gradually steps in a row and a nonlinear function is applied to images. These functions include maximizing, averaging, and even least-square norm. Fully connected layers include neurons that connect to the feature map from the pooling layer. The flattened matrix goes through a fully connected layer to classify the images. In order to feature extraction from CT COVID-19 scan images, the GoogleNet and resnet18 are used in this paper. The experiments in Balavand (2021) show that these models extract fewer features with powerful and informative quality. In the following, the structures of GoogleNet and ResNet are investigated schematically.

According to Fig. 11.2, GoogleNet (Szegedy et al. 2015) is a small network that includes two convolutional layers, three pooling layers, and nine inception layers each inception layer includes six convolutional layers and two pooling layers. Resnet18 (He et al. 2016) has five convolutional layers, one average layer, and one fully connected layer. According to Fig. 11.3, a good network has a balance between accuracy and prediction time. According to Fig. 11.4, between pre-trained convolution neural networks, GoogleNet and ResNet have acceptable accuracy with fewer prediction times. Figure 11.4 shows that as the accuracy of the classification increases, so does the prediction time. Indeed, there is a positive relationship between accuracy and prediction time.

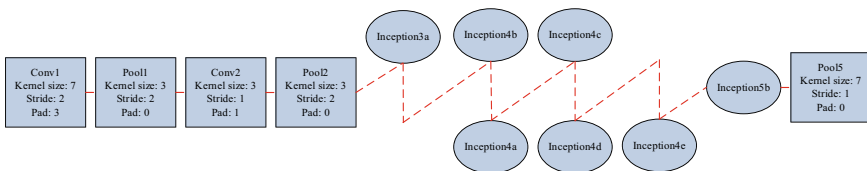


Fig. 11.2 GoogleNet structure

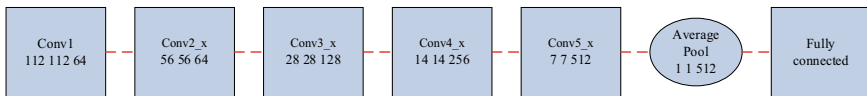
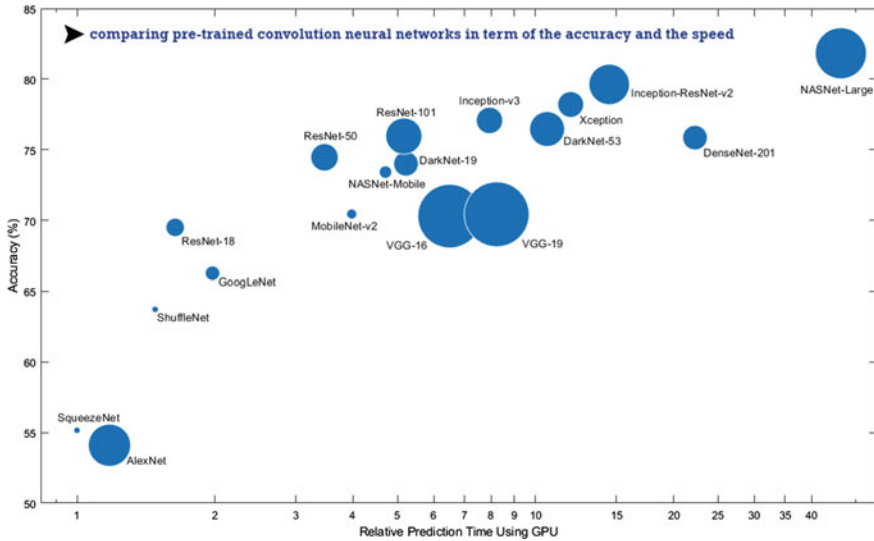


Fig. 11.3 Resnet18 structure



**Fig. 11.4** Comparing accuracy and prediction time among pre-trained convolution neural networks. *Note* This figure was produced by MathWorks company (<https://www.mathworks.com/help/deeplearning/ug/pretrained-convolutional-neural-networks.html> 2021)

### 11.3.3 Background and Strategy of Curling Game

Curling has been originated in Scotland in the mid-sixteenth century. Since 1924, Curling had been a part of the Olympics and in 1998, it was introduced at the Nagano Winter Olympics. Curling needs social activities and swarm intelligence has played a vital role in this game. This sport at the same time simplicity is known as chess on ice. In order to score in Curling, the rocks must be closer to the center than your opponent’s rocks. There are several strategies in curling that are used in different situations of a game. According to Turriff and Curling (2016), there are three strategies of offense, defense, and balance in curling. In offense strategy, the players try to keep rock in play. In this strategy, the players intend to rest in the playing area with a draw shot according to Fig. 11.5. The guard shots are usually softer and lighter than other shots. Guard stones are used to limit access to the center.

Defense strategy is the opposite of offense strategy. According to Fig. 11.6, in defense strategy, the players intend to remove the opponent’s stones by shoots that have more power and speed. This strategy does in the mid of the game when there are still several stones in the game. Balance strategy is between defense and offense strategy. This strategy has been applied when two teams do not want to take a risk in the game. In order to design a curling optimization algorithm, the strategies should be simulated.

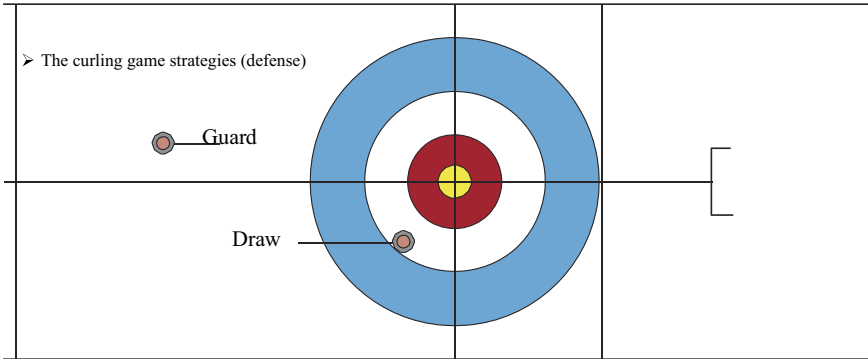


Fig. 11.5 Draw and guard examples

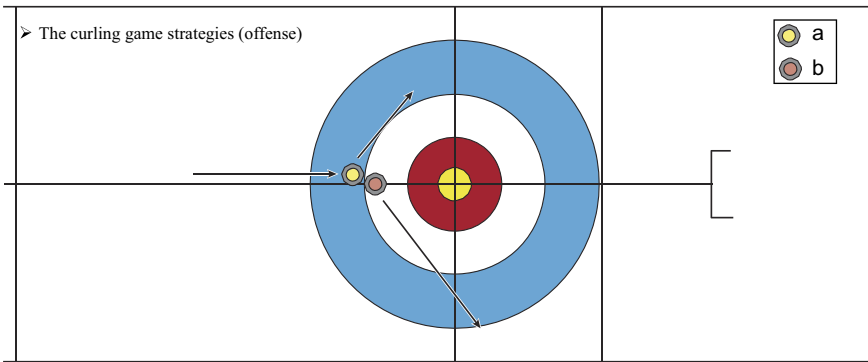


Fig. 11.6 Hit and roll: a stone (yellow) contacts the guard (red) and b moves it out of the way, but the stone stays in play

### 11.3.4 Curling Optimization Algorithm (COA)

COA is placed in the category of the population-based algorithm that can solve optimization problems with continuous and discrete solutions. Like other algorithms in this field, COA creates information flow through the collaboration of the population. As with other population-based algorithms, several initial solutions are randomly generated. In fact, these randomized solutions constitute the initial population called stones. After the initialization step, the algorithm enters the main phase. In the main phase, there are two phases of offense and defense strategy. The offense and defense phase is inspired by the offense and defense strategy of the curling game, respectively. The main phase has an iterative manner and after passing a number of iterations, COA stops and the best solution reports. In order to simulate COA algorithm, definitions and formulas of each section of the algorithm will be explained in the next section.



### 11.3.4.1 Initialization

Some initial parameters must be set after generating initial solutions. The number of population (Npop), the lower bound of variables ( $LB$ ), the upper bounds of variables ( $UB$ ), max iteration (Maxit), and the size of variables (Varsize) are the initial parameters. Then, to the number of the npop, random solutions ( $X$ ) are generated based on Eq. (11.1). Also, rand is a uniform random variable that is generated between zero and one. Then this solution is evaluated based on the objective function and is known as the best solution ( $x_{best}$ ).

$$X = LB + \text{rand}(\text{Varsize}) \times (UB - LB) \quad (11.1)$$

### 11.3.4.2 Exploitation and Exploration

In the initialization phase of COA, a number of solutions are randomly generated and evaluated. These solutions are known as stones of curling. Then, among these solutions, a solution is chosen as the best solution. This solution has a better position and is closer to the center of the circle compared to other stones. In order to make the best solutions, the initial solutions are ordered ascendingly based on the objective function and a member of the population ( $G$ ) is selected as the best solution. Then, the algorithm enters the main phase loop. There are two main rules in curling: Defense strategy and attacking strategy. In defense strategy, the stone is thrown with low speed and power and the player intends to get a better position around the best stone without hitting other rocks. So exploitation is done in this phase. In attacking strategy, the stone is thrown with high speed and power and the stone may get a better position by hitting other stones. Exploration is done in this phase. So, these strategies are used to simulate two main phases of COA. The main loop of COA is divided into two main phases. As mentioned before, the first phase is exploitation and the second phase is the exploration phase. In the first phase, the solutions move to the best solutions with small mutations and try to get a new position around the best solution. In the second phase, the solutions move to the best solutions with bigger mutations. Indeed, searching for the best solution is done in the first phase, and discovering new spaces is done in the second phase. In order to simulate the two main phases of the algorithm, the solution updating operators are proposed in the next sections.

### 11.3.4.3 Main Phase

As it was said, there are two strategies in the curling game. In the main phase of COA algorithm, each solution is updated according to offense or defense strategy randomly. Thus, the selection of each strategy is quite random. In Eq. (11.2), the update process in the curling algorithm is shown.

$$\begin{cases} x_c^{i,t+1} = x_c^{i,t} + r(x_{\text{best}} - x_c^{i,t}) \forall i \text{ if } r \leq 0.5 \\ x_c^{i,t+1} = \text{new crossover} \forall i \text{ if } r > 0.5 \end{cases} \quad (11.2)$$

In the top section of Eq. (11.2), in order to generate a new solution  $(x_c^{i,t+1})$ ,  $x_c^{i,t}$  with a random coefficient ( $r$ ) is moved toward  $x_{\text{best}}$  or best solution that denotes the center of the curling game. In fact, this section of the equation simulates the offense strategy in which each stone is thrown toward the center with soft and low power. The bottom section of Eq. (11.2) simulates the defense strategy in which stones are thrown with more power to remove the opponent's stones. So, for simulating the defense strategy, a new crossover operation is introduced. For generating solutions based on the crossover, pseudo-code is implemented according to Fig. 11.7.

This new crossover differentiates this algorithm from other population-based optimization algorithms. In order to implement the new crossover, the current solution must be close to the best solutions. The best solutions include the three first solutions that have a minimum objective function compared to other members of the population. So, the best solutions must be updated as soon as a better solution is found. In order to select one of the best solutions for crossover, the roulette wheel method is used in COA algorithm. The new crossover is shown schematically according to Fig. 11.8.

The crossover process is shown in Fig. 11.8 with two solutions. According to the top left section of this figure, the crossover is done between one of the best solutions and the current solution. A permutation vector with three members is generated. Indexes of this vector include 1, 4, and 8 which values corresponding to these vectors are 0.3, 0.2, and 0.3. These selected elements are replaced instead of the first, fourth, and eighth members of the current solution according to the bottom left section of Fig. 11.8. According to the top right section of Fig. 11.8, a new permutation vector is generated that the members of this vector are 1, 4, 6, 8, and 10. Values corresponding to this vector are 0.2, 0.1, 0.5, 0.5, and 0.1. These selected members of the best solution are replaced instead of the current solution according to the right bottom section of Fig. 11.8. This new method is proposed for the first time in this paper that has a significant effect on the performance of CSMA.

---

```

1.  $n = \text{generate random integer number}$  between 1 and max number of variables
2.  $n1 = \text{randperm}(\text{max number of variables}, n)$ 
3.  $n2 = \text{randperm}(\text{max number of variables}, n)$ 
4. For  $k=1$ :number element of  $n1$ 
5.      $\text{Pop.position}(n1(k)) = \text{Best.position}(n2(k))$ 
6. End for

```

---

**Fig. 11.7** Pseudo-code of crossover operation

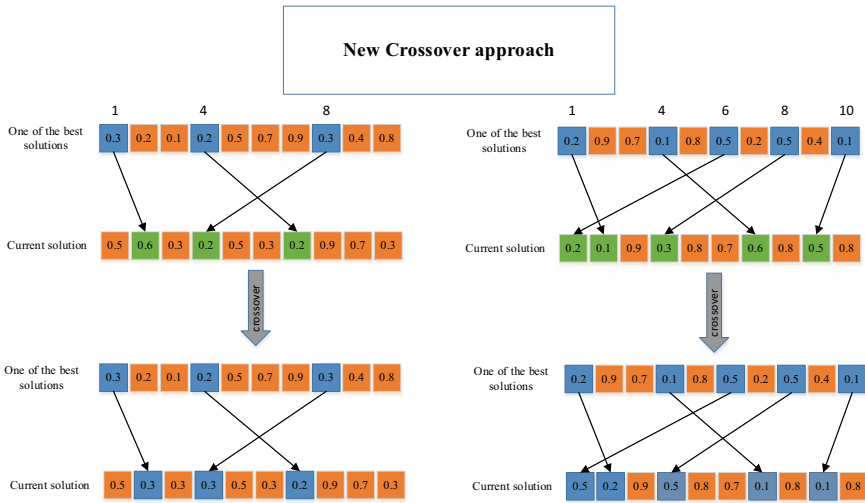


Fig. 11.8 Crossover operation process

### 11.3.5 Feature Selection by COA and DBSCAN

In most classification algorithms, the feature selection method is the main stage of the classification algorithm. Decreasing the dimension of data, improving classification accuracy, and increasing classification speed is the main advantage of feature selection. Feature selection based on a metaheuristic algorithm has had high performance (Agrawal et al. 2021). In this paper, a new feature selection method is introduced. This method is a combination of Db-Scan and COA algorithms that are introduced in this paper. The pseudo-code of this algorithm is shown in Fig. 11.9.

### 11.3.6 Binary SVM

Support vector machine is a supervised binary classifier that has been considered by researchers (Mantero et al. 2005). SVM is an algorithm that finds the maximum margin of a hyperplane using special linear and nonlinear equations. The maximization margin of the hyperplane leads to maximum separation among classes. Assume that training data is  $[x_i, y_i]$  that  $x_i \in R$  and  $y_i \in$  linearly separable, SVM separates the classes according to Eq. (11.1):

$$Y = \text{sign} \left( \sum_{i=1}^N y_i a_i K(X \times X) \right) + b \tag{11.3}$$

<p><b>COA algorithm</b></p> <ol style="list-style-type: none"> <li>1 set initial parameters</li> <li>2 best solution=<math>+\infty</math></li> <li>• <b>Initializing</b></li> <li>3 <b>For</b> each population</li> <li>4 Generate random values of <math>\epsilon</math> and <math>\minpts</math></li> <li>5 Evaluation clustering by <b>Cost function</b></li> <li>6 Update the best solution and current solution</li> <li>7 <b>End for</b></li> <li>8 dividing the population into the chasers and ambushers</li> <li>• <b>Main loop</b></li> <li>9 <b>While</b> it <math>\leq</math> <b>maxit</b></li> <li>15 <b>For</b> each population</li> <li>16 If <math>(r) \leq 0.5</math></li> <li>17 Implementing the above section of Eq(2)</li> <li>18 <b>Else if</b> <math>(AC) &gt; 0.5</math></li> <li>19 Implementing bottom section of Eq(2)</li> <li>20 <b>end if</b></li> <li>21 evaluate solutions by <b>Cost function</b></li> <li>22 Update the best solution and current solution</li> <li>23 <b>End for</b></li> <li>24 <math>It=It+1</math></li> <li>25 <b>End while</b> (main loop)</li> <li>26 Report the best solution</li> </ol>	<p><b>Cost function</b></p> <ol style="list-style-type: none"> <li>1 Input parameters <math>D, \epsilon, \minpts</math></li> <li>2 <math>C=0</math></li> <li>3 <math>Penalty=0</math></li> <li>4 <math>IDX=dbscan(D,\epsilon,\minpts)</math></li> <li>5 <math>Percent\_of\_noises = \frac{n\_noises}{n\_data}</math></li> <li>6 <math>N\_clusters=</math> Calculate number of clusters</li> <li>7 <b>If</b> or <math>(\frac{\text{number of object of each cluster}}{n\_data} &lt; 0.1, Percent\_of\_noises)</math></li> <li>8 <math>C=C+penalty</math></li> <li>9 <b>End</b></li> <li>10 divide train and test by three-fold-cross-validation</li> <li>10 <b>for</b> each fold</li> <li>11 <math>Model=train</math> SVM binary</li> <li>12 <math>Accuracy=</math> calculate classification error in each fold</li> <li>14 <b>end for</b></li> <li>13 Report classification error, <math>\epsilon, \minpts</math>, and data</li> </ol>
---------------------------------------------------------------------------------------------------------------------------------------------------------------------------------------------------------------------------------------------------------------------------------------------------------------------------------------------------------------------------------------------------------------------------------------------------------------------------------------------------------------------------------------------------------------------------------------------------------------------------------------------------------------------------------------------------------------------------------------------------------------------------------------------------------------------------------------------------------------------------------------------------------------------------------------------------------------------------------------------------------------------------------------------------------------------------------------------------------------------------------------------------	----------------------------------------------------------------------------------------------------------------------------------------------------------------------------------------------------------------------------------------------------------------------------------------------------------------------------------------------------------------------------------------------------------------------------------------------------------------------------------------------------------------------------------------------------------------------------------------------------------------------------------------------------------------------------------------------------------------------------------------------------------------------------------------------------------------------------------------------------------------------------------------------------------------------------------------

**Fig. 11.9** Feature selection by COA and DBSCAN

where  $Y$  is output,  $y_i$  are classes of train data,  $X$  is train data, and the values of  $a_i$  and  $b$  are adjustable and form the parameters of the hyperplane. If data do not be linearly separable, SVM separates the classes according to Eq. (11.2):

$$Y = \text{sign} \left( \sum_{i=1}^N y_i a_i K(X \times X_i) \right) + b \quad (11.4)$$

$K(X \times X_i)$  is a kernel function that for creating different machines in data space generates internal multiplication. In binary SVM definition, two classes are separated by a hyperplane (Weston and Watkins 1998). In order to create a hyperplane that can classify all classes into correct classes, an optimization problem is defined as Eq. (11.3).

$$\min Q_p(W^{kl}, b^{kl}, \xi^{kl}) = \frac{1}{2} (W^{kl})^T (W^{kl}) + C \sum_{i=1}^m \xi_i^{kl}$$

Subject to :

(11.5)

$$(W^{kl})^T \cdot \phi(x_i) + b^{kl} \geq 1 - \xi_i^{kl}, \text{ if } y_i = k,$$

$$(W^{kl})^T \cdot \phi(x_i) + b^{kl} \geq -1 + \xi_i^{kl}, \text{ if } y_i = 1,$$

$$\xi_i^{kl} \geq 0, i = 1, \dots, m \text{ and } k, l = 1, \dots, n.$$

where  $W$  is a weight vector,  $b$  is a bias vector that calculates hyperplane distance to origin coordinates,  $C$  is the penalty factor that balances the complexity of the model

with the classification error. A high value of  $C$  causes overfitting.  $\xi = \{\xi_1, \dots, \xi_m\}$  are Slack Variables.  $\phi(x_i)$  is a nonlinear transform that transforms the sample into a larger point space called the feature space.  $i = 1, \dots, m$  represents the number of train data and  $n$  shows the dimensions of data and  $y_i$  is a label of train data.

## 11.4 Experimental Results

In this section, the results of implementing the proposed algorithm are presented. This section is divided into two main subsections. In the first subsection, the results of classification along with the confusion matrix are presented based on ResNet18 features and in the second subsection, GoogleNet features are classified. In addition, the results of COA and DBSCAN are compared with other well-known dimension reduction algorithms.

In order to evaluate the performance of classification, three indices of accuracy, sensitivity, and specificity along with a confusion matrix are used. Formulas are presented to calculate these indicators in Eq. (11.6), Eqs. (11.7), and (11.8).

$$CA = (TP + TN)/(TP + TN + FP + FN) \quad (11.6)$$

$$\text{Sensitivity} = TP/TP + FN \quad (11.7)$$

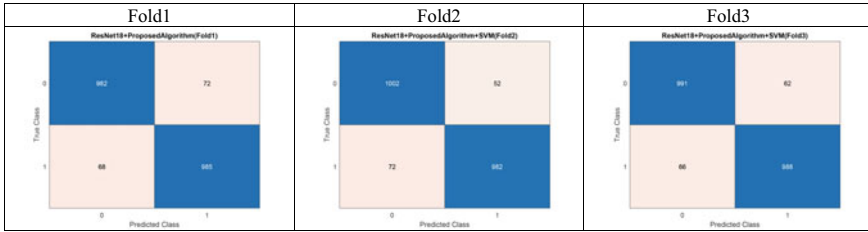
$$\text{Specificity} = TN/TN + FP \quad (11.8)$$

$TP$  indicates correctly classified positive cases,  $TN$  represents correctly classified negative cases,  $FP$  represents incorrectly classified negative cases, and  $FN$  represents the incorrectly classified positive cases.

### 11.4.1 Classification Results on ResNet18 Features

In this section, the results of classification based on ResNet18 are shown. Given that three-fold cross-validation has been used for dividing data into train and tests. So, the results of classification are shown in three folds. According to Fig. 11.10, the proposed algorithm has had good performance in all folds.

Table 11.1 shows the results of classification based on confusion matrixes. In this table, the results of classification are shown in rows and each row shows the results of a classification in each fold. Also, the values of accuracy, sensitivity, and specificity are shown in columns. In the last rows of Table 11.1, the average accuracy, sensitivity, and specificity are calculated in all folds. According to Table 11.1, the accuracy of classification of the proposed algorithm is 93.80%. The optimal values of



**Fig. 11.10** Confusion matrices in each fold based on classification results on ResNet18 features+the proposed method

**Table 11.1** The value of accuracy, sensitivity, and specificity based on classification results on ResNet18+ the proposed method

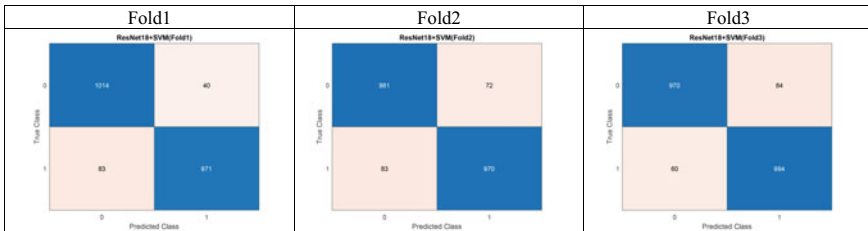
Folds	Accuracy (%)	Sensitivity (%)	Specificity (%)
1	93.93	92.79	95.07
2	93.55	92.79	94.30
3	93.93	92.79	95.07
<b>Mean</b>	<b>93.80</b>	<b>92.79</b>	<b>94.81</b>

*eps* and *minpts* are 271.28 and 769 respectively has been achieved from the Curling algorithm.

Table 11.2 represents the performance of the classification and Fig. 11.11 shows the confusion matrix based on SVM and ResNet18 features. By comparing the comparative results of Tables 11.1, and 11.2, it is concluded that the proposed algorithm has had a better performance in terms of accuracy and specificity.

**Table 11.2** The value of accuracy, sensitivity, and specificity based on classification results on ResNet18 without the proposed method

Folds	Accuracy (%)	Sensitivity (%)	Specificity (%)
1	93.17	94.31	92.03
2	92.64	92.12	93.16
3	93.17	94.31	92.03
<b>Mean</b>	<b>92.99</b>	<b>93.58</b>	<b>92.41</b>

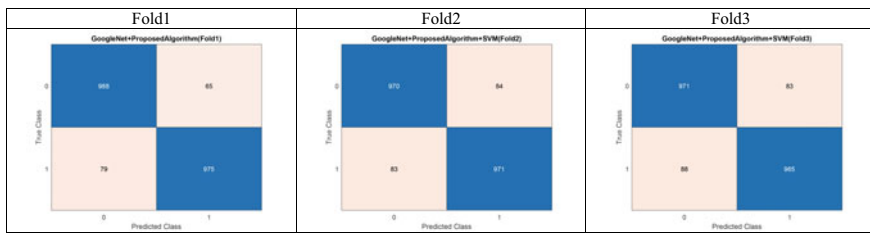


**Fig. 11.11** Confusion matrices in each fold based on classification results on ResNet18 features without the proposed method

### 11.4.2 Classification Results on GoogleNet Features

The performance of classification based on GoogleNet features is shown in Fig. 11.12. This figure shows that there are two classes of 0,1 in the confusion matrix. Indeed, the number of properly predicted rows has been shown in blue color and the incorrectly predicted classes have been shown in cream color. For example, according to the confusion matrix in fold1, the number of test data in class zero is 1053. Among 1053 test data, 988 of them are predicted properly and 65 of them are predicted incorrectly. According to this Table 11.3, the proposed algorithm has reached 91.95% classification accuracy. Also, the values of *eps* and *minpts* are 167.92 and 618, respectively.

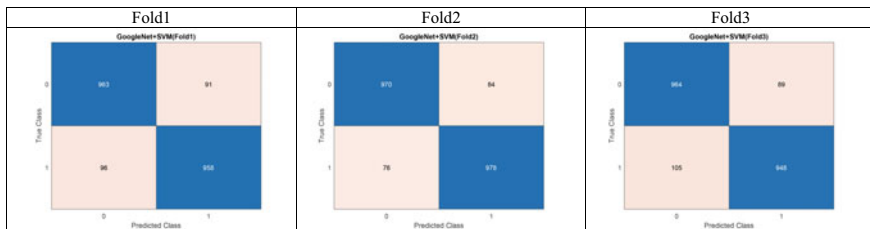
Figure 11.13 represents the confusion matrices in three folds that have been achieved by the combination of GoogleNet features and SVM classification algorithm. Table 11.4 represents the results of classification based on SVM and GoogleNet



**Fig. 11.12** Confusion matrices in each fold based on classification results on GoogleNet features+ the proposed method

**Table 11.3** The value of accuracy, sensitivity, and specificity based on classification results on GoogleNet+ the proposed method

Folds	Accuracy (%)	Sensitivity (%)	Specificity (%)
1	91.88	91.64	92.13
2	92.08	92.13	92.03
3	91.88	91.64	92.13
<b>Mean</b>	91.95	91.80	92.09



**Fig. 11.13** Confusion matrices in each fold based on classification results on GoogleNet features without the proposed method

**Table 11.4** The value of accuracy, sensitivity, and specificity based on classification results on GoogleNet without the proposed method

Folds	Accuracy (%)	Sensitivity (%)	Specificity (%)
1	90.79	90.03	91.55
2	92.41	92.79	92.03
3	90.79	90.03	91.55
<b>Mean</b>	91.33	90.95	91.71

features. The results of Table 11.4 show that the classification accuracy is 91.33% that this accuracy is less than the accuracy obtained from the proposed algorithm according to Table 11.3.

### 11.4.3 Comparing Experimental Results with Similar Works

In this section, the results of the proposed algorithm have been compared with other experimental results. Accordingly, Zulfaezal et al . (Rahman et al. 2021) have been selected that have had the most similarity with the proposed algorithm. In Rahman et al. (2021), there have only been experimental results with Resnet18 and comparative results have been summarized in Table 11.5.

Table 11.5 shows that in total, the proposed algorithm has had better results in comparison with Zulfaezal et al. (Rahman et al. 2021). According to this table, there have only been experimental results with Resnet18 with a different number of images. We concluded that as the number of images increases, the accuracy also increases. So, using data augmentation can have a big effect on the result of classification.

**Table 11.5** Comparative results of the proposed algorithm with state of art

Paper	Model	Number of images	Accuracy (%)	Sensitivity (%)	Specificity (%)
Zulfaezal et al. (Rahman et al. 2021)	Resnet18	3616	92.23	92.22	94.66
Zulfaezal et al. (Rahman et al. 2021)	Resnet18	1765	77.3	71.8	71.9
Proposed algorithm	Resnet18	6322	<b>93.93</b>	<b>92.79</b>	<b>95.07</b>



### 11.4.4 Evaluation of COA Algorithm

In this section, COA algorithm is evaluated with 12 classic benchmark functions. Also, COA is compared with four well-known optimization algorithms. According to Table 11.6, these functions have been divided into two groups: unimodal and multimodal functions.

In particular, unimodal functions were useful tools for benchmarking exploitation. In contrast, multimodal functions had many local optima and are suitable tools to evaluate the ability of exploration algorithms. In Fig. 11.14, a perspective view of the classical test functions is displayed. In this study, the number of function evaluation (*nfe*) has been used for stopping criteria. Given that the value of *nfe* is equal to 45,000. In order to validate the results, COA algorithm has been compared with four well-known algorithms as follows:

- (Ant Colony Optimization) ACO
- (Differential Evolution) DE
- (Genetic Algorithm) GA
- (Particle Swarm Optimization) PSO

The results obtained in Table 11.7 are shown that in all functions  $f_1$  to  $f_{12}$ , the COA algorithm has reached the optimal solution and has had better performance in  $f_5$ ,  $f_6$ ,  $f_{10}$  compared to the other algorithms. These results are based on (Balavand 2022). In total, among the 12 classic functions, the COA algorithm has reached the optimal solution in 17 functions that among 17 functions, three functions are multimodal and the rest of them are unimodal. In all of the classical test functions, in terms of the best solution, none of the algorithms are able to provide a better solution which this performance indicates a good balance between the exploration and exploitation of COA.

## 11.5 Conclusion

In this paper, a new classification algorithm was proposed that was used for the detection of COVID-19 in CT images. This algorithm included three-phase of feature extraction, dimension reduction, and classification by SVM. ResNet and GoogleNet were used to feature extraction from 6322 CT images. In the dimension reduction phase, a new algorithm was proposed in which a new metaheuristic algorithm called COA was proposed. COA is inspired by Curling game. The dimension reduction algorithm used the combination of DBSCAN and COA for dimension reduction of features. In this way the values of *eps* and *minpts* were generated by COA and by using these values, clustering was performed by DBSCAN. In DBSCAN algorithm, the outlier features are detected and removed from features. Detection of outlier features made the dimension of features decreased. SVM algorithm was used for the

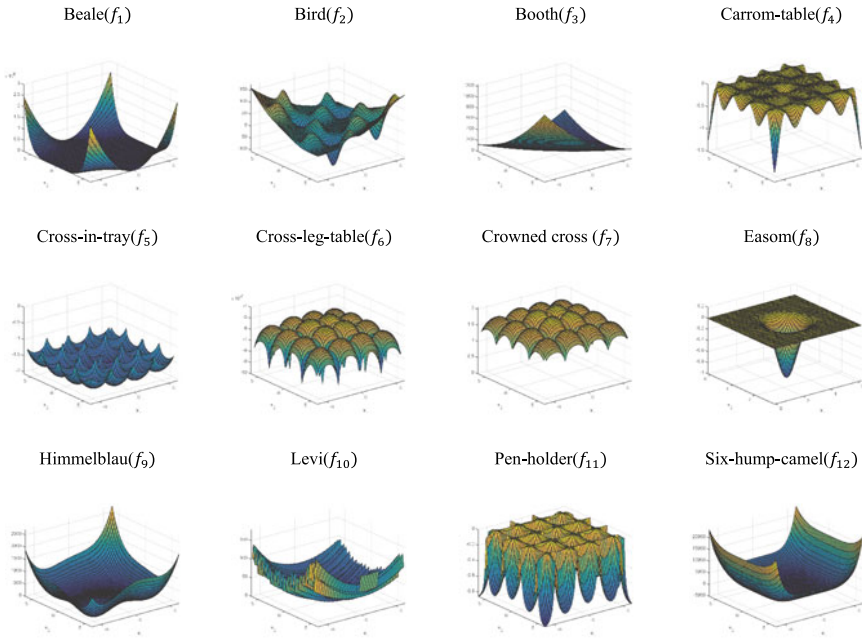
**Table 11.6** Benchmark functions (NF: Number of Functions, D: Dimension, U: Unimodal, M = Multimodal)

NF	Function	Range	D	Formulation	Min	Type
(f <sub>1</sub> )	Beale	[-4.5, 4.5]	2	$f(x) = (1.5 - x_1 + x_1x_2)^2 + (2.25 - x_1 + x_1x_2^2)^2 + (2.625 - x_1 + x_1x_2^3)^2$	0	U
(f <sub>2</sub> )	Bird	[-2π, 2π]	2	$f(x) = \sin(x_1) \cdot [\exp[1 - \cos(x_2)]^2 + \cos(x_2)] \cdot \exp[1 - \sin(x_1)^2] + (x_1 - x_2)^2$	-106.76	M
(f <sub>3</sub> )	Booth	[-10, 10]	2	$f(x) = (x_1 + 2x_2 - 7)^2 + (2x_1 + x_2 - 5)^2$	0	M
(f <sub>4</sub> )	Carrom- Table	[-10, 10]	2	$f(x) = \left[ \frac{[-\cos^2(x_1) \cdot (x_2)] \cdot \exp\left[\frac{1 - \sqrt{x_1^2 + x_2^2}}{\pi}\right]^2}{30} \right]$	-24.157	M
(f <sub>5</sub> )	Cross-in-tray	[-10, 10]	2	$f(x) = -0.0001 \cdot \left[ \sin(x_1) \cdot \sin(x_2) \cdot \exp\left[100 - \frac{(\sqrt{x_1^2 + x_2^2})}{\pi}\right] + 1 \right]^{0.1}$	-2.0626	M
(f <sub>6</sub> )	Cross-Leg -Table	[-10, 10]	2	$f(x) = - \left[ \frac{1}{\sin(x_1) \cdot \sin(x_2) \cdot \exp\left[100 - \frac{(\sqrt{x_1^2 + x_2^2})}{\pi}\right] + 1} \right]^{0.1}$	-1	M
(f <sub>7</sub> )	Crowned cross	[-10, 10]	2	$f(x) = 0.0001 \left[ \sin(x_1) \cdot \sin(x_2) \cdot \exp\left[100 - \frac{(\sqrt{x_1^2 + x_2^2})}{\pi}\right] + 1 \right]^{0.1}$	0.0001	M
(f <sub>8</sub> )	Easom	[-100, 100]	2	$f(x) = -\cos(x_1) \cdot \cos(x_2) \cdot \exp[-(x_1 - \pi)^2 - (x_2 - \pi)^2]$	-1	U
(f <sub>9</sub> )	Himmelblau	[-5, 5]	2	$f(x) = (x_1^2 + x_2 - 11)^2 + (x_1 + x_2^2 - 7)^2$	0	M

(continued)

**Table 11.6** (continued)

NF	Function	Range	D	Formulation	Min	Type
( $f_{10}$ )	Levi	[-10, 10]	2	$f(x) = \sin^2(3\pi x_1) + (x_1 - 2)^2 \left[ 1 + \sin^2(3\pi x_2) \right] + (x_2 - 1)^2 + \left[ 1 + \sin^2(2\pi x_2) \right]$	0	U
( $f_{11}$ )	Pen-holder	[-11, 11]	2	$f(x) = -\exp \left[ -\cos(x_1) \cdot \cos(x_2) \cdot \exp \left[ \left[ 1 - \sqrt{\frac{x_1^2 + x_2^2}{\pi}} \right] \right] \right]^{-1}$	-0.9635	M
( $f_{12}$ )	Six-hump-camel	[-5, 5]	2	$f(x) = \left( 4 - 2.1x_1^2 + \frac{x_1^4}{3} \right) x_1^2 + x_1 x_2 + (4x_2^2 - 4)x_2^2$	-1.0316	M



**Fig. 11.14** Perspective view of classical benchmark functions

classification phase in which remaining features from the previous step was classified by SVM. In this paper, three-fold cross-validation was used for dividing data into test and train. In the experimental result section, the results of the proposed algorithm were compared in two states. In the first state, the proposed algorithm was a part of classification and in the section state, the proposed algorithm was removed from the classification process. The comparative results showed that the proposed algorithm achieved better performance in terms of accuracy based on ResNet18 and GoogleNet features. In order to evaluate the performance of COA, this algorithm was compared with four well-known algorithms with 12 classical benchmark functions. The comparative results were shown that COA was better in most benchmark functions. For future work, the imbalance classification can be combined with the proposed dimension reduction.

**Table 11.7** Comparative results of COA with other algorithms in two-dimensional

Function	Parameters	ACO	DE	GA	COA	PSO
$f_1$	Best	3.1299E-06	0	0	0	0
	Mean	7.2459E-03	2.0855E-03	7.1999E-04	9.9847E-04	2.4908E-04
	Variance	1.8852E-03	3.4810E-04	1.2648E-04	2.1815E-04	2.1766E-05
$f_2$	Best	-1.0676E+02	-1.0676E+02	-1.0676E+02	-1.0676E+02	-1.0676E+02
	Mean	-1.0663E+02	-1.0664E+02	-1.0674E+02	-1.0664E+02	-1.0676E+02
	Variance	1.8801	3.5385E-01	1.0570E-01	1.8609	1.0316E-03
$f_3$	Best	5.2994E-25	0	0	0	0
	Mean	1.3102E-02	1.6698E-02	2.0382E-03	5.8687E-03	2.4578E-03
	Variance	1.7423E-02	1.1987E-02	5.4230E-04	7.4065E-03	2.1372E-03
$f_4$	Best	-2.4157E+01	-2.4157E+01	-2.4157E+01	-2.4157E+01	-2.4157E+01
	Mean	-2.4068E+01	-2.4135E+01	-2.4147E+01	-2.4137E+01	-2.4149E+01
	Variance	1.8050E-01	4.3429E-02	1.8200E-02	6.0485E-02	1.3318E-02
$f_5$	Best	-2.0626	-2.0626	-2.0626	-2.0626	-2.0626
	Mean	-2.0625	-2.0625	-2.0625	-2.0625	-2.0626
	Variance	2.9410E-07	3.5329E-06	6.9213E-07	3.2354E-06	2.4876E-10
$f_6$	Best	-8.4778E-02	-8.4778E-02	-6.6915E-03	-1	-8.0623E-02
	Mean	-4.2833E-02	-5.3238E-02	-4.1231E-03	-8.1339E-01	-3.1645E-02
	Variance	1.6981E-03	1.3978E-03	4.4315E-06	1.4710E-01	1.2390E-03
$f_7$	Best	8.7228E-03	1.1795E-03	1.2072E-03	1E-04	1.7250E-04
	Mean	4.7605E-01	8.3609E-02	3.1267E-02	3.6059E-02	1.3636E-01
	Variance	3.2127E-02	2.9777E-02	1.0944E-02	1.5789E-02	4.6630E-02

(continued)

Table 11.7 (continued)

Function	Parameters	ACO	DE	GA	COA	PSO
$f_8$	Best	-1	-1	-1	-1	-1
	Mean	-9.5938E-01	-9.1725E-01	-9.8690E-01	-9.7104E-01	-9.8763E-01
	Variance	3.4239E-02	6.9652E-02	1.1600E-02	2.6247E-02	8.7122E-03
$f_9$	Best	0	0	0	0	0
	Mean	3.0493E-02	1.4539E-02	2.1529E-03	1.9308E-02	6.3186E-03
	Variance	7.0564E-02	6.1932E-03	8.0876E-04	5.0114E-02	7.6783E-03
$f_{10}$	Best	5.8729E-11	1.3558E-37	1.3771E-69	0	6.1101E-46
	Mean	9.2793E-04	8.9400E-04	1.4052E-04	4.6047E-05	1.2764E-05
	Variance	1.0982E-04	4.8239E-05	2.8590E-06	3.8939E-07	1.7103E-08
$f_{11}$	Best	-9.6353E-01	-9.6353E-01	-9.6350E-01	-9.6353E-01	-9.6353E-01
	Mean	-9.6350E-01	-9.6348E-01	-9.6350E-01	-9.6352E-01	-9.6353E-01
	Variance	3.1196E-08	2.3385E-07	1.2342E-07	6.0357E-08	2.6682E-09
$f_{12}$	Best	-1.0316	-1.0316	-1.0316	-1.0316	-1.0316
	Mean	-1.0288	-1.0289	-1.0313	-1.0284	-1.0316
	Variance	2.4713E-03	1.3459E-03	3.8049E-05	3.9305E-03	1.8816E-07

## References

- Aggarwal P et al (2022) COVID-19 image classification using deep learning: Advances, challenges and opportunities. *Comput Biol Med* 105350
- Agrawal P et al (2021) Metaheuristic algorithms on feature selection: a survey of one decade of research (2009–2019). *IEEE Access* 9:26766–26791
- Apostolopoulos ID, Mpesiana TA (2020) Covid-19: automatic detection from x-ray images utilizing transfer learning with convolutional neural networks. *Phys Eng Sci Med* 1
- Balaha HM, El-Gendy EM, Saafan MM (2021) CovH2SD: a COVID-19 detection approach based on Harris Hawks optimization and stacked deep learning. *Expert Syst Appl* 186:115805
- Balaji K, Lavanya K (2019) Medical image analysis with deep neural networks. *Deep learning and parallel computing environment for bioengineering systems*. Elsevier, Amsterdam, pp 75–97
- Balavand A (2021) A new feature clustering method based on crocodiles hunting strategy optimization algorithm for classification of MRI images. *Vis Comput* 1–30
- Balavand A (2022) Crocodile Hunting Strategy (CHS): a comparative study using benchmark functions. *Iran J Numer Anal Optim*
- Balavand A, Hosseinzadeh Kashan A, Saghaei A (2019) Combination of support vector machine and pretrained convolutional neural network models to classify brain tumors in MRI images. *Mod Res Decis Making* 4(1):55–77
- Balavand A, Husseinzadeh Kashan A (2020) A package including pre-processing, feature extraction, feature reduction, and classification for MRI classification. *Optimization in machine learning and applications*. Springer, Berlin, pp 51–68
- Carvalho ED et al (2021) An approach to the classification of COVID-19 based on CT scans using convolutional features and genetic algorithms. *Comput Biol Med* 136:104744
- Challenge LSVR (2012) ImageNet. <http://www.image-net.org/challenges.LSVRC/2012/results.html>
- Chowdhury ME et al (2020) Can AI help in screening viral and COVID-19 pneumonia? *IEEE Access* 8:132665–132676
- Gao XW, Hui R, Tian Z (2017) Classification of CT brain images based on deep learning networks. *Comput Methods Programs Biomed* 138:49–56
- Gopatoti A, Vijayalakshmi P (2022) CXGNet: a tri-phase chest X-ray image classification for COVID-19 diagnosis using deep CNN with enhanced grey-wolf optimizer. *Biomed Signal Process Control* 103860
- He K et al (2016) Deep residual learning for image recognition. In: *Proceedings of the IEEE conference on computer vision and pattern recognition* <https://www.mathworks.com/help/deeplearning/ug/pretrained-convolutional-neural-networks.html> (2021)
- Jaiswal A et al (2020) Classification of the COVID-19 infected patients using DenseNet201 based deep transfer learning. *J Biomol Struct Dyn* 1–8
- Kashan AH et al (2021) The league championship algorithm: applications and extensions. *Handbook of AI-based metaheuristics*. CRC Press, Boca Raton, pp 201–218
- Ko H et al (2020) COVID-19 pneumonia diagnosis using a simple 2D deep learning framework with a single chest CT image: model development and validation. *J Med Internet Res* 22(6):e19569
- Li D et al (2020) False-negative results of real-time reverse-transcriptase polymerase chain reaction for severe acute respiratory syndrome coronavirus 2: role of deep-learning-based CT diagnosis and insights from two cases. *Korean J Radiol* 21(4):505–508
- Loey M et al (2020) A hybrid deep transfer learning model with machine learning methods for face mask detection in the era of the COVID-19 pandemic. *Measurement* 108288
- Mantero P, Moser G, Serpico SB (2005) Partially supervised classification of remote sensing images through SVM-based probability density estimation. *IEEE Trans Geosci Remote Sens* 43(3):559–570
- Minaee S et al (2020) Deep-covid: predicting covid-19 from chest x-ray images using deep transfer learning. [arXiv:2004.09363](https://arxiv.org/abs/2004.09363)

- Murugan R et al (2021) WOANet: Whale optimized deep neural network for the classification of COVID-19 from radiography images. *Biocybern Biomed Eng* 41(4):1702–1718
- Pathak Y et al (2020) Deep transfer learning based classification model for COVID-19 disease. *IRBM*
- Rahimzadeh M, Attar A (2020) A modified deep convolutional neural network for detecting COVID-19 and pneumonia from chest X-ray images based on the concatenation of Xception and ResNet50V2. *Inf Med Unlocked* 100360
- Rahman T et al (2021) Exploring the effect of image enhancement techniques on COVID-19 detection using chest X-ray images. *Comput Biol Med* 132:104319
- Russakovsky O et al (2015) Imagenet large scale visual recognition challenge. *Int J Comput vis* 115(3):211–252
- Shibly KH et al (2020) COVID faster R-CNN: a novel framework to diagnose novel coronavirus disease (COVID-19) in X-ray images. *medRxiv*
- Steger C, Ulrich M, Wiedemann C (2018) *Machine vision algorithms and applications*. Wiley
- Szegedy C et al (2015) Going deeper with convolutions *CVPR*
- Tian D (2013) A review on image feature extraction and representation techniques. *Int J Multimedia Ubiquitous Eng* 8(4):385–396
- Toğaçar M, Ergen B, Cömert Z (2020) COVID-19 detection using deep learning models to exploit social mimic optimization and structured chest X-ray images using fuzzy color and stacking approaches. *Comput Biol Med* 103805.
- Turriff S (2016) Curling: steps to success. *Human Kinetics*
- Ucar F, Korkmaz D (2020) COVIDiagnosis-Net: deep bayes-SqueezeNet based diagnostic of the coronavirus disease 2019 (COVID-19) from X-ray images. *Med Hypotheses* 140:109761
- Wallis LA (2020) COVID-19 severity scoring tool for low resourced settings. *Afr J Emerg Med*
- Weston J, Watkins C (1998) Multi-class support vector machines. *Citeseer*
- Yoo SH et al (2020) Deep learning-based decision-tree classifier for COVID-19 diagnosis from chest X-ray imaging. *Front Med* 7:427
- Zhang Y et al (2020) CT image classification based on convolutional neural network. *Neural Comput & Appl*
- Zhou B et al (2016) Places: an image database for deep scene understanding. [arXiv:1610.02055](https://arxiv.org/abs/1610.02055)
- Zouch W et al (2022) Detection of COVID-19 from CT and chest X-ray images using deep learning models. *Ann Biomed Eng* 1–11



# Chapter 12

## Deep Learning Framework for Brain Tumor and Alzheimer Disease Prognosis Using MRI Images



Aditee Patil, Bhavana Tiple, and Madhura Phatak

**Abstract** Brain Tumor (BT) and Alzheimer Disease (AD) are considered as the deadliest brain disease by many health organizations across the world. For the examination of both these diseases, professional health expert used MRI images because it provides detailed information about brain structures. In the proposed research work, BT and AD are distinguished using MRI. Additionally, Brain Tumor also has significant three types which get identified in the proposed model. The research model is ordered into five classes Glioma Tumor (GT), Meningioma Tumor (MT), Pituitary Tumor (PT), Alzheimer's disease (AD), and No Tumor. This proposed system works on the pre-trained models that are VGG16, VGG19, DenseNet201. In the research, for training purpose 75% images are considered as well as for testing 25% of images are set up from dataset. The best model, i.e., DenseNet201 is considered for the final analysis. The Accuracy rate, Precision, Recall, F1-Score are considered as the parameters of evaluation.

**Keywords** Brain tumor · Alzheimer's disease · Glioma tumor · Meningioma tumor · Pituitary tumor · VGG 16 · VGG 19 · DenseNet201

### 12.1 Introduction

All around the globe, brain diseases are considered as dangerous and it may harm to any level to a human being. Brain is a delicate organ which consists of many sensitive cells. The uncontrollable cell division in brain is called brain tumor.

---

A. Patil (✉) · B. Tiple · M. Phatak  
MIT World Peace University, Pune, India  
e-mail: [aditeepatil24@gmail.com](mailto:aditeepatil24@gmail.com)

B. Tiple  
e-mail: [bhavana.tiple@mitwpu.edu.in](mailto:bhavana.tiple@mitwpu.edu.in)

M. Phatak  
e-mail: [madhura.phatak@mitwpu.edu.in](mailto:madhura.phatak@mitwpu.edu.in)

There are many ways to categorize brain tumor but significant three types are glioma, meningioma, and pituitary. Other death-causing brain disease is Alzheimer. Alzheimer is a disease where cell is not growing instead cell death occurs. AD is an irreversible and progressive disease of the brain. In cell levels, various obsessive components are in like manner among tumor and AD growth. In recent years, many researchers have found that there is a relationship and link between AD and BT (<https://www.cancernetwork.com/view/growing-link-between-cancer-and-alzheimers-disease>, view, growing-link-between-cancer-and-alzheimers-disease). In case of AD and BT, the different clinical indications of comparable causes and conditions have baffled scientists for a long time.

One of the contagious diseases is BT and AD has rapidly found around the globe and due to these diseases humans of every age suffer to any extent. The obvious reason for dementia is AD and BT is considered as cancer causing and led to death. BT and AD both have some common symptoms like behavior changes, confusion generation, balancing and coordination issue, difficulty in concentration, weakness, troubling in hearing, speaking and vision at certain age.

The testing for BT and AD is done by taking brain structure images. There are many ways to take these images, for instance, X Rays scan, PET (Positron Emission Tomography) scan, MRI (Magnetic Resonance Imaging). MRIs are considered as best way to analyze brain anomalies; therefore MRI is mostly used by neurologist and neuropathy experts. MRI images resulted in far superior findings in contrast with the scans and other systems in terms of image etiology examination. Even a specialist radiologist or neurologist takes time to study and understand MRI scans. To reduce efforts and time, an automatic system is required and due to this the proposed system can be beneficial to health workers.

The proposed research is useful for detection of BT and AD from MRI images. The proposed work is split into 2 phases: 1. Preparation of data, 2. Brain disease prognosis. In phase one, collection of data and all the augmentation of data is performed. To add more data in dataset, augmentation of images step was performed. Also, for deep learning (DL) model huge size of data is required and to avoid overfitting this needs to be in large size. In phase two, MRI images categorized into five classes GT, MT, PT, AD, and No tumor. The responsibility of the proposed research work can be summarized as the new way of thinking with the original data which is increment on the limited dataset and is used to orchestrate the new dataset. The deep learning models, i.e., VGG16, VGG19, DenseNet201 are used to get better results and through this work try to contribute in medical health research.

The aim of this paper is to investigate the evolution of the brain disease prognosis frameworks using deep learning. Technical scientific division is presented that orchestrates the investigated structure subject to deep learning pre-prepared techniques. The paper includes the proposed work methodology in Sect. 12.2, architecture of system in Sect. 12.3, experiments in Sect. 12.4, results in Sect. 12.5, discussions in Sect. 12.6, last in Sect. 12.7 conclusion.

## 12.2 Related Work

This section provides a review about the research work which is carried out on the Brain Tumor and Alzheimer disease detection by the convolution neural networks using MRI images.

Shelke (2018) proposed the system in which CNN and KNN methods are used. CNN method provides highest 92.86% of Accuracy than KNN. The proposed system has two classes such as non-tumor and tumor. The system used MRI images in dataset and performed patch extractions, features extraction in pre-processing then classified the images using CNN. The aim of this system is to increase accuracy percentages and decrease the error percentages. 7.14% was the error rate of the implemented system. Sensitivity and specificity was 100% achieved.

Qayyum et al. (2020) presented an approach using two models of deep neural learning and comparing this with the proposed CNN method. The DenseNet201 achieved the highest accuracy of 99.51%. The InceptionV3 achieved accuracy of 99.34%. 3064 images were in the MRI image dataset. The system has three tumor classes such as GT, MT, and PT. Accuracy score, F1-score, Precision rate, Recall rate parameters are considered as examination parameters.

Azmi et al. (2020) developed a system of 12 layers CNN for automatic detection and classification of Alzheimer disease. In system CNN and Transfer learning models VGG19, InceptionV3, MobileNet V2, and Xception were compared to achieve better result. In the proposed system Oasis image dataset was used and it was classified into two classes demented and non-demented. The performance evaluation is done based on Accuracy, Precision, F1-score, Recall, Specificity, and Sensitivity. The model shows the accuracy by CNN is 97.75% VGG19 is 50%, InceptionV3 is 90.62%, MobileNet V2 is 81.24%, Xception is 84.37% which is achieved.

Sim et al. (2020) represented an automatic system using a two-DCNN for detection of tumor. The system uses 2D CNN and achieved 91.3% accuracy. The dataset includes three tumor types of MRI images glioma, meningioma, and pituitary. The proposed system classifies images into normal brain and abnormal brain images. The Evaluation parameters are Precision and Recall.

Marghalani and Arif (2019) developed a system for prognosis and categorization for brain diseases. The implemented model consists of 3 classes such as name of the classes Brain tumor, Alzheimer disease, and Normal brain. There are more than 1200 images in the dataset which is collected from oasis, cancer archives. In developed system SVM was used as classifier and it achieved 97% accuracy for all three classes.

The research gaps are as follows:

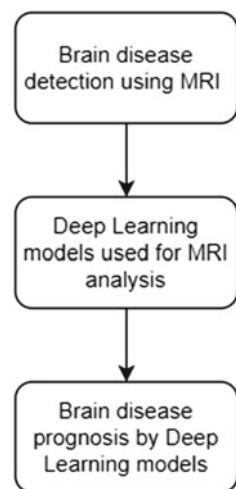
1. Most of the papers have been worked to classify maximum of only three classes.
2. Many research work is based on single brain disease only. No two combined disease detection was found on web sources.
3. Reviewed research papers used smaller dataset so this may result in bias and mistraining of deep learning models.

### 12.3 Proposed System

Machine Learning's subfield is deep neural networks. This subfield totally depends on calculations of models and elements which is having similarities brain-like structures called artificial intelligence (AI). AI is a combination of machine and human thinking. Deep learning helps the machine to solve difficult data problems regardless of dataset size, computation time. Deep learning-based model provides better result with huge data. In recent years, in the health industry deep learning is growing popularity. It helps in clinical research, new development of clinical equipment, medical data analysis, etc. The deep neural network models are utilized for forecasting brain diseases and it includes some steps, for example, collection of data, creation of new data, Fetching elements, categorization, and calculation of gathered information. Figure 12.1 illustrates the proposed prognosis system which depends upon Deep learning.

The first step of proposed system is data gathering, and for collection public web repositories. For large data two public dataset were collected and merged into one dataset. The next step is preparation of data which molds the data into proper format as collected data is not in desired format. Data augmentation was performed using Keras. Augmentation steps like image resizing, horizontal flipping, rotational range, width shifting, height shifting are performed to make optimized system which will provide good accuracy. The subsequent step of it is portioning of data, in this data set is divided into 75–25% ratio for training and testing. Also images are categorized into five classes such as GT, MT, PT, AD, and No Tumor. For feature extraction, it is done by DL models, i.e., VGG16, VGG19, DenseNet201. The most important step is this extraction of required features for prognosis of brain diseases. Lastly, performance was tested by taking into consideration of following parameters: Accuracy, Precision, F1-score, Recall, and support.

**Fig. 12.1** Prognosis of brain disease using deep learning



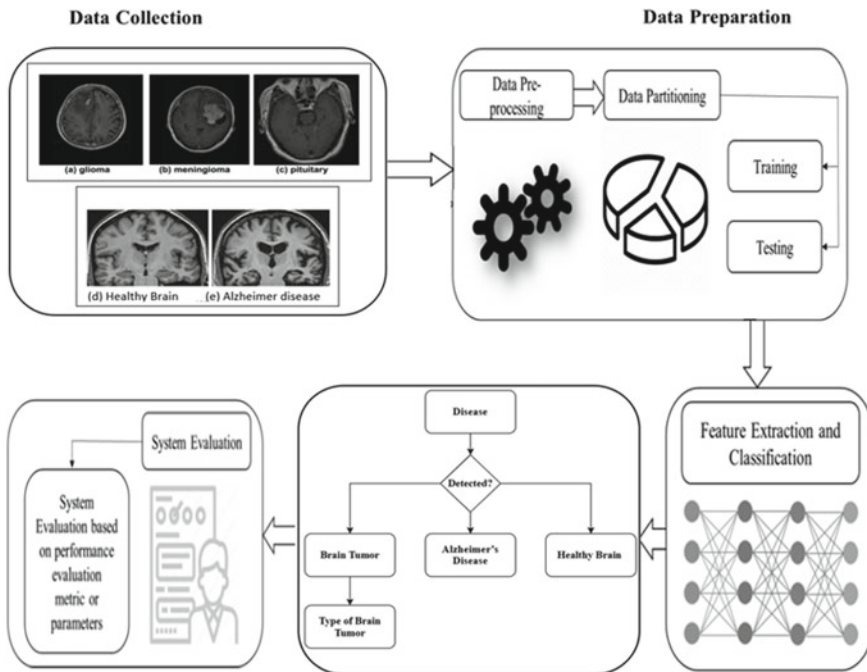


Fig. 12.2 The proposed methodology

Phase two consists of prognosis of brain diseases, and this step depends on five classes. Compare three models of DL for checking which model provides better result and which one is more optimized to use. Most of the operations are performed by deep learning’s model which is pre-trained. Therefore, it extracts features rapidly and classification is also done by the model. The proposed system does not focus on only a single tumor but it also focuses on types of tumors. Additionally it is also checking with other brain diseases, i.e., AD and if no disease is found then it also checks whether it is health brain which is no tumor (Fig. 12.2).

## 12.4 Architecture

The deep learning pre-prepared models are made to take care of a specific issue which anybody can utilize it to tackle a comparable issue. CNN stands for convolutional neural network which is mainly utilized to solve classification problem in picture datasets. The model which is having a huge scope, precise, and various picture information base is ImageNet. To organize the pictures in this dataset WordNet progressive system is utilized. For this research, three deep learning models which pre-trained over ImageNet were utilized and tested. The utilized models are as below:

VGG16: VGG16 network model has 16 layers. The dataset named ImageNet, includes fourteen million images that belong to 1000 classes used for pre-training VGG16. The model received accuracy of 92.7% for top 5 test on that dataset. But problem with this model is that it takes time to train fast and trained imagenet weight itself is 528 MB; therefore, it requires lots of disk space.  $224 \times 224$  is the input size of images.

VGG19: VGG19 network has weight layers 19 and convolution layers 16, lastly 3 totally connected layers. The pre-processed data use Image Data Generator of Keras library. The standard input image size is  $224 \times 224$ .

DenseNet201: DenseNet201 network is 201 layers deepest in size. DenseNet stands for dense coevolutionary network, which is attached with each and every layer in forward feed way. This network can easily divide one image into 1000 classes, for instance, pen, bottle, birds. Standard Input Image size for this network model is  $224 \times 224$ . Advantages: computational and parameter's good efficiency, features are more expanded, good flow of gradient.

## 12.5 Experimental Analysis

### 12.5.1 Dataset

The two datasets were collected from public dataset repository like Kaggle (<https://www.kaggle.com/sartajbhuvaji/brain-tumor-classification-mri>; <https://www.kaggle.com/tourist55/alzheimers-dataset-4-class-of-images>). These two datasets are combined to form one large dataset. The collected dataset is divided into 75% training and 25% testing. Total collected data size is 6975 images. The collected images were categorized into five classes, namely, GT, MT, PT, AD, and No Tumor. Each classes' number of image samples are not same. GT includes 895 images, MT includes 1895 images, PT images are 1395, AD includes 2395 images, and no tumor includes 395 images. All the collected image data goes through image augmentation process to achieve better accuracy with desired cleaned images.

### 12.5.2 Experimental Setup

In the experimental setup, for backend tool TensorFlow used version 2.8.0 and TensorFlow with Keras framework is used. Hardware accelerator set as GPU for fast processing and deep learning models are large in size, so it is necessary to use GPU. GPU also known as Tesla P4 is provided by Google in its Google Collaboratory.

Python is used as programming language. The techniques like VGG16, VGG19, Densenet201 are used to perform processing. Keras gives pre-prepared loads to pre-arranged models. Regardless of the manner, models trained with ImageNet dataset

images and the images present on this dataset accumulated to make task useful and provides better results. In like manner, pre-arranged loads lessen the essential of a colossal volume for training of the dataset. For training purpose, Adam Optimizer with Categorical cross-entropy is used. Adam optimizer is also a substitute optimization method for stochastic gradient descent and this is mostly used in DL models (Kasgari et al. 2021).

Experimenting with different epochs sizes to get maximum accuracy but for considering model loss with the help of graphs decided to set it to 10. Batch size is set to 128. From dataset equally 500 images were used for each class in the model. All the five classes were trained and tested with augmented images (Anitha et al. 2021).

## 12.6 Results

Table 12.1 provides information about accuracy values by three models, i.e., VGG16, VGG19, DenseNet201. The highest accuracy 94% was achieved by DenseNet201. Lowest Accuracy of 84% was achieved by VGG19. The VGG16 obtained 90% accuracy. Table 12.2 outlines the parameters for evaluation of three models individually and it is different for each class. Parameters are accuracy rate, precision, recall, and F1-scores. The maximum macro avg precision of model was 94% achieved by Densent201 and the lowest macro avg precision by model was 88% achieved by VGG19. For DenseNet201 precision is more than 0.5 therefore it is considered as more robust model.

The confusion matrix tables in percentage by VGG16, VGG19, DenseNet201 for all the five classes' names are shown in Figs. 12.3, 12.4, and 12.5. Figures 12.6, 12.7, and 12.8 provide information about true labels vs predicated labels in confusion matrix by three models. Confusion matrix provides models performance prediction in multi-class classification. In the proposed system total five classes are present, so confusion matrix be  $5 \times 5$  matrix.

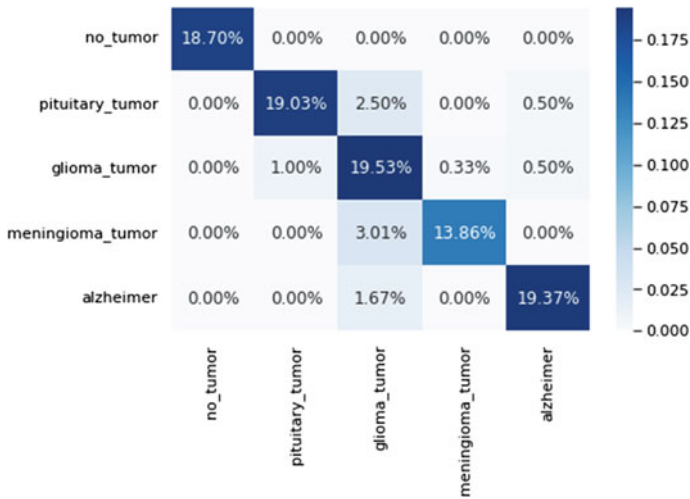
Experimental model loss and model accuracy graphs for all the three proposed models are presented in Figs. 12.9, 12.10, 12.11, 12.12, 12.13, and 12.14. For the model loss graph, Epoch upon X coordination axis and on Y coordination axis has been set to loss rate. Similarly, for model accuracy graph, on coordination axis of X epoch has been set and accuracy onto Y coordination of axis has been set. Blue line and Red line indicate Training and Testing progress of the model. These graphs are useful to decide whether the model is working in proper order or not. Loss

**Table 12.1** Accuracies by proposed models

Method	Accuracy
VGG16	0.90
VGG19	0.84
DenseNet201	0.94

**Table 12.2** Evaluation parameters matrix

Models	Evaluation parameters	No tumor	Pituitary	Glioma	Meningioma	Alzheimer
VGG16	Precision	1.00	0.95	0.73	0.98	0.95
	Recall	1.00	0.86	0.91	0.82	0.92
	F1-score	1.00	0.90	0.81	0.89	0.94
VGG19	Precision	1.00	0.99	0.59	0.93	0.91
	Recall	1.00	0.53	0.91	0.87	0.91
	F1-score	1.00	0.69	0.72	0.90	0.91
DenseNet 201	Precision	1.00	0.95	0.83	0.99	0.95
	Recall	1.00	0.92	0.92	0.91	0.94
	F1-score	1.00	0.93	0.87	0.95	0.95



**Fig. 12.3** Result of VGG16 confusion matrix

infers how inadequately or well a model acts after every cycle of optimization. An accuracy graph is utilized to quantify the calculation’s presentation in an explainable manner. The model accuracy is determined after the model boundary parameter and is determined in the percentage form. The loss in the model is the summation of the errors made during each cycle of training and validation.

The purposed implemented system has five classes that are GT, MT, PT, Alzheimer, and no tumor. The size of image datasets is also comparatively higher than existing reviewed system which has less size of data. Accuracy rate, Precision score, Recall rate, and F1-scores are points considered for model examination and evaluation. There are three different methodologies utilized, i.e., VGG16, VGG19, DenseNet201. The DenseNet201 has given the highest accuracy of 94% as well as



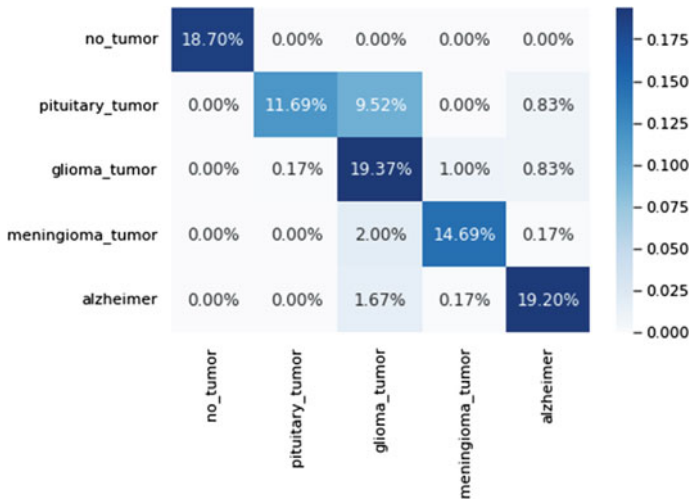


Fig. 12.4 Result of VGG19 confusion matrix

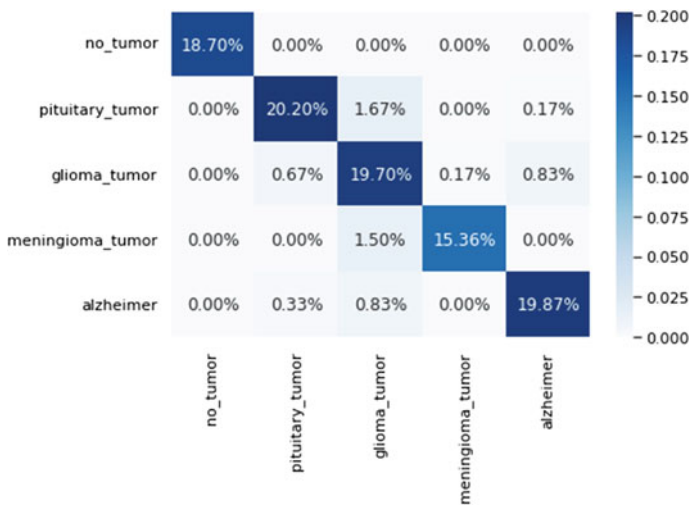
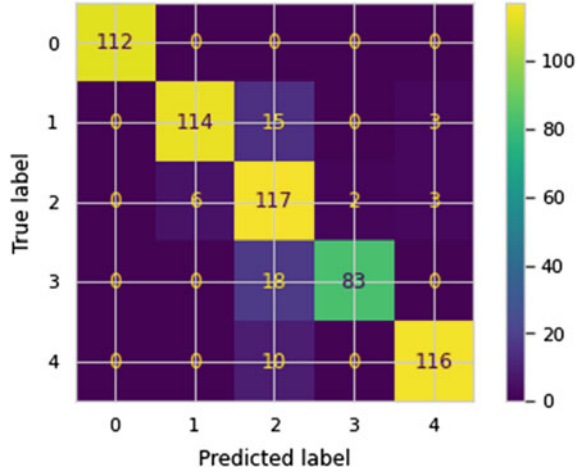


Fig. 12.5 Result of DenseNet201 confusion matrix

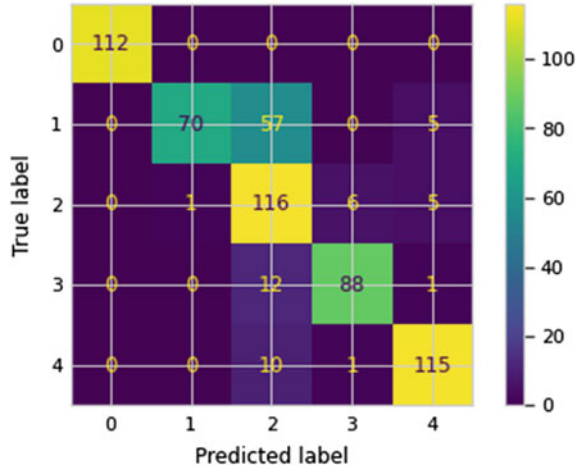
testing accuracy of 100%. The precision is also maximum for DenseNet201 (Table 12.3).

From all the reviewed research work, it is crystal clear that there is very less work found out with five classes. In proposed system, this gap trying to fill. Also it can be seen that the dataset used in existing systems are not more than 500 to 2000 images therefore taking into consideration this point, the developed system used

**Fig. 12.6** True versus predicted labels VGG16 confusion matrix



**Fig. 12.7** True versus predicted labels VGG19 confusion matrix



more number of images, that is, more than 2000 images. All these new implemented points make proposed system unique than others.

## 12.7 Discussion and Future Scope

The discussion section provides information about the research work which based on the Brain Tumor and Alzheimer disease detection by the deep learning framework models using MRI images and suggests future scope of implemented system.

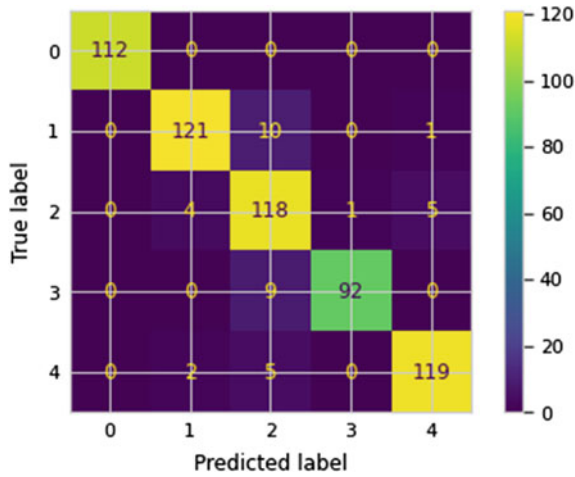


Fig. 12.8 True versus predicted labels confusion matrix of DenseNet201

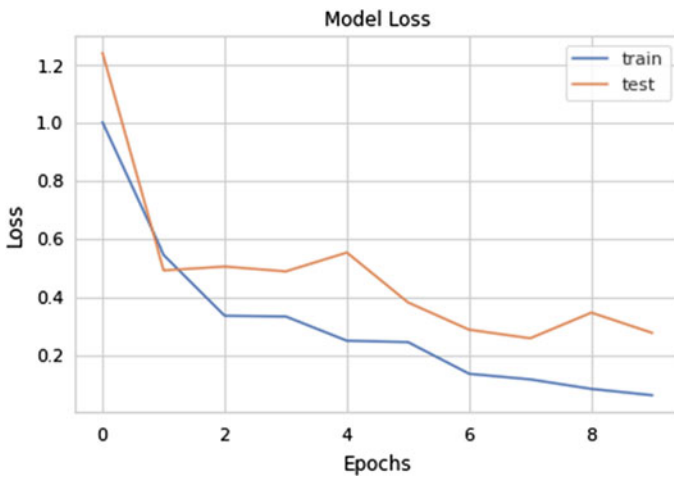


Fig. 12.9 Model loss for VGG16

The deep neural learning methods and calculations are used for prognosis of the brain diseases. To foster a strong framework enormous measure of dataset is required for analysis. For analysis of BT and AD, many researchers used old standard image information which resulted in poor performance of models. Also, old medical image dataset is not enough for this advanced era because new brain diseases have been found and most importantly polluted environment factors also hamper the human body. Considering all these elements there is a need to explore new ways to collect new medical data and new techniques for diagnosis. Internet sources are the best

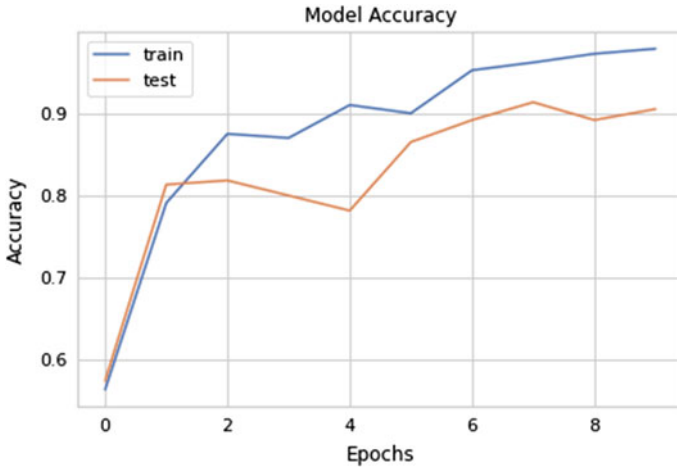


Fig. 12.10 Model accuracy graphs for VGG16

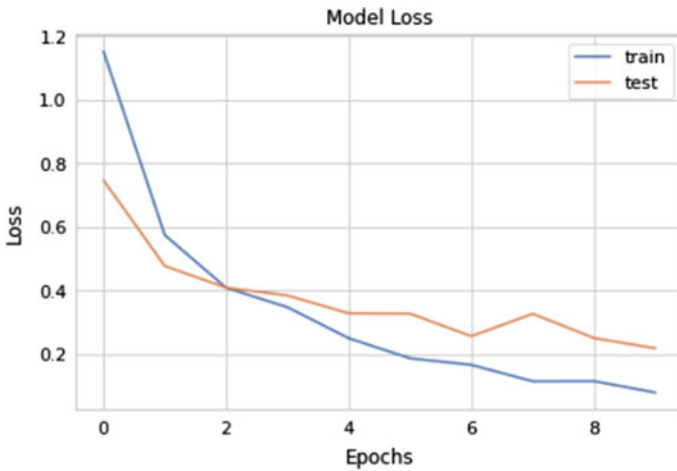


Fig. 12.11 Model loss graphs for VGG19

way to provide data but the collected dataset from web repositories are mostly imbalanced therefore before processing that data cleansing, data normalization is required (Ramana and Nandhagopal 2021; Yakub et al. 2020).

In the training phase of images in the deep learning, irregularity in data is viewed as biased. There are less positive number of samples, because of this it becomes hard to maintain balance data. In testing phase, absence of confidence intervals is another challenge. Confidence of prediction is provided by deep neural network model as output where it represents as output indicator. The low confident interval in brain disease prediction system is generally not desirable. The optimized deep learning

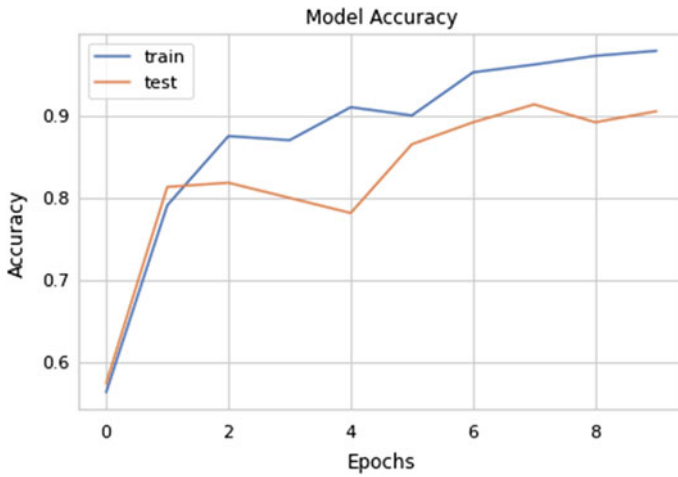


Fig. 12.12 Model accuracy graphs for VGG19

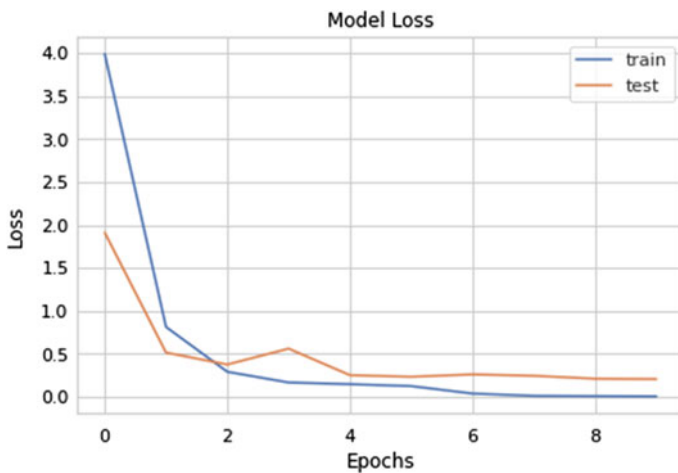


Fig. 12.13 Model loss graphs for DenseNet201

architecture model can manage a number of data and be considered by the research scholars to eliminate these challenges.

Data augmentation is the possible solution to overcome the data challenges of medical image processing. Deep neural networks model with optimized approach are beneficial to reduce huge training and testing computing time (Raju et al. 2020). Due to complexity of brain cells in brain it is feasible to use deep neural networks to process and extract many features as input data travels from one layer to other deep layers (Kamorudeen et al. 2021).

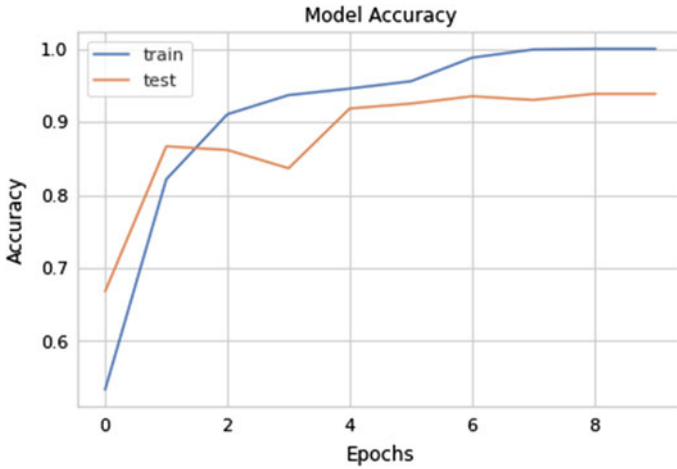


Fig. 12.14 Model accuracy graphs for DenseNet201

Table 12.3 Table of comparison with parameters of evaluation

Author name	Model	Accuracy (%)	Precision	Sensitivity/Recall	F1-score (%)
Shelke et al. (2018)	InceptionV3	92.86%	–	100%	–
Qayyum et al. (2020)	InceptionV3	99.34%	–	–	–
	DensNet201	99.51%	–	–	–
	12 layers CNN	97.75%	100% 93%	92% 100%	97% 98%
	VGG19	50%	0% 50%	0% 100%	0% 67%
Azmi et al. (2020)	MobileNetV2	81.24%	92% 75%	69% 94%	79% 83%
	InceptionV3	90.62%	93% 88%	88% 94%	90% 91%
	Xception	84.37%	100% 76%	69% 100%	81% 86%
Sim et al. (2020)	CNN	91.3%	91%	88%	–
Marghalani and Arif (2019)	SVM	97%	100% 98% 99%	100% 99% 98%	– – –
	VGG16	90%	92%	90%	91%
Proposed system	VGG19	84%	88%	84%	84%
	DenseNet201	94%	94%	94%	94%

The following may be considered in future scope:

1. different deep learning models such as GoogleNet, ResNet, and AlexNet will be applied for new brain disease detection systems.
2. Other brain diseases like Parkinson, Epilepsy, etc. can be included in research work as future development.
3. Large number of different scans like PET, CT dataset can be used for extensive research using advance methods of deep learning (Khan et al. 2022).
4. The real-life dataset should be used instead of web-based repositories and other open-source datasets to enhance results of detection system (Divyamary et al. 2020).

## 12.8 Conclusion

Globally brain diseases like brain tumor and Alzheimer are considered as dangerous and treatments of this diseases are also expensive (Lascu et al. 2019). The proposed system may provide guidance and help for the patients who needs more knowledge about disease and medical condition. The implemented system is also helpful for doctors and other health workers, researchers who want to do research in this field and want to innovate new medicine to cure these diseases. The proposed technique is user-friendly therefore it is easy to use. The system classifies the MRI images into five classes Glioma Tumor (GT), Meningioma Tumor (MT), Pituitary Tumor (PT), Alzheimer Disease (AD), and No Tumor. According to requirement collected MRI image dataset was resized and processed. To increase the quality of images dataset and size data augmentation is performed (Thejaswini et al. 2019). Deep Learning models VGG16, VGG19, and DenseNet201 used for prognosis of BT and AD of brain disease. Also their performances were tested. ImageNet database used by models therefore they have pre-trained weights and they are pre-prepared. The proposed system is categorized into 5 classes. In the experimenting results, the maximum high accuracy achieved by DenseNet201 is 94%. Furthermore, DenseNet201 has maximum precision. VGG19 achieved the least accuracy. It is fitted to take a note that deep Learning plays a vital role in medical industry research.

## References

- Ajagbe SA, Amuda KA, Oladipupo MA, Oluwaseyi FAFE, Okesola KI (2021) Multi-classification of Alzheimer disease on Magnetic Resonance Images (MRI) using Deep Convolutional Neural Network (DCNN) approaches. *Int J Adv Comput Res* 11(53):51–60. <https://doi.org/10.19101/Ijacr.2021.1152001>
- Anitha A, Kokila B, Devadharshini MS, Sankar SA (2021) Brain tumor detection and classification using deep learning techniques based on MRI images. *Proc J Phys: Conf Ser* 1916(1):012226. Iop Publishing. <https://doi.org/10.1088/1742-6596/1916/1/012226>

- Azmi T, Hussain E, Hasan M, Hassan SZ, Rahman MdA, Parvez MZ (2020) Deep learning based binary classification for Alzheimer's disease detection using brain MRI images. In: 2020 15th IEEE Conference on Industrial Electronics and Applications (ICIEA), Kristiansand, Norway, 09 November 2020, pp 1115–1120. <https://doi.org/10.1109/ICIEA48937.2020.9248213>
- Divyamary D, Gopika S, Pradeeba S, Bhuvanewari M (2020) Brain tumor detection from MRI images using naive classifier. In: 2020 6th International Conference on Advanced Computing and Communication Systems (ICACCS), Coimbatore, India, 23 April 2020, pp 620–622. <https://doi.org/10.1109/ICACCS48705.2020.9074213>
- <https://www.cancernetwork.com/view/growing-link-between-cancer-and-alzheimers-disease>
- <https://www.kaggle.com/sartajbhuvaji/brain-tumor-classification-mri>
- <https://www.kaggle.com/tourist55/alzheimers-dataset-4-class-of-images>
- Kasgari AB, Ranjbarzadeh R, Ghoushchi SJ, Anari S, Naseri M, Bendechache M (2021) Brain tumor segmentation based on deep learning and an attention mechanism using MRI multi-modalities brain images. *Sci Rep* 11(1):1–17. <https://doi.org/10.1038/S41598-021-90428-8>
- Khan A, Abbas S, Adnan Khan M, Farooq U, Khan W, Siddiqui S, Ahmad A (2022) Intelligent models for brain tumor identification using deep learning. *Appl Comput Intell Soft Comput* 2022. Article Id – 8104054. <https://doi.org/10.1155/2022/8104054>
- Lascu M, Mircea G, Luscu D (2019) Tumor detection and classification of MRI brain image using different wavelet transforms and support vector machines. In: 42nd international conference on Telecommunications and Signal Processing's (TSP), Budapest, Hungary, 25 July 2019, pp. 505–508. <https://doi.org/10.1109/TSP.2019.8769040>
- Marghalani B, Arif M (2019) Automatic classification of brain tumor and Alzheimer's disease in MRI. *Procedia Comput Sci J Elsevier Sciencedirect* 163:78–84. <https://doi.org/10.1016/J.Procs.2019.12.089>
- Qayyum A, Noreen N, Palaniappan S, Ahmad I, Imran M, Shoaib M (2020) A deep learning model based on concatenation approach for the diagnosis of brain tumor. *IEEE Access* 8:55135–55144. <https://doi.org/10.1109/ACCESS.2020.2978629>
- Raju M, Gopi VP, Anitha VS, Wahid KA (2020) Multi class diagnosis of Alzheimers disease using cascaded three dimensional convolutional neural network. *Phys Eng Sci Med* 1219–1228. <https://doi.org/10.1007/S13246-020-00924-W>
- Ramana TV, Nandhagopal SM (2021) Alzheimer disease detection and classification on Magnetic Resonance Imaging (MRI) brain images using Improved Expectation Maximization (IEM) and Convolutional Neural Network (CNN). *Turk J Comput Math Educ* 12(11):5998–6006
- Shelke SM (2018) Automated segmentation and detection of brain tumor from MRI. In: 2018 International Conference on Advances in Computing, Communications and Informatics (ICACCI), Bangalore, India, 02 December 2018, pp 2021–2026. <https://doi.org/10.1109/ICACCI.2018.8554807>
- Sim, Sarkar S, Kumar A, Chakraborty S, Aich S, Kim HC (2020) A CNN based approach for the detection of brain tumours using MRI scans. *Test Eng Manag* 83:16580–16586
- Thejaswini P, Bhat B, Prakash K (2019) Detection and classification of tumour in brain MRI. *Int J Eng Manuf* 9(1):11–20. <https://doi.org/10.5815/ijem.2019.01.02>
- Yakub B, Kamalakannan A, Rajamanickam G (2020) Detection and classification of brain tumor in MRI images using deep convolutional network. In: 2020 6th International Conference on Advanced Computing & Communication Systems (ICACCS), Coimbatore, India, 6–7 March 2020, pp. 248–252. <https://doi.org/10.1109/Icaccs48705.2020.9074375>



**Part IV**  
**Miscellaneous**

# Chapter 13

## Genetic Algorithm to Maximize the Tourist's Satisfaction: An Assessment of Technology Adoption for a Tourist App



M. A. Cosío-Léon, Anabel Martínez-Vargas, Misael Lopez-Sanchez, and Viridiana Silva-Rodríguez

**Abstract** Tourism has a positive effect on economic growth in large and small countries. The combination of technology and applications is referred to as Tourism 3.0. In this chapter, we propose a tourism app to produce personalized trip itineraries. The app has embedded a genetic algorithm that searches for the best choices of places to maximize the tourist's satisfaction. However, running a genetic algorithm in a standard smartphone suppose to be a challenge since a standard smartphone is a constrained device. The above may affect the tourists' behavior towards using our proposed tourism app. Then, to evaluate tourists' attitudes toward using our tourism app based on a genetic algorithm, we apply the technology acceptance model. Results show that most test participants found our tourism app easy to use. They also show a strong positive correlation between attitude towards use and intention to use.

**Keywords** Technology acceptance model · Genetic algorithm · Itinerary · Tourism app

---

M. A. Cosío-Léon · A. Martínez-Vargas (✉) · M. Lopez-Sanchez  
Universidad Politécnica de Pachuca, Zempoala, Hidalgo, Mexico  
e-mail: [anabel.martinez@upp.edu.mx](mailto:anabel.martinez@upp.edu.mx)  
URL: <http://www.upp.edu.mx>

M. A. Cosío-Léon  
e-mail: [ma.cosio.leon@upp.edu.mx](mailto:ma.cosio.leon@upp.edu.mx)

M. Lopez-Sanchez  
e-mail: [misael.lopez@micorreo.upp.edu.mx](mailto:misael.lopez@micorreo.upp.edu.mx)

V. Silva-Rodríguez  
Universidad Autónoma de San Luis Potosí, San Luis Potosí, San Luis Potosí, Mexico  
e-mail: [viridiana.silva@uaslp.mx](mailto:viridiana.silva@uaslp.mx)  
URL: <http://www.uaslp.edu.mx>

## 13.1 Introduction

There is a positive relationship between tourism and economic growth in developing and developed economies. Some spillover tourism effects include increased employment, added income earnings, a source of government revenue, foreign exchange earnings, and balance of payment support (Scarlett 2021).

Recently, the combination of technology and applications with travel has changed the travel model for tourists. The above is referred to as Tourism 3.0 which is tourist-centric model (Páez-Quinde et al. 2020). Currently, tourists can download apps to help them decide to visit new attractions or try specific activities at the destination. Also, tourists use apps to search for information related to transportation, housing, food, maps, points of interest (POIs), shopping, and city overviews. Mainly, tourists search for the above information to reduce potential risks during their trips. Tourism apps contribute to increasing the growth rates for tourism sites (Lin et al. 2020). Hence, it is paramount to understand the items and stuff that tourists search for when they use tourism apps.

In this work, we present a tourism app to maximize tourist satisfaction according to their travel time in the place. The proposed tourism app generates a personalized trip itinerary composed of some POIs. To do so, our search engine takes data available on Google APIs about POIs to produce recommendations. This is a challenge since a large volume of data (specifically for large cities) is processed to generate good recommendations. To cope with, we integrated a genetic algorithm in the search engine. The above enables our tourism app to work worldwide and give personalized itineraries in seconds.

Most research works focus on discovering how to provide users with the best itineraries to optimize tourist visits instead of focusing on how users interact with recommender system applications. However, recommender systems should be evaluated in terms of effectiveness, efficiency of recommendations, and users' perception of usefulness and ease of use.

To evaluate users' attitudes toward using our tourism app to generate their personalized trip itinerary, we apply the technology acceptance model (TAM) (Davis et al. 1989). TAM helps to understand why people accept or reject using an IT system. It should be noted that our focus in the app evaluation is to analyse how the tourist reacts to the personalized trip itinerary generated by a genetic algorithm. The tourists do not have the notion that a genetic algorithm generates their itineraries. No research to date, to the best of our knowledge, has evaluated users' attitudes toward personalized trip itineraries produced by a genetic algorithm on a mobile device with average resources.

There are previous works that apply the TAM methodology in tourism apps. For example, a study in Lin et al. (2020) explores why independent foreign travelers use apps to search for tourism information. The authors evaluated at the terminal of Taiwan Taoyuan International Airport. Regarding the usage attitude of apps, the study found that if independent foreign travelers believe that an app is helpful, they exhibit a positive attitude towards operating the app. On the other hand, the study

found that independent foreign travelers have problems with the app user interfaces or app designs flawed. Another work is Lin et al. (2014) in which the authors apply TAM to evaluate an app that provides digitized information on mountaineering trails in Daken, Taiwan. Their app monitors energy expenditure for health promotion under the Android platform. The subjects answered a questionnaire for two months. Results show that the app is useful for community tourism and health promotion in Daken. Consequently, work in Páez-Quinde et al. (2020) proposes an app focused on Pilahuín, Ecuador. The authors developed the app for iOS and Android. The app promotes cultural tourism and gastronomic tourism in the town. Then, the authors apply the TAM methodology to measure the acceptability of the inhabitants of Pilahuín. As a result, the authors find out that the community of Pilahuín agrees to offer digital tourism. In addition, work in Xia et al. (2018) shows the official app of the Macau government tourist office, called “Experience Macau.” The app includes information provision, trip planning, navigation, and entertainment functions. Through TAM authors found that more attention should be paid to navigation and content quality. These two factors impact in perceived effectiveness. Content quality was the most unsatisfactory function, consequently, the information on the features of Macau was insufficient considering users’ experience.

The above studies do not have a metaheuristic embedded in your apps. Furthermore, the apps focus on tourist attractions from specific areas.

Although work in Tenemaza et al. (2020) does not apply the TAM methodology (instead, it undergoes an analysis of users’ perceptions), it generates itineraries through a genetic algorithm along with  $k$ -means. The authors apply  $k$ -means to cluster preferences based on the number of days a tourist will visit a place. After that, a genetic algorithm optimizes the itinerary. Then, the authors present an analysis of users’ perceptions that identifies factors influencing user preference and quality of the experience. Their evaluation shows that the POIs in the itinerary helps tourist enjoy the place without affecting their interests. Unlike work in Tenemaza et al. (2020), we only apply a genetic algorithm to produce personalized trip itineraries. Likewise, the work in Tarantino et al. (2019) is based on an evolutionary optimizer that allows to determine, in an acceptable time, a near-optimal user-adapted tour for each day of the visit considering different conflicting objectives. The functionalities and interactive facilities provided by the application are illustrated together with the model used to adapt the tourist itinerary to the user’s preferences and constraints. Besides putting emphasis on the usability of the application and its graphical user interface together with the user satisfaction through the application of two questionnaires: usefulness, satisfaction and ease of use questionnaire (USE), and user experience questionnaire (UEQ).

This chapter is organized as follows: Sect. 13.2 describes the tourist recommended system design. Section 13.3 explains the system evaluation. Section 13.4 shows the results and discussion. Finally, Sect. 13.5 provides the conclusions and indicates future research directions.

## 13.2 Tourist Recommended System Design

### 13.2.1 Optimization Model

The knapsack problem (KP) (Martello et al. 1990) as its name suggests deals with the problem of selecting those items that maximize profit without overloading the knapsack. Each item has a profit and a weight.

Formally the KP is described as follows: given a number of items  $n$ , a set of profits  $P = \{p_1, \dots, p_n\}$ , a set of weights  $W = \{w_1, \dots, w_n\}$ , and a capacity  $C$ ; find the subset of items to maximize profit while the total weight is below  $C$ . Then the optimization model is

$$\text{Maximize } P(x) = \sum_{i=1}^n x[i] \cdot P[i] \quad (13.1)$$

s.t.

$$\sum_{i=1}^n x[i] \cdot W[i] \leq C \quad (13.2)$$

$$x \in \{0, 1\}, i = 1, 2, \dots, n \quad (13.3)$$

where Eq. (13.1) is the objective function to maximize profit. There  $x[i] = 1$ , if the  $i$ -th item is included in the knapsack, otherwise  $x[i] = 0$ . On the other hand, Eq. (13.2) constraints the total weight of selected items.

Then, the KP is mapped to the tourist trip design problem (TTDP) which maximizes the travelers' satisfaction (Tlili and Krichen 2021). Unlike the KP, the TTDP has a set of points of interest (POIs) to visit. These POIs are visited in such a way that the overall profit is maximized without violating a set of constraints. The solution is a POIs route for a tourist.

To propose personalized trip planning to a tourist, we consider the KP optimization model to address the TTDP as follows (Lopez-Sanchez et al. 2021):

- *Travel time* (capacity). The tourist sets travel time (days or hours). Our app converts travel time to seconds.
- *Solution size* ( $n$ ). It is the cardinality of the set of POIs in the coverage area of the current tourist location.
- *Rating* (profit). It is given by Google *Places* API metadata. It is the average of ratings, determined by people's experience with each POI.
- *Time by place* (weight). It is time in seconds. This data is gathered using *Directions* API. Time by place is computed as the time to move from the tourist location to the POI (go and back) plus stay time as Eq. (13.4) shows:

$$T = (t \cdot 2) + t_p \quad (13.4)$$

**Table 13.1** Values for  $t_p$  according to the types of POIs (Gartner and Huang 2021; Sumiya et al. 2015)

Types of POIs	Stay time (s)
Museum	3600
Park	9900
Amusement park	28,800
Zoo	7200
Historical places	1800

where  $t$  is the transportation time given by *Directions API*. Conversely,  $t_p$  is the stay time to visit a type of POI which is set according to Table 13.1.

### 13.2.2 System Architecture

The proposed tourism app generates a personalized trip itinerary, suggesting the most convenient POIs to visit. This is done through travel time, destination location, and personal preferences. The above is the user profile knowledge. Our tourism APP gathers POIs data from external data sources. The collected data complies with the user profile. Then, the collected data is processed by a steady-state genetic algorithm (SSGA). When the SSGA concludes its searching process to find the subset of POIs that maximizes tourist satisfaction subject to travel time, the tourist obtains a personalized trip itinerary.

Figure 13.1 shows the system architecture comprised by three modules: (a) views, (b) travel plan manager, and (c) search engine based on a genetic algorithm.

Our tourism app takes into account POIs contents that are collectively generated by tourists. To do so, we use Google Places API. As shown in Fig. 13.1, it keeps a database created by crowdsourcing. Then the tourists can add, modify, and update the POIs' information like photographs, opinions, ratings, etc. Another data source is Google Directions API which computes time and distance between two coordinates in a map. The units are seconds for time and meters for distance.

A tourist can interact with our tourism app through the graphical user interface (GUI). The above makes our tourism app reactive when the tourist triggers events using the GUI and the app performs those actions. In terms of the system architecture shown in Fig. 13.1, this is the views module. Figure 13.2 shows the GUI of the app.

The travel plan manager module shown in Fig. 13.1 gathers data to create a personalized trip itinerary. It collects knowledge about the tourist (travel time, location, and personal preferences) to acquire POIs information. A tourist sets travel time in days or hours as Fig. 13.2d shows. However the tourist app converts the travel time in seconds according to Eq. 13.5:

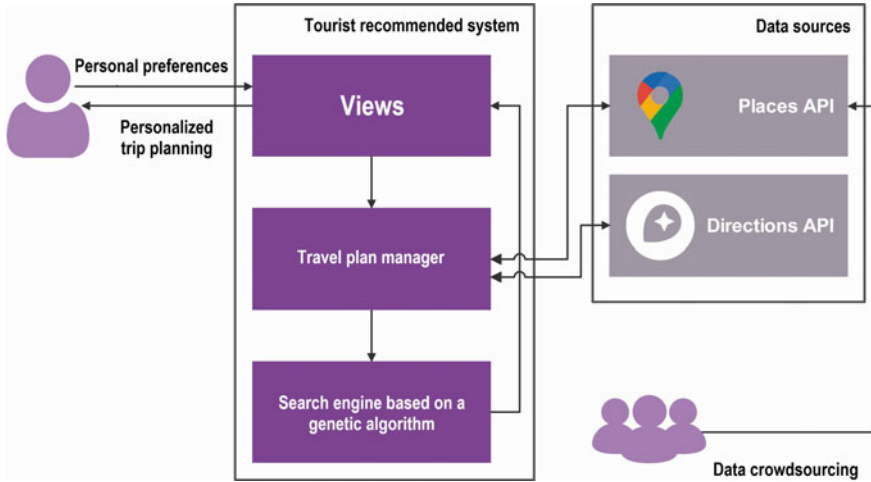


Fig. 13.1 System architecture



Fig. 13.2 GUI of the APP. a Initial screen. b Main menu. c Help screen. d Travel time screen. e Location screen. f Map screen to manually enter location. g Personal preferences menu screen. h Search by proximity screen. i Personalized trip itinerary screen. j Information of a POI screen

$$D_{\text{travel}} = \begin{cases} (t_{\text{tourist}} \cdot 12) \cdot 3600, & \text{If } \textit{unit} = \textit{days} \\ t_{\text{tourist}} \cdot 3600, & \text{If } \textit{unit} = \textit{hours} \end{cases} \quad (13.5)$$

where  $t_{\text{tourist}}$  is travel time value. *unit* uses the days or hours metrics. When travel time is set to days, each day is equal to 12h to enjoy the trip. Then, the hours are

converted to seconds. In contrast, when a tourist sets travel time to hours, they simply are converted to seconds.

In contrast, location is the geographic coordinates (latitude and longitude) in which the tourist is located. A tourist can choose to set their location in two ways: manually or automatically (see Fig. 13.2e). The tourist automatically sets their location by doing one click of the gray button. Conversely, the tourist manually sets their location by using a map as Fig. 13.2f shows.

The last piece of information is personal preferences which are the kind of places a tourist will visit. Our app has four places to visit: museums, zoos, parks, and historical places (see Fig. 13.2g). In this way, the tourist selects the kind of POIs that build up their personalized trip itinerary.

When the travel plan manager module finished its task, it shares its collected data with the search engine based on a genetic algorithm module.

In work in Lopez-Sanchez et al. (2021), we reported that the random decoder (Michalewicz 1996) would be implemented in our tourism app accompanied by the SSGA because it gives a personalized trip itinerary with different POIs. Moreover, the random decoder achieves a knapsack (travel time) almost loaded. The above means that tourist has a day full of entertainment. Therefore the search engine based on a genetic algorithm module has a random decoder coupled with the SSGA.

Decoders use integer representation (ordinal representation). Each individual has a length  $n$ , then the  $i$ -th component of the vector is an integer in the range  $[1, n - i + 1]$ . The ordinal representation references a list  $L$  of POIs that is created randomly. We apply the decoder procedure (Michalewicz 1996) shown in Algorithm 13.1.

---

### Algorithm 13.1: Random decoder procedure

---

**Data:** Individual vector ( $x$ ), profits vector ( $P$ ), and weights vector ( $W$ ).

```

1 build a list  $L$  of items;
2  $i = 1$ ;
3  $WeightSum = 0$ ;
4  $ProfitSum = 0$ ;
5 while  $i \leq n$  do
6    $j = x[i]$ ;
7   remove the  $j$ -th item from the list  $L$ ;
8   if  $WeightSum + W[j] \leq C$  then
9      $WeightSum = WeightSum + W[j]$ ;
10     $ProfitSum = ProfitSum + P[j]$ ;
11  end
12   $i = i + 1$ ;
13 end
14 End;
```

---

Take, for example, the individual vector  $x = [10, 3, 7, 9, 5, 6, 1, 4, 4, 2, 1, 1]$ , the list  $L = [1, 2, 3, 4, 5, 6, 7, 8, 9, 10, 11, 12]$ , the profits vector  $P = [3.7, 2.8, 3.7, 4.4, 4.4, 4.5, 4.8, 2.8, 3.5, 4.7, 4.8, 4.0]$ , the weights vector  $W = [4213, 4100, 4544, 10882, 10536, 29768, 7681, 8153, 2309, 2269, 2488, 2603]$ , and the capacity



$C = 43200$ . Then considering the Algorithm 13.1, we obtain that the POIs vector [10, 3, 8, 12, 9, 1, 7, 11, 2] builds up the personalized trip itinerary that is represented by the individual  $x$ . Therefore, its fitness is 34.8 points, and its total weight is 38360s. Table 13.2 illustrates step by step the decoder procedure shown in Algorithm 13.1.

To obtain the best-personalized trip itinerary, we apply the SSGA shown in Algorithm 13.2. SSGA randomly starts to generate the population. It applies tournament selection to create two parents. To do so, it randomly picks  $k$  individuals from the population. Then it selects the best performer (based on fitness that is calculated according to Algorithm 13.1) from the  $k$  individuals. The best performer is the parent (Eiben and Smith 2015). That procedure is repeated twice.

After that, SSGA performs the one-point crossover operator for the ordinal representation as suggested in Michalewicz (1996). SSGA applies the one-point crossover as long as a random number in the range [0, 1] is below the crossover probability. Otherwise, the offspring are the two parents. Consequently, SSGA undergoes a mutation similar to the bit-flip for the binary representation. It takes a random value (with uniform distribution) from the range [1,  $n - i + 1$ ] for the  $i$ -th position to be mutated (Michalewicz 1996).

In an SSGA, parents and offspring compete for survival. In this work, we apply elitist recombination (Herrera et al. 2008) in which the best two parents and offspring go to the next generation.

When the SSGA reaches a predefined number of cycles, it returns the best-personalized trip itinerary as a solution.

---

### Algorithm 13.2: SSGA

---

**Data:** Population size, crossover probability, mutation probability, and number of iterations. Travel time, profits vector (rating), and weights vector (time by place).

**Result:** The best personalized trip itinerary.

```

1 Generate population randomly;
2 repeat
3   | Select two parents using a tournament selection;
4   | if random_number <= crossover_probability then
5   |   | Perform one-point crossover;
6   | else
7   |   | offspring_1 = Parent_1;
8   |   | offspring_2 = Parent_2;
9   | end
10  | Mutate the two-resulting offspring;
11  | Perform replacement strategy;
12 until number_of_cycles > total_number_of_cycles;
13 Select the best solution from population;
14 End;
```

---

**Table 13.2** Decoder procedure using  $x = [10, 3, 7, 9, 5, 6, 1, 4, 4, 2, 1, 1]$

$i$	$x[i]$	$j$	$L$	WeightSum	POI included in the itinerary?	ProfitSum
1	$\overset{i}{[10, 3, 7, 9, 5, 6, 1, 4, 4, 2, 1, 1]}$	10	$[1, 2, 3, 4, 5, 6, 7, 8, 9, \overset{j}{10}, 11, 12]$	$0 + 2269 = 2269$	Yes	$0 + 4.7 = 4.7$
2	$[10, \overset{i}{3}, 7, 9, 5, 6, 1, 4, 4, 2, 1, 1]$	3	$[1, 2, \overset{j}{3}, 4, 5, 6, 7, 8, 9, 11, 12]$	$2269 + 4544 = 6813$	Yes	$4.7 + 3.7 = 8.4$
3	$[10, 3, \overset{i}{7}, 9, 5, 6, 1, 4, 4, 2, 1, 1]$	7	$[1, 2, 4, 5, 6, 7, \overset{j}{8}, 9, 11, 12]$	$6613 + 8153 = 14966$	Yes	$8.4 + 2.8 = 11.2$
4	$[10, 3, 7, \overset{i}{9}, 5, 6, 1, 4, 4, 2, 1, 1]$	9	$[1, 2, 4, 5, 6, 7, 9, 11, \overset{j}{12}]$	$14966 + 2603 = 17567$	Yes	$11.2 + 4.0 = 15.2$
5	$[10, 3, 7, 9, \overset{i}{5}, 6, 1, 4, 4, 2, 1, 1]$	5	$[1, 2, 4, 5, \overset{j}{6}, 7, 9, 11]$	$17569 + 29768 = 47337$	No	
6	$[10, 3, 7, 9, 5, \overset{i}{6}, 1, 4, 4, 2, 1, 1]$	6	$[1, 2, 4, 5, 7, \overset{j}{9}, 11]$	$17569 + 2309 = 19878$	Yes	$15.2 + 3.5 = 18.7$
7	$[10, 3, 7, 9, 5, 6, \overset{i}{1}, 4, 4, 2, 1, 1]$	1	$[\overset{j}{1}, 2, 4, 5, 7, 11]$	$19878 + 4213 = 24091$	Yes	$18.7 + 3.7 = 22.4$
8	$[10, 3, 7, 9, 5, 6, 1, \overset{i}{4}, 4, 2, 1, 1]$	4	$[2, 4, 5, \overset{j}{7}, 11]$	$24091 + 7681 = 31772$	Yes	$22.4 + 4.8 = 27.2$
9	$[10, 3, 7, 9, 5, 6, 1, 4, \overset{i}{4}, 2, 1, 1]$	4	$[2, 4, 5, \overset{j}{11}]$	$31772 + 2488 = 34260$	Yes	$27.2 + 4.8 = 32.0$
10	$[10, 3, 7, 9, 5, 6, 1, 4, 4, \overset{i}{2}, 1, 1]$	2	$[\overset{j}{2}, 4, 5]$	$34260 + 10882 = 45142$	No	
11	$[10, 3, 7, 9, 5, 6, 1, 4, 4, 2, \overset{i}{1}, 1]$	1	$[\overset{j}{2}, 5]$	$34260 + 4100 = 38360$	Yes	$32.0 + 2.8 = 34.8$
12	$[10, 3, 7, 9, 5, 6, 1, 4, 4, 2, 1, \overset{i}{1}]$	1	$[\overset{j}{5}]$	$38360 + 10536 = 48846$	No	

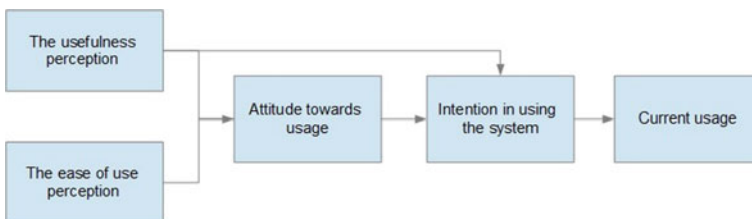
## 13.3 System Evaluation

### 13.3.1 Evaluation Model

Human-computer interaction (HCI) is a field of study focusing on the design of computer technology for human users as well as the main phenomena that surround them. HCI evaluation mainly follows three objectives: assess the scope and accessibility of system functionality, assess users' experience in the interaction, and identify any system-specific issues (Dix et al. 2003). The above can be developed into four time stages of the system age: (a) *On the planning stage* with the aim of informing its design and the system development, (b) *On the system design stage*, a formative assessment, it contributes to system development, identifying design problems early, whether in drawings, mockups, or non-functional prototypes, (c) *During system development*, evaluating functional prototypes allows us to identify particular usability problems, (d) *After system implementation stage*, acceptance tests can be performed to identify improvement features for a second system version; and in this last stage, we apply an assessment of technology adoption and user experience of the system.

The assessment in this study was based on the TAM which was developed by Davis (1989) (see Fig. 13.3). TAM defines perceived ease of use as the ease of understanding and learning to use an interactive system. TAM questionnaire is used as a measure of acceptance and use of an interactive system because it is based on the significant relationship between perceived usefulness, perceived ease of use, and attitudes towards system use. This model proposes that perceptions of usefulness and ease of use by a person about an information system are conclusive to determining their intention towards the system (Santana-Mancilla and Anido-Rifón 2017). TAM explains the reasons for the users' technology acceptance. In the following section, we will describe the protocol for the evaluation process to gather information about *Turisteando Ando* app.

The TAM questionnaire based on the Likert-type scale (Summers 1976) was used for a subjective evaluation of aspects related to user interaction with a mobile application. The Likert-type scale measures attitudes and behaviors by means of a



**Fig. 13.3** Technology acceptance model (TAM). Modified from Davis et al. (1989)

series of options that oscillate between two contrasting extremes of perception. In addition to the easy comprehension so that the user can determine an answer about his personal opinion.

### 13.3.2 Description of the Evaluation Protocol

The protocol that guides this study consists of the following seven sequential stages:

**i. Establish Research Hypotheses.** The proposed work focuses on the application of a genetic algorithm to provide a good solution as a response to a traveler's request on its smartphone. Genetic algorithms are a challenge to work in an average smartphone, so *this can reduce the user intention towards the system*. Therefore, it is necessary to evaluate the proposal in terms of ease of use and usefulness, for which the following hypotheses guided the evaluation.

- There is a significant relationship between perceived ease of use, usefulness, attitude, and intention to use the *Turisteando Ando app*.
- Perceived ease of use has a positive impact on users' attitudes and intention to use the *Turisteando Ando app*.
- Perceived usefulness has a positive impact on users' attitudes and intention to use the *Turisteando Ando app*.

**ii. Elements of the Study and Criteria.** Its elements are evaluation objective, methods, sample size and its characteristics, and data gathering process. So, a sample of 14 Spanish speakers was established for the evaluation of *Turisteando Ando app*. The subjects who evaluated the application were recruited through social networks. Each participant completed an initial questionnaire, which evaluated their age and the number of trips made during 2019. Those subjects who met the criteria established in the second bullet of the inclusion and exclusion list shown above were contacted via email. Finally, a virtual meeting was scheduled through videoconferencing platforms where the participant carried out the evaluation.

The inclusion and exclusion criteria were

1. Each subject must be at least 18 years old to be part of this study.
2. Each subject must have at least three travels through 2019 (given that in March of 2020 when this research was being carried out, it was not possible to travel due to the COVID-19 health contingency).
3. Each subject must have an Android device.

**iii. Establishing Evaluation Tools and Auxiliary Forms.** This work used a descriptive research method to develop a quantitative design of the relationship between the four dimensions of the TAM questionnaire. For this purpose, the TAM questionnaire was adapted to the context of *Turisteando Ando app* from Santana-Mancilla and Anido-Rifón (2017). Then, we translated the questionnaire from English to Spanish. Also, we make a video (see <https://youtu.be/O7j7js9dpKE>) to explain the problem

**Table 13.3** Personal information and technological experience

Personal information		Technological experience	
Question	Options	Question	Options
Age		Experience using tourism applications	
Sex			I have not used any
	Man		I know them
	Woman		I have used some
	I prefer not to say		I use them on every trip
Employment			
Residence			

that *Turisteando Ando app* addresses, how the problem is solved, and a comparison with other apps available on the market. Finally, we established an informed consent form for the evaluation.

**iv. Recruit Participants.** It consists of collecting participants to conduct the technology assessment. We recruited the subjects who evaluated the app through social networks. Each participant completed an initial questionnaire (see Table 13.3). Those subjects who met the age requirement (be above 18 years old) and the number of trips requirement during 2019 (three or more trips) were contacted via email. Finally, we scheduled a personal virtual meeting where the participant performed the evaluation.

**v. Conduct the Data Collection Sessions.** In this stage, we collected textual data (adapted TAM questionnaire) and non-textual data (video in which the participant interacts with the app). Our focus was to carry out the events through which the evaluation data will be collected. To achieve data collection, a sequential set of activities must be conducted, they are described in Table 13.4. Activity four includes dialogues and tasks related to the interview-evaluation-data collection process. The above is described in Algorithm 13.3.

**Table 13.4** Initial configuration to conduct the data collection sessions

Step	Activities
1	Schedule convenient day, time and videoconference platform for each participant
2	Prepare installation material for the <i>Turisteando Ando app</i> (apk, as well as the installation manual)
3	Request to subjects download the <i>Turisteando Ando app</i> .apk as well as the installation manual; to ask them to show up for the evaluation with the app installed
4	Prepare interview-evaluation-data collection material (see Algorithm 13.3)

---

**Algorithm 13.3: Interview-Evaluation-Data collection Algorithm**


---

**Data:** Interview dialogues, TAM questionnaire, Tasks

**Result:** Data collected about *Turisteando Ando app* evaluation.

- 1 Prepare recording software to start the interview;
  - 2 **The interview starts** = Thank you for participating in the evaluation of the *Turisteando Ando app*. My name is: \_\_\_\_\_ during the following minutes, I will accompany you to evaluate the *Turisteando Ando app*. We conduct an evaluation of a mobile application to support travelers in planning their activities during their trips. Hence, we require the validation of our proposal to understand how active travelers perceive our app, how useful the app is, how easy to learn the app is, and if the traveler would use the app on their next trips. Also, we are interested to know the advantages and disadvantages that the traveler identifies in *Turisteando Ando app*;
  - 3 /\* After introducing yourself to the participant, tell the participant that to make a reliable assessment, you will read some parts of the evaluation. \*/
  - 4 Signature of the consent form;
  - 5 Play video about *Turisteando Ando app*;
  - 6 /\* After the video, you will solve general questions. \*/
  - 7 **The interview continues** = You saw a semblance of our proposal, which focuses on a tool to support travelers in selecting the tourist attractions to visit on their trips. So that at the end of their trips to maximize their satisfaction. Do you have any questions? We introduced the *Turisteando Ando app*. Firstly, we will ask you to perform some tasks within the app. Afterward, you will let us know your opinion thinking out loud and in writing. Do you have any questions?;
  - 8 /\* The participant will perform three tasks to explore the ways in which the app can create an itinerary. \*/
  - 9 Confirm the requirements for successful installation of the *Turisteando ando app*;
  - 10 /\* Prepare subjects for *Turisteando Ando app* evaluation \*/
  - 11 Task 1();
  - 12 Task 2();
  - 13 Task 3();
  - 14 TAM questionnaire;
- 

### Task 1 [Directions]

- Please read carefully the task with the title: **Review help information**.
- Open *Turisteando Ando app*.
- At main menu, select “AYUDA”.
- Read the help information.
- Press “OK”.

### Task 2 [Directions]

- Please carefully read the task with the title: **Create itinerary for your vacation before traveling**. Suppose you plan to travel your next vacation, so you want to know what tourist attractions you will be able to visit during your trip. Then, you create an itinerary using *Turisteando Ando app*. To create your itinerary, you will enter the duration in days, for example, seven days. In addition, you will enter the location manually using a map within the app. You can repeat the directions for

*this task as many times as you want, trying different configurations to create the itinerary (for example, modify the duration (in days) of the trip and the location of the destination, etc.).*

- At main menu, select “INICIAR VIAJE”.
- Enter travel time in days (minimum three days, maximum 15 days).
- Press the “SIGUIENTE” button.
- Select “SELECCIONAR UBICACIÓN”. Choose a point on the map. Prefer a city that has a large number of tourist attractions (for example, México City). Press the “SIGUIENTE” button.
- Press the “SELECCIONAR” button.
- Press the “SIGUIENTE” button.
- From personal preferences menu, select one or more types of tourist attractions.
- Press the “BUSCAR” button.
- Wait while *Turisteando Ando app* build the itinerary (here the genetic algorithm builds your itinerary).
- Review the list of places that *Turisteando Ando app* suggests as your itinerary.
- Choose a place of your itinerary.
- Review the information of the place.
- Review the information of some or all the places in your itinerary.
- Close *Turisteando Ando app*

### **Task 3 [Directions]**

- *Please carefully read the task with the title: **Create itinerary for a short visit.** Suppose you visit a business place or you visit a relative. You have some hours left before going back home. Therefore, you want to know what tourist attractions you can visit during those remaining hours. Create your itinerary using *Turisteando Ando app*. To create your itinerary, you will enter the travel duration in hours, for example, 12h. Since you are already in the place, allow *Turisteando Ando app* automatically find your location. You can repeat the steps for this task as many times as you wish, trying different configurations to create your itinerary (i.e., change the travel duration (in hours) and the location of your destination).*
- At main menu, select “INICIAR VIAJE”.
- Enter travel time in hours (between 10 and 24h).
- Press the “SIGUIENTE” button.
- Press the “LOCALIZAME” button.
- Press the “SIGUIENTE” button.
- From personal preferences menu, select one or more types of tourist attractions.
- Press the “BUSCAR” button.
- Wait while *Turisteando Ando App* build the itinerary (here the genetic algorithm builds your itinerary).
- Review the list of places that *Turisteando Ando App* suggests as your itinerary.
- Choose a place of your itinerary.

- Review the information of the place.
- Review the information of some or all the places in your itinerary.
- Close *Turisteando Ando app*.

The last task is the application of the TAM questionnaire. The subjects select the option that best fit their perception about the app. We asked the subjects to thinking out loud the reasons to rate each item. The above is known as the thinking aloud method. The thinking aloud method is a usability tool that consists on asking test participants to verbalizing their thoughts as they move through the user interface (Nielsen 1993). We use the above usability tool to find out the participants' comments about the app, both positive and negative.

**vi. Analyze the Data Collected.** Data obtained were categorized and quantified (see Sect. 13.3.3). We gathered notes and other non-textual materials from the transcripts of interviews to increase our understanding of how the participant perceived the *Turisteando Ando app*.

**vii. Report Results.** The results obtained from the evaluation are documented and reported in Sect. 13.4 *Results and discussion*. As well as, the acceptance or rejection of the hypothesis defined in the first stage of this methodology. The results contribute to the validation of the proposal or idea, and give guidelines for new research or future work.

### 13.3.3 The Intervention Instrument

For the evaluation, this research uses an instrument based on the TAM questionnaire (Santana-Mancilla and Anido-Rifón 2017). This was translated into Spanish language and adapted to the context of *Turisteando Ando App*. The TAM questionnaire was composed of 15 items grouped into four dimensions: (1) perceived ease of use, (2) perceived usefulness, (3) attitude towards the utilization of the software, and (4) intention to use. For each item, the answer used a Likert-type scale (Summers 1976). The measurement items employed in this study were constructed from previous literature studies, resulting in the TAM questionnaire shown in Table 13.5, Items use a Likert-type scale of seven options (see Table 13.6).

## 13.4 Results and Discussion

This section is devoted to results analysis and discussion. To show the reliability coefficient of the measurement scale, Table 13.7 shows the reliability statistics based on Crombach's  $\alpha$  coefficient. The TAM questionnaire scale has a coefficient of 0.9 which means that the 7-point Likert-type scale has high reliability for *Turisteando*



**Table 13.5** TAM questionnaire’s dimensions and items (Spanish language)

Acronym	Item
<i>Dimension 1. Utilidad Percibida [Perceived Utility]</i>	
QUP1	En general, usar <i>Turisteando Ando App</i> en mi viaje puede ser útil
QUP2	Usar <i>Turisteando Ando App</i> me permite realizar la planeación del itinerario de viaje más rápidamente
QUP3	Para mí, usar <i>Turisteando Ando App</i> haría más efectivo el proceso de planear un itinerario de viaje
QUP4	Si uso <i>Turisteando Ando App</i> , podría ahorrar costos relacionados con el tiempo y el esfuerzo al planear un itinerario de viaje
<i>Dimension 2. Facilidad de Uso Percibida [Perceived Ease of Use]</i>	
QFUP5	Aprender a usar <i>Turisteando Ando App</i> es fácil para mí
QFUP6	La interacción con <i>Turisteando Ando App</i> es clara y comprensible
QFUP7	Dominar el uso de <i>Turisteando Ando App</i> es una tarea fácil
QFUP8	Me sería fácil utilizar <i>Turisteando Ando App</i> para obtener los itinerarios de viaje
<i>Dimension 3. Actitud Hacia el Uso [Attitude Towards Use]</i>	
QAHU9	No me disgusta la idea de usar <i>Turisteando Ando App</i>
QAHU10	Tengo una actitud favorable hacia el uso de <i>Turisteando Ando App</i>
QAHU11	Considero que es bueno el uso de <i>Turisteando Ando App</i>
QAHU12	Usar <i>Turisteando Ando App</i> para planear itinerarios de viaje es una buena idea
<i>Dimension 4. Intención de Uso [Intention to use]</i>	
QIU13	Asumiendo que <i>Turisteando Ando App</i> se encuentra disponible para su descarga y uso. En el futuro, estoy dispuesto a usar <i>Turisteando Ando App</i> para mis viajes
QIU14	Asumiendo que <i>Turisteando Ando App</i> se encuentra disponible para su descarga y uso. Yo utilizaría <i>Turisteando Ando App</i> de forma regular para la planeación de mis próximos viajes
QIU15	Asumiendo que <i>Turisteando Ando App</i> se encuentra disponible para su descarga y uso. Tengo la intención de utilizar <i>Turisteando Ando App</i>

**Table 13.6** Likert-type scale of seven options in the TAM questionnaire Spanish–English

Likert	Spanish language*	English language
Scale values		
1	Totalmente en desacuerdo	Totally disagree
2	Bastante en desacuerdo	Quite disagree
3	En desacuerdo	In disagreement
4	Neutro	Neutral
5	De acuerdo	Agree
6	Bastante de acuerdo	Quite agree
7	Totalmente de acuerdo	Totally agree

**Table 13.7** Frequentist scale reliability statistics

Estimate	Cronbach’s $\alpha$	Mean	SD
Point estimate	0.900	96.500	8.428
95% CI lower bound	0.840	92.085	6.110
95% CI upper bound	0.945	100.915	13.579

*Note* The following items correlated negatively with the scale: QFUP5, QFUP6

**Table 13.8** Maximal and expected values on dimensions for the TAM questionnaire

Dimensions	Number of items	Maximum accumulated of items values on Likert scale	Expected value
Perceived utility	4	28	24
Perceived ease of use	4	28	24
Attitude towards use	4	28	24
Intention to use	3	21	18

*Ando app* evaluation even though two items have a negative correlation. If we remove them is highly likely to improve the Cronbach’s  $\alpha$  coefficient.

Now, we define reference values for this analysis. Using the Likert-type scale of seven options for items related to four dimensions on the TAM questionnaire. We build Table 13.8, and it shows the maximum value accumulated by dimension. The maximum value is obtained by adding each item with its highest value on Likert-type scale of seven options in each dimension. On the other hand, the expected value on items is stated for this app on *Quite agree* as the best option of acceptance.

Table 13.9 shows the summary of answers on the modified TAM questionnaire’s items. Skew column shows negative values related to the median value. The above implies on Likert-type scale a skew to positive responses on four dimensions about the *Turisteando Ando app*. Excess of positive kurtosis describes a leptokurtic curve. This means high data concentration around of a narrow region as on items QFUP5 and QFUP7 with high frequency of Likert-type scale of seven options (Totally agree). On the other hand, negative kurtosis describes a platykurtic curve on items from dimension 1 and 3, they do not have extreme number of positive or negative opinions. In this case, subjects’ opinions are distribute over positive region as values on Skew column suggest.

Mean and median have similar values, both skew to high values from the Likert-type scale (Totally agree). Standard deviation (SD) confirms this behavior, due to SD on items are around of 1; the above means near of mean, which has values around 6.0; therefore, as we expected *Turisteando Ando app* has a *Quite agree* acceptance level.

As we analyze dimensions instead of questions, results in Table 13.10 show differences on the mean. Although, media of dimensions outperformances the expected

**Table 13.9** Descriptive statistics of modified TAM questionnaire

Item	n	Mean	SD	Median	Min	Max	Range	Skew	Kurtosis
<b>Dimension 1. Perceived utility</b>									
QUP1	14	6.00	0.96	6.00	4.00	7.00	3.00	-0.48	-0.99
QUP2	14	6.00	1.11	6.00	4.00	7.00	3.00	-0.63	-1.11
QUP3	14	5.79	1.05	6.00	3.00	7.00	4.00	-1.09	0.98
QUP4	14	6.21	1.05	7.00	4.00	7.00	3.00	-0.76	-1.03
<b>Dimension 2. Perceived ease of use</b>									
QFUP5	14	6.93	0.27	7.00	6.00	7.00	1.00	-2.98	7.41
QFUP6	14	6.79	0.43	7.00	6.00	7.00	1.00	-1.25	-0.47
QFUP7	14	6.93	0.27	7.00	6.00	7.00	1.00	-2.98	7.41
QFUP8	14	6.50	0.94	7.00	4.00	7.00	3.00	-1.55	1.10
<b>Dimension 3. Attitude towards use</b>									
QAHU9	14	6.64	0.74	7.00	5.00	7.00	2.00	-1.49	0.46
QAHU10	14	6.71	0.47	7.00	6.00	7.00	1.00	-0.85	-1.36
QAHU11	14	6.57	0.65	7.00	5.00	7.00	2.00	-1.04	-0.20
QAHU12	14	6.57	0.76	7.00	5.00	7.00	2.00	-1.21	-0.21
<b>Dimension 4. Intention to use</b>									
QIU13	14	6.29	1.20	7.00	3.00	7.00	4.00	-1.49	1.22
QIU14	14	6.29	1.14	7.00	3.00	7.00	4.00	-1.68	2.16
QIU15	14	6.29	1.14	7.00	3.00	7.00	4.00	-1.68	2.16

**Table 13.10** Results on TAM questionnaire by dimension

Dimension	Mean	SD	Median	Min	Max	Range	Confidence interval	
							Lower	Upper
1	24	3.35	25	18	28	10	22.065	25.935
2	27.14	1.03	27.5	25	28	3	26.55	27.736
3	26.5	1.83	27.5	23	28	5	25.444	27.556
4	18.86	3.42	21	9	21	12	16.885	20.83

value, the SD on dimension 1 and 4 is greater than 3; this is influenced by the atypical opinions, and not a problem on *Turisteando Ando app*, which can be seen in the min column values of Table 13.9, and median column values.

Table 13.11 shows the results of the statistical  $\chi^2$  test. We found that most users of the *Turisteando Ando app* found it easy to use and useful. Also, there was a positive attitude towards it.

There were differences among the means on the four dimensions. Therefore to know if the differences are statistically significant, we performed a Chi-squared test because the data type is ordinal. The null hypothesis in this test is: The averages of the four dimensions are equal, while the alternative hypothesis is that at least one of the four dimensions is different. The  $\chi^2$  calculated is 0.301, and the value on

**Table 13.11** Results of TAM questionnaire statistical  $\chi^2$  test

Dimension	Observed (O)	Expected (E)	$(O - E)^2$	$(O - E)^2/E$
1	24	24	0	0
2	27.14	24	9.86	0.411
3	26.5	24	6.25	0.26
4	18.86	18	0.74	0.041
			$\chi^2$ value is	0.301

**Table 13.12** Spearman correlation level

Range	Relation
0.00	There is no correlation
$\pm 0.01$ to $\pm 0.10$	Weak positive correlation
<b><math>\pm 0.11</math> to <math>\pm 0.50</math></b>	<b>Positive correlation media</b>
<b><math>\pm 0.51</math> to <math>\pm 0.75</math></b>	<b>Positive correlation considerable</b>
<b><math>\pm 0.75</math> to <math>\pm 0.90</math></b>	<b>Very strong positive correlation</b>
$\pm 0.91$ to $\pm 1.00$	Perfect positive correlation

**Table 13.13** Spearman correlation among dimensions

Dimension	Perceived Utility	Perceived Ease of Use	Attitude Towards Use	Intention to use
<b>Perceived Utility</b>	1.0000000			
<b>Perceived Ease of Use</b>	0.4949678	1.0000000		
<b>Attitude Towards Use</b>	0.8143172	0.7462145	1.0000000	
<b>Intention to use</b>	0.8829847	0.4896789	0.8935476	1.0000000

tables of  $\chi^2_{0.95,3}$  is 7.8147. Therefore, the null hypothesis cannot be rejected, and the acceptance level is statistically similar among four dimensions.

Table 13.13 shows the Rho Spearman coefficient; pairs of dimensions on TAM questionnaire. **Perceived Utility** and **Perceived Ease of Use**, as well as **Intention to use** and **Perceived Ease of Use** have the lowest correlation values, around of 0.5 (see Table 13.12) which is a medium positive correlation. The subjects’ opinion of **Perceived Ease of Use** has a relevant impact on **Perceived Utility** and **Intention to use**, with a 95% of confidence level. However, **Perceived Ease of Use** is most relevant on **Attitude Towards Use**; because it is has a Rho Spearman of 0.746 and  $p$ -value = 0.002176. Most of the test participants found *Turisteando Ando* app easy to use. They also consider our app as one they could frequently use. However, the test participants pointed out some limitations, for example, GUI flaws (overlapped objects). Another

limitation is the way to search for destinations. The subjects suggest having more options in the personal preferences menu screen and arranging the itinerary by day.

For most subjects, **Perceived Utility** has a very strong positive correlation with **Attitude Towards Use** and **Intention to use**. The above is a significant finding for this research. The utility pursued is mainly generated by the way the problem is approached and solved. A genetic algorithm is responsible for generating good solutions as fast as possible in the tourist smartphone. The above is a challenge on devices with constrained resources like the tourist smartphones.

Items by dimension offered relevant information about specific topics. So, in dimension 1 (**Perceived Utility**), the first item is related to the use of *Turisteando Ando app* during a trip; while, the last three questions are related to **Perceived Utility** before traveling. Answers have Likert-type scale values equal to or higher than four in QUP1, QUP2, and QUP4 (see Fig. 13.4). On the other hand, QUP3, which is personal opinion has one low evaluation of 3 on the Likert-type scale. The general perception of the utility of planning travel is 71%, which is 11% greater than the expected value (see Fig. 13.4 and Table 13.11).

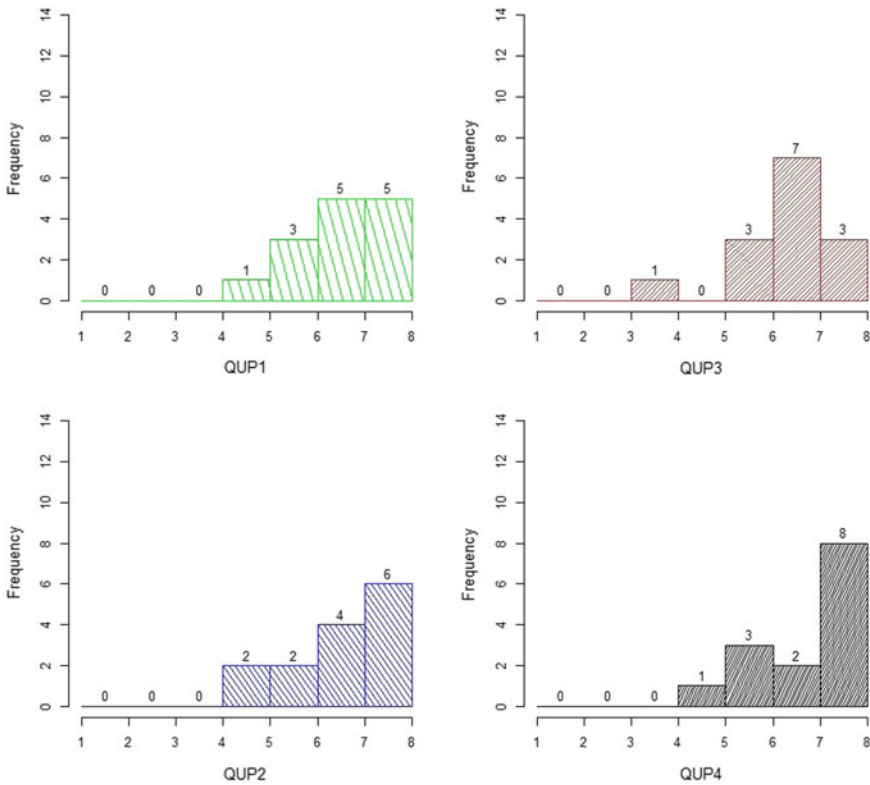
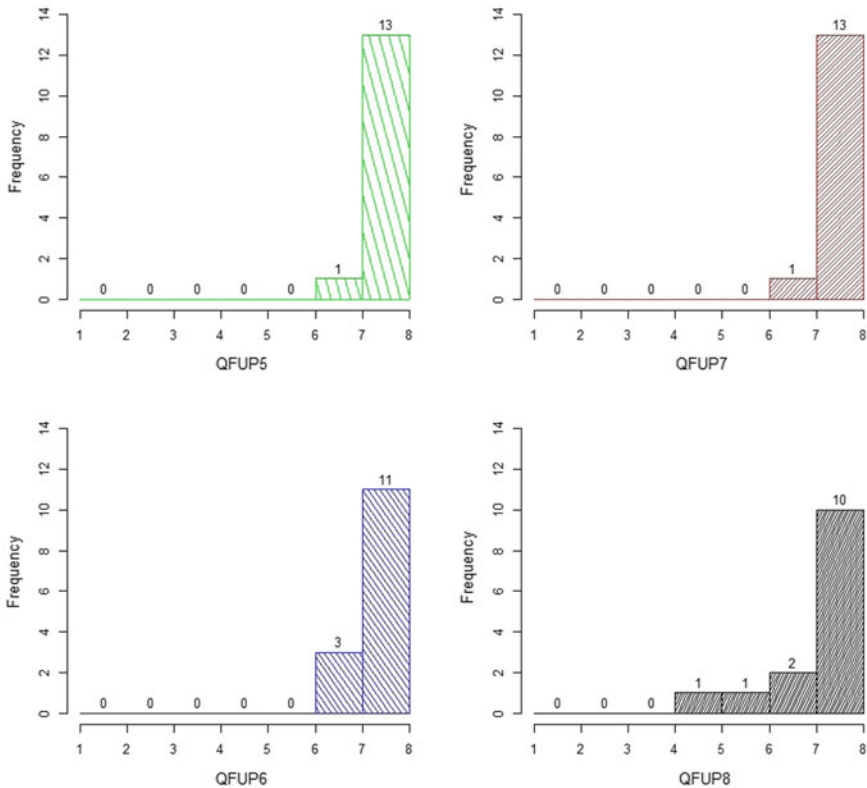


Fig. 13.4 Dimension 1. Perceived utility



**Fig. 13.5** Dimension 2. **Perceived ease of use**

In the results of items in dimension 2 (**Perceived Ease of Use**), users believed that the *Turisteando Ando app* is easy to use. From Fig. 13.5, expected values on the Likert-type scale are overcome again. Results have a high skew to *Totally agree* on four items, the lowest value was set by one subject specifically on the item QFUP8, again a question in first person, as in the previous dimension on item QUP3. This behavior can be related to personal preferences.

Regarding dimension 3 (**Attitude Towards Use**), the *Turisteando Ando app* (see Fig. 13.6) obtained a positive response; around 71.4% felt *Totally agree* on the specific topics in items. It is relevant to mention that all items are questions in the first person (see Table 13.5), and different from previous behavior where these kinds of items were evaluated low; in this dimension, the lowest value is 5 on the Likert-type scale.

Finally, in dimension 4 (**Intention to use**) again appears a low evaluation by one subject. The above opens the opportunity to analyze their point of view and to filter relevant opinions to this work. The rest of the subjects mentioned that they would use and download the app for regular use; 64.28% of them set 7 on a Likert-type

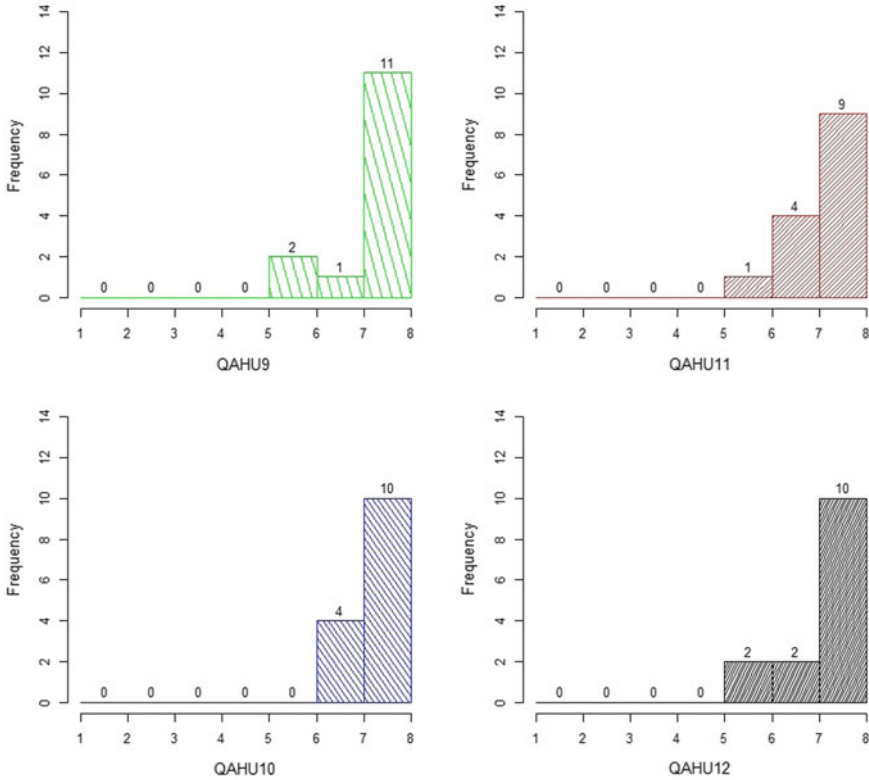
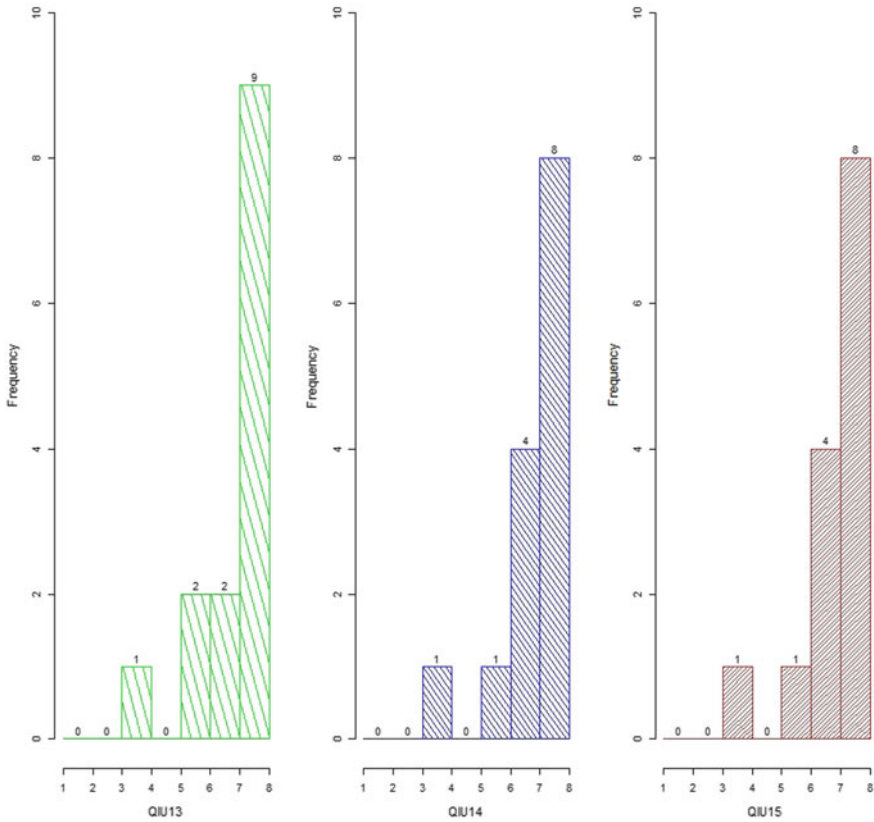


Fig. 13.6 Dimension 3. Attitude Towards Use

scale to items in this dimension. On the other hand, the rest of the subjects use 5 or 6 on a Likert-type scale. The result here also surpasses expected values (Fig. 13.7).

Most apps we mentioned in related work do not have a metaheuristic embedded to efficiently produce itineraries. Furthermore, those tourist apps focus on specific regions of the world. Unlike those works, the *Turisteando Ando* app has a search engine based on a metaheuristic that efficiently generates a personalized itinerary in polynomial time that tourists considered acceptable. From the thinking aloud method through the four dimensions, no tourist complained about the time their itinerary was displayed on their smartphone. The above contrasted with work in Tenemaza et al. (2020), in which authors generate itineraries through a genetic algorithm and a *k*-means algorithm. This can be costly computationally in a standard smartphone. Also, work in Tenemaza et al. (2020) analyzed users' perceptions; unlike work in Tenemaza et al. (2020), we applied TAM methodology, and through thinking aloud method, we obtained users' perceptions in each question in the four dimensions.

Another *Turisteando Ando* app key feature is that it gathers POIs information from any region in the world within a 30km radius from the current tourist location. The above is help full since we did not receive from the thinking aloud method



**Fig. 13.7** Dimension 4. Intention to use

implemented in the four dimensions negative feedback about this aspect. On the other hand, like work in Xia et al. (2018), we found that more attention should be paid to navigation.

### 13.5 Conclusion and Future Work

This chapter presents a tourism app based on a genetic algorithm to produce personalized trip itineraries. For a standard smartphone, running a genetic algorithm is a demanding task. The above may affect the way that a tourist perceives the interaction with our tourism app. To evaluate the adoption of our proposed app, we applied TAM.

The results showed that most tourists found our tourism app easy to use and useful. Also, there was a positive attitude towards it. Furthermore, tourists considered our



app as one they could frequently use. Results also showed a strong positive correlation between attitude towards use and intention to use.

However, the test participants pointed out some limitations, for example, GUI flaws (overlapped objects). Another limitation was the way to search for destinations. The subjects suggested having more options in the personal preferences menu screen and arranging the itinerary by day.

For future work we plan to improve the GUI and include more options in the personal preferences menu. Furthermore, since the POIs contents that Google keeps in its data storage are gathered from the tourists' opinions, the type of POI highly depends on the tourist's point of view. The above sometimes leads that the type of POI does not correspond to the correct one. For example, there were cases where a graffiti wall was classified by a tourist as a historical place. Then, the accurate POI contents that our tourism app shows mainly depend on the tourist's point of view. Therefore, another future work is to verify the type of POI before SSGA processes the POIs contents to display the correct kind of POI when the tourist obtains a personalized trip itinerary.

## References

- Davis F, Bagozzi R, Warshaw P (1989) User acceptance of computer technology: a comparison of two theoretical models. *Manag Sci* 35:982–1003. <http://www.jstor.org/stable/2632151>
- Dix A, Finlay J, Abowd G, Beale R (2003) *Human-computer interaction*, 3rd ed. Prentice-Hall Inc
- Eccles D, Aarsal G (2017) The think aloud method: what is it and how do I use it?. *Qual Res Sport Exerc Health* 9:514–531. <https://doi.org/10.1080/2159676X.2017.1331501>
- Eiben A, Smith J (2015) *Introduction to evolutionary computing*. Springer Publishing Company, Incorporated
- Gartner G, Huang H (2011) Using context-aware collaborative filtering for POI recommendations in mobile guides. In: *Advances in location-based services: 8th international symposium on location-based services*, Vienna, pp 131–147. [https://doi.org/10.1007/978-3-642-24198-7\\_9](https://doi.org/10.1007/978-3-642-24198-7_9)
- Lin K, Chang L, Tseng C, Lin H, Chen Y, Chao C (2014) A smartphone APP for health and tourism promotion. *Math Probl Eng* 2014:583179 (2014, 5). <https://doi.org/10.1155/2014/583179>
- Lin S, Juan P, Lin S (2020) A TAM framework to evaluate the effect of smartphone application on tourism information search behavior of foreign independent travelers. *Sustainability* 12. <https://www.mdpi.com/2071-1050/12/22/9366>
- Lopez-Sanchez M, Cosío-Léon M, Martínez-Vargas A (2021) Comparative analysis of constraint handling techniques based on Taguchi design of experiments. In: *Constraint handling in meta-heuristics and applications*, pp 285–315. [https://doi.org/10.1007/978-981-33-6710-4\\_14](https://doi.org/10.1007/978-981-33-6710-4_14)
- Lozano M, Herrera F, Cano J (2008) Replacement strategies to preserve useful diversity in steady-state genetic algorithms. *Inf Sci* 178:4421–4433. <http://www.sciencedirect.com/science/article/pii/S0020025508002867>. Including special section: genetic and evolutionary computing
- Martello S, Toth P (1990) *Knapsack problems: algorithms and computer implementations*. Wiley. ISBN 0471924202
- Michalewicz Z (1996) *Genetic algorithms + data structures = evolution programs*, 3rd ed. Springer. ISBN 3540580905
- Nielsen J (1993) Usability testing. In: *Usability engineering*, pp 165–206. <https://www.sciencedirect.com/science/article/pii/B9780080520292500097>

- Páez-Quinde C, Torres-Oñate F, Rivera-Flores D, Chimbo-Cáceres M (2020) Tourism 3.0 and indigenous food cultures: case study Pilahuín. *Technol Innov* 166–178
- Santana-Mancilla P, Anido-Rifón L (2017) The technology acceptance of a TV platform for the elderly living alone or in public nursing homes. *Int J Environ Res Public Health* 14:617
- Scarlett H (2021) Tourism recovery and the economic impact: a panel assessment. *Res Global* 3:100044. <https://www.sciencedirect.com/science/article/pii/S2590051X21000095>
- Sumiya K et al (2015) A route recommender system based on the user's visit duration at sightseeing locations. In: *Software engineering research, management and applications*, pp 177–190. [https://doi.org/10.1007/978-3-319-11265-7\\_14](https://doi.org/10.1007/978-3-319-11265-7_14)
- Summers G (1976) Una técnica para medir actitudes. Trillas (ed)
- Tarantino E, De Falco I, Scafuri U (2019) A mobile personalized tourist guide and its user evaluation. *Inf Technol Tour* 21:413–455. <https://doi.org/10.1007/s40558-019-00150-5>
- Tenemaza M, Luján-Mora S, De Antonio A, Ramírez J (2020) Improving itinerary recommendations for tourists through metaheuristic algorithms: an optimization proposal. *IEEE Access* 8:79003–79023
- Tlili T, Krichen S (2021) A simulated annealing-based recommender system for solving the tourist trip design problem. *Exp Syst Appl* 186:115723. <https://www.sciencedirect.com/science/article/pii/S0957417421011040>
- Xia M, Zhang Y, Zhang C (2018) A TAM-based approach to explore the effect of online experience on destination image: a smartphone user's perspective. *J Destin Market Manag* 8:259–270. <https://www.sciencedirect.com/science/article/pii/S2212571X16300245>